THE EFFECT OF DRILLED HOLES ON NOTCH TOUGHNESS

by

Charles Alfred Rau, Jr.

April, 1967

SU-DMS Report No. 67-12

THE EFFECT OF DRILLED HOLES ON NOTCH TOUGHNESS

by

Charles A. Rau, Jr.

Department of Materials Science

Stanford University

Stanford, California

April, 1967

Technical Report #6

Prepared for the

National Aeronautics and Space Administration

Under NASA Contract NSG-622

ABSTRACT

The effect of mechanically drilled holes on the notch toughness of iron-base alloys has been investigated by means of instrumented impact-bend, slow-bend, and tension testing. Although one small hole (diameter = 0.0292") drilled at or below the notch tip produces insignificant or adverse effects on the Charpy-V transition behavior, two holes located on each side of the notch produce considerable improvements. The important geometric parameters which determine the magnitude of the improvement were investigated. The impact transition temperature of drilled specimens can be as much as 60°C lower than that of standard Charpy samples. In addition, two holes increase the load carrying capacity of Charpy samples by as much as 100% at low temperatures where both specimens fracture completely by cleavage prior to general yielding.

A photoelastic stress analysis revealed that these improvements are obtained without markedly reducing the elastic stress concentration factor of the notch. However, metallographic examination of etch-pitted specimens of Fe-3% Si showed that two holes cause a marked redistribution of local plastic strains away from the notch tip and between the notch side and each hole. As a result, two holes reduce the rate at which the plastic stress concentration factor builds up with applied load, and thus holes increase the applied load required to produce the critical fracture stress or strain below the notch root. In addition, when ductile tearing occurs to both holes, the resulting "hammerhead" notch is so blunt that fracture reinitiation requires much higher energy. Other geometries such as increased hole size and additional number of holes were able to further improve the nominal notch strength

at low temperatures, but they tended to be less effective than two 0.0292" holes at higher temperatures. Similar improvements were also obtained in Charpy type samples of reduced thickness and sheet tension samples, indicating that plane strain conditions are not a prerequisite for improvement with holes.

Although a general geometric effect, the magnitude of the improvement from hole drilling varies with microstructure. In a series of hypoeutectoid steels, holes increased the notch strength by similar amounts when failure occurred prior to general yielding. However, the reduction in the ductility transition temperature due to holes increased rapidly with the steel's carbon content in mild steels (%C < 0.2) and then decreased with additional carbon content. The percentage increase in the shelf energy of fully ductile samples showed no such maximum and increased continuously as the ductile tear energy decreased.

ACKNOWLEDGMENTS

The author wishes to express his gratitude to:

Dr. A. S. Tetelman, his thesis advisor, for his constant encouragement and guidance, and especially for the intense interest which he maintained and instilled in the author through the course of this study;

Dr. T. R. Wilshaw, who so freely gave his time and ideas in discussions which stimulated development of many concepts necessary for this work;

Dr. O. D. Sherby and Dr. M. Hetenyi, for their interest and time in reading the manuscript;

His fellow students and associates at Stanford, who both stimulated the author's technical development and joined him in necessary temporary relapses;

His wife, Brooke, for her patience and understanding while contributing many lonely nights toward completion of this work;

Phyllis E. Dillman, for typing the manuscript;

Jim Forsberg, for preparing many of the drawings;

The research laboratories of the Ford Motor Company, Jones and Laughlin Steel Company, and Lockheed Missiles and Space Company, for supplying some of the alloys used in this study;

The National Aeronautics and Space Administration, in particular, Dr. R. R. Nash, for providing encouragement and financial support under Contract NASA-NSG-622.

TABLE OF CONTENTS

TABLE OF CONTENTS

TABLE OF CONTENTS

TABLE OF CONTENTS

TABLE OF CONTENTS

LIST OF TABLES

LIST OF ILLUSTRATIONS

LIST OF ILLUSTRATIONS

LIST OF ILLUSTRATIONS

LIST OF ILLUSTRATIONS

LIST OF ILLUSTRATIONS

LIST OF ILLUSTRATIONS

LIST OF ILLUSTRATIONS

LIST OF SYMBOLS

Symbol	Meaning
a	Net depth of a notched sample
a_o	Lattice parameter
b	Burgers vector of a dislocation
c	(a) One-half the length of an internal crack (b) Depth of an external crack or notch
k	Yield strength in shear
n	Integer (a) the number of dislocations in a pile-up (b) the order of the photo-elastic fringe
r	Radial distance from the tip of a blocked slip band
t	Specimen thickness
x	Distance (and direction) ahead of the notch tip
y	Distance (and direction) perpendicular to the plane of the notch
A	Minimum area over which σ_f must exist to cause cleavage
E	(a) Elastic modulus (b) Impact energy absorbed in Charpy test
E_a	Uncorrected energy calculated from a load-time trace
E_o	Initial energy of the Charpy pendulum on impact
E_{max}	Charpy shelf energy
ΔE_{max}	Difference between the shelf energy of Charpy and drilled samples
G	Shear modulus
G_c	Toughness, work done in initiating unstable fracture at the tip of a notch or crack
G_{Ic}	Plane strain fracture toughness (tensile loading)
H	Superscript or subscript, associated with two drilled holes

List of Symbols (Cont'd.)

Symbol	Meaning
H_D	Hole diameter
I	Moment of inertia
K_Y	Parameter that determines the grain size dependence of the yield strength
K_σ	Elastic stress concentration factor of a notch
K_σ^H	Elastic stress concentration factor of a notch modified by two holes
$K_{\sigma(p)}$	Plastic stress concentration factor
$K_{\sigma(p)}^H$	Plastic stress concentration factor in a drilled sample
$K_{\sigma(p)}^F$	Critical plastic stress concentration factor
$K_{\sigma(p)}^{max}$	Maximum plastic stress concentration factor
$K_{\sigma(p)}^{max,H}$	Maximum plastic stress concentration factor in a drilled sample
$K_{\sigma(p)}^{EFF}$	Effective plastic stress concentration factor resulting from both triaxiality and increased strain rate
$K_{\sigma(p)}^{\infty}$	Hypothetical plane strain, plastic stress concentration factor for a thin sample
L	(a) Length of a slip band (b) One-half the total support length for a beam loaded in three-point bending (c) Constraint factor, ratio of the general yield load of a notched section to that of an unnotched section of the same dimensions
M	Applied bending moment
P	Applied load
P_F	Applied load to cause fracture
P_F^H	Applied load to cause fracture of a drilled sample
P_{ULT}	Applied ultimate load (plastic instability)

List of Symbols (Cont'd.)

Symbol	Meaning
P_{LY}	Applied load to cause local yielding
P_{GY}	Applied general yield load
R	(a) Plastic zone size (b) Radial distance from the center of curvature of the notch tip to the center of the drilled holes (c) Relative retardation (phase shift) of one light wave with respect to another
R_{β}	Plastic zone size at which maximum triaxiality is produced
R^{F}	Plastic zone size required to cause fracture
T	Temperature (^{o}C)
T_{Do}	Nil-ductility transition temperature of a smooth sample
T_{So}	Initiation transition temperature of a smooth sample
T_{D}	Nil-ductility transition temperature of a notched sample
T_{N}	Ductility transition temperature of a notched sample
T_{S}	Initiation transition temperature of a notched sample
T_{50}	50% E_{max} transition temperature of a notched sample
T_{DH}	Nil-ductility transition temperature of a drilled sample
T_{NH}	Ductility transition temperature of a drilled sample
T_{SH}	Initiation transition temperature of a drilled sample
T_{50H}	50% E_{max} transition temperature of a drilled sample
T_{i}^{t}	"i-type" transition temperature of a notched sample of thickness t
T_{iH}^{t}	"i-type" transition temperature of a drilled sample of thickness t
T_{D}^{ω}	Nil-ductility transition temperature of a Charpy type sample with flank angle ω
ΔT_{i}	Difference between the "i-type" transition temperature of drilled and standard samples

LIST OF ILLUSTRATIONS

List of Symbols (Cont'd.)

Symbol	Meaning
ΔT_i^t	Difference between the "i-type" transition temperature of drilled and notched samples of thickness t
V_o	Initial striker velocity on impact
V(c)	Notch tip displacement
V*(c)	Critical notch tip displacement to cause cleavage in a notched sample
V**(c)	Critical notch tip displacement to cause cleavage ahead of the notch in a drilled sample
V*(c + H)	Critical notch tip displacement to cause fracture ahead of one hole in a drilled sample
$V_s^*(c)$	Critical notch tip displacement to initiate fibrous tear-in a notched sample
$V_H^*(c)$	Critical notch tip displacement to initiate fibrous shear failure between the notch side and a drilled hole
$V^{RLX}(c)$	Notch tip displacement at which the large tensile stresses are relaxed
$V^{RLX,t}(c)$	Notch tip displacement at which the large tensile stresses are relaxed in a sample of thickness t
$V_H^{RLX}(c)$	Notch tip displacement at which the large tensile stresses are relaxed in a drilled sample
X(R,t)	Factor $X < 1$ representing the deviation from plane strain conditions in a sample of thickness t
α	Redistribution coefficient $\alpha \geq 1$ describing the amount of plastic strain concentrated away from the notch tip in drilled samples
β	Factor relating the strain at the notch tip to that at the point of maximum constraint (R_β)
β_H	Factor relating the strain at the hole to that at the point of maximum constraint ahead of the hole
γ_s	True surface energy

List of Symbols (Cont'd.)

Symbol	Meaning
γ_m	Work done near the tip of a cleavage crack that is propagating within a single crystal or grain of a polycrystal
γ_{GB}	Work done in propagating a cleavage crack through a high angle grain boundary
δ	Deflection at the central loading point in three-point bending
$\dot{\delta}$	Deflection rate at the central loading point in three-point bending
ϵ	True tensile strain
ϵ_f	Critical cleavage strain in a smooth sample
ϵ_F	Critical cleavage strain at the point of maximum constraint in a notched sample
ϵ_F^H	Critical cleavage strain at the point of maximum constraint in a drilled sample
ϵ_F'	Critical cleavage strain ahead of one hole at the point of maximum constraint
ϵ_F^t	Critical cleavage strain at the point of maximum constraint in a notched sample of thickness t
ϵ_{yy}	Tensile strain in the y direction
ϵ_s	Tensile strain to cause fibrous tearing
$\dot{\epsilon}$	True strain rate
λ	Wave length
ρ	Radius of curvature of the notch root
ρ_{min}	Notch root radius below which toughness (cleavage controlled) is independent of ρ
$\rho_{min,s}$	Notch root radius below which toughness (fibrous controlled) is independent of ρ
ρ_H	Radius of curvature of a blunted hole

List of Symbols (Cont'd.)

Symbol	Meaning
θ	Angular coordinant of the holes from the plane of the notch
σ	Tensile stress
$\sigma_{yy} \equiv \sigma_y$	Tensile stress in y direction
$\sigma_{xx} \equiv \sigma_x$	Tensile stress in x direction
σ_Y	Uniaxial yield stress, static loading
σ_Y^*	Uniaxial yield stress at appropriate strain rate ahead of the notch
σ^{max}	Maximum local tensile stress
σ_f	Critical local tensile stress required for cleavage fracture
σ_i	Lattice friction stress in tension
σ_N	Applied nominal stress
σ_1, σ_2	Principal stresses
σ_F	Applied nominal stress to produce σ_f locally and cause cleavage fracture
σ_{GY}	Applied nominal stress to produce general yielding
σ_{LY}	Applied nominal stress to produce local yielding
$\Delta\sigma$	Amount the tensile flow stress is raised by strain hardening
$d\sigma/d\varepsilon$	Strain hardening rate
τ	Shear stress
τ^{max}	Maximum shear stress
τ_{xy}	Shear stress on x plane in y direction
τ_i	Lattice friction stress in shear
ω	Notch flank angle

CHAPTER I

INTRODUCTION

In choosing materials for engineering structures, one must consider not only their strength under appropriate service conditions but also their toughness. Because flaws or necessary design configurations can act as stress and strain concentrators, the strength of semi-brittle materials can be reduced considerably and normally ductile materials may appear brittle. The useable strength of a material therefore depends on the specific nature of the concentration and the material's intrinsic ability to relax local concentrations. To understand what improvements are possible in both, it is first necessary to define the conditions which control brittle fracture.

1.1 Fracture of Unnotched Polycrystalline Materials

1.1-1 Griffith Theory of Crack Propagation

Cleavage fracture occurs when tensile stresses are able to break atomic bonds across crystallographic planes. In a completely brittle material, the work done in breaking these bonds is essentially twice the intrinsic surface energy of the crystal.

Griffith[1, 2] in 1920 proposed that brittle materials fracture below their theoretical strengths because microscopic flaws are present. These flaws or cracks propagate under a given stress when the elastic strain energy released by an increment of crack extension is greater than the energy required to create the two new surfaces. For a crack of length 2c, fracture occurs at a stress (σ_f) where

$$\sigma_f = \text{const.} \times \sqrt{\frac{E\gamma_s}{c}} \qquad (1.1)$$

E is the elastic modulus and γ_s is the surface energy.

In metals, equation (1.1) is not exactly applicable because plastic deformation around the moving crack requires the expenditure of additional energy. Orowan and his co-workers[3, 4, 5] modified Griffith's equation to account for this additional energy. Equation (1.1) becomes

$$\sigma_f = \text{const.} \times \sqrt{\frac{E(\gamma_s+\gamma_m)}{c}} \qquad (1.2)$$

where γ_m is the elastic energy dissipated by plastic deformation around the moving crack. In practical structural metals, $\gamma_m \gg \gamma_s$ so that γ_s is negligible in equation (1.2).

In polycrystals, energy must also be expended in propagating a cleavage crack through high angle grain boundaries. The Griffith equation may again be modified to

$$\sigma_f = \text{const.} \times \sqrt{\frac{E\gamma_{GB}}{c}} \qquad (1.3)$$

where γ_{GB} is the energy spent in crossing the grain boundary. Normally, when a crack has spread to one or more boundaries, its length 2c has increased markedly. Therefore γ_{GB} must be extremely high relative to γ_m to stop a moving cleavage crack. For this reason, non-propagating cracks are only observed in special cases where the crack is initiated at very low stresses (low γ_m) and when they are quite short[6-9].

1.1-2 Crack Nucleation in Metals

It is presently accepted that pre-existing flaws are not required for low stress brittle fracture in metals. Some plastic deformation always precedes fracture and is responsible for nucleating microcracks which may propagate unstably when equations (1.2) and (1.3) are satisfied. Numerous microscopic mechanisms have been proposed whereby inhomogeneous deformation can produce cleavage cracks. Zener[10] and Stroh[11] have considered a slip band and edge dislocation pile-up respectively as producing large tensile stresses when blocked by a strong obstacle such as a grain boundary. These tensile stresses are given by

$$\sigma = (\tau - \tau_i) \left(\frac{L}{r}\right)^{1/2}$$

where

τ = resolved shear stress

τ_i = lattice friction stress

L = length of slip band

r = radial distance from the tip of the blocked dislocation group.

They proposed that when this stress at $r = a_0$ (the lattice parameter) is greater than the theoretical cleavage strength of the crystal $[\sqrt{2G\gamma_s/a_0}]$, a crack is nucleated. That is,

$$\tau - \tau_i \geq \sqrt{\frac{2G\gamma_s}{L}} \,. \tag{1.4}$$

Similarly, mechanical twins produce large local tensile stresses when they are blocked by an obstacle. Hull[12, 13] and Honda[14] have shown clear experimental evidence for the initiation of cracks at twin

intersections. The effectiveness of any one of these mechanisms will depend on

(1) The intensity of the blocked shear band[15, 16, 17]

(2) How easily the large stresses at its tip may be relaxed by slip[18, 19].

By analogy with crack propagation, the total work done in crack nucleation is γ_m rather than γ_s in equation (1.4) because some elastic energy is expended in plastic deformation. In this light, brittle second phases such as carbides at ferrite grain boundaries ease crack formation by providing a barrier in which relaxation by slip is difficult during crack formation[8]. Consequently, γ_m is lowered.

1.1-3 The Critical Step for Fracture

Tetelman and McEvily[20] have pointed out that there are three criteria which must be fulfilled for cleavage to occur. They are: 1) crack nucleation, 2) initial propagation, and 3) propagation through the first few grain boundaries. The criteria which requires the largest applied stress will be the critical one. Nucleation (eq. 1.4) and propagation through the grain boundaries have been discussed previously. It was pointed out then that grain boundaries would only stop cracks under special conditions. Quantitative arguments[20-22] have also shown that nucleation is not the critical stage. This leaves initial growth as the process which requires the maximum applied stress in most alloys.

Cottrell[21] has derived an expression for the stress required for first growth using a dislocation coalescence model. His criterion

is given by the relation

$$\sigma_f nb = 2\gamma_m \tag{1.5}$$

where n is the number of dislocations coalescing to form the crack, b is their Burgers vector, and γ_m is the surface energy modified by the plastic work which accompanies cleavage. Equation (1.5) may be rewritten substituting an expression for the plastic displacement (nb). Noting that plastic displacement relieves elastic shear stresses in the shear band

$$(\tau-\tau_i)\,\frac{d}{G} = nb$$

and that

$$\tau-\tau_i = k_Y d^{-1/2} \qquad \text{(Petch}^{(23)}\text{ equation)},$$

the plastic displacement is given by

$$nb = (\tau-\tau_i)\,\frac{d}{G} = (k_Y d^{-1/2})\,\frac{d}{G} = k_Y \frac{d^{1/2}}{G}$$

Equation (1.5) becomes

$$\sigma_f = \frac{2G\gamma_m}{k_Y d^{1/2}} \tag{1.6}$$

1.1-4 The Ductile to Brittle Transition

A specimen is considered completely brittle if fracture occurs on initial yielding. This requires from equation (1.6) that

$$\sigma_f \leq \sigma_Y$$

$$\frac{2\gamma_m G}{k_Y} d^{-1/2} \leq \sigma_i + k_Y d^{-1/2} \qquad T \leq T_{Do} \tag{1.7}$$

where σ_i = lattice friction stress in uniaxial loading. In body-centered-cubic metals, σ_i increases[24-28] while γ_m decreases[16, 17] with decreasing temperature. Thus equation (1.7) is satisfied below some temperature (T_{Do}) but not for temperatures above T_{Do}.

As the temperature is decreased, twinning may replace slip as the primary deformation mode[28]. Hull[28] has shown that k_Y for twinning is very much greater than k_Y for slip. Therefore σ_f is lower, and equation (1.7) can be satisfied at a higher temperature (i.e., T_{Do} is higher) when twinning is the primary mode of deformation.

Above T_{Do} fracture does not occur on yielding. However, cleavage may occur after work hardening ($\Delta\sigma$) raises the flow stress up to σ_f. Specifically, the fracture criteria becomes

$$\sigma_Y + \Delta\sigma = \sigma_f \tag{1.8}$$

If the σ-ε curve is approximated as shown in Figure 1.1, the necessary work hardening is related to the tensile ductility (ε_f) through the work hardening coefficient ($d\sigma/d\varepsilon$) by

$$\Delta\sigma = \varepsilon_f \frac{d\sigma}{d\varepsilon}$$

The fracture criterion above T_{Do} may be written

$$\sigma_Y + \frac{d\sigma}{d\varepsilon}\,\varepsilon_f = \sigma_f = \frac{2G\gamma_m}{k_Y}\,d^{-1/2} \tag{1.9}$$

or

$$\varepsilon_f = \frac{\sigma_f - \sigma_Y}{d\sigma/d\varepsilon} \tag{1.10}$$

Since σ_Y decreases with increasing temperature in B.C.C. metals, ε_f

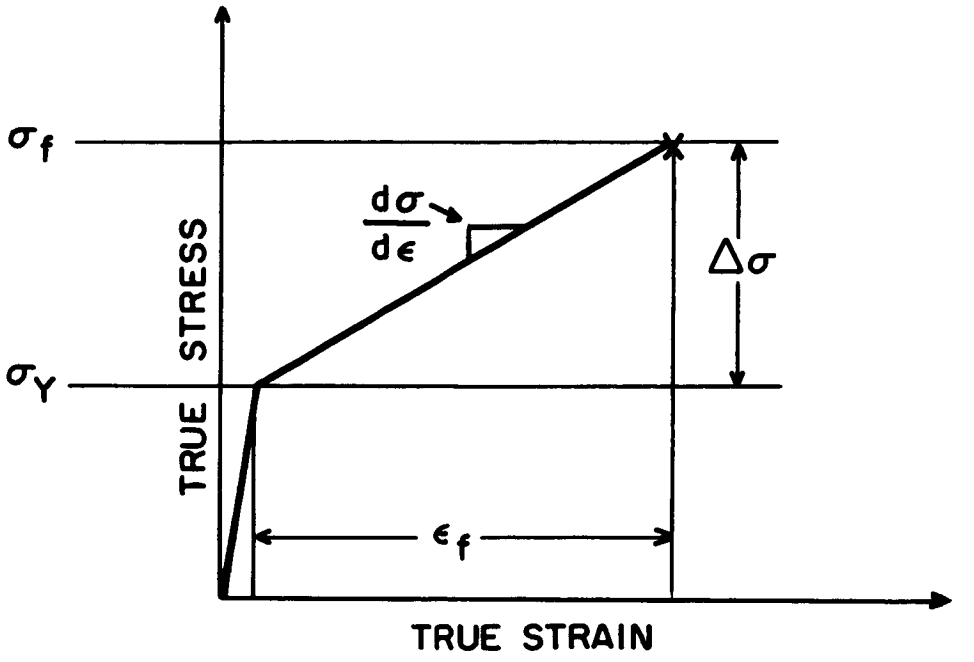

Figure 1.1 An idealized stress-strain curve relating the tensile ductility (ϵ_f) to the difference between the yield (σ_Y) and fracture stress (σ_f) and the strain hardening rate ($d\sigma/d\epsilon$).

increases with temperature at a rate determined by $d\sigma/d\epsilon$ and the temperature dependence of $\sigma_f - \sigma_Y$. It should be noted that σ_f may increase or decrease with temperature depending on the effects of temperature and plastic strain on σ_f [equation (1.3) or (1.6)]. In low carbon alloys, γ_m/k_Y [equation (1.6)] increases with temperature[16, 20, 29-31] so that σ_f increases with temperature. In materials containing large second phases, microcracks grow easily (low γ_m) to a grain boundary, and σ_f depends on equation (1.3). In these cases, strain may (1) reduce σ_f if microcracks are sharpened or grow in length or (2) raise σ_f if the cracks are blunted[32].

At some higher temperature (T_{So}), the strain (ϵ_f) required to reach σ_f is so high that the material fails by ductile tearing before equation (1.10) can be satisfied[8, 9]. That is

$$\epsilon_s < \epsilon_f \qquad T > T_{So} \tag{1.11}$$

where ϵ_s is the strain required for ductile failure.

1.2 The Effect of Notches or Other Macroscopic Discontinuities on the Ductile-to-Brittle Transition

It is common knowledge that notches, cracks, or other stress raisers "embrittle" normally ductile metals and increase the ductile-to-brittle transition temperature from T_{Do} to T_D. A notch modifies the local stresses and strains in its vicinity, but it cannot itself change the material's deformation or fracture properties. Consider the external notch shown in Figure 1.2 of depth c, tip radius ρ and flank angle ω in a thick tensile sample. Cottrell[33] has shown that the material at the

notch tip may be regarded as a "miniature tensile specimen" of gauge length 2ρ. Therefore, notch brittleness may be examined in terms of (1) the effect of the adjacent notch on the ductility of the "miniature specimen" and (2) the relationship between the ductility of the specimen and the structure's ductility.

Local yielding begins in the "miniature tensile specimen" when the nominal stress σ_N is raised by the elastic stress concentration factor K_σ to the material's yield stress ($\sigma_Y = 2k$, Tresca yield criterion)

$$\sigma_N = \sigma_{LY} = \frac{\sigma_Y}{K_\sigma} . \tag{1.12}$$

With further increases in applied stress, σ_Y is exceeded further away from the notch and the plastic zone extends. However, because the plastic region is surrounded by elastic material, the notched sample appears elastic until the plastic zones extend entirely across the section at the general yield stress

$$\sigma_{GY} = L\, \sigma_Y \tag{1.13}$$

where $L > 1$ is the constraint factor which depends on notch and specimen geometry.

A notch has an embrittling effect for primarily three reasons. The first two result because the notch reduces the tensile ductility of the "miniature specimen" below that given by equation (1.10).

(1) For a given applied loading rate, there is a <u>higher local strain rate $\dot{\epsilon}$</u> (strain concentration) at the notch tip. In B.C.C. metals, the yield stress increases with increasing strain rate[34-37] so that

the actual yield stress in the "miniature specimen" is $\sigma_Y^* > \sigma_Y$.

(2) Because a triaxial stress state is set up ahead of a notch by plastic constraint, the maximum local tensile stress (which does not exceed the yield criteria) is raised from σ_Y^* up to $K_{\sigma(p)}\ \sigma_Y^*$. The plastic stress concentration factor $K_{\sigma(p)}$ is a function of specimen and notch geometry and the amount of local strain at the notch tip[3, 38-44]. It increases from a value of unity at the onset of local yielding up to $K_{\sigma(p)}^{max} < 3$ (which also depends on notch geometry[38, 39]) at general yield.

(3) Due to strain concentration at the notch tip, the "miniature specimen" can deform plastically before failure while the notched sample is still nominally elastic. Moreover, regardless of how ductile the "miniature specimen" is, the notched bar will always be somewhat less so.

Figure 1.3 illustrates how the first two changes raise the nil-ductility temperature. The cleavage stress is assumed to vary only slightly with temperature while the yield stress increases quite rapidly with decreasing temperature. As a result there is the temperature T_{Do} below which smooth samples fail on yielding. In the notched sample, the maximum local stress developed prior to general yielding is raised by both (1) and (2) from σ_Y up to $K_{\sigma(p)}^{max} \cdot \sigma_Y^*$. Consequently, there is some higher temperature $T_D > T_{Do}$ below which $K_{\sigma(p)} \cdot \sigma_Y^* = \sigma_F$ is produced locally while $\sigma_F < \sigma_{GY}$.

The plastic strains developed at notches like that shown in Figure 1.2 are small prior to general yield so that the contribution of local strain hardening can be neglected. However, at temperatures above T_D, plastic constraint alone is not sufficient to raise the local tensile

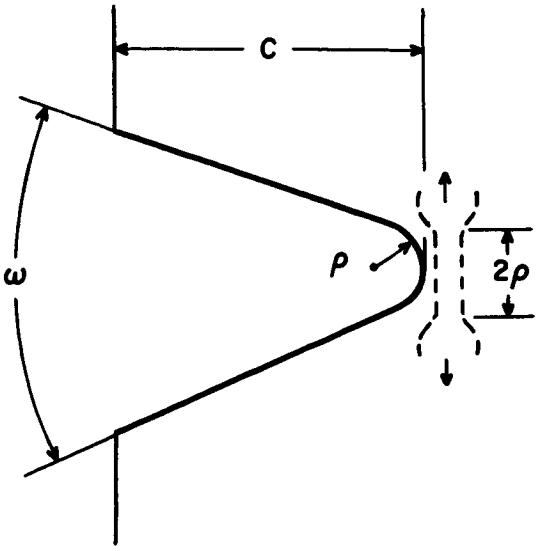

Figure 1.2 The hypothetical miniature tensile specimen below an external notch.

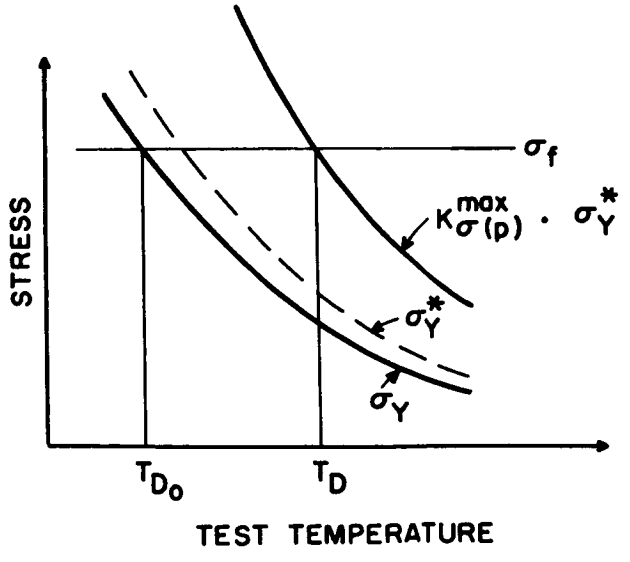

Figure 1.3 The effect of increased strain rate and a triaxial stress state on the nil-ductility temperature of a B.C.C. metal.

stresses in the plastic zone up to σ_f. General yielding and some strain hardening are required to reach σ_f. The fracture criteria becomes

$$K^{max}_{\sigma(p)} \left[\sigma^*_Y + \frac{d\sigma}{d\epsilon}\, \epsilon_F\right] = \sigma_f \tag{1.14}$$

Rewriting (1.14), the tensile ductility of the "miniature specimen" is

$$\epsilon_F = \frac{\sigma_f - K^{max}_{(p)}\, \sigma^*_Y}{K^{max}_{\sigma(p)}\, d\sigma/d\epsilon} \quad . \tag{1.15}$$

Equation (1.15) is similar in form to equation (1.10), but the notch reduces the rate at which ϵ_F increases with temperature

$$\frac{d\epsilon_F}{dT} = \frac{1}{K^{max}_{\sigma(p)}} \cdot \frac{d\epsilon_f}{dT} \qquad \frac{d\sigma^*_Y}{dT}\,,\ \frac{d\sigma}{d\epsilon} = \text{const.}$$

The critical notch root displacement to obtain ϵ_F is a measure of the apparent ductility of the notched sample. It is given by

$$2V^*(c) = \beta(2\rho)\ \epsilon_F$$

or

$$V^*(c) = \beta\rho \left[\frac{\sigma_f - K^{max}_{\sigma(p)}\, \sigma^*_Y}{K^{max}_{\sigma(p)}\, d\sigma/d\epsilon}\right] \tag{1.16}$$

where 2ρ is the gauge length of the "miniature specimen" and β is a geometrical factor, proportional to ρ, which relates the strain at the notch tip to the strain at the point of maximum stress. Equation (1.16) indicates that even when the section is fully plastic, the notch reduces the effective ductility through strain concentration (small ρ) as well as plastic constraint ($K^{max}_{\sigma(p)}$) and increased strain rate (σ^*_Y).

1.3 Notch Toughness

For a notch of a given depth, cleavage fracture initiates below the root at a critical notch displacement V*(c) where

$$\sigma^{max} = K_{\sigma(p)} \cdot \sigma_Y^* = \sigma_f \qquad K_{\sigma(p)} = f(V(c))$$

is produced locally. Bilby et al[45] have shown that these considerations lead to a form of the Griffith - Orowan[3] and Irwin[46] relations for fracture [analogous to equation (1.2)]

$$\sigma_F = \sqrt{\frac{E\,G_c}{\pi c(1-\nu^2)}} \qquad \sigma_F \ll \sigma_{GY} \tag{1.17}$$

where

$$G_c \cong 2\sigma_{GY}\, V^*(c) \tag{1.18}$$

is the notch toughness. Physically, G_c represents the work done in initiating and propagating a unit area of fracture in a given notched sample. For the limiting case of a sharp crack under plane strain conditions, $G_c = G_{Ic}$ the material's plane strain fracture toughness. Notch toughness is therefore a measure of a material's resistance to brittle fracture in the presence of a particular notch and under specified test conditions (temperature, $\dot{\epsilon}$). That notch which produces the most strain concentration, $\dot{\epsilon}$ increase, and plastic constraint will yield the lowest G_c and consequently the lowest σ_F at low temperatures where equation (1.17) is obeyed. When failure occurs near or above P_{GY} (i.e., at higher temperatures), equation (1.17) is no longer applicable[42]. However, the notch toughness is still given by equation (1.18). Comparing equations (1.16) and (1.18) shows that any change in the notch

geometry which lowers the (1) strain concentration, (2) effective $\dot{\epsilon}$ (σ_Y^*), or (3) triaxiality ($K_{\sigma(p)}^{max}$) of the notch will increase G_c.

Toughness Evaluation - The Instrumented Charpy Test

A variety of laboratory tests have been developed to evaluate a material's toughness under different service conditions ($\dot{\epsilon}$, temperature, notches). Some of these tests emphasize initiation of cleavage while others, the stopping of a fast running cleavage crack. Because the specimen geometry and loading rate differ, these tests yield the notch toughness under different conditions.

The most common laboratory test for toughness is the Charpy V-notch impact test. A small rectangular bar of square cross section (10 mm x 10 mm) containing a notch is broken in three-point bending by means of a pendulum dropped from known height. The energy absorbed in deformation and fracture at a particular test temperature is determined from the height to which the pendulum rises after impact. Recently the pendulum striker has been instrumented by various authors[47-52] to measure directly the applied load on the sample during impact, and this has permitted a much more meaningful interpretation of the toughness measurements. An idealized load-time trace is shown in Figure 1.4 with the various stages of deformation labeled.

The physical significance of the various portions of these traces has been discussed by Biggs[53] and Fearnehough and Hoy[52]. On initial impact, the specimen deforms elastically with increasing load. At small loads, still within the nominally elastic portion of the curve, plastic deformation occurs at the notch tip and extends with increasing load.

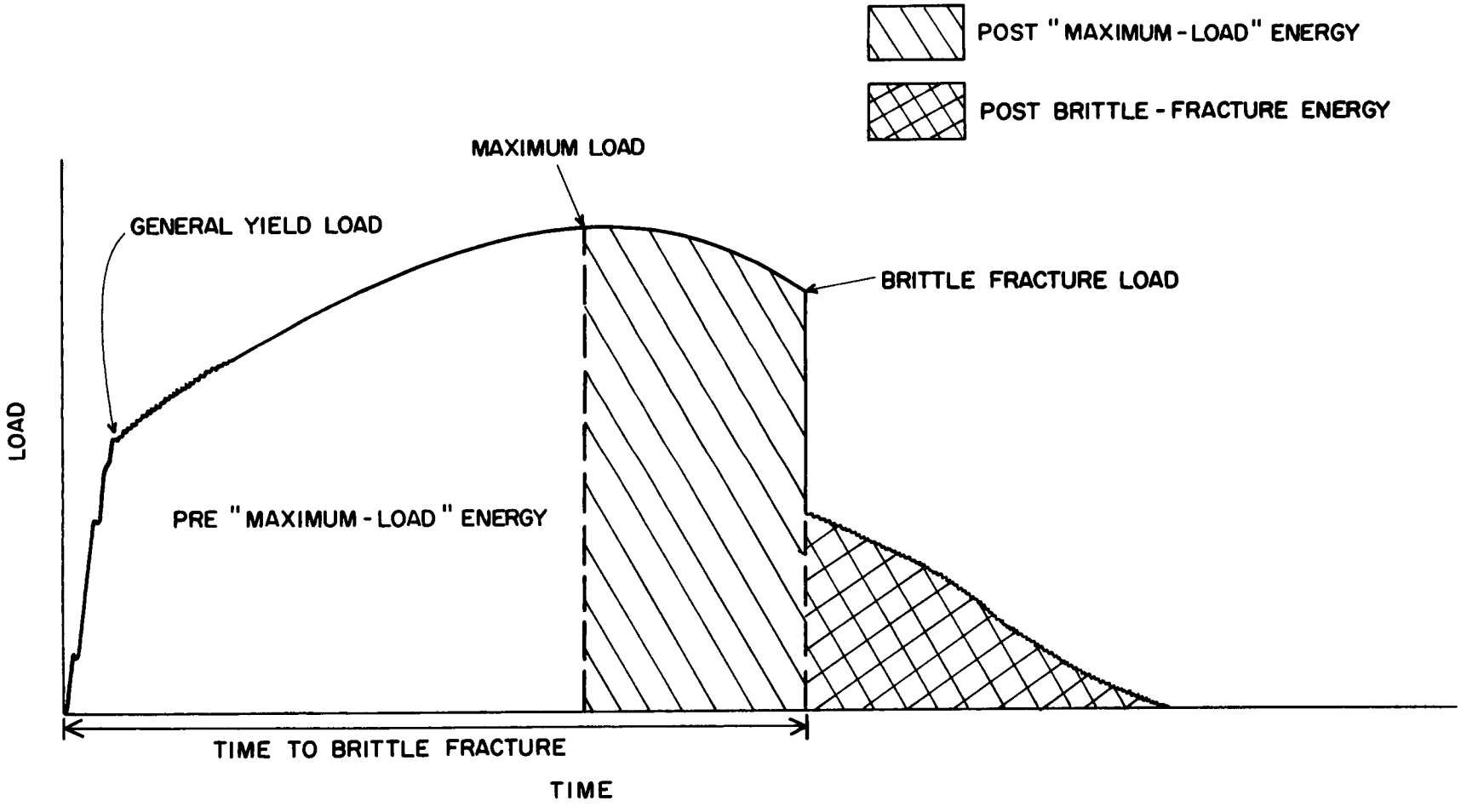

Figure 1.4 An idealized load-time trace for an impacted Charpy V-notch sample.

Several small jogs in the load occur at about the same time in all curves. These jogs are caused by reflected stress waves within the striker itself and do not result from nor affect the deformation markedly.

Eventually, a load is reached at which the plastic zones extend across the entire section, and general yielding occurs. In some alloys, there may be an instability associated with general yield[52, 54] which results in an upper and lower yield point. However, in materials where this instability is quite small, general yield is characterized only by a change in slope of the load-time trace. The bar now deforms continuously around the plastic "hinges" with a less rapid increase in the applied load. A maximum load, P_{ULT}, is reached beyond which the load decreases gradually to zero if brittle fracture does not intervene.

Brittle fracture, resulting in a sudden drop in load, may occur in any one of the three regions; that is, nominally elastic prior to P_{GY}, plastic prior to P_{ULT}, or plastic after P_{ULT}. If brittle fracture occurs prior to P_{GY} or soon after it, a brittle crack has been nucleated directly, in the high stress region below the root. On the other hand, Lubahn[55] has shown that in mild steel a fibrous tear is formed at the notch root midway through the thickness prior to ultimate load. This tear spreads laterally with increasing load, extends across the entire thickness at maximum load, and then advances with decreasing load. Thus, if brittle fracture occurs near or after P_{ULT}, it has nucleated from a fibrous tear which has sharpened the "effective notch". Moreover, when cleavage is initiated after maximum load, the fracture load has little physical significance since instability has already occurred.

The "post-brittle" energy region (Figure 1.4) results from the

deformation of (1) shear lips along the specimen sides and (2) material along the compression side ahead of the arrested brittle crack. The magnitude of this energy will vary with temperature and material[52, 53] and may be present regardless of whether the brittle crack initiates directly or forms from a fibrous tear.

The total impact energy measured on the machine is simply the sum of the work done in deformation and fracture of the Charpy sample plus the small kinetic energy transferred to the pieces of the fractured sample. The impact energy (E_a) is approximately the total area under the load-time curve times the initial hammer velocity. Since the hammer is deaccelerating constantly during the test, the actual energy will be lower than calculated in this manner. Augland[49] has shown that the actual energy E may be obtained from the uncorrected one, E_a, by the formula

$$E = E_a - \frac{E_a^2}{4E_o} \tag{1.19}$$

where E_o is the initial hammer energy (240 ft.lb. in this case). The corrected energy E agrees within 10% with that measured directly on the machine[52]. In the same way, the specimen deflection $\delta(t)$ at any time t is given

$$\delta(t) = V_o t \left(1 - \frac{E_a(t)}{960}\right) \tag{1.20}$$

where V_o = the initial hammer velocity (17 ft./sec.) and $E_a(t)$ is the uncorrected energy at time t.

Instrumentation of the Charpy striker thus allows extensive and meaningful information to be obtained from the simple Charpy test.

1.4 Deformation and Fracture of Notched Bars in Bending

Detailed experimental studies of notched bars in bending have been performed by Green and Hundy[39], Crussard et.al.[56], Knott[57], Fearnehough and Hoy[52], and Wilshaw[54]. These studies have shown that the notch strength and toughness of polycrystalline mild steel varies with temperature as shown in Figure 1.5. Tetelman and McEvily[58] have pointed out that four temperature regions (corresponding to ranges in material's fracture toughness) may be identified. Within each region, failure is associated with another stage in the development of the elastic - plastic, stress - strain state of the bar.

1.4-1 Region 1 - Cleavage on Local Yielding

At very low temperatures $\sigma_Y^* \geq \sigma_f$, and cleavage occurs on local yielding. The nominal stress to cause both is

$$\sigma_F = \sigma_N = \frac{\sigma_Y^*}{K_\sigma} \tag{1.21}$$

where $\sigma_N = \frac{Mc}{I}$ from the familiar beam formula. Since actually plastic deformation must extend over at least one grain to produce a micro-crack[41], K_σ in (1.21) is approximately the elastic stress concentration factor at the first grain boundary. In this range, the notch strength increases with decreasing temperature ($\sigma_Y^* \uparrow$) and is inversely proportional to K_σ.

1.4-2 Region 2 - Cleavage due to Plastic Constraint

Because σ_Y^* decreases with increasing temperature and σ_f remains about constant, yielding in the first grain at the notch can no

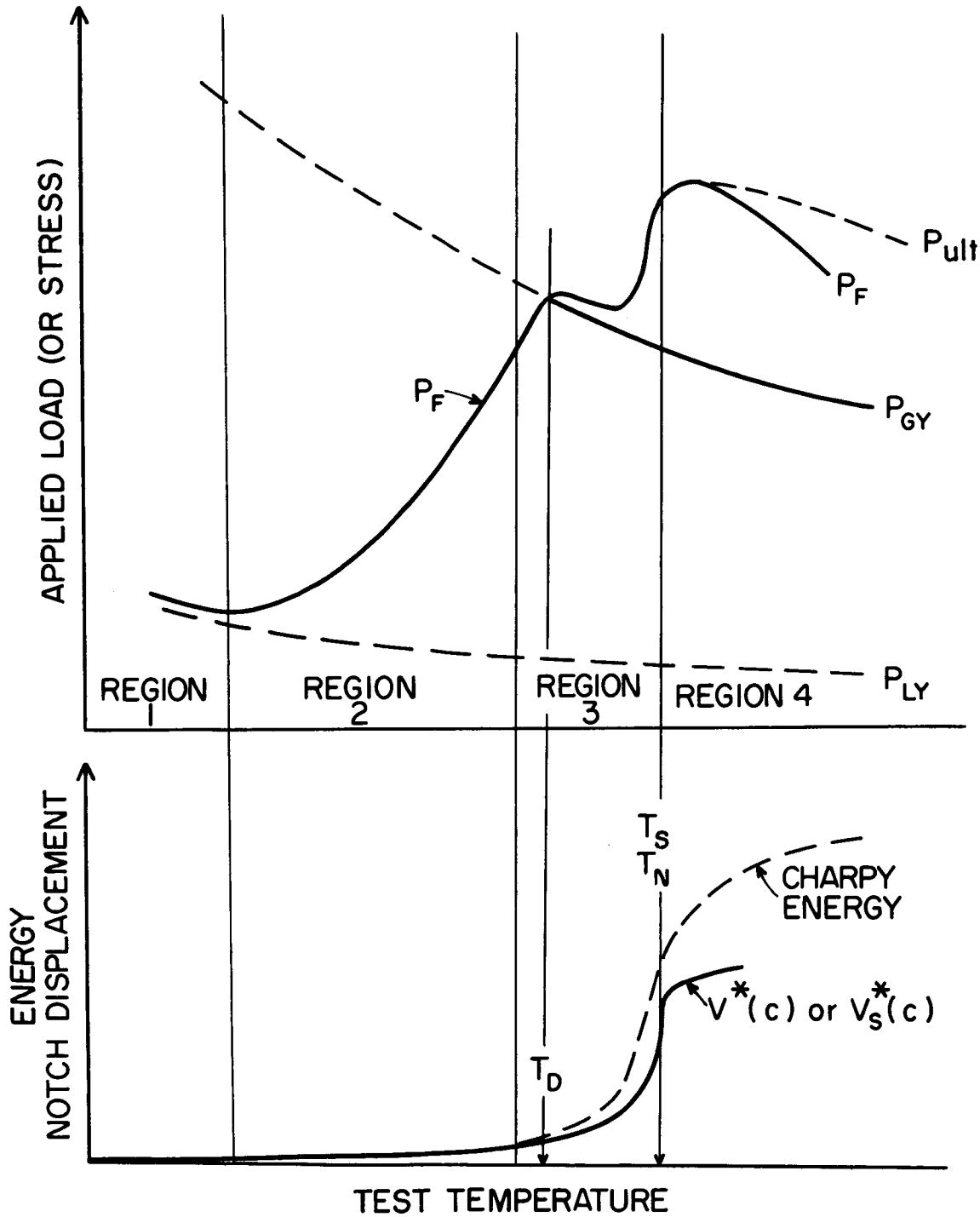

Figure 1.5 The nominal fracture strength and energy absorbed by notched bars of mild steel tested at various temperatures.

longer produce cleavage ($\sigma_Y^* < \sigma_f$). Some additional plastic deformation is required to produce plastic constraint (triaxiality, $K_{\sigma(p)}$) and raise the maximum local stress from σ_Y^* to $K_{\sigma(p)}\sigma_Y^*$. The crtieria for fracture of the "miniature specimen" is then

$$\sigma^{max} = K_{\sigma(p)}\sigma_Y^* = \sigma_f \tag{1.22}$$

where

$$K_{\sigma(p)} = f(V(c)) \quad = f'(\sigma_N/\sigma_Y^*)$$

With increasing temperature, the required $K_{\sigma(p)}$ increases (due to lower σ_Y^*), and the critical displacement and applied fracture load also increase.

In a non-strain hardening material deforming in plane strain, Hill[38] has shown that $K_{\sigma(p)}$ increases with the plastic zone size (R) relative to the root radius (ρ)

$$K_{\sigma(p)} = [1 + \ell n\ (1 + R/\rho)]\ . \tag{1.23}$$

The maximum possible value of $K_{\sigma(p)}$ is defined by the notch geometry[38,39]

$$K_{\sigma(p)}^{max} = 1 + \frac{\pi}{2} - \frac{\omega}{2} \tag{1.24}$$

but depends only on the notch flank angle ω (Figure 1.2). The rate at which R (and $K_{\sigma(p)}$) increases with applied load does, however, depend on the other aspects of the notch and specimen geometry. Recently, Wilshaw, Rau, and Tetelman[59] have developed a model to predict this relationship for an arbitrary notch and specimen geometry in plane strain bending. Their predictions agree well with experimental observations of yield zones and fracture behavior. Wilshaw and Pratt[60] have experimentally

measured R as a function of applied load in mild steel Charpy samples; and using equation (1.23), related $K_{\sigma(p)}$ to applied load (σ_N/σ_{GY}). These results indicate that in the Charpy sample, $K_{\sigma(p)}$ increases with applied load until $\sigma_N/\sigma_{GY} = 0.8$ whereupon $K^{max}_{\sigma(p)}$ is reached. Combining equations (1.23) and (1.24), yields the plastic zone size R_β at which $K^{max}_{\sigma(p)}$ is achieved

$$R_\beta = \rho \quad \exp\ (K^{max}_{\sigma(p)} - 1) - 1 \tag{1.25}$$

With further increases in applied load, the plastic zone may extend, but there is no additional increase in triaxiality.

1.4-3 Region 3 - Cleavage due to Plastic Constraint and Work Hardening

As the temperature is increased still further, the required $\sigma^{max} = \sigma_f$ cannot be achieved by constraint alone (i.e., $K^{max}_{\sigma(p)} \cdot \sigma^*_Y < \sigma_f$ for $\sigma_N/\sigma_{GY} > 0.8$). Some strain hardening $\Delta\sigma$ is required in addition to constraint to produce σ_f locally at R_β.

$$K^{max}_{\sigma(p)} \ (\sigma^*_Y + \Delta\sigma) = \sigma_f$$

The critical displacement required to produce this $\Delta\sigma$ is given by equation (1.16)

$$V^*(c) = \beta\rho\epsilon_F = \beta\rho \left[\frac{\sigma_f - K^{max}_{\sigma(p)} \ \sigma^*_Y}{K^{max}_{\sigma(p)} \ d\sigma/d\epsilon} \right] \tag{1.16}$$

Because elastic material surrounds the plastic zone prior to σ_{GY}, the plastic strain ϵ_F remains small; and the applied load required to produce $V^*(c)$ increases rapidly with temperature up to T_D.

At T_D, the plastic "hinges or arcs" traverse the entire sample[39, 61-63] ($\sigma_N = \sigma_{GY}$, $P = P_{GY}$) before V*(c) is reached. Green and Hundy[39] have calculated the theoretical relationship (assuming an ideal plastic material and plane strain conditions) between the uniaxial yield stress and the applied moment to cause general yielding. For the Charpy V-notch sample loaded in three-point bending, the general yield load is

$$P_{GY}(\text{lb.}) = 0.030\ \sigma_Y^* \ (\text{psi}) \tag{1.26}$$

where $\sigma_Y^* = 2k$ for the Tresca or $\sqrt{3}\ k$ for Von Mises' yield criterion.

After general yielding, the applied load to produce V*(c) continues to increase but much less rapidly than prior to σ_{GY}[52, 54]. The rate at which σ_F/σ_{GY} increases with temperature depends on (1) how rapidly the toughness [V*(c)] increases with temperature [i.e., $d\sigma_Y^*/dT$, $d\sigma/d\varepsilon$, $d\sigma_f/d\varepsilon$, $\rho(V(c))$] and (2) how rapidly the notch displacement [V(c)] increases with applied load [$d\sigma/d\varepsilon$]. Both (1) and (2) will vary with the material's microstructure, and the overall effect of increased carbide content is to reduce $d(\sigma_F/\sigma_{GY})/dT$ and spread out the transition region[64, 65]. The total Charpy energy also increases with V*(c) but somewhat more rapidly since it also includes the energy to propagate fracture in the plane stress regions near the free surfaces.

At some higher temperature, the ductility transition T_N, there is a sharp rise in toughness [V*(c)] and the corresponding applied load. This behavior results from a change in the stress state which reduces $K^{max}_{\sigma(p)}$ in equation (1.16). Specifically, Knott[66] and Sakui et.al.[67] have observed that T_N is extremely sensitive to specimen thickness. This indicates that plastic deformation occurs through the thickness

at some $\left[V^{RLX}(c)\right]$ and relaxes the triaxial stress state. Wilshaw[54] has noted in Charpy samples that T_N is coincident with formation of plastic "wings" between the plastic "hinges" and the notched surface. This plane strain type deformation may also cause a reduction in $K^{max}_{\sigma(p)}$ or simply be coincident with relaxation through the thickness. The relative importance of each has not yet been defined.

1.4-4 Region 4 - Fibrous Initiation of Failure

In low carbon irons where the ductile failure strain is very high, cleavage can be initiated directly at temperatures above T_N at a much larger V*(c). However, at some higher temperature, the initiation transition T_S, V*(c) is so large that the ductile tearing strain ϵ_S [equation (1.11)] is exceeded at the notch root before V*(c) can be obtained[41, 56], i.e.

$$V^*(c) > V^*_S(c) = \rho\epsilon_S \tag{1.27}$$

where $2V^*_S(c)$ is the critical notch displacement necessary to produce ϵ_S.

In mild steel and most structural materials, ϵ_S is much smaller due to the larger number second phase particles. The sharp increase of V*(c) at T_N is usually sufficient to satisfy equation (1.27) and cause fibrous initiation. As a result $T_N = T_S$, and the ductility and initiation transitions are coincident. In some high strength materials where ϵ_S is very low, equation (1.27) may be satisfied prior to $V^{RLX}(c)$ ($T_S < T_N$); and there is no sharp increase in toughness prior to or accompanying fibrous initiation.

As stable fibrous tearing occurs, the effective notch deepens

and sharpens, especially if it links up with stable microcracks[54]. Consequently, the strain concentration, effective $\dot{\epsilon}$, and $K^{max}_{\sigma(p)}$ all increase to the point where unstable cleavage can be initiated from the tear[68]. The amount of fibrous tearing and sharpening which is required to produce cleavage increases with temperature until at $T > T_p$ failure is 100% fibrous. The total energy absorbed increases with temperature until failure is 100% fibrous after which it is nearly constant.

1.5 The Effect of Deformation Rate

In B.C.C. metals, these four temperature (σ_f/σ^*_Y) regions are observed in Charpy type samples over a wide range of applied loading rates[52, 69]. There are, however, three effects of increased loading rate (i.e., from slow-bend to Charpy impact) which affect the form of Figure 1.5. (1) Because the cleavage stress remains nearly constant while the yield stress increases with increasing loading rate ($\dot{\epsilon}$), the transition region is shifted to higher temperatures (analogous to Figure 1.3). (2) Because the transition region occurs at a higher temperature and the temperature dependence of the yield stress decreases with increasing temperature, region 2 is extended over a wider temperature range (i.e., a given change in σ_f/σ^*_Y requires a larger change in temperature). (3) Because the rate of strain hardening decreases with increasing strain rate[36], V*(c) [equation (1.16)] increases more rapidly with increasing temperature (σ_f/σ^*_Y) and this tends to reduce the difference between T_D and T_N and constrict region 3.

1.6 Variation in Notch and Specimen Geometry

1.6-1 Notch Root Radius (ρ)

It is well known that the notch toughness decreases with decreasing root radius (sharper notches). More specifically, lower toughness is observed in each of the four regions previously described. In region 1, this results because the elastic stress concentration factor, K_σ [equation (1.21)], increases with decreasing ρ[70]. Moreover, the elastic solutions are known for simple notch configurations[70] so that accurate predictions of the nominal fracture strength can be made.

In regions 2 and 3, toughness also decreases with decreasing ρ because (1) the local strain rate increases (for a given loading rate) and σ_Y^* is correspondingly larger in equations (1.22) and (1.16) and (2) triaxiality ($K_{\sigma(p)}$) increases more rapidly with applied load[59]. Both these effects reduce the nominal fracture strength and toughness [$V^*(c)$] at a given temperature and thereby shift regions 2 and 3 to higher temperatures. In region 4, smaller ρ causes reduced notch-toughness since the fibrous tearing strain (ε_s) can be produced by a smaller notch displacement [$V^*(c)$ in equation (1.27)].

Since the plastic deformation processes which nucleate cleavage require a minimum volume (determined by some microstructural feature such as grain size, particle spacing, etc.) to operate, toughness does not decrease indefinitely with decreasing ρ. Various authors have observed[41, 43, 71] that for $\rho < \rho_{min}$, notch toughness is independent of ρ and behaves as if $\rho = \rho_{min}$. In region 4, there is also a $\rho_{min,s}$ below which fibrous tearing at the notch root occurs at the same $V_s^*(c) = \rho_{min,s}\ \varepsilon_s$[72].

1.6-2 Notch Flank Angle (ω)

Notch toughness also decreases with decreasing ω, at least in regions 1 and 2. Neuber[70] has shown that the elastic stress concentration factor (K_σ) increases with decreasing ω thereby reducing σ_F [equation (1.21)] in region 1. Because the maximum triaxiality, $K^{max}_{\sigma(p)}$ [equation (1.24)] increases with decreasing ω, region 2 is extended to higher temperatures and T_D is increased[66]. Although no experimental studies have reported results above general yield, the larger $K^{max}_{\sigma(p)}$ should also reduce the critical notch displacement [V*(c) in equation (1.16)] which is required for cleavage in region 3. This would, in turn, extend region 3 to higher temperatures.

1.6-3 Specimen Thickness (t)

Little is known about the effect of thickness on notch toughness in regions 1 and 2 where deviations from plane strain conditions might reduce $K_{\sigma(p)}$. On the other hand, various authors[66, 67, 73] have observed that the nil-ductility temperature (T_D, where $\sigma_N = \sigma_{GY}$) decreases gradually with decreasing thickness between 0.5 and 0.1". Knott[66] observed no significant change in the general yield load with thickness and concluded that the lower T_D results from a lower $K^{max}_{\sigma(p)}$ in thinner samples.

In going from samples of t = 0.3" to t = 0.2", a sharp decrease in the initiation transition temperature (T_S) was observed while for t > 0.3", T_S was independent of thickness[66]. This sharp transition has been attributed[66] to an increase in the material's intrinsic σ_f with plastic strain as the required amount of local work hardening increases. However, this explanation is not consistent with the effect

of reduced thickness. Additional explanations have been discussed[74], but a more realistic model which incorporates relaxation of triaxiality has not yet been developed.

There may also be metallurgical differences between thin and thick bars (or plates) due to different cooling rates[75]. Since these changes can also produce considerable changes in notch-toughness in addition to those associated with the mechanics of deformation, care must be taken in interpreting the toughness of different thickness samples.

1.6-4 Notch Depth (c) and Specimen Size (a+c=d)

In the past there has been much controversy and misunderstanding regarding the "size effect" (reduced notch-toughness of larger samples). In most cases, the confusion has resulted from a lack of appreciation of the important variables. For instance, the elastic stress concentration factor (K_σ) increases with (1) $\sqrt{c/\rho}$ for shallow notches ($c \ll a$) and (2) $\sqrt{a/\rho}$ for deep notches ($a \ll c$). For most specimens used in toughness testing, K_σ is a complex function of both $\sqrt{c/\rho}$ and $\sqrt{a/\rho}$[70]. Neuber[70] has derived a geometrical averaging technique for the general case which allows accurate prediction of K_σ and therefore notch-toughness in region 1. In region 2, a recently developed model[59] predicts that notch-toughness depends on K_σ in a more complex but qualitatively similar way.

In many experimental studies of size effect, the ratio c/a has been maintained constant while both c and a were increased. When ρ was also kept constant, K_σ increased due to the larger $\sqrt{c/\rho}$ and $\sqrt{a/\rho}$, and reduced toughness was observed. However, in geometrically similar

samples where ρ is also scaled up no difference in deformation mechanics or toughness are predicted for region 1[70] or region 2[59]. In general, it is the ratios $\sqrt{c/\rho}$ and $\sqrt{a/\rho}$ which control K_σ and indirectly the notch-toughness in regions 1 and 2. Consequently, increasing notch depth (c) at constant ρ and d (decreasing a) may either increase (for $c/d < .3$) or decrease (for $c/d > .3$) K_σ[70] and thus notch-toughness[59].

There are several exceptions to the previous conclusions which may produce an apparent size effect in geometrically similar samples. First, if $\rho < \rho_{min}$ in the smaller or both sizes, K_σ will differ because $\sqrt{c/\rho_{min}}$ and $\sqrt{a/\rho_{min}}$ differ. Second, since the effective K_σ or $K_{\sigma(p)}$ is the minimum value over at least one grain, a larger sample with the same grain size has an effective K_σ or $K_{\sigma(p)}$ which is closer to the predicted value[76]. Third, by similar argument, a given microstructure contains a statistical distribution of fracture nucleation sites[77], and a larger sample has a higher probability of containing a favorably oriented site in the maximum stress region[76]. Finally, as in thicker samples, there may be metallurgical differences (due to different cooling rates) which reduce the notch-toughness of larger samples. All of these effects may lead to apparent size effects in addition to that resulting from increases in $\sqrt{c/\rho}$ and $\sqrt{a/\rho}$.

1.7 Plan of the Investigation

It has been shown that a notch or crack embrittles normally ductile metals for primarily three reasons. First, the triaxial tensile stresses ahead of the notch raise the effective yield stress. Second, the increased strain rate at the notch tip (for a given loading rate)

raises the yield stress in most B.C.C. metals. Third, strain concentration at the notch tips produces high local strains at low nominal displacements.

If, then, notch toughness of a structure is to be improved there must be a reduction in the plastic constraint, the effective strain rate, or the strain concentration of a notch. This is possible in anisotropic materials[78] such as fiber composites[79, 80] or wrought alloys[81, 82]. In these cases, the transverse tensile stresses are able to crack relatively weak interfaces which are perpendicular to the maximum stress, thereby relaxing the triaxial stress state and increasing the notch toughness. Similarly, in extruded AgCℓ compacts containing dispersed particles of $Aℓ_2O_3$, the particle-matrix interface separation results in a reduction of constraint and an impact transition temperature some 70°C below that of pure AgCℓ[83].

The present study was undertaken to determine whether small, mechanically-drilled holes could similarly improve notch toughness. Because of its convenience and widespread use, the Charpy V-notch specimen was chosen for the majority of toughness evaluations. The relevant geometrical parameters which define the optimum improvement in toughness were first determined. A photoelastic stress analysis and dislocation etch-pitting studies were performed to evaluate the effect of two holes on the distribution of stress and strain around the notch.

Impact-bend, slow-bend, and tension tests were performed on mild steels at various temperatures to evaluate the improvements in load carrying capacity and notch ductility obtained through hole drilling. The study was then extended to more complex notches, arrays of holes,

and variable thickness specimens.

Although a general geometric effect, the magnitude of improvement with hole drilling depended on the microstructure of the material. Impact bend transition studies on a series of hypoeutectoid steels and selected other materials served to define the important microstructural features.

CHAPTER II

EXPERIMENTAL METHODS AND MATERIALS

2.1 Materials

Experiments to define the important geometrical parameters which locate the holes relative to the notch tip were performed on two mild steels (0.025 and 0.24, Table 2.1). Steel 0.025 was a low carbon iron containing carbides in 5 - 10% of the grain boundary area (Fig. 2.1). This alloy was chosen because it has a very sharp ductile to brittle transition at a well defined temperature. It was therefore possible to use changes in this transition temperature as a measure of changes in notch toughness. The second steel 0.24 was a commercial mild steel consisting of 25% by volume pearlite colonies and some semi-continuous carbides (see Fig. 2.2) at the ferrite grain boundaries. Extensive fracture experiments to determine improvements in load carrying capacity with two holes and other more complex geometries were also performed on these two materials. In both cases, the material was used in the hot worked conditions except where specified otherwise. Certain critical experiments were repeated using other steels listed in Table 1.

Hahn[84], Tetelman[85], and Griffiths[86] have used dislocation etch-pitting[87] in Fe - 3% Si to reveal both microscopic and macroscopic plastic deformation around cracks and notches. Because of their high sensitivity to small plastic strains, Fe - Si alloys were used to directly observe the effect of drilled holes on the distribution of plastic strain around a notch. Fracture experiments on this single phase material were useful since the transition from shear to cleavage

Table 2.1

Composition of the alloys used in this study

Alloy Designation	All figures are percent by weight						$d(10^{-3}$ in.)
	C	Mn	Si	Ni	P	S	
0.025	0.025	0.22	0.24	2.14	0.002	0.006	1.1
0.24	0.24	0.47	0.031	-	0.007	-	0.8
0.020	0.020	0.26	0.23	2.08	0.010	0.004	2.4
0.10	0.092	0.21	0.15	3.52	0.006	0.005	0.67
0.11	0.096	0.22	0.15	2.02	0.004	0.005	0.74
0.20	0.20	0.30	0.062	0.041	0.010	-	1.2
0.40	0.406	0.01	-	-	-	-	1.1
0.41	0.401	1.50	-	-	-	0.060	
0.57	0.572	-	-	-	-	-	
0.72	0.726	-	-	-	-	-	
18-8	0.015	-	0.025	18.87	0.002	0.008	
	(7.89 Co, 4.90 Mo, 0.31 Ti, 0.11 Aℓ)						
Fe-Si 1	0.007	-	3.25	-	-	-	20
Fe-Si 2	0.010	-	3.25	-	-	-	21

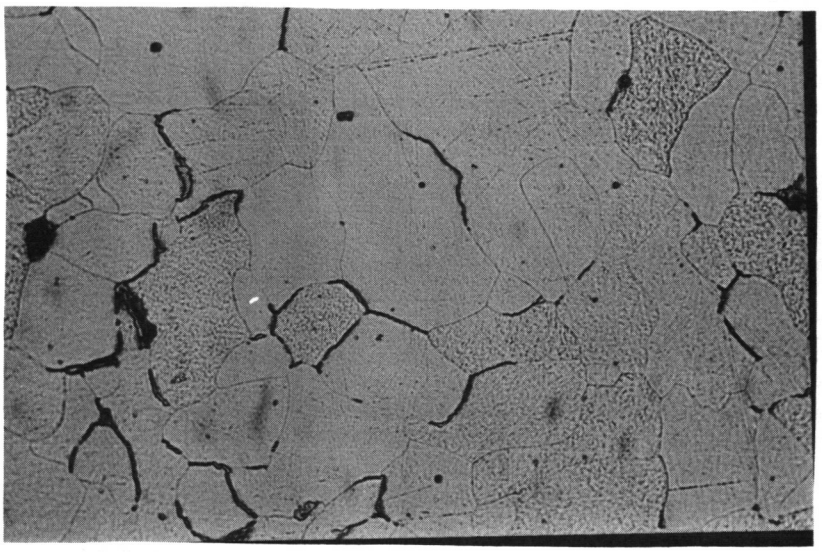

Figure 2.1 Microstructure of steel 0.025; etched 4% nitol, magnification = 556X.

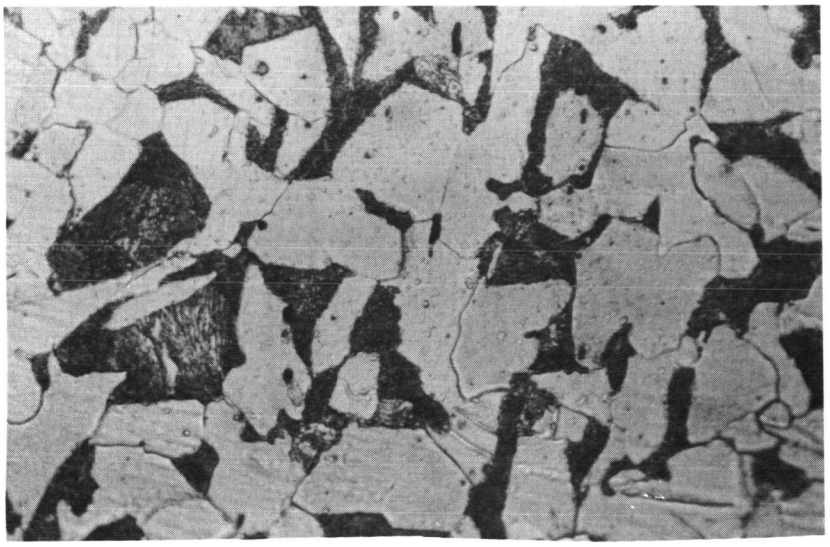

Figure 2.2 Microstructure of steel 0.24; etched 4% nitol, magnification = 556X.

fracture is not complicated by brittle carbides and fibrous crack nucleation. Two heats of Fe-Si (Fe-Si 1, Fe-Si 2, Table 2.1) were warm rolled to approximately 0.50 inch plate. After specimen preparation, annealing was performed at $875^{o}/900^{o}C$ in vacuum to obtain equiaxed ferrite grains.

In order to evaluate the generality of the improvements observed in the two steels and, more specifically, to determine the effects of microstructure on the improvement from hole drilling, a series of hypoeutectoid steels (0.020, 0.10, 0.20, 0.40, 0.41, 0.57, 0.72, Table 2.1) were studied for a specific hole geometry. These steels were hot worked to 0.50" plate (courtesy of Jones & Laughlin Steel Corporation) and consisted of equiaxed colonies of fine pearlite in a ferrite matrix. There were massive carbides at ferrite grain boundaries in some alloys and these carbides tended to be aligned parallel to the rolling direction. Figures 2.3 - 2.9 show the microstructures of these alloys.

Some tests were performed on an 18 Ni - 8 Co maraging steel (250 ksi yield strength) to examine the toughness improvements that are possible in high strength materials that fail by low energy tearing.

2.2 Specimen Preparation

The Charpy V notch impact specimen was selected for toughness measurement because it is the most widely used fracture test and the mechanics of its deformation are well established. The specimen is a rectangular prismatic bar 10 mm x 10 mm x 55 mm containing a 2 mm deep notch in the center of one side (Fig. 2.10a). Charpy specimens were prepared to ASTM specifications by surface grinding all surfaces prior to milling the V-notch with a specially prepared cutter. All specimens were

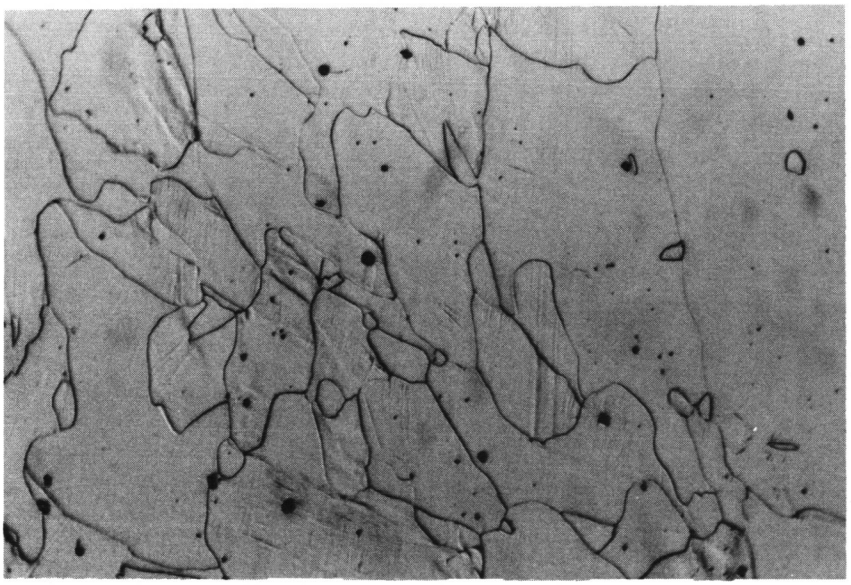

Figure 2.3 Microstructure of steel 0.010; etched 4% nitol, magnification= 226X.

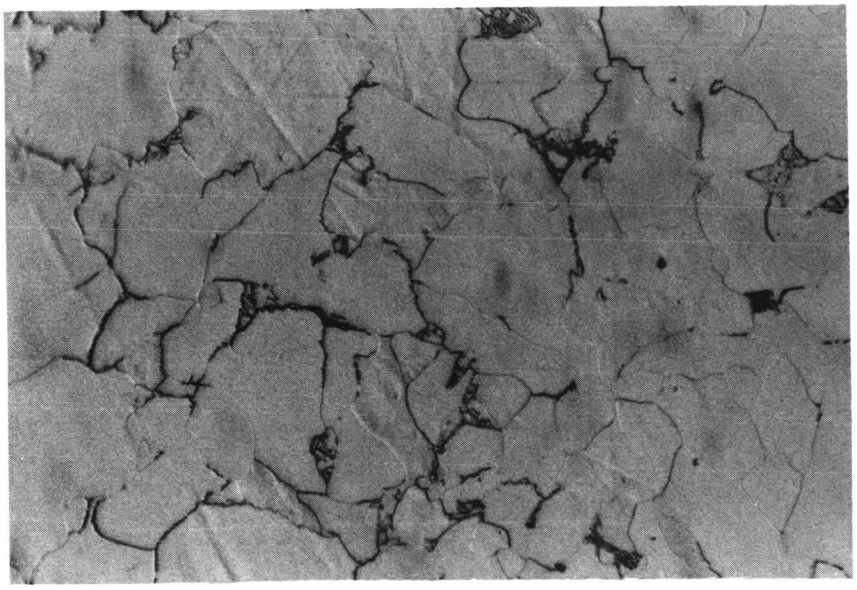

Figure 2.4 Microstructure of steel 0.10; etched 4% nitol, magnification = 556X.

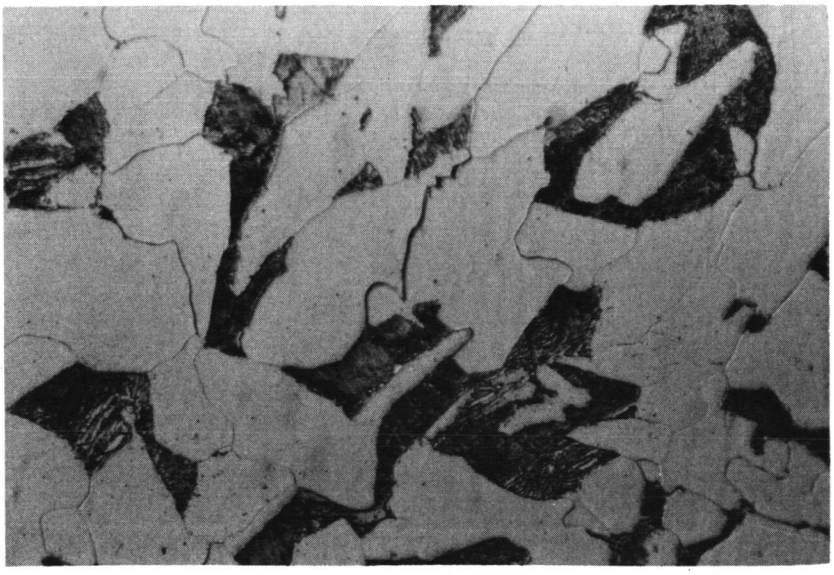

Figure 2.5 Microstructure of steel 0.20; etched 4% nitol, magnification = 556X.

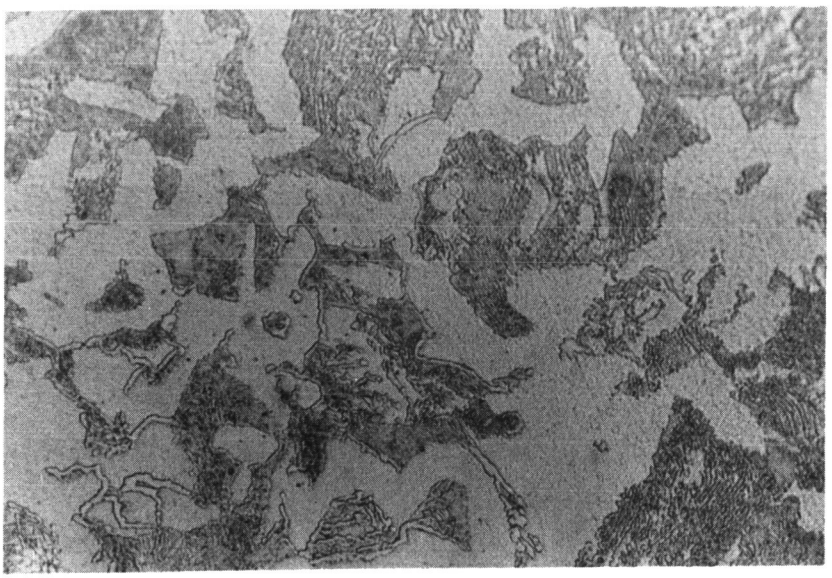

Figure 2.6 Microstructure of steel 0.40; etched 4% nitol, magnification = 556X.

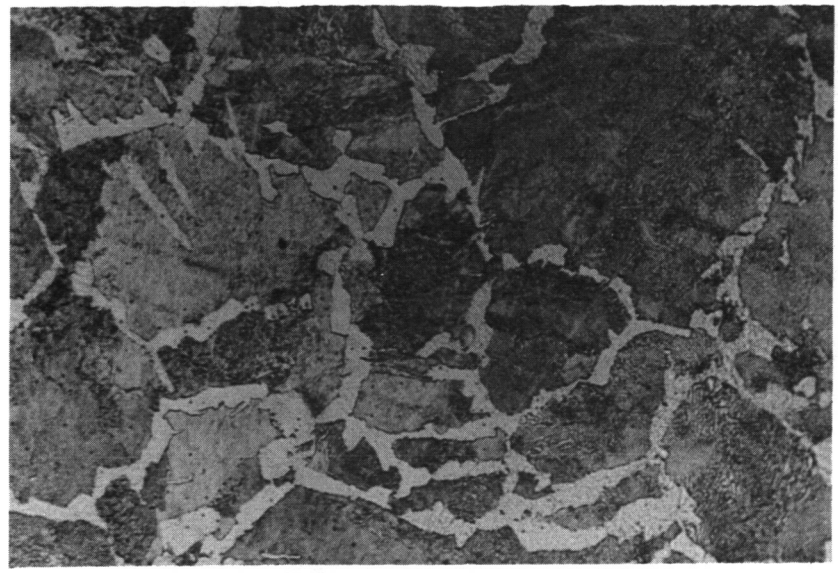

Figure 2.7 Microstructure of steel 0.41; etched 4% nitol, magnification = 556X.

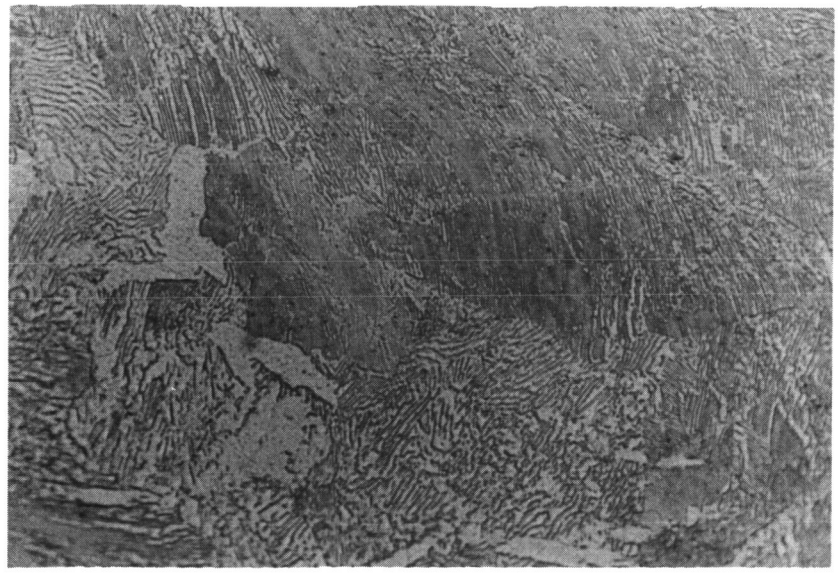

Figure 2.8 Microstructure of steel 0.57; etched 4% nitol, magnification = 556X.

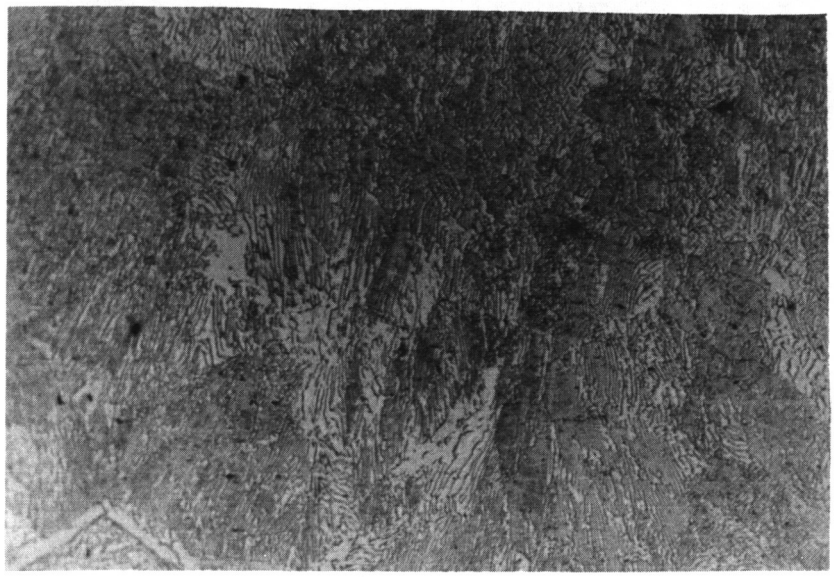

Figure 2.9 Microstructure of steel 0.72; etched 4% nitol, magnification = 556X.

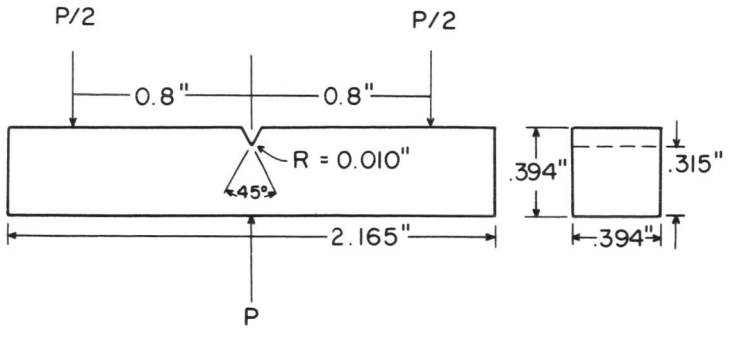

(a)

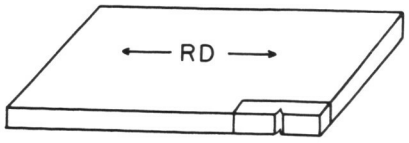

(b)

Figure 2.10 The Charpy V-notch specimen and the orientation from which they are cut in a rolled plate.

oriented with respect to the plate as shown in Fig. 2.10b. Thus, failure propagated neither perpendicular nor parallel to plane of the plate which might contain elongated second phases.

Slow bend samples were prepared in the same manner with three additional slots milled as shown in Fig. 2.11a to locate the loading rollers. A limited number of tests were performed in four-point loading using the specimen shown in Fig. 2.11b.

Cylindrical holes were located relative to the notch tip and drilled mechanically using a "jig bore". This machine was equipped with an optical device which enabled the holes to be positioned within $\pm$ 0.0005". The position of the holes relative to the notch tip is described by the coordinates (R, θ) shown in Figure 2.11c. All holes were 0.0292" in diameter and were drilled completely through the specimen thickness unless otherwise stated.

Charpy impact and slow bend-fracture tests were performed on the "as-machined" specimens without subsequent heat treatment except where specified. Experiments will be described which show that the small, localized machining and drilling strains did not play an important role in the observed effects. Fe-Si 2 samples for dislocation etch-pit studies and variable thickness fracture experiments were prepared as above. They were then annealed in vacuum for one hour at various temperatures to obtain a uniform ferrite grain size (Table 2.1).

Sheet tensile specimens of steel 0.40 and Fe-Si 1 were prepared from 0.050" sheet which had been warm rolled from 1/2 inch plate. Specimen blanks were sheared so that the tensile axis would lie parallel to the rolling direction. In the case of steels 0.24 and 0.20, tension

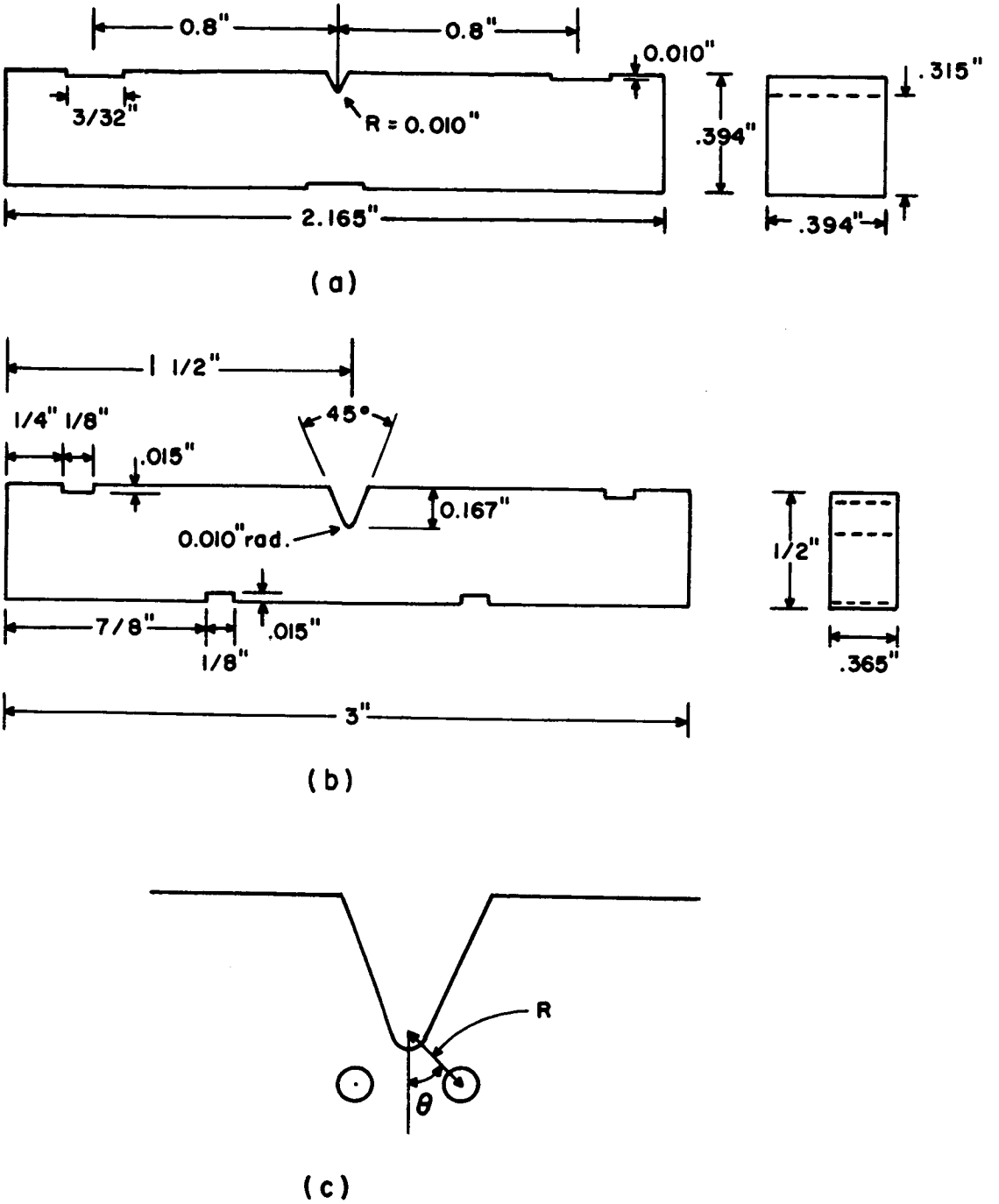

Figure 2.11 Slow bend specimens and the coordinants of drilled holes;

(a) Three-point loading
(b) Four-point loading
(c) Coordinants of drilled holes.

blanks were cut directly from the 1/2" thick plate. All tension blanks were surface ground to 0.040" thick prior to machining the final form. Master templates were designed and purchased so that the blanks could be machined on the laboratory's "Tensilkut" machine. The specimen designs which were employed are shown in Figure 2.12. Charpy-V notches were milled in the conventional manner while holes were again positioned and drilled on the "jig-bore".

The photoelastic model material and specimen preparation are described separately in Chapter IV.

2.3 Mechanical Testing

The effect of drilled holes on the (1) load carrying capacity, (2) impact transition temperature and (3) ductility of notched samples was studied by means of slow - bend, impact bend, and tension tests over a range of temperatures.

2.3-1 Slow Bend Tests

Slow bend tests were performed on an Instron testing machine using a specially constructed bend jig and cryostat (Figure 2.13). The jig was designed for both three and four-point bend specimens with the loading rollers positioned by slots in the specimens.

All tests were performed at a crosshead velocity of 0.10"/min. Various test temperatures (+ 300°C to - 196°C) were obtained by immersing the entire bend jig in an appropriate liquid bath (salts, oils, acetone, ethyl alcohol, isopentane, or liquid nitrogen). Specimen temperature was measured by a thermocouple taped just below the notch root and was recorded continuously throughout a test on an x-y recorder.

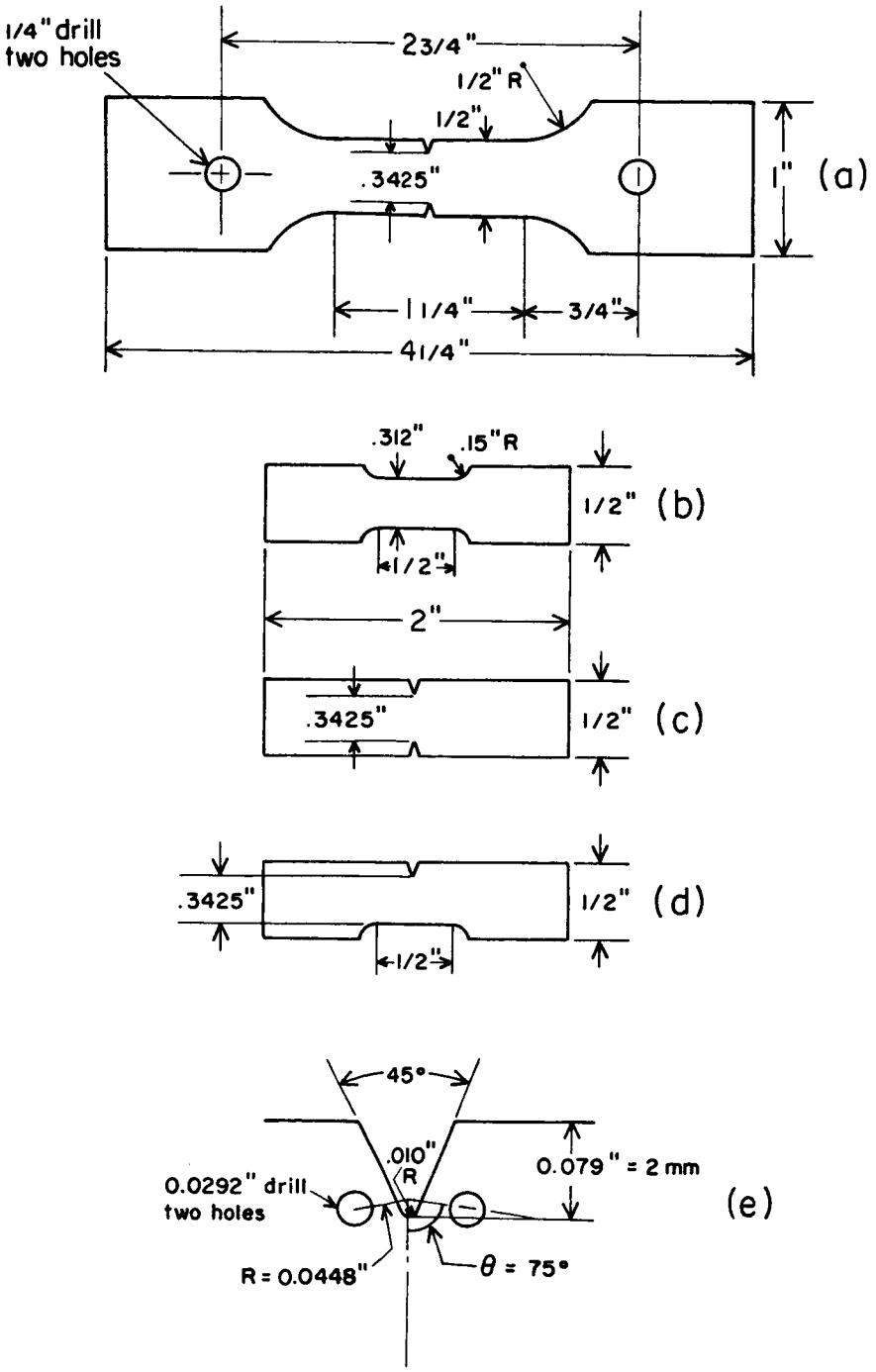

Figure 2.12 Sheet tensile specimens.

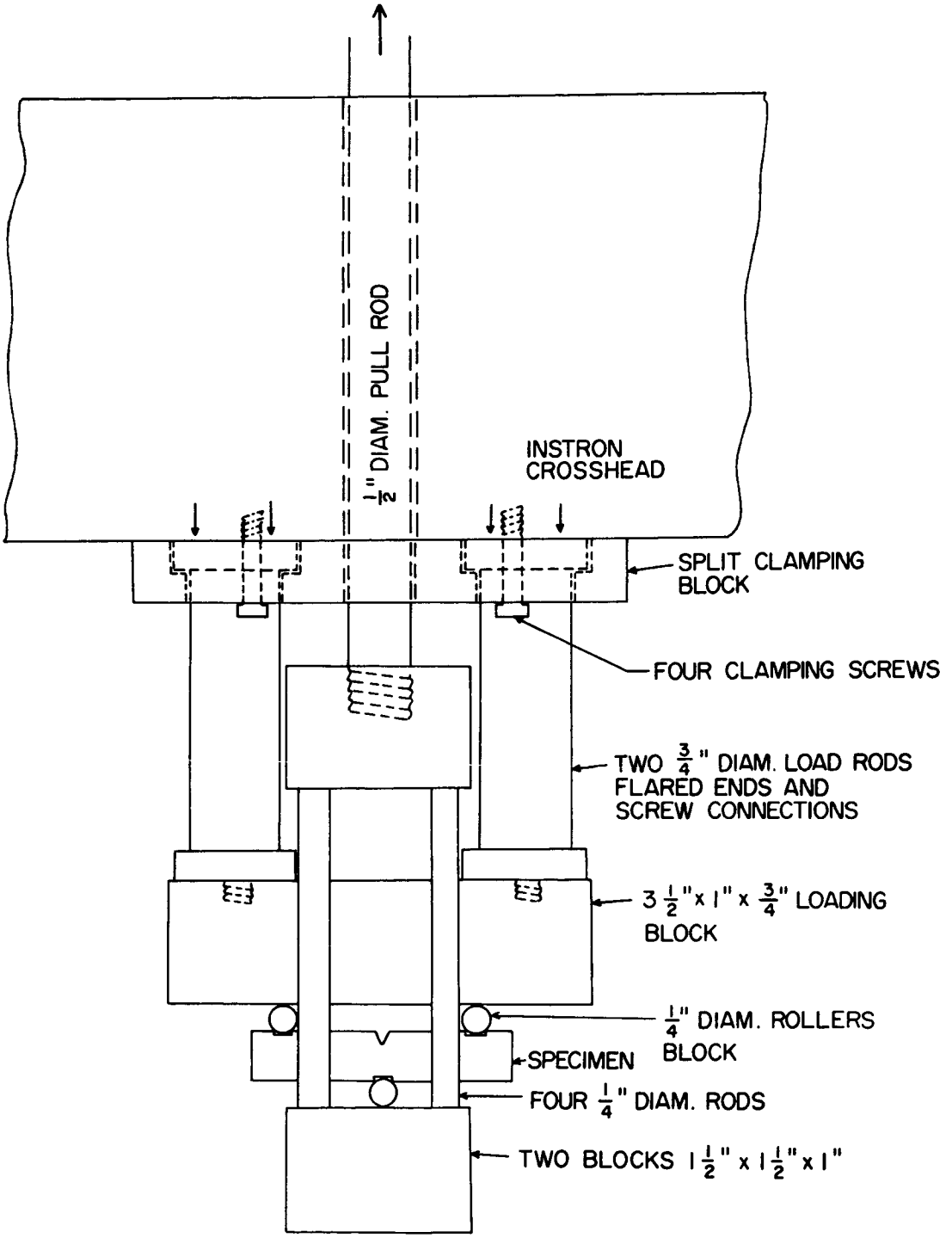

Figure 2.13 A schematic drawing of the bend jig used for testing in controlled temperature baths.

A special technique was devised to obtain temperatures between -188°C and -150°C where no liquid bath is available. A metal dewar was partially filled with boiling nitrogen and positioned around the bend jig on an adjustable jack. The liquid bath could then be moved up or down relative to the specimen with the adjustable hand jack. The entire jig and specimen were first cooled to -196°C after which the specimen was allowed to warm up to the test temperature in the cold vapors above the liquid. By controlling the bath level throughout a test, temperatures between -188°C and -150°C could be maintained $\pm$ 0.5°C over the entire sample.

2.3-2 Tension Tests

Tension tests were performed on an "Instron" testing machine at a loading rate of 0.10"/min. or 0.5"/min. The Fe-Si samples shown in Fig. 2.12a were pin loaded by means of pull rods between the crossheads (Fig. 2.14a). This facilitated rapid insertion and removal of specimens and avoided problems of alignment and grip slippage. A simple cryostat consisting of an insulated 3-inch diameter stainless steel can with a separable split bottom was fitted around the lower pull rod. Vacuum grease provided an adequate seal for tests in liquid nitrogen, isopentane, or alcohol.

For temperatures between -188°C and -150°C where no liquid bath was available, nitrogen was sprayed as a vapor mist on the specimens wrapped in "saran wrap". Following Wessel and Olleman[88], nitrogen was forced under pressure through a solenoid valve and a controllable constant flow line to an insulated specimen chamber. Temperatures were maintained by a combination of constant flow and the periodic flow

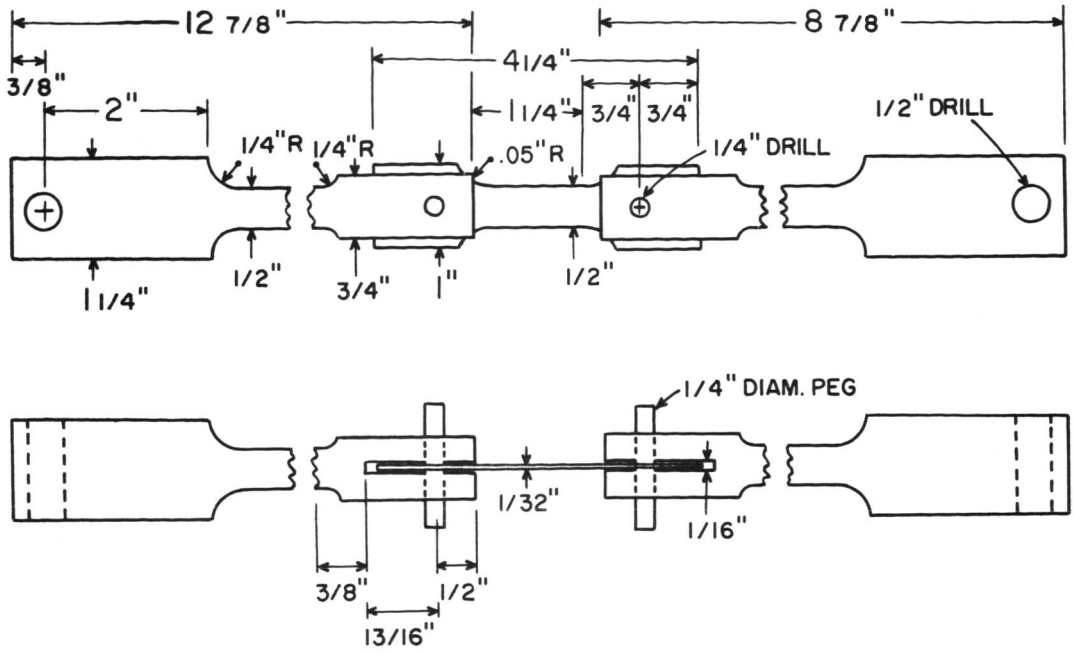

(a)

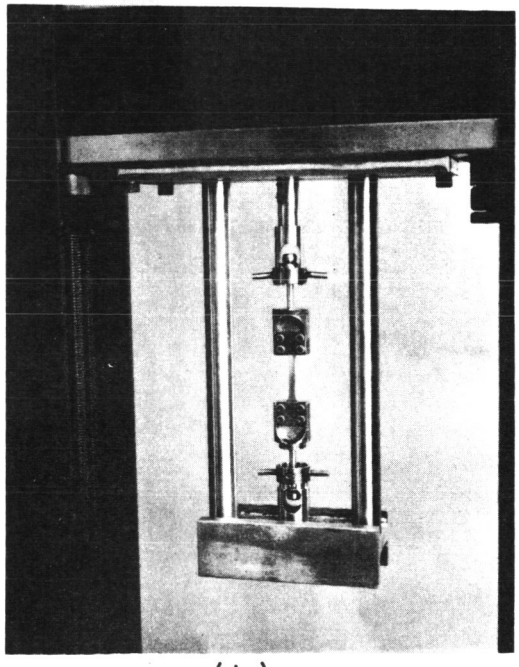

(b)

Figure 2.14 Loading fixtures for tension testing at controlled temperatures.

through the solenoid valve operated by a controller. With this apparatus temperatures were maintained $\pm$ 2°C.

Steel 0.40 specimens shown in Fig. 2.12-b, c, d were tested beneath the instron crosshead in the tensile bridge shown in Figure 2.14b. This fixture was designed to provide more rapid insertion and removal from the temperature baths while providing the clamp gripping necessary for these smaller specimens.

2.3-3 Impact-bend Tests

Impact bend tests were performed on a Wiedemann-Baldwin SI-1 impact machine. The Charpy V-notch specimen shown in Fig. 2.10a is loaded in three-point bending by a striker attached to a swinging pendulum. The 53.2 pound pendulum is released from 4.51 ft. reaching a velocity of 17 ft/sec. at the time of impact (the bottom of its swing). The energy absorbed in failure of the specimen is obtained from the height of the fall minus the height of the rise less any losses due to friction and kinetic energy of the fractured pieces. A pointer on the machine is calibrated to give the impact energy directly.

Various test temperatures were obtained by stabilizing samples for ten to sixty minutes in large, stirred, constant temperature baths (salt, oil, alcohol, isopentane, or liquid nitrogen). Specimens were transferred from the bath to the impact machine in special tongs which insured that the specimen was positioned correctly in the loading anvil (i.e., with the notch directly opposite the striker). The time between removal from the bath and impact was approximately three seconds, never exceeding five seconds. Experimental measurements showed that for tests

below room temperature no significant warm-up of the samples occurred in this time. Evaporation of coolant from the specimen surface is partially responsible for preventing warm-up. At temperatures above room temperature but below 200°C, specimens cooled less than 2°C in this time interval prior to impact.

2.4 Instrumentation to Measure Dynamic Load-Time Curves

In order to obtain more extensive information from the Charpy test, the pendulum striker was instrumented to record dynamically the load applied to the specimen during the test. As shown in Fig. 2.15, a 0.050" deep slot was milled and polished on each side of the striker and two similar slots were introduced on the massive base of the striker. Foil resistance strain gauges (Budd type 384-B-350Ω, gauge factor = 3.33) were applied symmetrically, one in each slot, using standard adhesives and techniques. Each slot was then filled with a very hard and tough epoxy ("crystal clear epoxy") to protect the gauges. Each of the four gauges form one arm of a wheatstone bridge circuit. The two gauges on the striker are the active measuring gauges while the two arms on the base serve only to complete the bridge and insure temperature compensation (see Fig. 2.16). During loading of the specimen, the striker is compressed and the resistance of the measuring gauges decreases causing a potential difference (V_{AB}) between points A and B. This potential difference was recorded on a Hewlett-Packard variable persistance (storage) oscilloscope.

The impact test now yields a curve of millivolt output (V_{AB}) as a function of time. No external triggering device is required to initiate recording since the oscilloscope can be internally set to

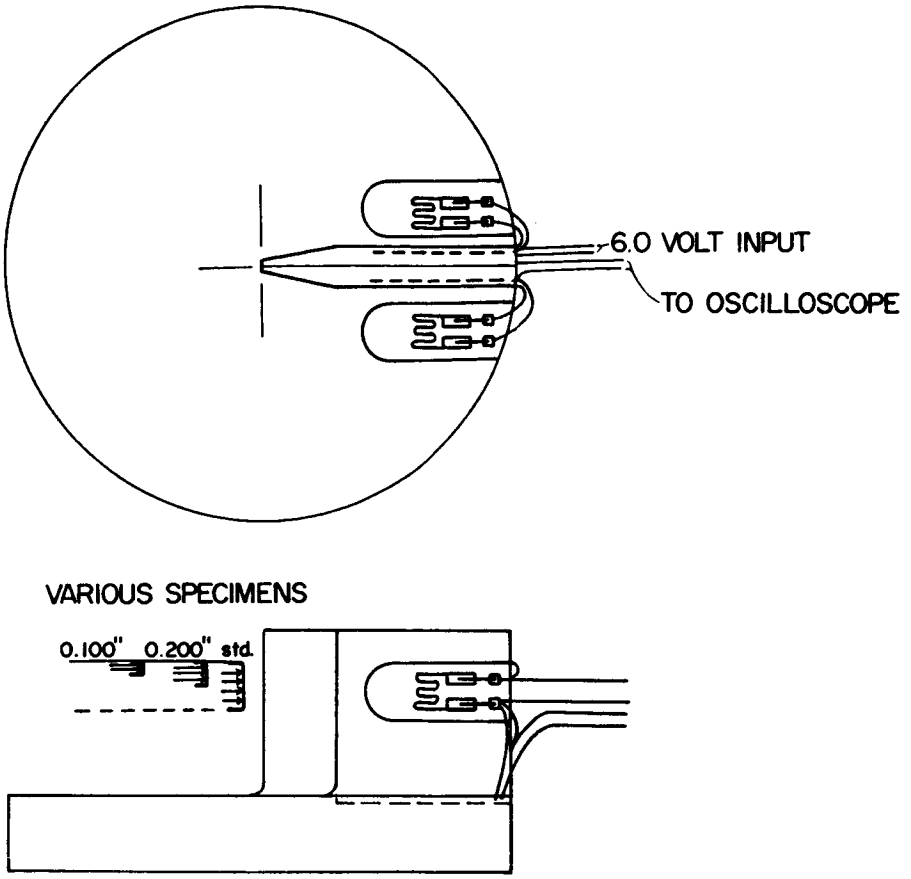

Figure 2.15 The location of foil strain gauges on the instrumented Charpy striker.

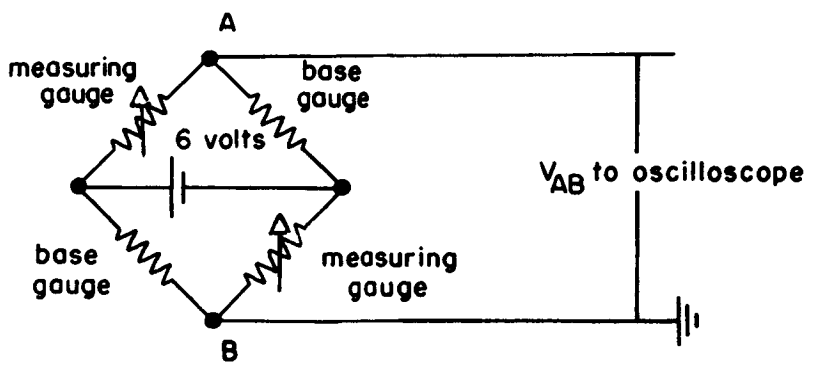

Figure 2.16 Schematic circuit diagram of the instrumented Charpy striker.

start recording whenever some small V_{AB} is exceeded.

Calibration of the instrumented striker was performed by removing the entire pendulum and loading it beneath the crosshead of the Instron as shown in Fig. 2.17. All the downward force from the crosshead is transmitted through that loading area on the striker which would contact the Charpy specimen during an actual test. The applied load is recorded on the Instron chart and the mv output on the oscilloscope. Typical calibration curves are shown in Figure 2.18. When specimens thinner than standard Charpy were tested, there was some question whether the calibration would be the same due to the reduced loading area. The calibration was therefore repeated for thicknesses of 0.200" and 0.100". The calibration curves, which are shown in Figure 2.18, indicate that the striker is 4.5% and 6% less sensitive when loaded by 0.200" and 0.100" thick specimens respectively. These calibrations were repeated from time to time to insure that no change resulted from large numbers of impact tests; no change was detected.

In order to check the calibration under dynamic conditions, Charpy impact and slow-bend samples of aluminum alloy 6061T6 were tested at room temperature and -196°C. This alloy is strain rate insensitive and therefore should yield the same load - deflection curve in both tests. The results summarized below indicate that the striker calibration is valid under test conditions.

23°C	Slow-bend	Impact
General yield load (lb.)	1500 ± 50	1500
Ultimate load (lb.)	1670 ± 10	1680
-196°C		
General yield load (lb.)	1800 ± 50	1750
Ultimate load (lb.)	2100	1950

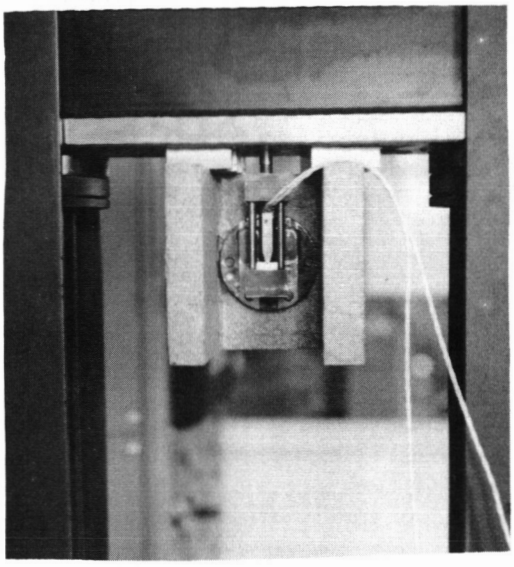

Figure 2.17 Loading of the instrumented Charpy striker beneath the crosshead of the Instron testing machine for calibration of the striker; the weight of the hammer plus the applied load from the machine are supported by that area on the striker which would contact the sample.

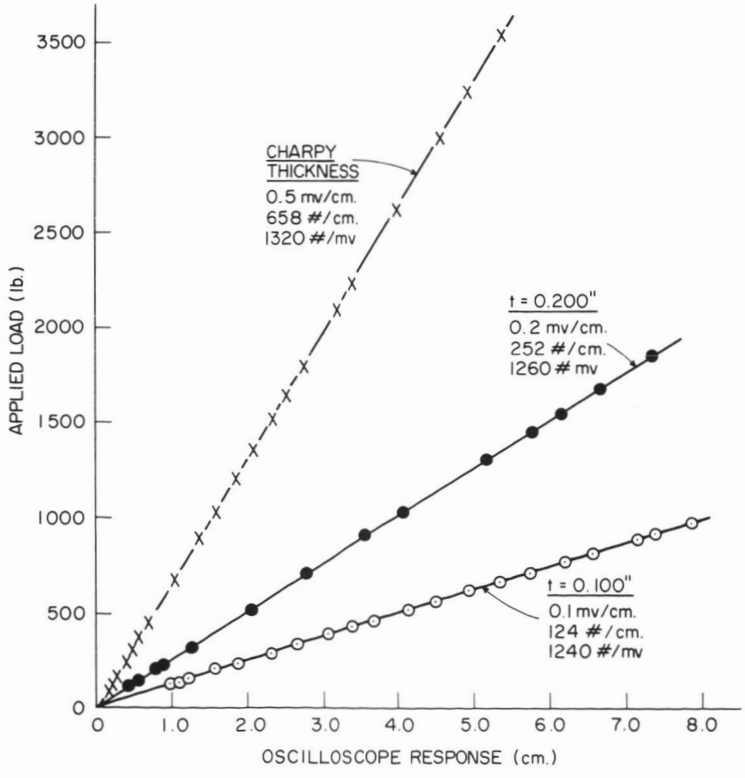

Figure 2.18 Calibration curves for various loading areas, corresponding to different thickness Charpy samples.

2.5 Dislocation Etch-Pitting

Various experiments were performed on well annealed iron - 3.25% silicon alloy to directly observe the effect of holes on local plastic deformation. After loading, specimens were aged twenty minutes at 160°C to permit carbon to diffuse to the dislocations. Specimens were polished mechanically, through 6 micron diamond paste, and then electrolytically. The solution for both electropolishing and etch-pitting was 50g CrO_3, 266 ml. glacial acetic acid, and 14 ml. water[89] stirred continuously and used between 5° and 15°C. Specimens (anode, with stainless steel cathode) were electropolished at 25 volts for five minutes and etch-pitted at 5 volts for four minutes.

2.6 Metallography

Photomicrographs were taken with a Leitz microscope equipped with 35 mm camera and focusing device. Low magnifications were obtained with the same camera and focusing device through one eyepiece of a B&L stereo microscope.

CHAPTER III

THE EFFECT OF HOLE POSITION ON NOTCH TOUGHNESS

3.1 Standard Charpy Specimens

The standard Charpy curve of alloy 0.025 showed a sharp rise in energy over a narrow temperature range so that the initiation transition temperature T_S was well defined at -58°C (Fig. 3.1). This sharp transition behavior is characteristic of clean, essentially single phase materials and results in the ductility (T_N), initiation (T_S), and 50% E_{max} (T_{50}) transition temperatures coinciding[64, 65].

Observation of fractured specimens indicated that at temperatures considerably below T_S, specimens had undergone general yielding prior to cleavage fracture. Above T_S specimens did not fracture but simply wrapped around the impact striker absorbing 240 ft.-lbs. of energy. This sharp transition behavior facilitated the evaluation of the effect of drilled holes on notch toughness.

3.2 One Hole Ahead of the Notch Root

One 0.0292" diameter hole was drilled beneath the notch root at distances R ranging from R = 0.010" (keyhole type specimen) to R = 0.070". The hole size of 0.0292" was chosen for this and for the initial two-hole studies because it was the smallest diameter that could be conveniently drilled through the Charpy specimen. As shown in Figure 3.1, the presence of one hole did not cause any appreciable change in the transition temperature, even when it was drilled directly at the notch tip. This result is not in conflict with differences that have

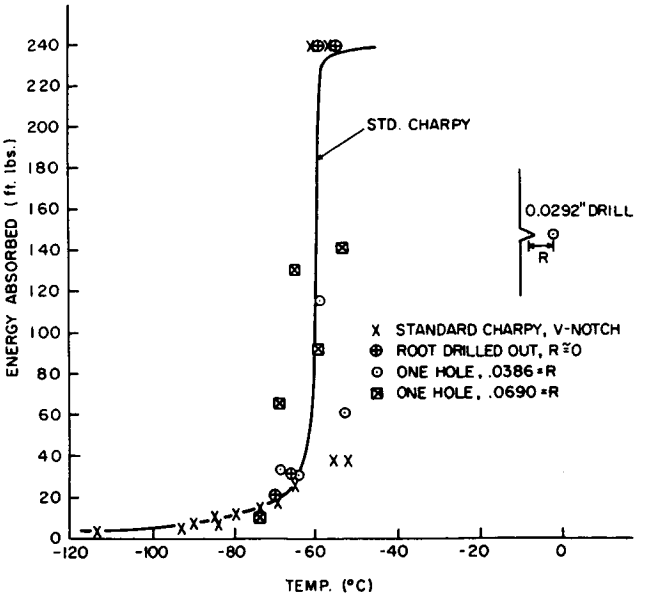

Figure 3.1 The effect of one 0.0292" diameter hole, drilled at various distances (R) below the notch tip center of curvature, on the Charpy impact transition curve of steel 0.025.

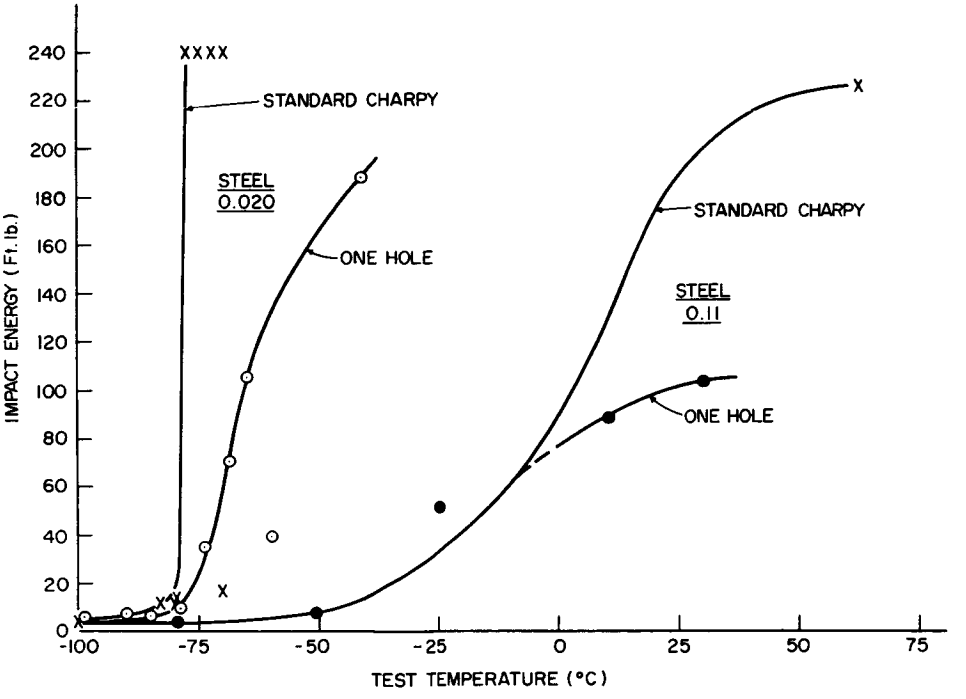

Figure 3.2 The effect of one 0.0292" diameter hole, drilled at R = 0.0448" below the notch tip center of curvature, on the Charpy impact transition curves of steels 0.020 and 0.11.

been reported between Charpy keyhole and V-notch specimens[90-92]. In the present work, the drilled ("keyhole") sample has a notch radius of $\rho = 0.0145"$, only 45% larger than the standard V-notch ($\rho = 0.010"$). On the other hand, the standard keyhole specimen has a root radius of $\rho = 0.0395"$ and should therefore result in a significantly lower transition temperature (Chapter I).

One 0.0292" hole was also drilled at R = 0.0448" in specimens of alloys 0.02 and 0.11. The impact energy transition curves were altered as shown in Figure 3.2. No increase in energy is observed in drilled specimens tested below the transition temperature T_S while above T_S, the energy absorbed is reduced by the presence of the hole. Thus in these alloys, one hole produces only small and adverse effects on toughness.

3.3 Two Holes

Although one hole produces insignificant or adverse effects on notch toughness, two 0.0292" holes drilled symmetrically about the plane of the notch result in pronounced improvements. Impact transition curves were obtained for alloy 0.024 specimens with two holes located at R = 0.0448" and various $\theta = 30, 45, 60, 75$ and 90°. The transition temperature T_S is lowered by $33^\circ C$ [i.e., down to $T_{SH} = -91^\circ C$., Figure 3.3] when R = 0.0448", $\theta = 75^\circ$. The reductions are significant but somewhat smaller for both smaller and larger values of θ. In future discussions, the additional subscript "H" on transition temperatures will denote that the samples contain two drilled holes.

Figure 3.4 shows the appearance of a standard Charpy and drilled specimen after impact at $-88^\circ C$, $30^\circ C$ below the standard transition temp-

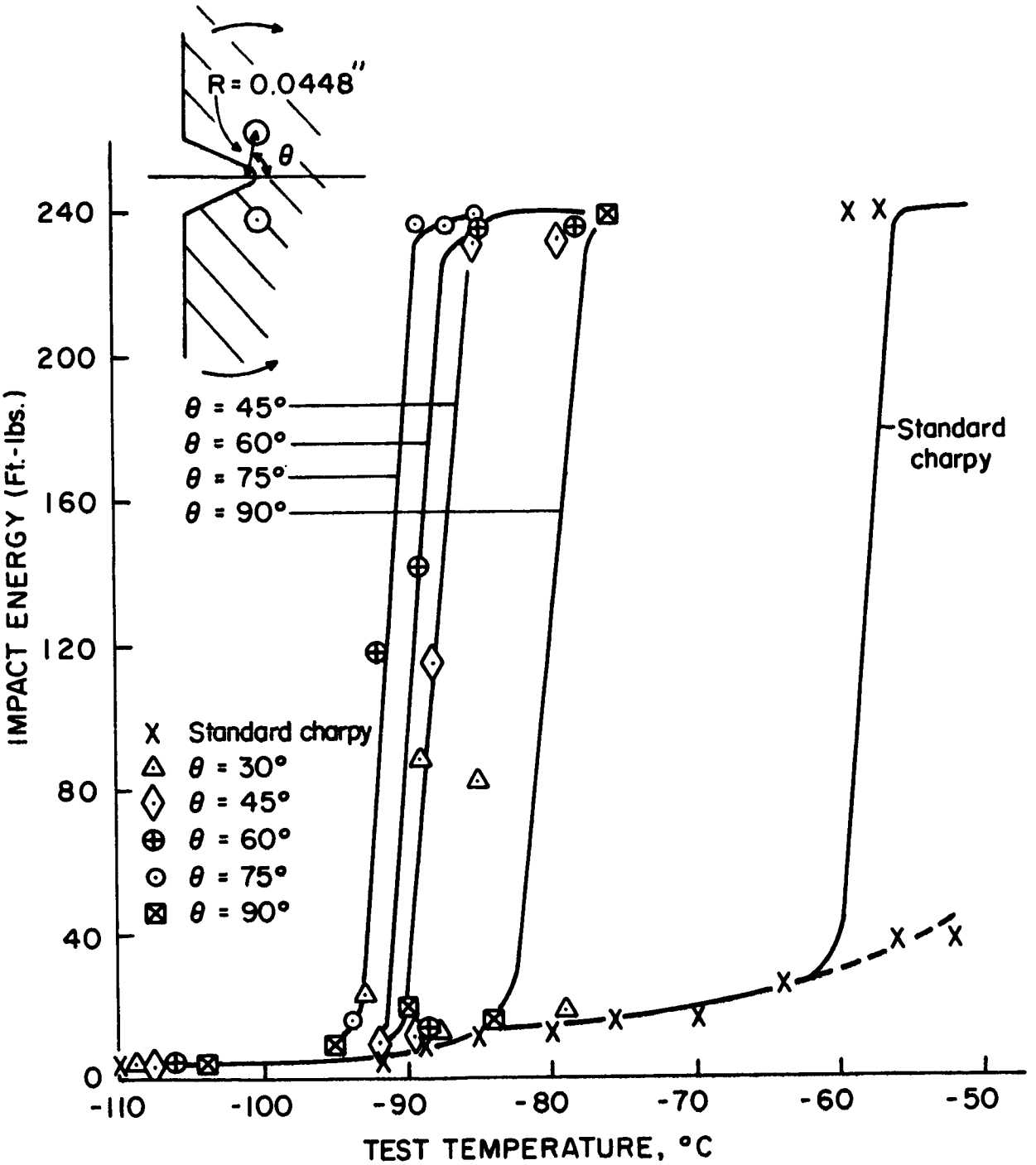

Figure 3.3 The effect of <u>two</u> 0.0292" diameter holes, drilled symmetrically about the notched section at R = 0.0448" and various θ, on the Charpy transition curve of steel 0.025.

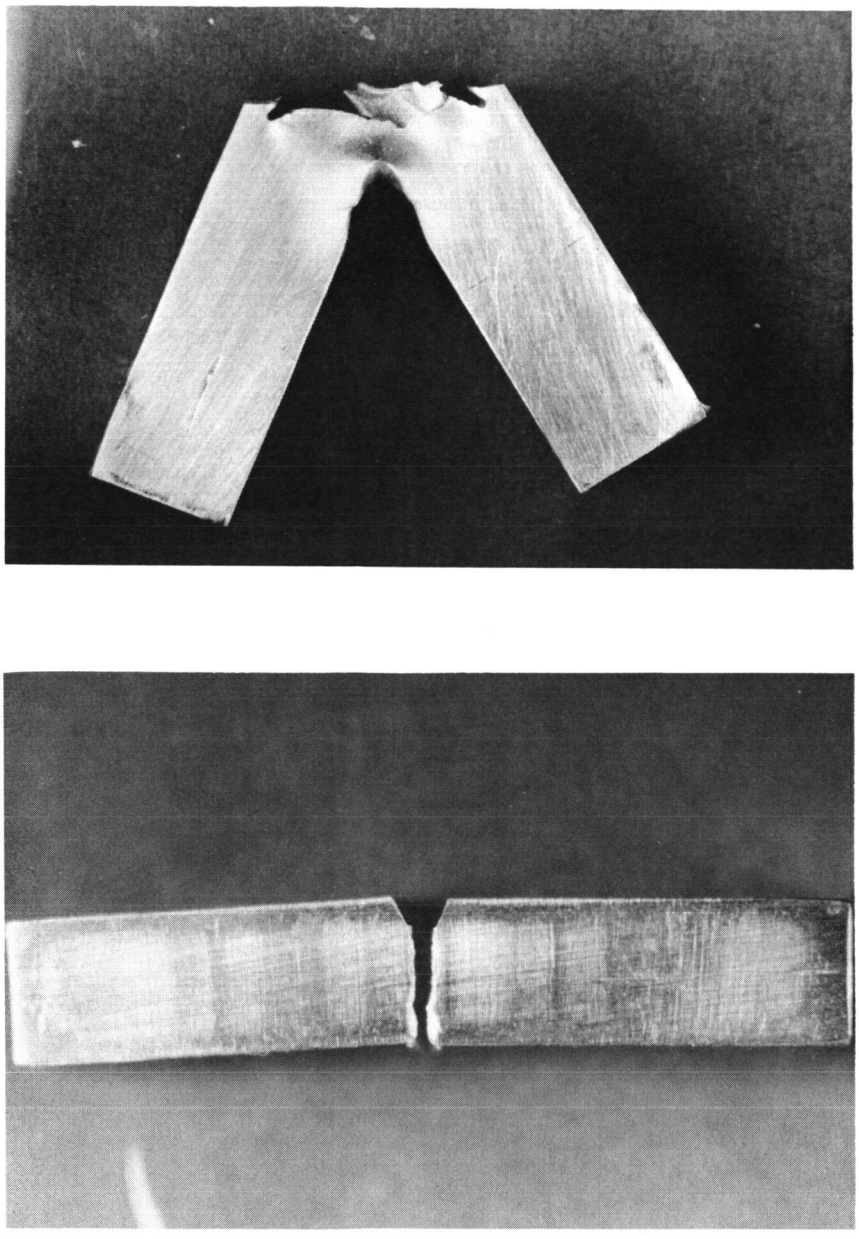

Figure 3.4 Comparison of standard Charpy and drilled samples of steel 0.025 after impact at -88°C (30°C below the initiation transition temperature of the standard Charpy);
(a) Two drilled holes (R = 0.0448", θ = 60°)
(b) Standard Charpy specimen.

erature. The standard sample fractures entirely by cleavage at this temperature and absorbs less than 10 ft.-lbs. of energy. In the drilled specimen, however, large amounts of deformation and fibrous tearing have completely prevented cleavage initiation; and the specimen absorbs the complete 240 ft.-lb. impact without breaking.

3.4 The Mechanisms of Fracture in Two-Hole Specimens

At low temperatures (below $T_{SH} = -91^{o}C$) even specimens with two holes fail by cleavage in one of two ways. (1) A fibrous shear crack forms between the notch side and one hole; subsequently, a dynamic cleavage crack is initiated near the other side of this hole and causes complete separation. (2) Cleavage nucleates ahead of the notch tip between the two holes and propagates to failure without encountering either hole. In either case, large scale tearing is not produced and energy absorbed is quite low.

The reduced impact transition temperature of drilled samples is achieved by drastically altering the mechanism of crack nucleation. Figure 3.5 shows schematically the fracture process in a drilled sample impacted above its transition temperature T_{SH}. Fibrous shear cracks form between the notch and both holes under the action of shear strains. The elongated holes are now the leading edges of two very blunt cracks which become blunter as bending proceeds. Still larger deflections may initiate a fibrous tear from either or both holes (Fig. 3.4b) but these tears cannot propagate at temperatures above $T_{SH} = -91^{o}C$ in alloy 0.025. At temperatures approximately equal to the transition temperature of drilled samples, a dynamic cleavage crack sometimes forms after about 50% fibrous tearing, and intermediate energy values are observed.

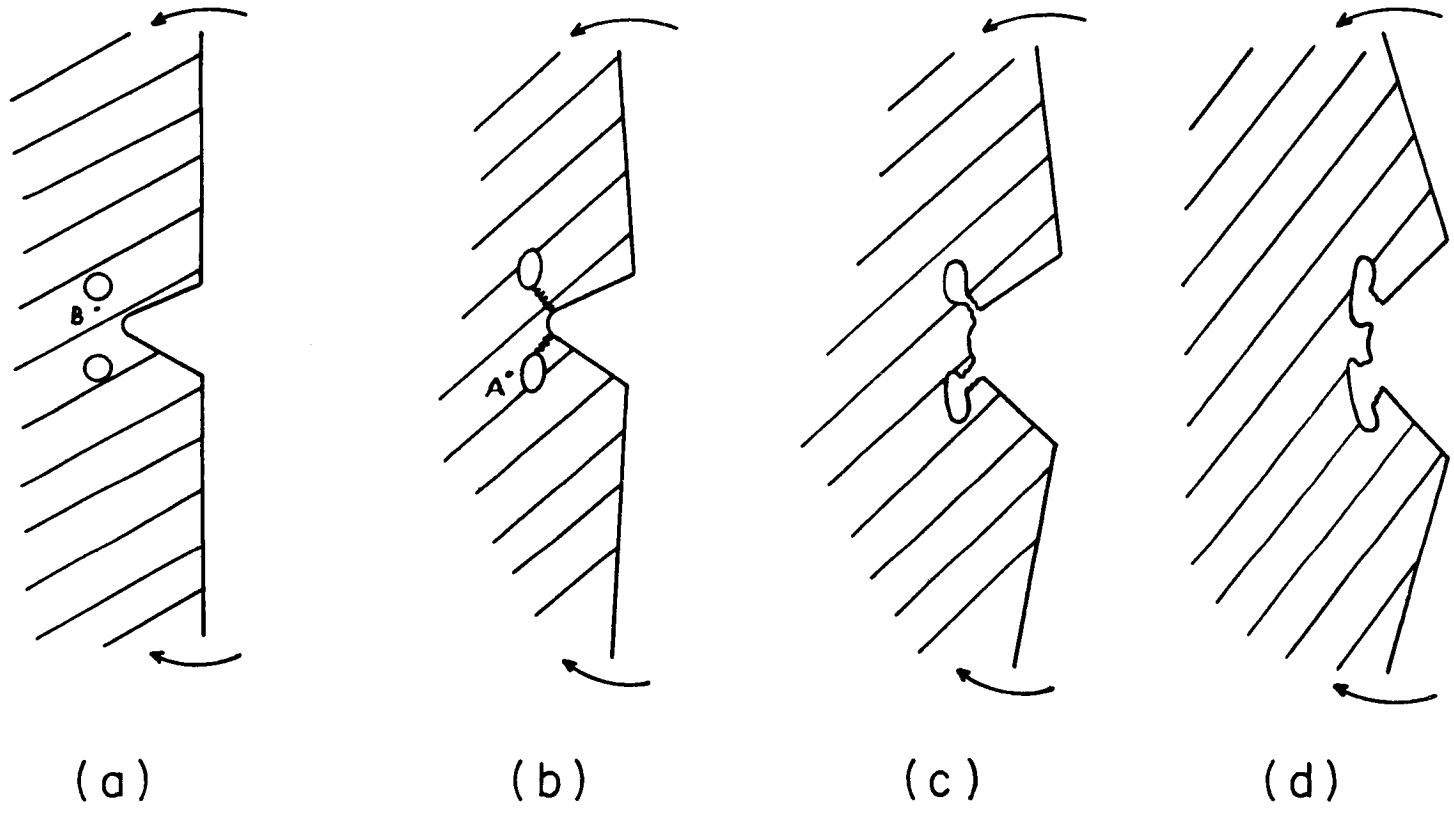

Figure 3.5 Schematic representation of the fracture mechanism in drilled samples tested at temperatures above the ductility transition temperature of drilled samples.

3.5 Summary of Geometric Parameters - Optimum Position

In the previous section, impact results for two holes drilled at constant R = 0.0448" and various θ were presented. Additional experiments were performed to determine the effect of increased radial spacing of the holes. Specifically, impact transition curves were obtained for R = 0.074" and θ = 30, 45, and 75°, for R = 0.0594", θ = 45°, and for R = 0.039", θ = 75°.

The effects of varying R and θ on the impact transition temperature of alloy 0.024 are summarized in Figure 3.6. At a constant value R = 0.0448", a substantial lowering of the transition temperature is obtained when θ is between 45° and 75°. The improvement is negligible at θ = 0° (one hole) and increases to a maximum at θ = 75°. At still higher angles the improvement is considerably less.

Since one hole drilled at the root (R = 0.010") has little effect on T_S while two holes at R = 0.0448" lowered T_S by about 30°C., the impact transition temperature decreases with increasing values of R, reaching a maximum reduction at R = 0.0448". However, when R is increased above 0.0448", T_{SH} increases and approaches that of the standard Charpy T_S as R approaches 0.074". Along line A-B in Figure 3.6, the trend is illustrated for θ = 45°. Consequently, there is an optimum position for two 0.029" diameter holes which occurs when R = 0.0448" and θ = 75°.

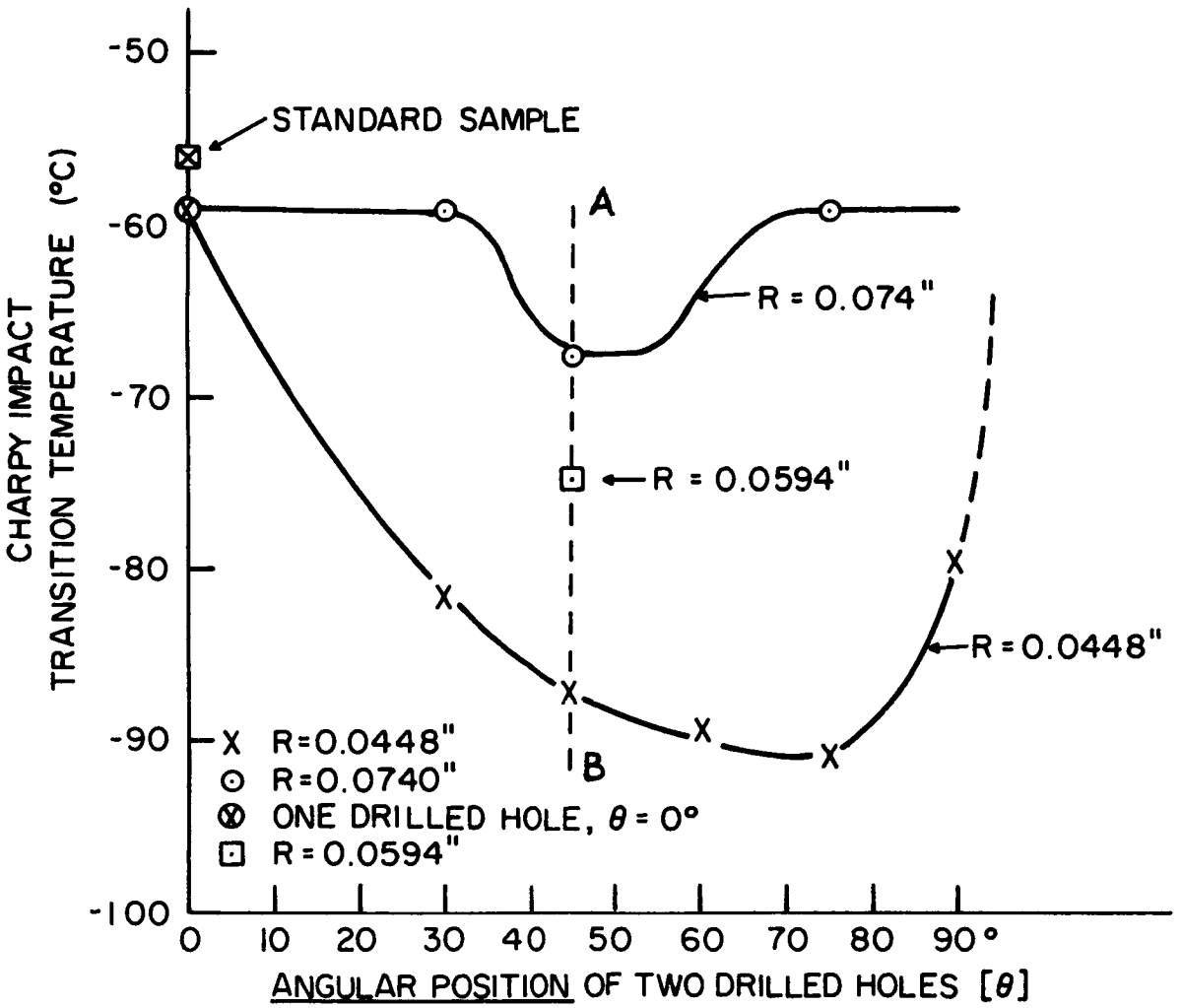

Figure 3.6 The impact transition temperature of steel 0.025 as a function of the location (R, θ) of two 0.0292" holes around the Charpy notch.

CHAPTER IV

CHANGES IN THE ELASTIC STRESS DISTRIBUTION PRODUCED BY TWO HOLES

In order to understand the lower impact transition temperature of drilled specimens compared with standard Charpy samples, the effect of two holes on the stress and strain distributions around a notch had to be determined. Analytical solutions to even the completely elastic problem were not possible at this time so that experimental methods were employed. More specifically, a photoelastic stress analysis was performed for both the Charpy geometry and the Charpy geometry modified by two drilled holes. The specific position of the holes was the experimentally determined optimum of $\theta = 75^{o}$, R = 0.0448" (Chapter III).

4.1 The Photoelastic Technique

This technique makes use of the physical property of birefringence[93]. That is, some transparent materials polarize visible light which passes through them into those planes which are parallel to the principal stress directions in the loaded material. A loaded planar model, therefore, separates incident plane polarized light into two-plane polarized waves. Each wave travels through the model at a velocity proportional to the magnitude of the principal stress in its plane. Since the magnitudes of the two principal stresses will in general be different, the two waves, which are initially in phase, move through the model at different velocities, and a phase difference results. If the two waves are passed through another plane polarizer after leaving the model, the components of the two waves in this one

plane interfere. Quantitative analysis of the resulting interference patterns yields the magnitudes and directions of the stresses in the plane of the model[94-97].

A schematic sketch of the experimental set-up (polariscope) is shown in Figure 4.1. The initial (polarizer) and final (analyzer) polarization directions are normally rotated 90^{o} with respect to each other so that the analyzer will remove all light which is transmitted through an unstressed model. An alternative alignment is with the polarization directions parallel so that the analyzer transmits all light which passes through an unstressed sample.

In a stressed model, the initial wave is split in two, and the relative retardation R of one wave with respect to the other within the model is given by

$$R = C\ t\ (\sigma_1 - \sigma_2) \tag{4.1}$$

where t is the model thickness, C a materials constant, and σ_1 and σ_2 are the principal stresses in the plane of the model. The intensity of transmitted light will therefore be a periodic function of t and $\sigma_1 - \sigma_2$ reaching a maximum whenever $R = n\lambda$ and zero (extinction) whenever $R = \frac{n\lambda}{2}$, n = integer. Therefore, extinction occurs whenever

$$n\,\frac{\lambda}{2} = C\ t\ (\sigma_1 - \sigma_2)$$

or

$$n = \frac{2C}{\lambda}\ t\ (\sigma_1 - \sigma_2)\ . \tag{4.2}$$

For a specific monochromatic light and model material, the constant $\frac{2C}{\lambda}$ may be evaluated experimentally using a known stress field. Once

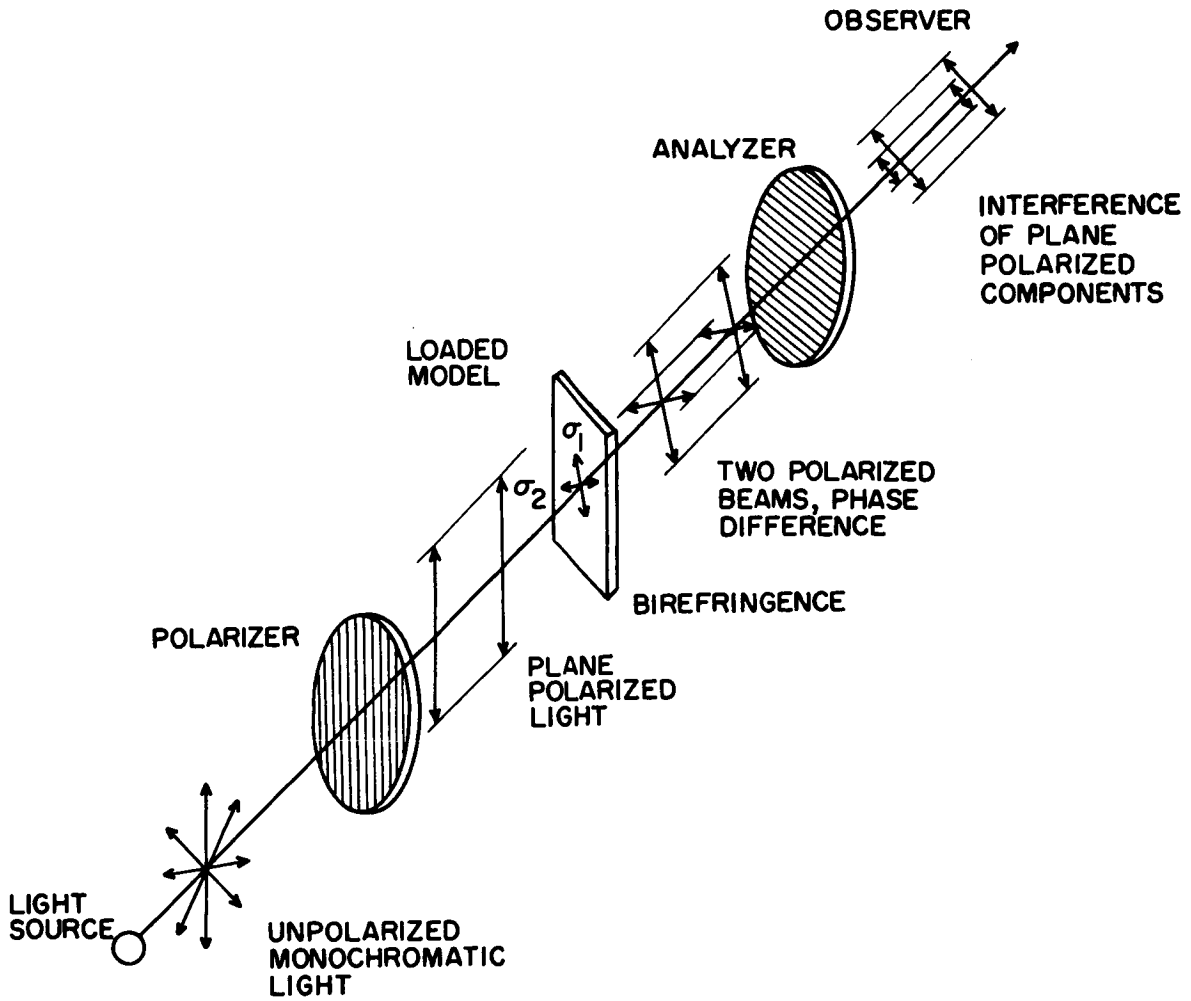

Figure 4.1 A schematic representation of the experimental apparatus (polariscope) which is used to observe the interference fringes resulting from the stresses (or strains) in a birefringent model.

evaluated, any complex stress state may be studied since the extinction fringes, known as isochromatics, represent loci of constant $\sigma_1 - \sigma_2$.

In order to fully describe a stress state, the directions of σ_1 and σ_2 as well as their magnitude must be evaluated. These may be determined experimentally since whenever σ_1 or σ_2 is parallel to the polarizer, extinction also results. That is because no splitting of the incident beam results in these cases, the analyzer (rotated 90^o) will completely remove the single transmitted beam. In a complex stress state, the resulting extinction fringe represents all points where σ_1 or σ_2 fall in the plane of the initial polarized beam. The coupled polarizer and analyzer may then be rotated to various angles to obtain other fringes where σ_1 or σ_2 are parallel to the polarization directions. These fringes are known as the "isoclinics" of the various directions. In this way, the direction of the principal stresses may be defined at all points in the model.

Obtaining the isochromatics and isoclinics for any model and known boundary conditions is usually sufficient to completely define the two-dimensional stress state.

4.2 Experimental Procedure

For this study photoelastic models were prepared from CR-39 resin, 0.259 inches thick and with a fringe constant of 100 psi per fringe per inch thickness. The model dimensions and loading pieces are those used in the Charpy impact-bend test, but all dimensions were scaled up by a factor of five to improve resolution. The model dimensions are shown in detail in Figure 4.2. An aluminum template was machined from two 1/8-inch thick strips so that the model sheet could be sandwiched be-

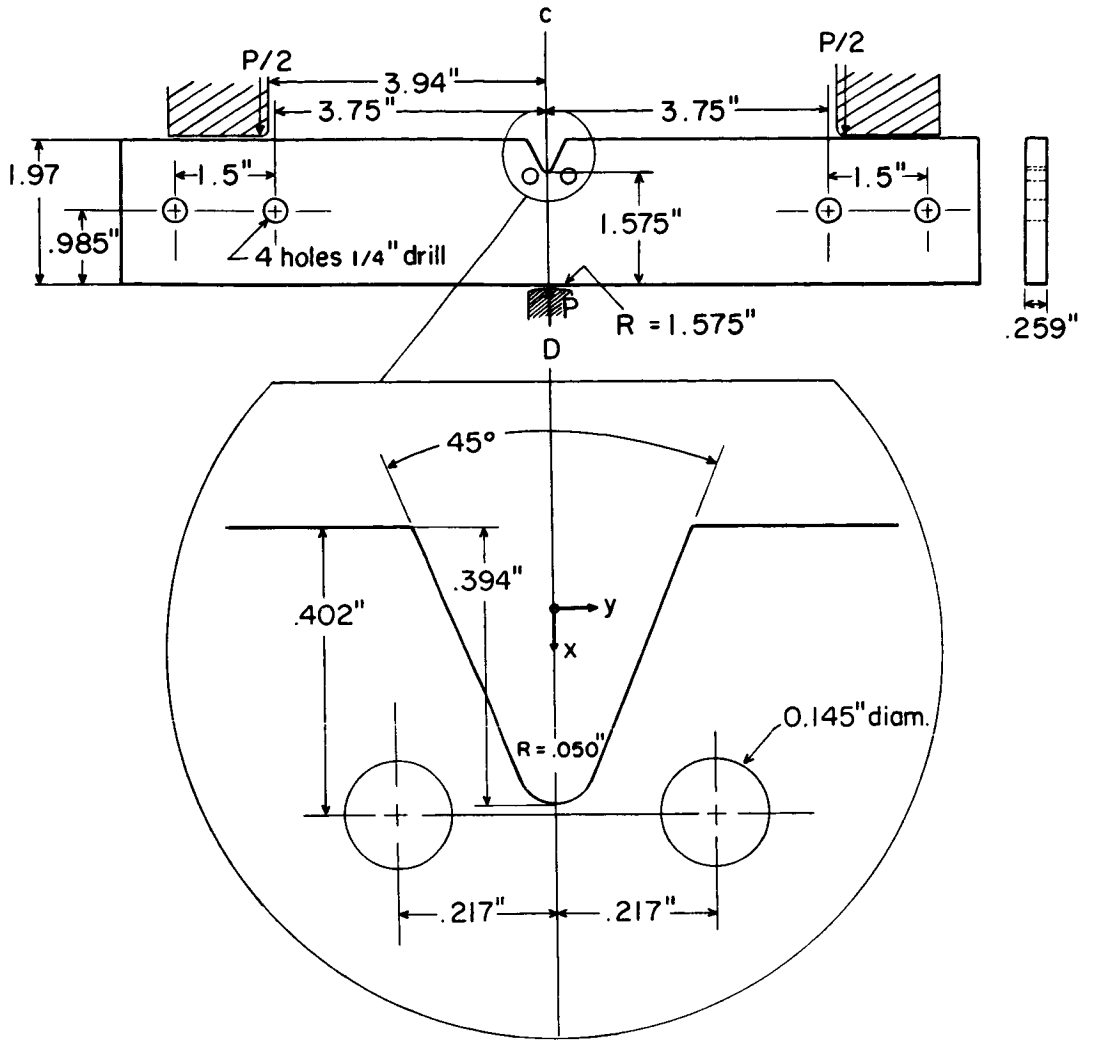

Figure 4.2 The photoelastic model and loading pieces; all dimensions are five times those of the standard Charpy specimen and striker except the model thickness.

tween them during preparation. This assured dimensional control and prevented chipping of the model edge during machining. The notch and holes were finished to final dimensions by fine filing to avoid residual thermal or mechanical stresses.

Models were observed in an eight-inch diameter collimated light polariscope* using a point source mercury green (λ = 5461 Å) arc. The camera assembly consisted of an independent collector lens and interchangeable magnification lenses of 1X and 5X. Isochromatics were photographed on polaroid 4" x 5" positive/negative (type 55) film using circularly polarized light to remove the isoclinics. The isoclinics were traced by hand in plane polarized light at a very low load where isochromatics are not well developed. Loading was accomplished by means of weights through a plunger assembly which was first calibrated to determine any frictional forces.

Because CR-39 undergoes a "time-edge" effect, the polariscope was completely prepared prior to final model filing; and the standard model was observed immediately after completion. After photographing, the model was removed from the polariscope, coated with protective tape, and placed in the template for drilling and filing of the two holes (Fig. 4.1). The drilled model was then loaded and observed as the standard Charpy model had been.

Measurement of fringe positions used in subsequent calculations were taken from photographic enlargements (15X) of the isochromatics. The principal stresses along the axis of symmetry were evaluated by means of integration of the equilibrium conditions in cartesian coordi-

---

* Courtesy of Dr. M. Hetenyi, Engineering Mechanics Department, Stanford University

nants[97]. The details of this analysis are described in section 4.4.

4.3 Isochromatics and Isoclinics

The fringe constant of the CR-39 sheet was 100 psi per inch thickness or 386 psi per fringe in the 0.259-inch thick model. The dark fringes are loci of constant difference between principal stresses $(\sigma_1 - \sigma_2)$, and the magnitude of the difference is given by 386 psi times the fringe number n. The magnitude of n is determined by reference to known boundary conditions and/or by observing the development of the fringes with increasing load. Since the maximum shear stress τ_{max} is given by

$$\tau_{max} = \frac{\sigma_1 - \sigma_2}{2} ,$$

these fringes also represent loci of constant maximum shear stress. Figures 4.3 to 4.6 compare the isochromatics of the standard Charpy with those of the Charpy-holes model under the same applied load. Figure 4.7 shows the labeled isochromatics at a somewhat higher load where the actual calculations were performed.

The isoclinics were constructed by rotating the coupled polarizer and analyzer and recording the extinction (dark) fringes at each angular position. From these loci, the directions of the principal stresses are defined at each point of the model. Figure 4.8 shows the observed isoclinics and the constructed directions of principal stress (stress trajectories) for the model containing two holes.

4.4 Calculation of the Principal Stresses Ahead of the Notch

The magnitude principal stress difference $\sigma_1 - \sigma_2$ is given

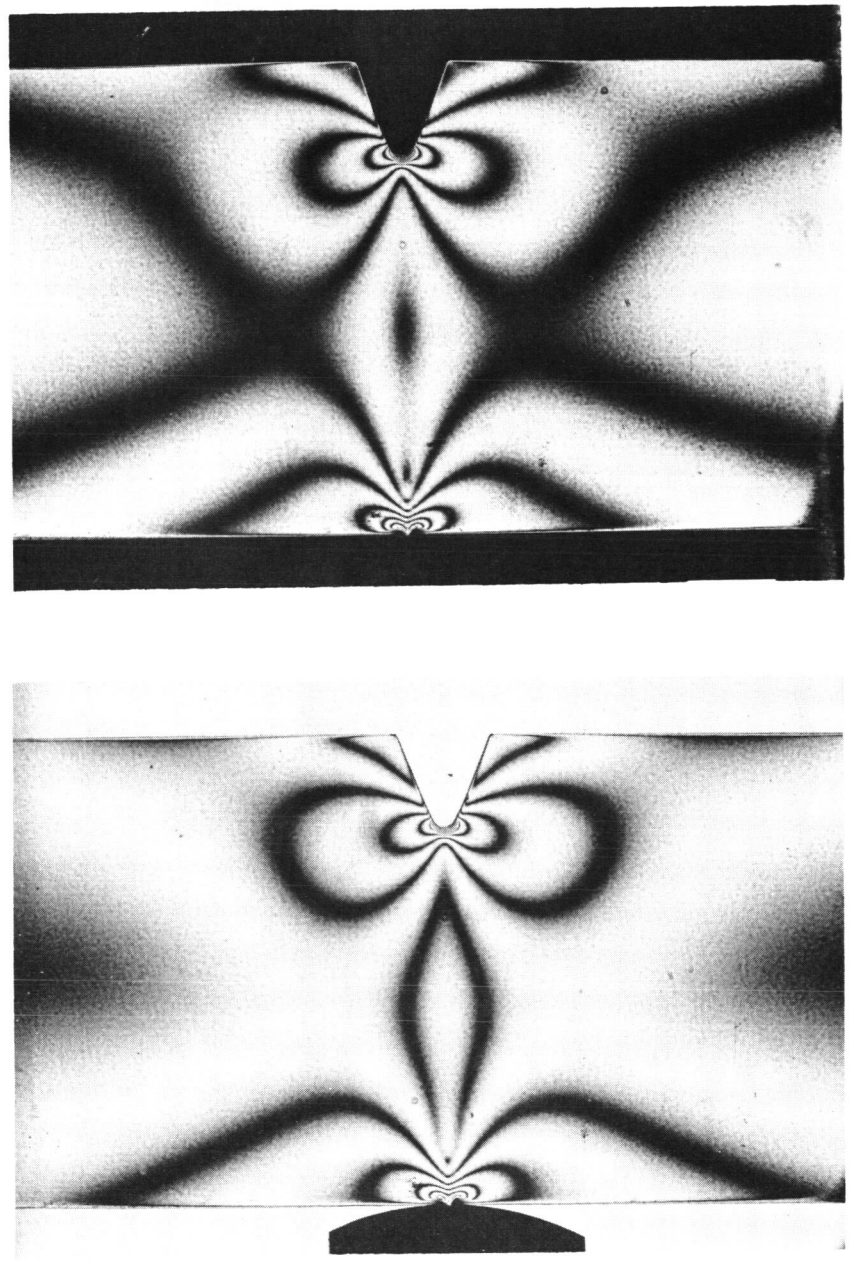

Figure 4.3 Isochromatics for the standard Charpy model loaded in three-point bending; load = 60.6 lb., magnification = 1.2X,

(a) Dark fringes are integer fringe numbers (n)
(b) Dark fringes are one-half integer fringe numbers (n+1/2).

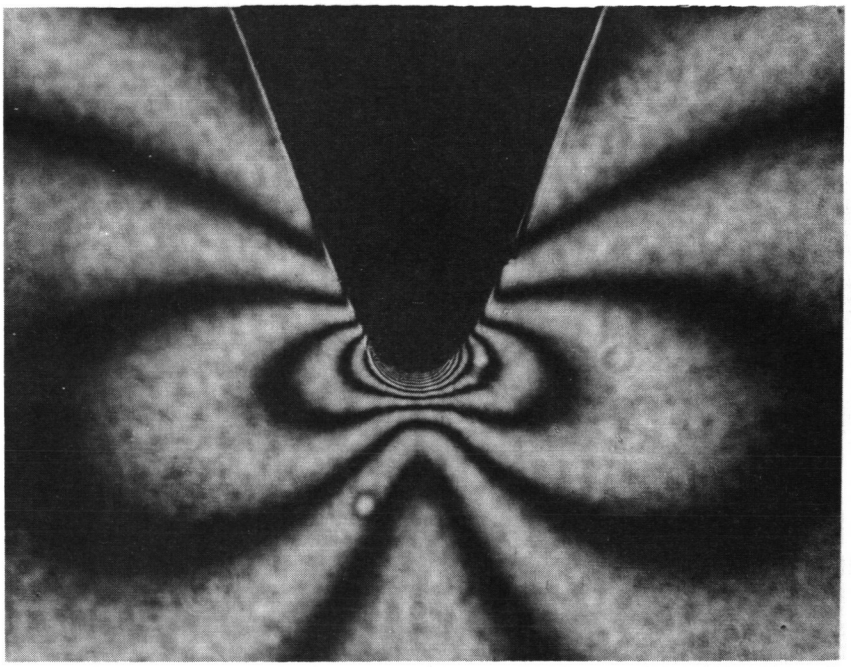

(a)

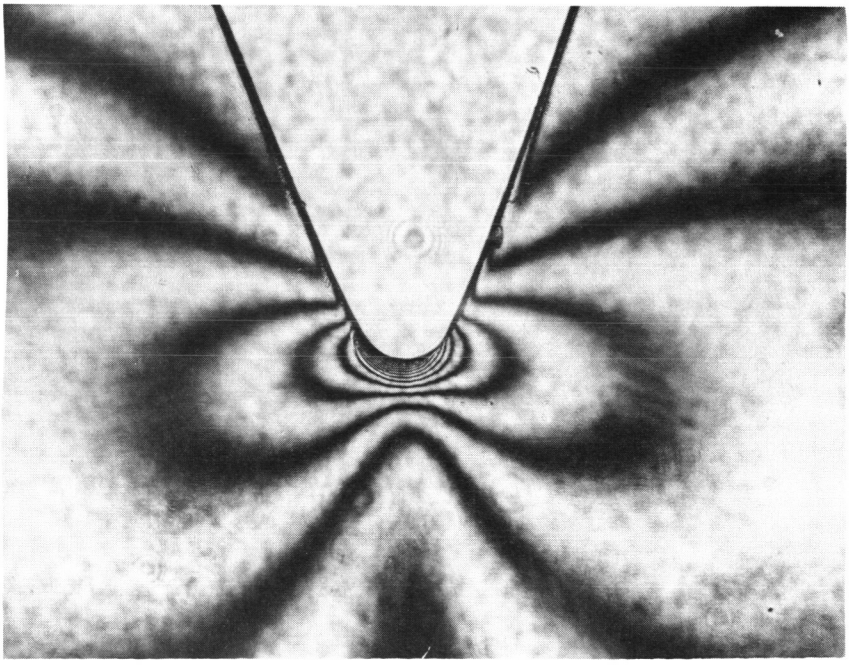

(b)

Figure 4.4 Isochromatics for the standard Charpy model loaded in three-point bending; load = 60.6 lb., magnification = 5X,

(a) Dark fringes are integer fringe numbers (n)
(b) Dark fringes are one-half integer fringe numbers (n+1/2).

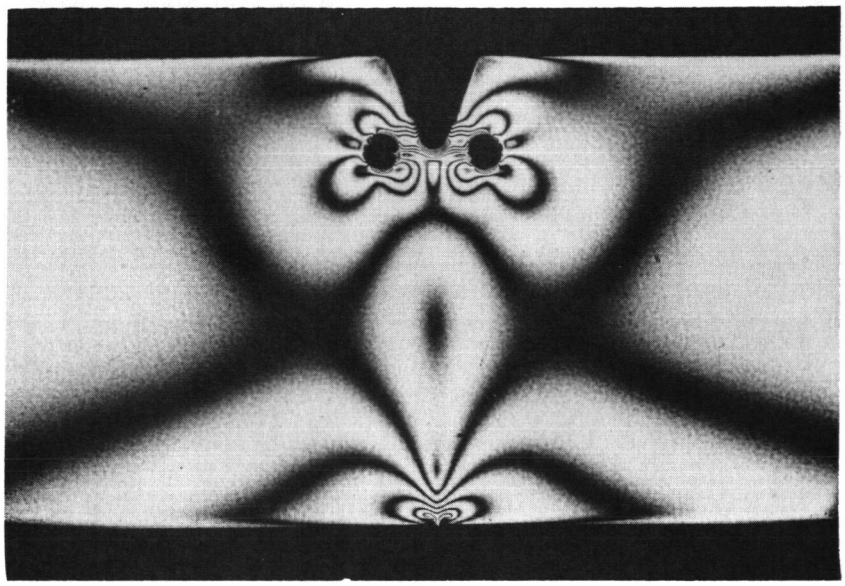

(a)

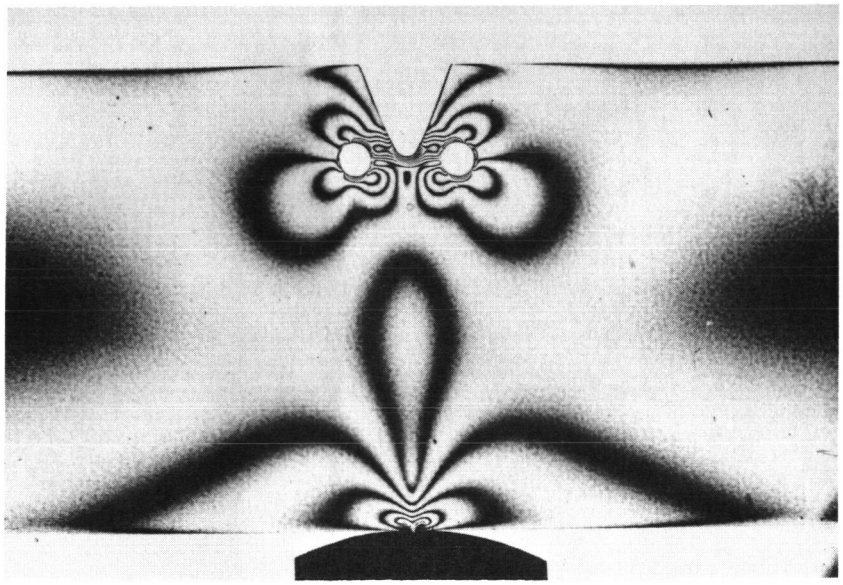

(b)

Figure 4.5 Isochromatics for the Charpy model modified by two drilled holes and loaded in three-point bending; load = 60.6 lb., magnification = 1.2X,

(a) Dark fringes are integer fringe numbers (n).
(b) Dark fringes are one-half integer fringe numbers (n+1/2).

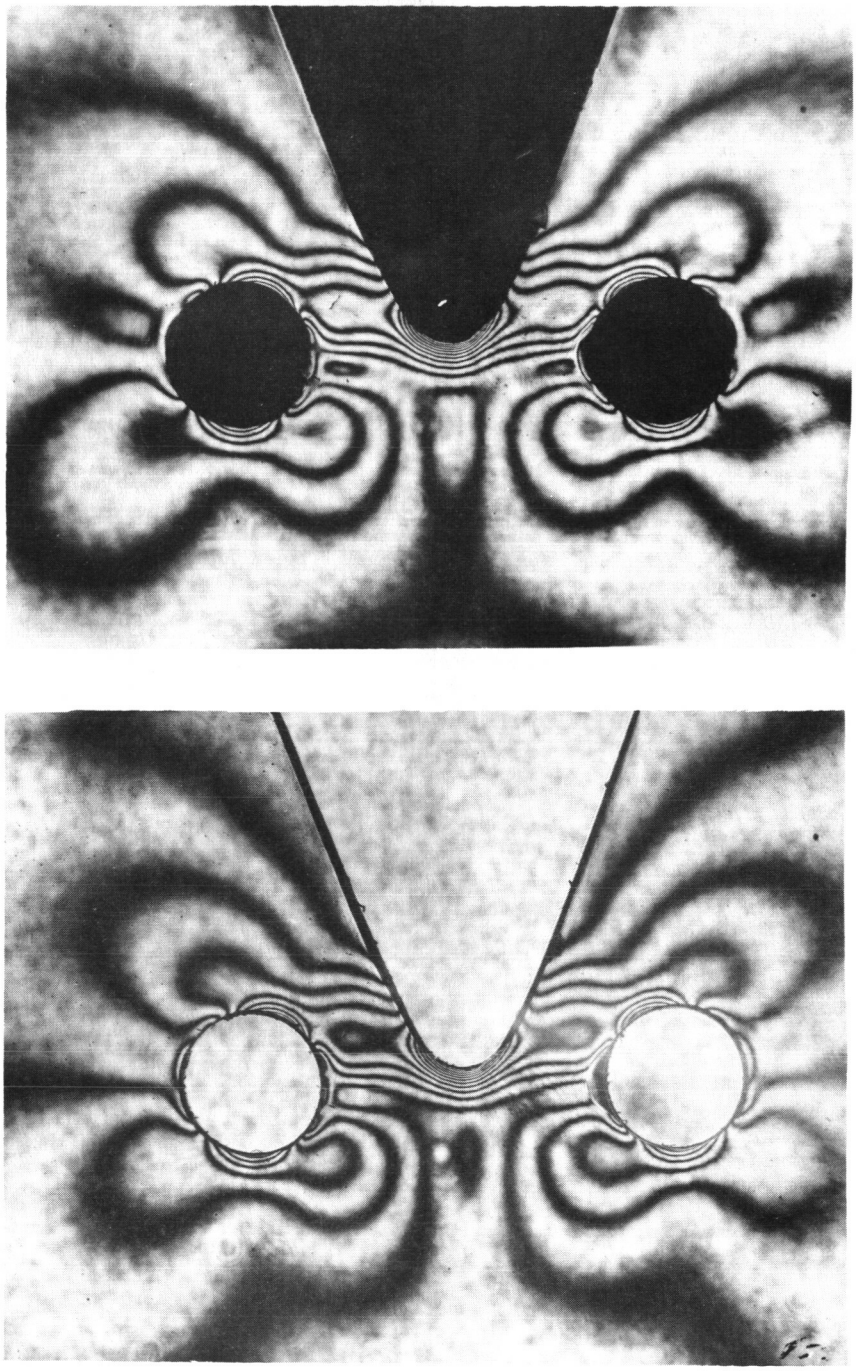

Figure 4.6 Isochromatics for the Charpy model modified by two drilled holes and loaded in three-point bending; load = 60.6 lb., magnification = 5X,

(a) Dark fringes are integer fringe numbers (n)
(b) Dark fringes are one-half integer fringe numbers (n+1/2).

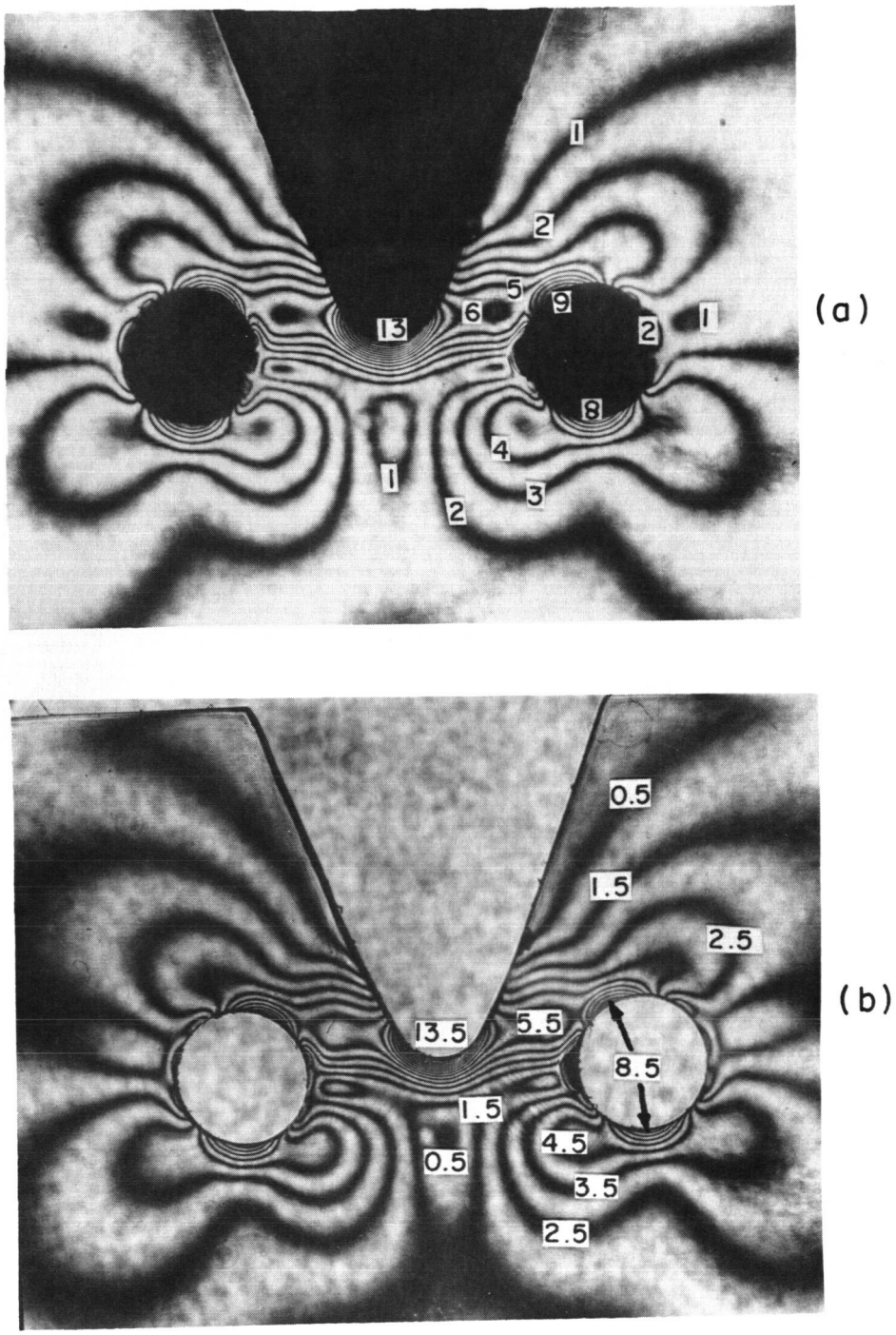

Figure 4.7 Isochromatics for the Charpy model modified by two holes and loaded in three-point bending; load = 75.6 lb., magnification = 5X,

(a) Dark fringes are integer fringe values (n)
(b) Dark fringes are one-half integer fringe values (n+1/2).

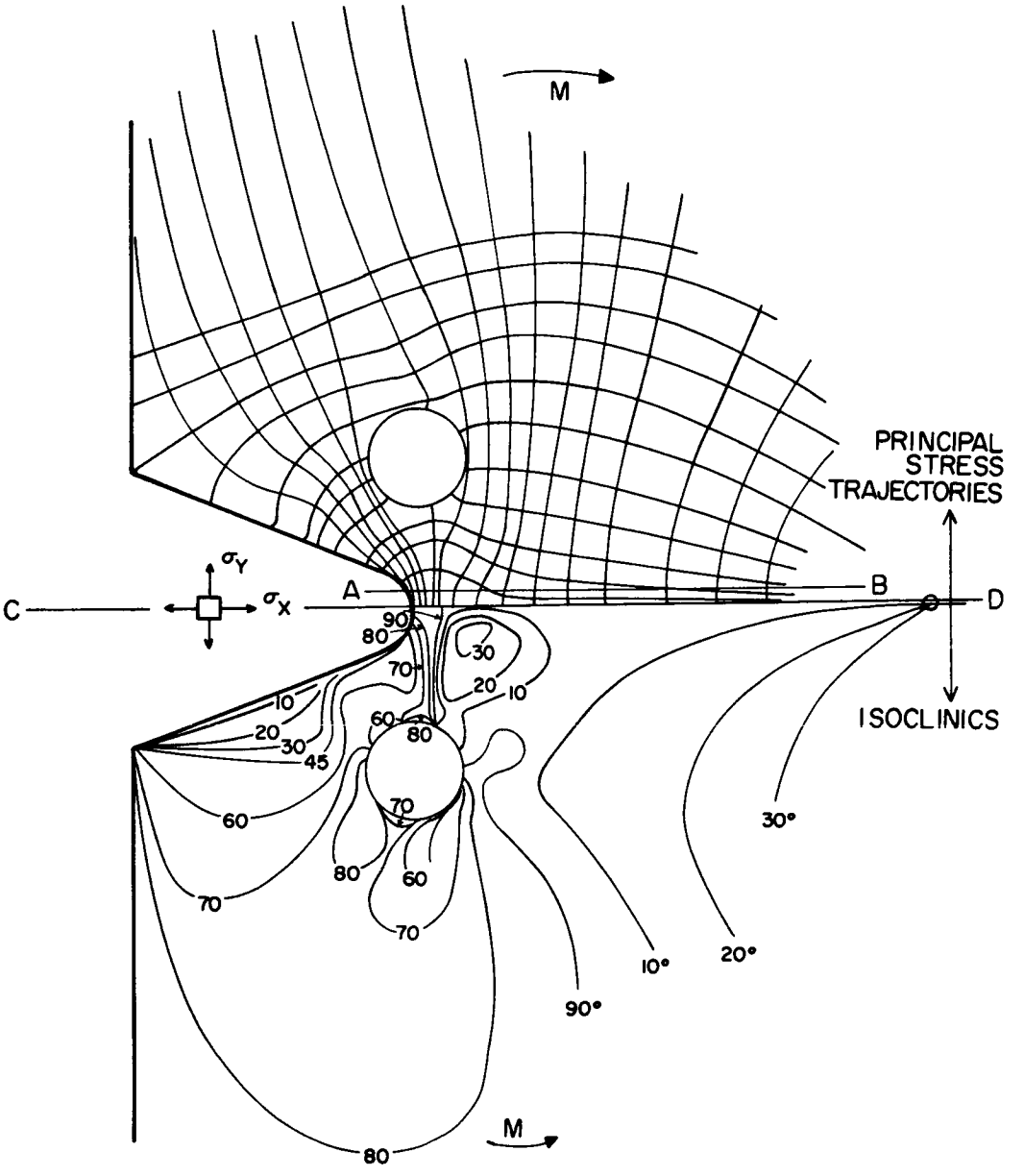

Figure 4.8 The isoclinics and principal stress trajectories (directions) for the Charpy model modified by two holes.

directly by the isochromatics. However, the value of each principal stress can only be determined by employing some additional measurement or calculation. The distribution of longitudinal tensile stress ahead of the notch root is of particular interest because it includes the largest tensile stresses. The "shear - difference" method (integration of an equilibrium condition) was employed to evaluate directly σ_Y and σ_x along the minimum section.

The equilibrium condition can be written in integral form as

$$\sigma_x(x=b) = \sigma_x(x=a) - \int_a^b \frac{\partial \tau_{xy}}{\partial y} dx \tag{4.3}$$

or approximately

$$\sigma_x(x=b) = \sigma_x(x=a) - \sum_{x=a}^{b} \frac{\Delta \tau_{xy}}{\Delta y} \Delta x \tag{4.4}$$

That is, the value of σ_x at point b is just its value at point a, minus the average rate of change of τ_{xy} across the section, times the distance between a and b. Since $\sigma_x = 0$ at the notch root (free surface), all other values of σ_x along CD can be obtained if $\frac{\Delta \tau_{xy}}{\Delta y}$ is evaluated along CD. At any point in the model, the shear stress is given by

$$\tau_{xy} = \frac{\sigma_1 - \sigma_2}{2} \sin 2\theta$$

where θ is the angle the x-axis makes with σ_1. Just above CD, along the section AB (Fig. 4.8), $\sigma_1 - \sigma_2$ can be obtained from the isochromatics and θ from the isoclinics. Moreover, since CD is a plane of symmetry, $\tau_{xy}(y=0) = 0$ and

$$\frac{\Delta \tau_{xy}}{\Delta y} \text{ (Along CD)} \cong \frac{\tau_{xy} \text{ (Along AB)}}{\Delta y} \tag{4.5}$$

The value of σ_x at all points along CD is thus calculated by

(1) dividing CD into segments, (2) evaluating the average τ_{xy} along AB for each segment, and (3) applying equation (4.4) to each segment starting at the notch root where $\sigma_x = 0$. Once σ_x is evaluated, σ_y is obtained directly from the isochromatics because

$$| \sigma_y - \sigma_x | = \sigma_1 - \sigma_2 .$$

The calculations are summarized in Table 4.1 and Figure 4.9.

It should be noted from Figure 4.9 that $(\sigma_1 - \sigma_2)$ and thus the maximum shear stress $\frac{\sigma_1 - \sigma_2}{2}$ go through a minimum, approximately equal to zero, at about two root radii below the notch root. The longitudinal tensile stress σ_y decreases monotonically with distance below the root but shows a plateau associated with the minimum in principal stress difference.

4.5 Calculation of the Total Bending Moment from the Photoelastic Results

In order to obtain a check on the photoelastic results, an approximation to the total bending moment was made from the photoelastic results. The calculation and assumptions concerning the stress distribution are shown schematically in Figure 4.10. Graphical integration of σ_y (from Figure 4.9) was performed between the notch root and the neutral axis. From the Wilson-Stokes theory a longitudinal tensile force of P/3.14 or 24 pounds in this case is produced near the loading point[98]. Equilibrium then requires that the compressive stresses must produce a total resultant force of 142.7 pounds (Figure 4.10). Following Wilson and Stokes, the compressive stress distribution was assumed linear, and the total bending moment (resultant couple produced by these forces) was then calculated from Figure 4.10 to be M = 127.1 inch-pounds.

Table 4.1

Calculation of the Principal Stresses Along the Section of Symmetry for the Drilled Sample Loaded in Three-Point Bending; P = 75.6#, M = 149 in.lb., σ_N = 1400 psi.

Distance from the Notch Root on Charpy	Model	Enlargement	Segment No.	Along Section AB (y = 0.0135") $\sigma_1 - \sigma_3$		θ	Sin 2θ	τ_{xy}	$\Delta x/\Delta y$	$\frac{\Delta \tau_{xy}}{\Delta y}\Delta x$	Along the Section of Symmetry CD σ_x	$\sigma_1 - \sigma_3$	σ_y	Δx Enlargement	Increment Force x 15 t	ΣF x15t	$\frac{\sigma_y - \sigma_x}{\sigma_N}$	$\frac{\sigma_x}{\sigma_N}$	$\frac{\sigma_y}{\sigma_N}$
(in.x10^{-3})	(in.x10^{-3})	(in.)		(Fringes)	(Psi)	(Degrees)		(Psi)		(Psi)	(psi)	(fringes)	(psi)	(in.)	(lbs.)				
0	0	0		13.9	5460	-15	-.500	1342			0	14.9	5760	.025	146	146	4.12	0	4.12
.667	3.33	0.05	1	12.5	4830	-13.5	-.454	1096	.2525	-308	308	13.3	5130	.05	272	413			
1.333	6.67	0.10	2	11.1	4290	-12.0	-.407	872	.2525	-249	557	11.9	4590	.05	257	670	3.28	0.40	3.68
2.00	10	0.15	3	9.65	3725	-10.5	-.358	667	.2525	-194	751	10.5	4050	.05	240	910			
2.67	13.3	0.20	4	8.25	3190	- 9.8	-.334	533	.2525	-152	903	9.1	3513	.05	221	1131	2.51	.65	3.15
3.335	16.65	0.25	5	7.05	2720	- 9.0	-.309	421	.2525	-121	1024	7.65	2953	.05	199	1330			
4.00	20.00	0.30	6	6.05	2340	- 8.0	-.2756	322	.2525	- 93.7	1118	6.50	2509	.05	182	1512	1.79	.80	2.59
4.67	23.3	0.35	7	5.10	1970	- 7.0	-.2419	238	.2525	- 70.5	1188	5.50	2123	.05	166	1678			
5.34	26.67	0.40	8	4.35	1680	- 6.0	-.208	175	.2525	- 52.2	1240	4.70	1814	.05	153	1831	1.30	.89	2.18
6.0	30.00	0.45	9	3.70	1430	- 5.0	-.174	124.5	.2525	- 37.8	1278	4.00	1544	.05	141	1972			
6.67	33.3	0.50	10	3.15	1217	- 3.8	-.131	79.6	.2525	- 25.9	1304	3.40	1312	.075	196	2168	.94	.93	1.87
8.00	40.0	0.60	11	2.30	888	- 1.5	-.052	23.1	.505	- 25.9	1330	2.55	984	.10	231	2399	.70	.95	1.65
9.34	46.7	0.70	12	1.73	668	+ 3.0	+.104	34.7	.505	+ 2.9	1327	1.88	726	.10	205	2604	.52	.95	1.47
10.67	53.3	0.80	13	1.32	510	14.0	.470	120	.505	39.0	1288	1.35	521	.15	271	2875	.37	.92	1.29
13.33	66.7	1.00	14	0.83	321	18.5	.602	96.6	1.01	109	1179	0.75	290	.30	441	3316	.21	.84	1.05
18.67	93.3	1.40	15	0.60	232	22.7	.707	820	2.02	180.5	999	0.50	193	.40	477	3793	.14	.71	.85
24.0	120	1.80	16	0.80	309	18.0	.588	90.9	2.02	175	824	0.65	251	.40	430	4223	.18	.59	.78
29.4	146.7	2.20	17	1.10	425	10.0	.342	72.4	2.02	164	660	1.05	405	.80	852	5075	.29	.47	.76
45.4	226.7	3.40	18	1.25	483	3.0	.104	50.2	6.06	372	288	1.20	463	1.20	901	5976	.33	.21	.54
61.4	306.5	4.60	19	1.00	386	2.0	.070	27.0	6.06	234	54	1.00	386	1.83	805	6781	.28	.04	.31
94.2	472	7.07	20	0.63	241	2.0	.070	16.9	12.5	274	-220	0.62	239	1.28	24	6805	.17	-.16	.01
149.4	747	11.20	21	0+				0	22.1	186.4	-406	0	0				0	-.29	-.29
ρ=.010"	ρ=.050"	ρ=.742"													.490 ΣF x=0	= 118.7#			

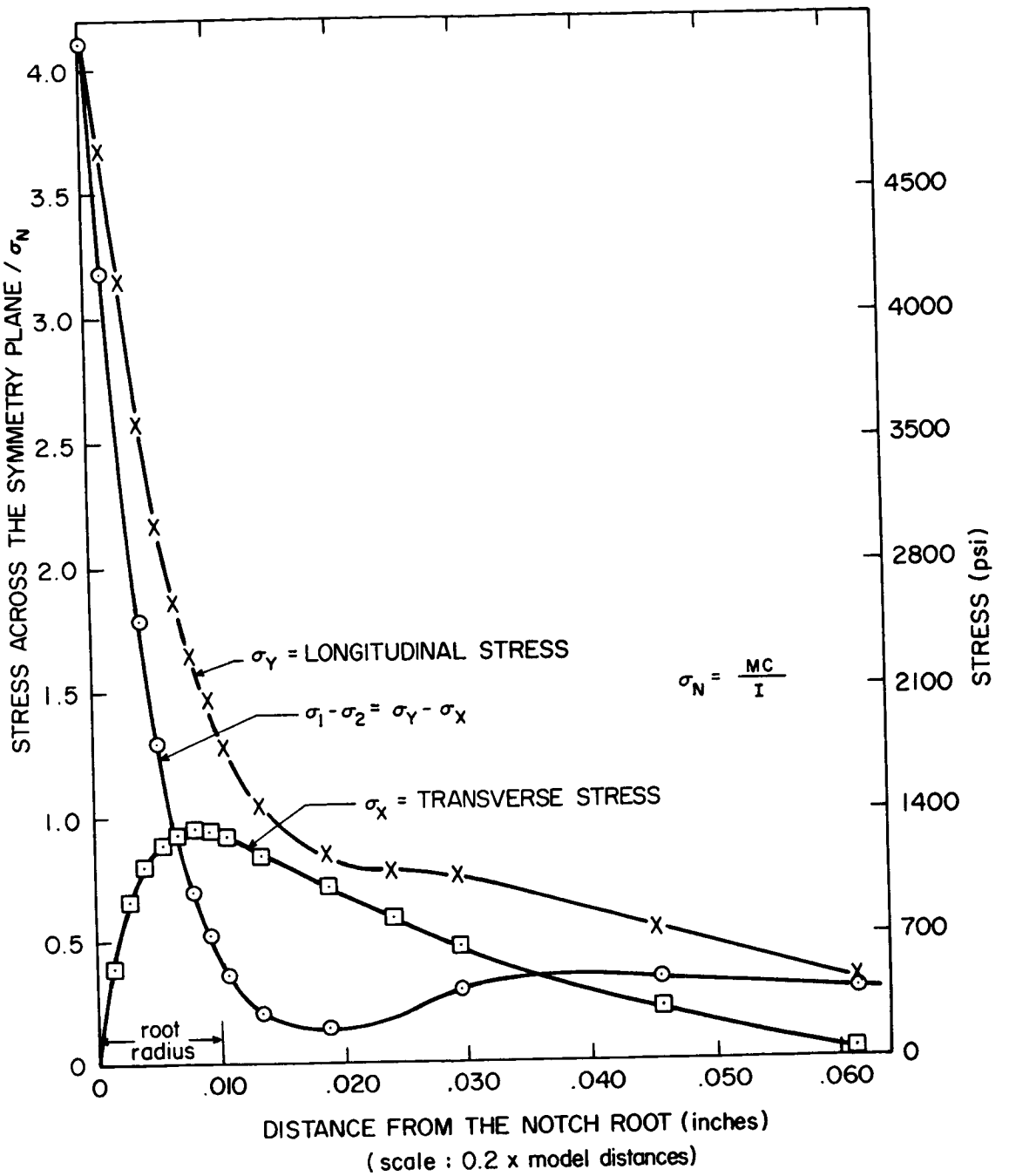

Figure 4.9 The elastic stress distribution below the Charpy notch modified by two drilled holes.

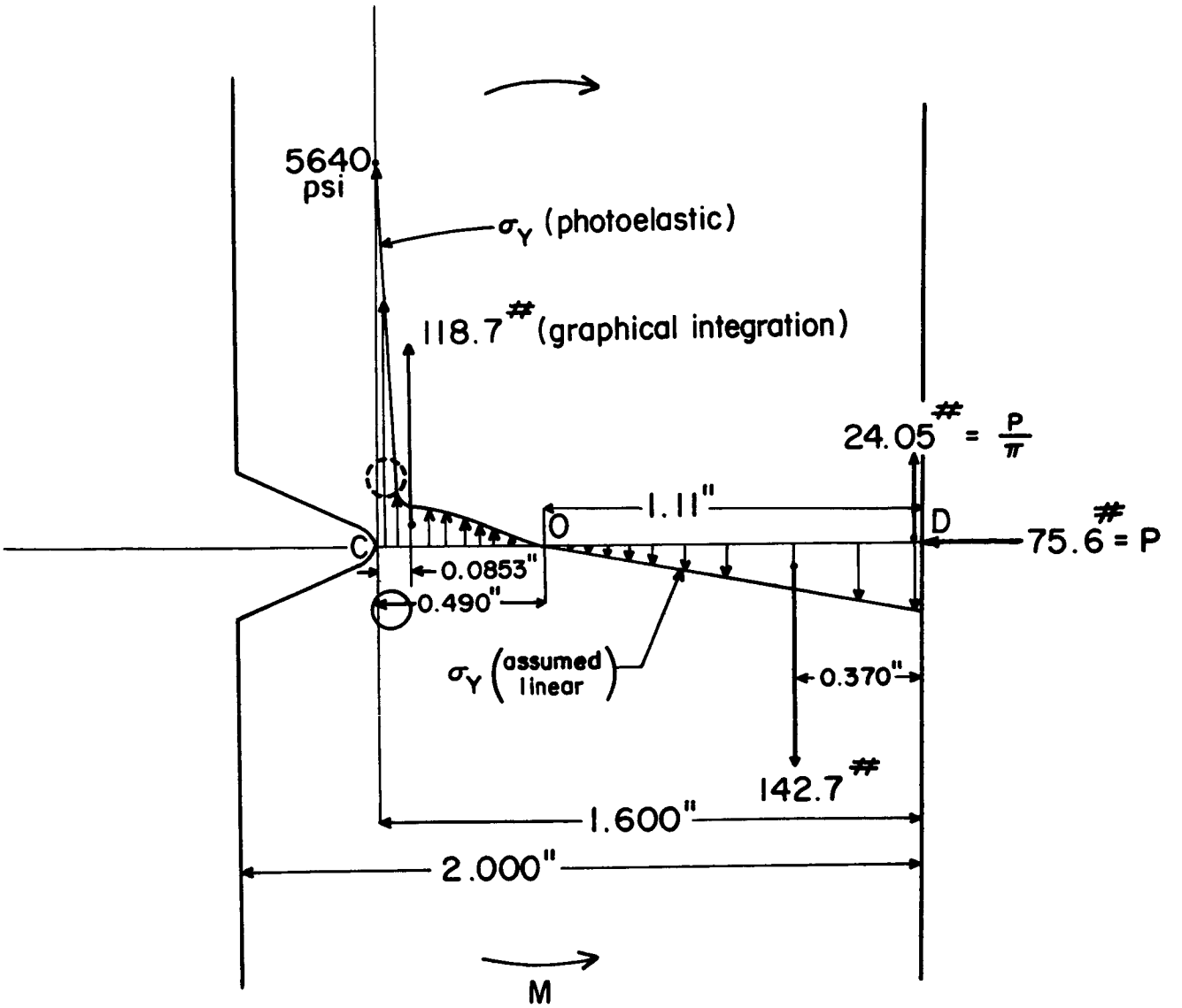

$$M = 24.05^{\#}\,(1.60") - 142.7\,(1.23") + 118.7\,(.0853")$$

$$M = 127.1$$

Figure 4.10 Schematic representation of the stress distribution used to estimate the total bending moment from the photoelastic results.

A slightly better approximation to the compressive stress distribution is given by Timoshenko and Goodier[99]. This slight modification yields M = 127.6 inch-pounds. The actual applied moment was 149 inch-pounds or an error of 14.8%. However, since the applied load is not really a point force but rather distributed over a small region, the 25-pound longitudinal force is actually located further away from the loading edge. This would increase the calculated M and reduce the error. Considering the assumptions made in this calculation, the agreement is acceptable.

4.6 Comparison of Standard Charpy and Drilled Specimens

Comparison of isochromatics in Figures 4.3 and 4.5 indicates that two holes produce local changes in the distribution of shear stress near the notch, but leave the long range distribution unaltered. More specifically, Figure 4.4 shows that in the standard specimen high shear stresses are concentrated near the notch tip. However, the two holes (Figure 4.6) produce regions of high shear stress which extend from the notch tip outward toward the top of both holes. At the same time, Figure 4.11 shows that τ_{max} drops off more rapidly with distance ahead of the notch root when two holes are present.

The elastic stress concentration factor in bending K_σ is defined as the ratio of maximum tensile stress σ^{max} to nominal stress σ_N. That is,

$$K_\sigma = \frac{\sigma^{max}}{\sigma_N} \tag{4.6}$$

where $\sigma_N = \frac{Mc}{I}$ is based on the minimum cross-sectional area. Figure 4.12 compares the stress distributions for the standard and drilled geometries

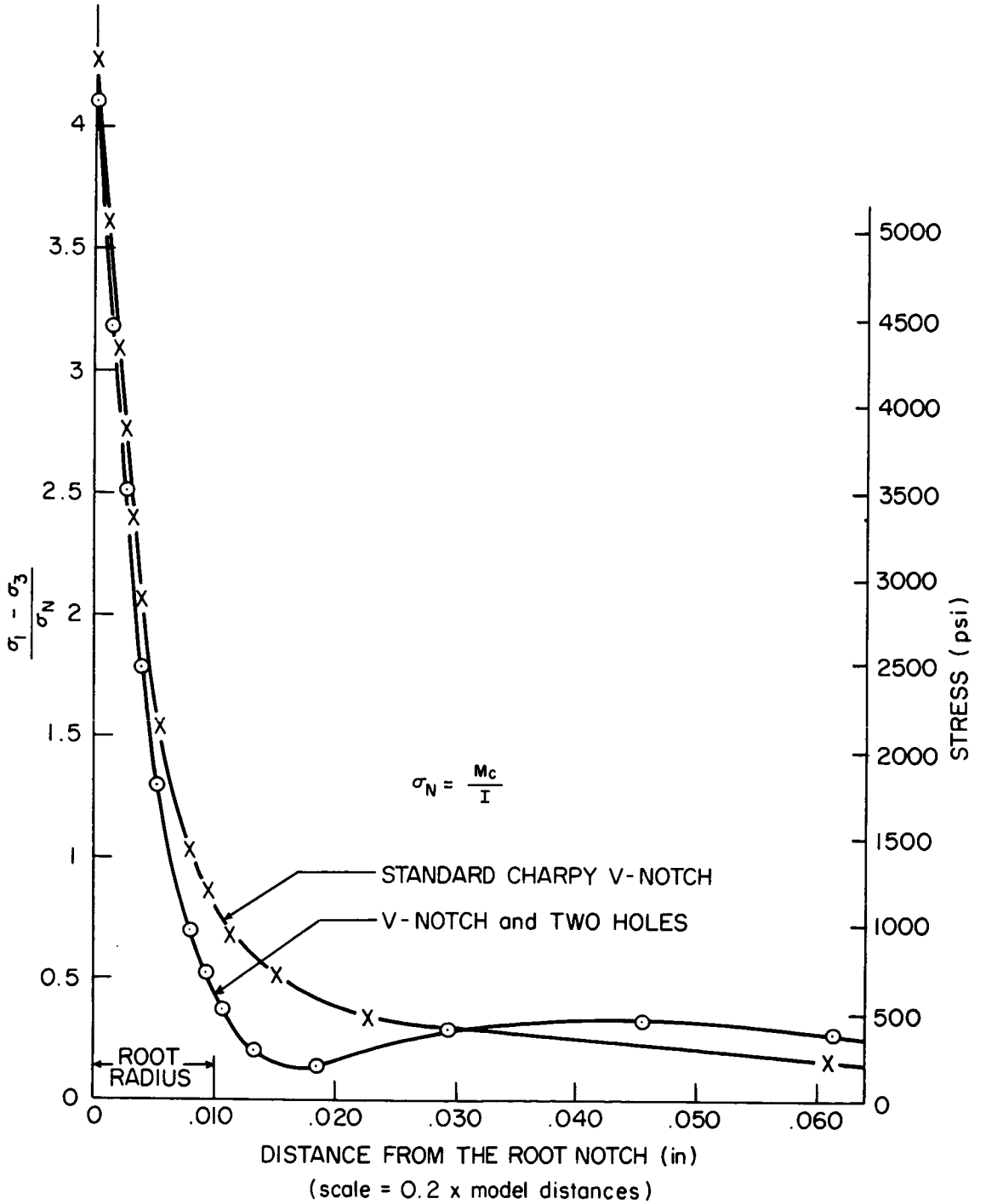

Figure 4.11 The effect of two holes on the principal stress difference (maximum shear stress) ahead of the Charpy notch.

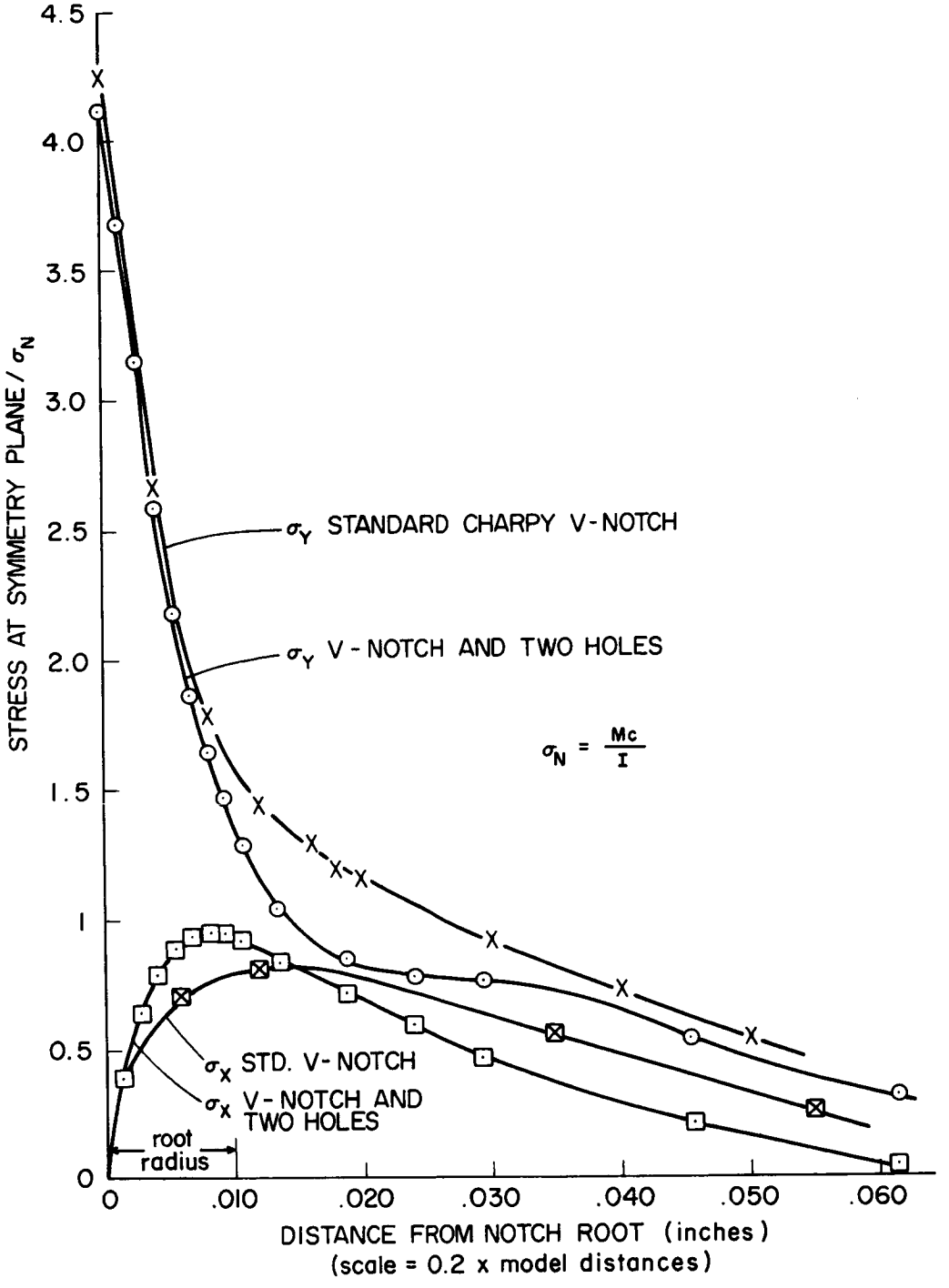

Figure 4.12 The effect of two holes on longitudinal and transverse stresses below the Charpy notch.

which were calculated from the photoelastic results. For the standard Charpy geometry, K_σ was measured to be 4.28. This agrees very well with Neuber's[70] analytical calculation of 4.2. For the geometry containing two holes, $K_\sigma^H = 4.12$, which is a reduction of less than four percent. Thus the two holes do not markedly reduce the elastic stress concentration factor of the Charpy notch. In addition, the longitudinal tensile stresses σ_y drop off only slightly more rapidly with distance ahead of the notch when holes are present.

The observed improvements in notch toughness with hole drilling are, therefore, not simply a result of reducing the elastic stress concentration factor. However, the local redistribution of shear stresses which two holes produce might cause pronounced differences in the local yielding characteristics. This is the topic of the following chapter.

CHAPTER V

CHANGES IN THE PLASTIC STRAIN DISTRIBUTION PRODUCED BY TWO HOLES

In the previous chapter, it was shown that two holes do not significantly reduce the elastic stress concentration factor of the Charpy notch. The observed improvements in notch toughness must therefore result from a modification of the elastic - plastic state which develops as plastic deformation takes place. In order to observe directly the effect of holes on the initial yielding around the notch, dislocation etch-pitting was employed.

Standard and drilled ($R = 0.0448''$, $\theta = 75^{o}$) samples of Fe - 3% Si alloy (FeSi 1, FeSi 2) were loaded at room temperature in three or four-point bending to various fractions of their respective general yield loads. Samples were then aged, sectioned, polished, and etch-pitted to reveal the yielded regions.

5.1 Plane Strain Deformation of Charpy Samples

In the Charpy specimen, deformation prior to general yielding occurs under conditions of primarily plane strain except near the specimen surface. The yield zones of standard and drilled samples were observed in the specimen's mid-plane after loading to varioud loads. Figures 5.1 - 5.5 compare the plastic zones which result with and without holes from loading to 750, 1250, 1750, and 2550 pounds respectively. Deformed specimens were mounted in bakelite and photographed under indirect lighting. As a result, the elastic (undeformed) regions appear dark because light is reflected away by the electropolished surface.

The yielded zones appear white because the irregular surface caused by the high density of dislocation etch-pits reflects light into the microscope. The light specks throughout the elastic regions are simply etched grain boundaries which happen to be oriented to reflect light into the microscope.

A notched specimen remains completely elastic until the applied nominal stress σ_N times the elastic stress concentration factor K_σ exceeds the uniaxial yield stress σ_Y of the material. That is yielding begins when

$$\sigma_N = \frac{\sigma_Y}{K_\sigma} \quad . \tag{5.1}$$

In three-point bending of the Charpy sample, the applied load to cause local yielding P_{LY} is given by

$$\frac{Mc}{I} = \frac{\sigma_Y}{K_\sigma}$$

$$\frac{P_{LY}(0.8)c}{I} = \frac{\sigma_Y}{K_\sigma}$$

$$P_{LY}(\text{lb.}) = 3.9 \times 10^{-3}\ \sigma_Y(\text{psi}) \tag{5.2}$$

For alloy FeSi 2, σ_Y = 78,000 psi, so that yielding should first occur at an applied load of about 300 pounds. In the drilled sample, yielding begins at a slightly higher load due to the small reduction in K_σ. As the load is increased above this value, plastic deformation extends ahead of the notch. However, the plastic zone is surrounded by elastic material until it extends across the entire sample, at the general yield load. The general yield load of the standard sample was measured to be 2280 pounds while that for specimens containing two holes was only 2100 pounds. This reduction of about 8 percent is in itself significant

because it implies a lower average constraint (triaxiality) in the drilled specimen. This will be discussed in more detail in Chapter VI.

Figure 5.1 shows the observed yielded regions, in samples with and without holes, after loading to P = 750 lb. which is approximately 35% of the general yield load. As predicted from the photoelastic results, yielding begins directly below the notch root in both standard and drilled specimens. Initial yielding of standard samples takes the form of the logarithmic spirals predicted from plane strain, slip line field analysis[38]. Of course, the orientation of individual grains around the notch root causes local deviations from the isotropic analysis. In the drilled sample, small amounts of yielding can also be detected between the notch side and the holes although most of it is concentrated at the notch tip.

As the load is increased, the logarithmic spirals increase in size in standard specimen as shown in Figure 5.2a. Some fine slip occurs outside the spirals, but yielding is still confined to the vicinity of the notch tip. Figure 5.2b shows the yield zones of the drilled sample after similarly loading to 1250 lb. or about 57% of the general yield load. In the drilled sample, plastic zones have developed between the notch side and each hole and are also forming below each hole.

Qualitatively, this zone shape corresponds to the distribution of maximum shear stress which was observed in the completely elastic state. For example, Figure 5.3 shows all points where the maximum shear stress, taken from the photoelastic results (Figure 4.5), is at least one-third of τ_{max} at the notch tip. Thus, if the elastic stress field were unperturbed by local yielding, Figure 5.3 would be the exact yield zones after applying a load three times that required to cause first slip at the

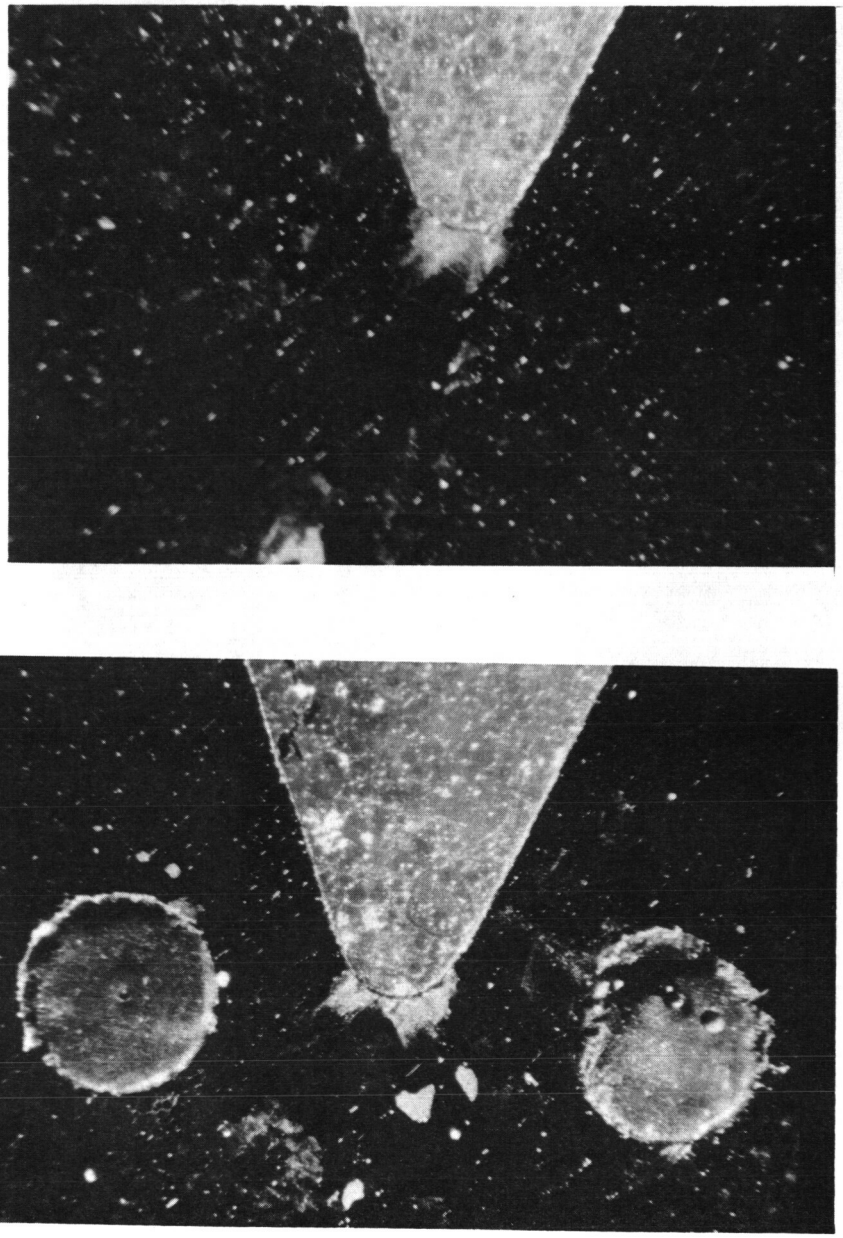

Figure 5.1 The effect of two holes (H_D = 0.0292", R = 0.0448", θ = 75°) on the yield zones produced by loading to P = 750 lb., P/σ_Y = 9.7 (10^{-3} in^2), magnification = 34.4X,

(a) P/P_{GY} = .33 (b) P/P^H_{GY} = .36 .

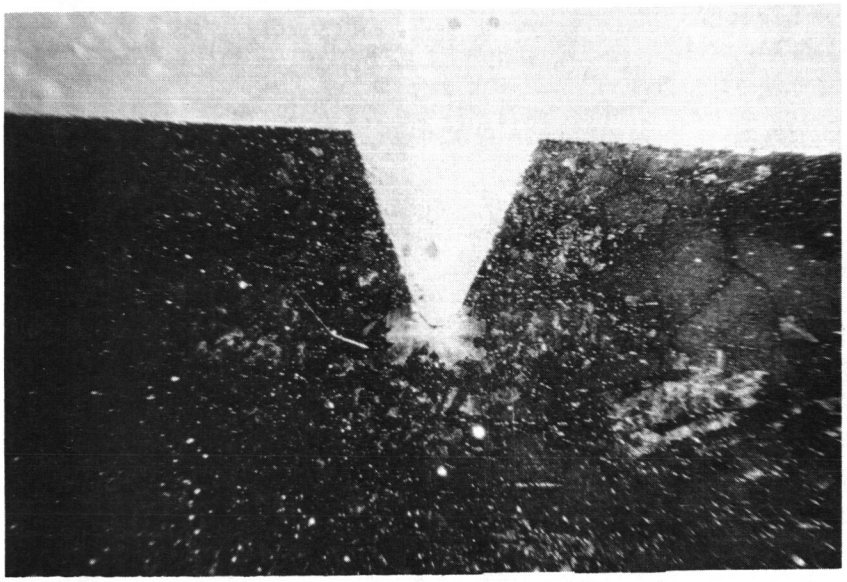

(a)

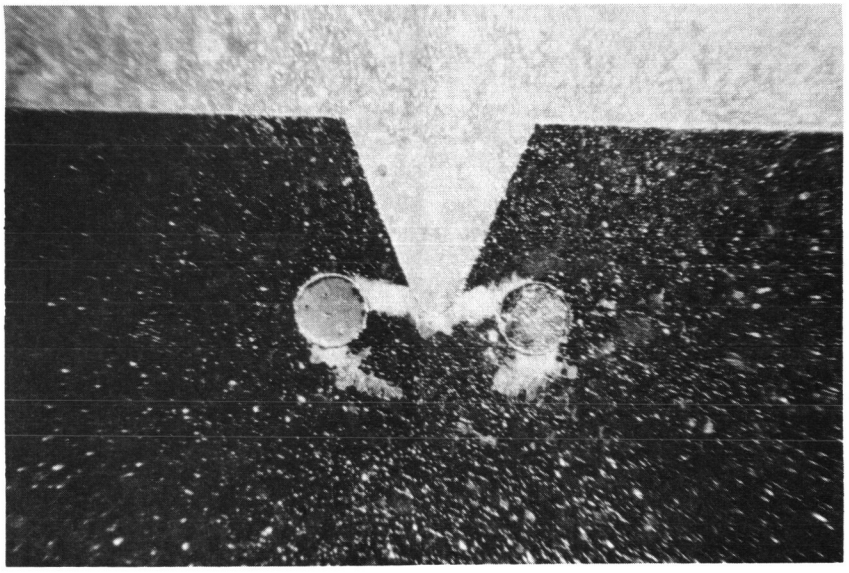

(b)

Figure 5.2 The effect of two holes on the yield zones produced by loading to P = 1250 lb., P/σ_Y = 16.0 (10^{-3} in ^{2}), magnification = 12.7X,

(a) P/P_{GY} = .53 (b) P/P^H_{GY} = .60 .

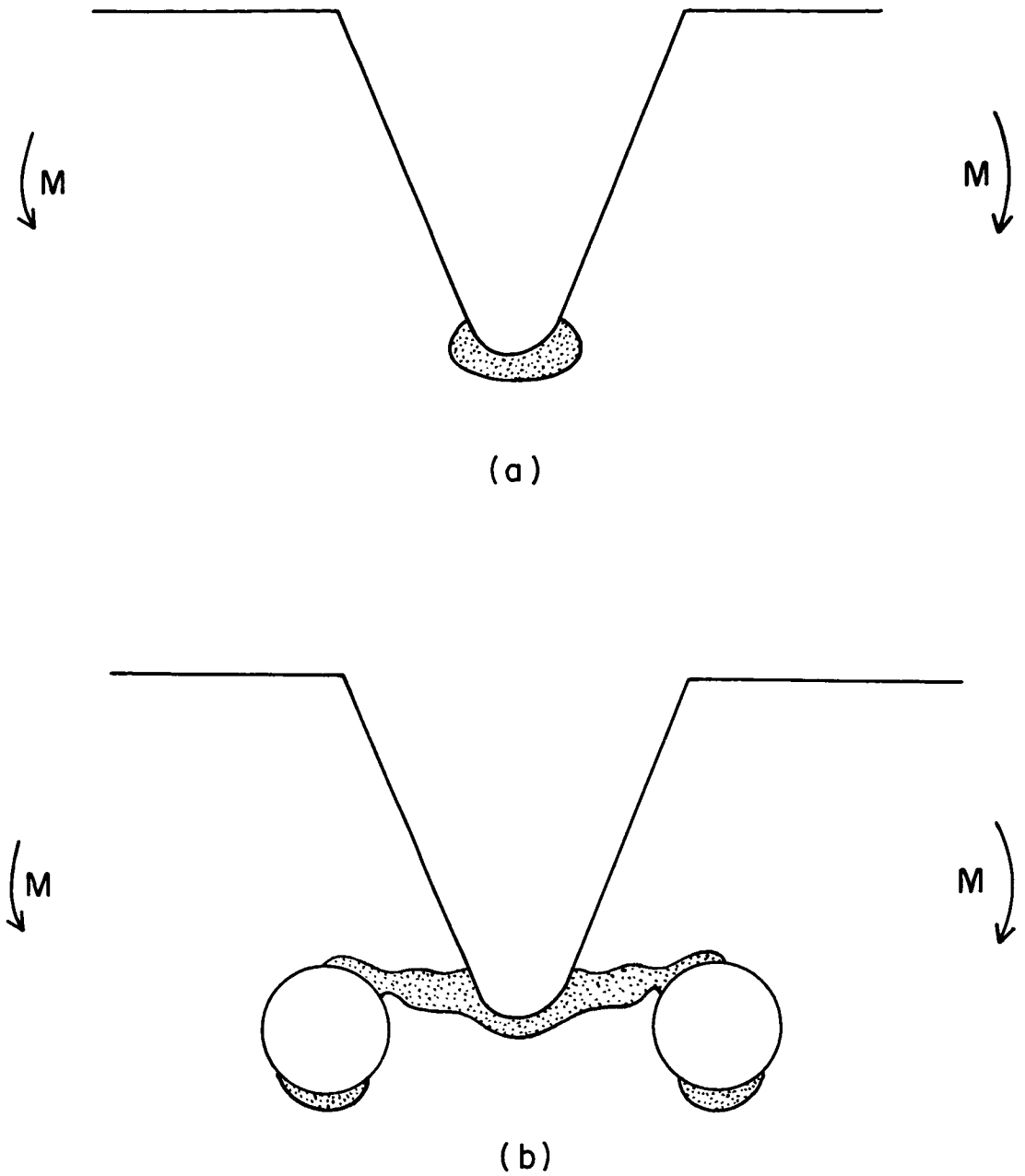

Figure 5.3 The distribution of maximum shear stress in the fully elastic state; shaded regions represent all points where τ_{max} is equal to or greater than one-third of τ_{max} at the notch tip (obtained from Figure 4.5).

notch tip. These regions are strikingly similar to the observed plastic zones of Fig. 5.2, where the applied load is about four times that required for first slip. Therefore, the effect of two holes on initial yielding is very similar to their effect on the elastic distribution of maximum shear stress.

Figure 5.4 compares the yield zones after loading up to 1750 pounds or approximately 80% of the general yield loads. As the applied load on a standard sample is increased from 1250 to 1750 pounds, the total plasticity is no longer confined to a logarithmic spiral, at least in Fe-Si. Instead, plastic hinges, which are characteristic of general yielding, start to form from the existing spiral as shown in Figure 5.4a. In mild steel which shows discontinuous yielding, Wilshaw[54] has shown that hinges do not form until just before general yielding, and the spirals grow to a larger size. However, even when the hinges form and grow, the maximum strain is located at the notch tip, and its magnitude increases continuously with applied load. In the drilled specimen (Figure 5.4b), the maximum strains occur between the notch side and each hole. Consequently, the holes allow a larger total volume of deformation but distribute it more homogeneously around the notch.

The effect of holes on the distribution of local plastic strain is continued when the bars are loaded beyond general yield. Figure 5.5 shows the yield zones at P = 2550 lb. or about 20% above the general yield loads. In the Charpy sample, the plastic hinges span the entire cross-section and plastic wings have started to form between the hinges and the top surface. Up to this load, however, the crack opening displacement (2V(c) = .168 mm) has been accommodated in hinge-type deformation which in turn requires a continuous increase in strain ahead of the root.

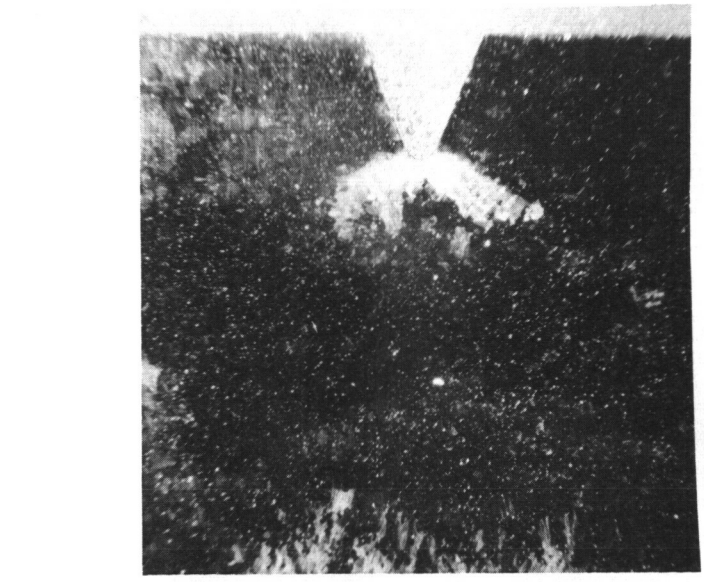

(a)

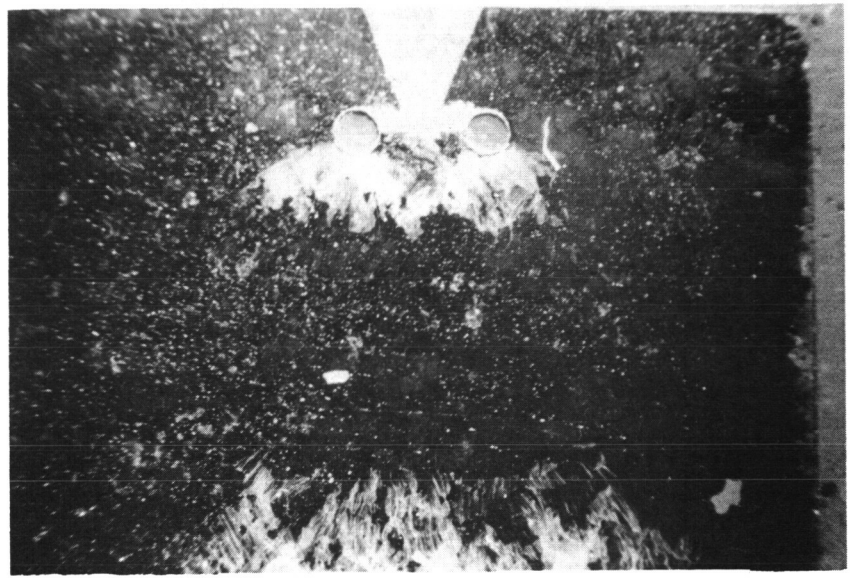

(b)

Figure 5.4 The effect of two holes on the yield zones produced by loading to P = 1750 lb., P/σ_Y = 22.4 (10^{-3} in^2), magnification = 8X,

(a) P/P_{GY} = .75, (b) P/P^H_{GY} = .82 .

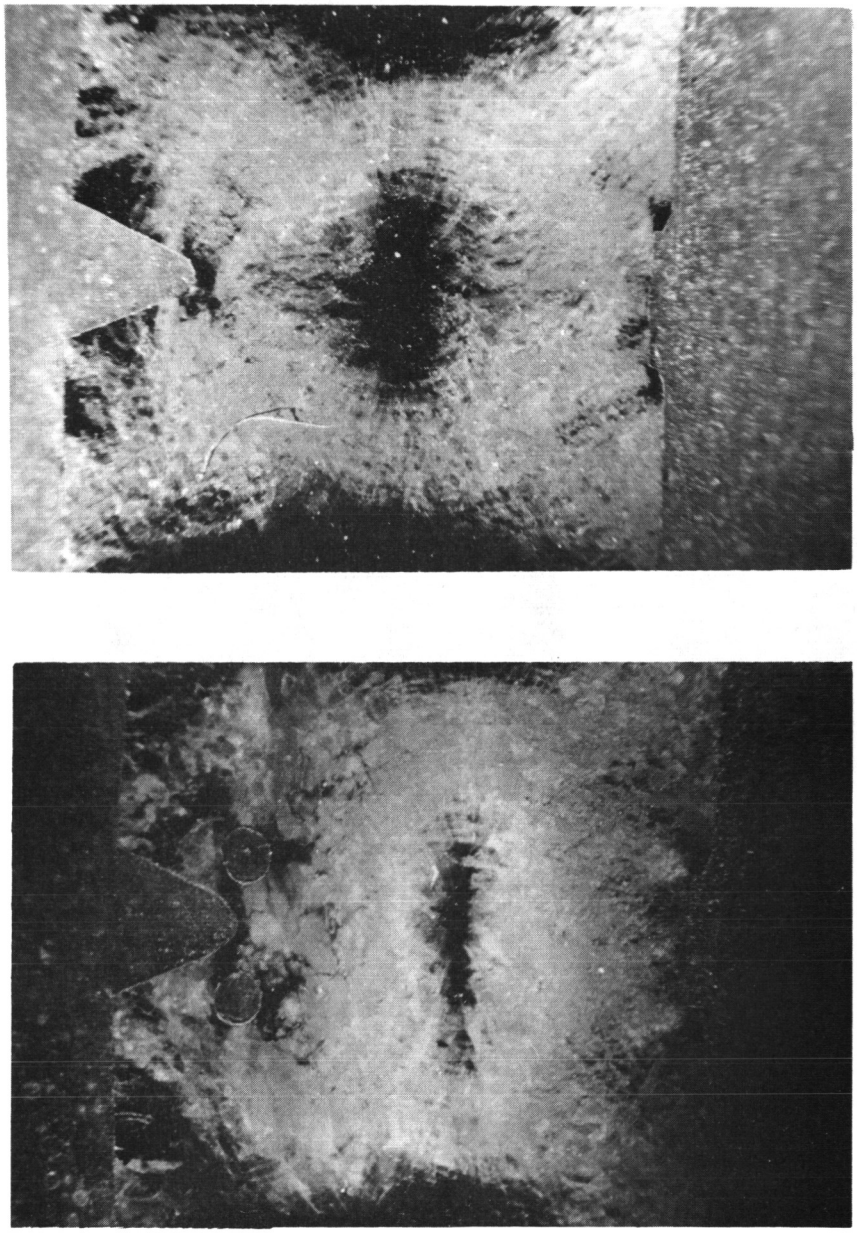

Figure 5.5 The effect of two holes on the yield zones produced by loading to P = 2550 lb., P/σ_Y = 32.7 (10^{-3} in^2), magnification = 8X,

(a) P/P_{GY} = 1.09, (b) P/P^H_{GY} = 1.20 .

Wilshaw[90] has observed an empirical relationship between the crack opening displacement [2V(c)] and the plastic strain (ϵ_{yy}) at a distance x below the Charpy notch,

$$\epsilon_{yy}(x) = \frac{8\,[2V(c)]}{x} \quad . \quad \begin{matrix} x > 0.1 \text{ mm} \\ V(c) \text{ in mm} \end{matrix} \qquad (5.3)$$

Equation (5.3) may be used to estimate the maximum strain resolvable by dislocation etch-pitting[91, 92] in alloy FeSi 2. In Figure 5.5a, the dark region directly below the notch contains strains too high to be resolved. Substituting 2V(c) = .168 mm, x = .3 mm, the maximum strain resolved is 4.5 percent, which is in agreement with measurements by other workers[84].

In the drilled sample (Figure 5.5b), the same load of 2550 lbs. produces a 2V(c) = 0.333 mm. In spite of this larger total displacement, the holes have maintained much lower strains below the notch. For example, in Figure 5.5b, the point where etch-pit resolution begins is defined as x = 0.137 mm, 2V(c) = 0.333 mm, ϵ_{yy} = 4.5%. For the same distance x and V(c), equation (5.3) predicts that the strain in an undrilled sample would be

$$\epsilon_{yy}(x = 0.137 \text{ mm}) = \frac{8\ (0.333)}{0.137} = 19.5\% \ .$$

Consequently, at this one point below the notch, holes reduce the strain concentration by more than a factor of four by redistributing the plastic strain. This reduction is achieved because the displacement is accommodated by plastic hinges that originate at the notch side rather than the notch tip. Regions of high strain are not eliminated but rather relocated at the notch sides where the tensile stresses are lower.

5.2 Variation of Yield Zones from Specimen Surface to Center (Plane Stress to Plane Strain)

A similar series of standard and drilled four-point bend samples (0.365" thick) were loaded to various fractions of their general yield load. The plastic zones were observed on the surface (plane stress), at the midsection (plane strain) and midway between the two (75% through the total thickness). In this way, the effect of two holes on the three-dimensional form of the localized yielding could be characterized.

Figure 5.6 shows the various sections after loading to 50% of the general yield load. Along the midsection (5.6 e, f), the plane strain plastic zones are very similar to those observed in the previous three-point bend samples. At 75% of the thickness (Fig. 5.6 c, d) the zones are the same implying that deformation is still occurring under conditions of plane strain. The surface zones (Figure 5.6a, b) are, however, more diffuse in both the standard and drilled sample. This reflects that some through-the-thickness or plane stress type deformation is occurring near the free surface.

Figure 5.7 shows similar sections after loading to 71% of general yield. The effect of holes on the deformation zones at the midsection are again consistent with those observed in three-point bending. The surface zones are more diffuse, but even there holes have prevented strain concentration at the notch tip. Figure 5.7(e) shows a section in which etch-pitting was incomplete although the same sample etched normally in other sections. Apparently, this behavior results from variations in the amount of carbon in solid solution, which is available to decorate the dislocations. The exact cause of such variations ("banding") is not completely understood.

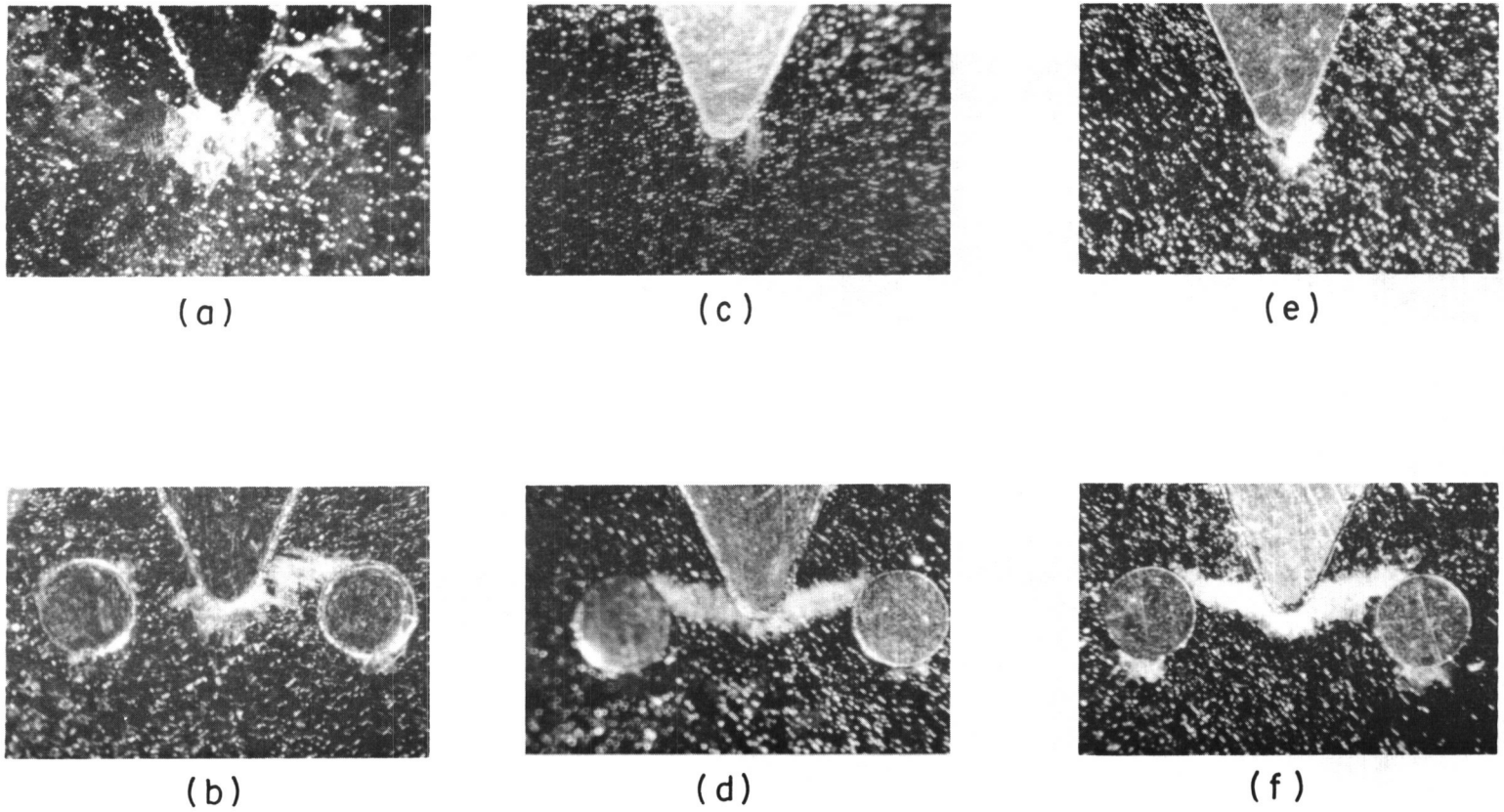

Figure 5.6 The variation of the plastic zones from specimen surface to midsection in both standard Charpy and drilled samples after loading P/P_{GY} = 0.50 in four-point bending; magnification = 18X; (a), (b) surface; (c), (d) midway between the surface and midsection; (e), (f) midsection.

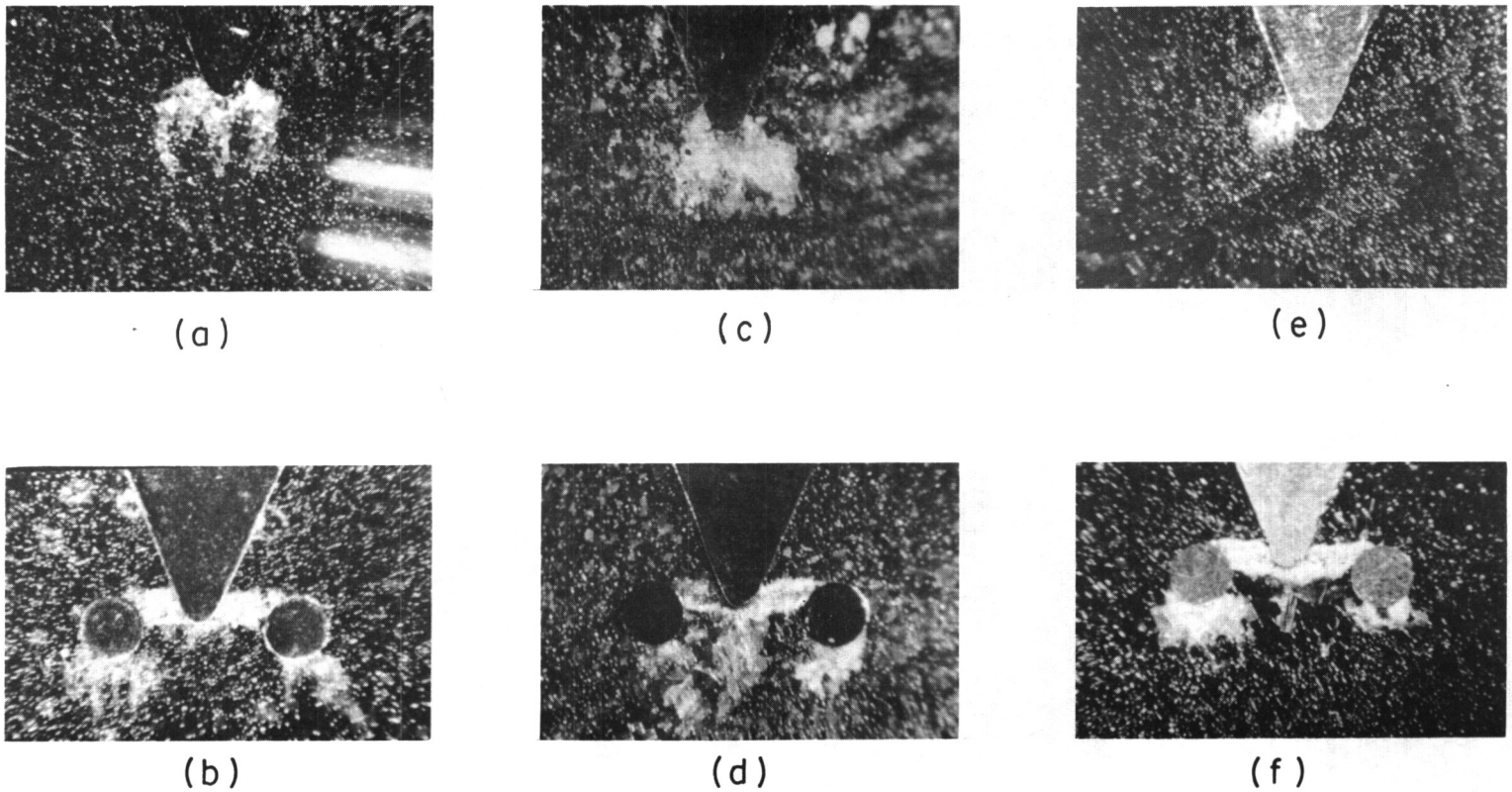

Figure 5.7 The variation of the plastic zones from specimen surface to midsection in both standard Charpy and drilled samples after loading to $P/P_{GY} = 0.715$ in four-point bending; magnification = 18X; (a), (b) surface; (c), (d) midway between the surface and midsection; (e), (f) midsection. Note: The etching is incomplete in (e).

Figure 5.8 shows a section parallel to the top surface and just below both holes in a sample loaded to 91% of general yield. This micrograph reveals that from the midsection to about .070" from the surface, the deformation ahead of each hole is normal to the micrograph (plane strain). Between the sample surface and a depth of .070", shear zones at 45^{o} to the surface and in the plane of the micrograph are noted. In this region, at least part of the total deformation occurs through the thickness thus encouraging conditions of plane stress. This is also consistent with the more diffuse plastic zones which are observed on the surface.

5.3 Strain Distribution within the Local Plastic Zones of Drilled Samples

It has been shown that two drilled holes allow a given displacement to be accommodated by plastic zones which do not require such high strains at the notch root. Also of interest are the relative magnitudes of the plastic strain within various portions of the plastic zone. As an illustration, consider the plane strain zone shown in Figure 5.9a for a drilled four-point bend sample loaded to 91% of general yield. Although yielding begins at the notch tip (Figure 5.1b), increases in load do not cause the plastic zone to extend below the notch. This is quite evident at the higher magnification of the notch root shown in Figure 5.9b. The plastic strains quickly decrease from about 5% at the notch root to zero at one root radius away.

A similar micrograph of the zone between the notch side and one hole (Figure 5.9c) reveals that strains exceed 5% at the notch side and the back of the hole. The strain midway between the notch and the

Figure 5.8 A section parallel to the notched surface revealing the plastic zones just below both holes in a sample loaded to P/P^{H}_{GY} = .91 in four-point bending; magnification = 15X.

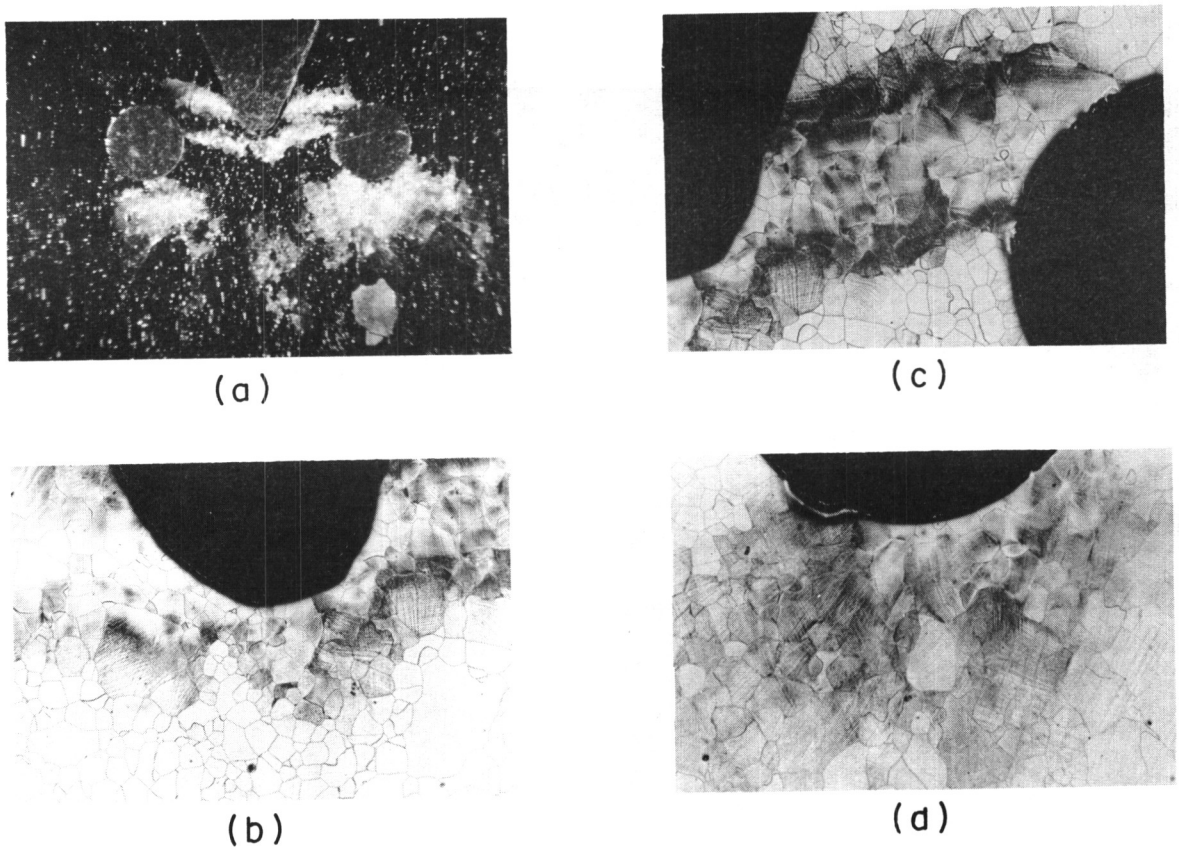

Figure 5.9 Various portions of the plane strain (midsection) plastic zone of a drilled sample loaded to P/P^{H}_{GY} = .915 in four-point bending;

(a) Entire notch region, magnification = 13.8X;
(b) The notch tip, magnification = 67X;
(c) Between the notch (left) and hole (right), magnification = 67X;
(d) Below one hole, magnification = 67X.

hole is somewhat less than 5% and still sensitive to etch-pitting. The plastic zone on the lower side of one hole is shown in Figure 5.9d. The strain at this side of the hole also exceeds 5% and drops off gradually with distance below the hole into a homogeneous plastic zone.

5.4 Summary

Two holes produce marked changes in the distribution of plastic strain around the Charpy notch. Yielding begins at the notch root in both standard and drilled samples, and holes have little effect on the initial plastic zone for loads up to 0.35 P_{GY} (i.e., $P/\sigma_Y < 10.5 (in^2 \times 10^{-3})$). With increasing load ($P > 0.35\ P_{GY}$), holes concentrate plastic deformation between the notch side and each hole and away from the notch tip. Consequently, with increasing applied load, two holes produce a larger relative reduction in the strain concentration below the notch. Moreover, in drilled samples, the regions of high strain, in order of decreasing strain, are (a) notch sides, (b) top of the holes, (c) below the holes and (d) the notch tip. This order is maintained even above general yielding when the strains become very large.

CHAPTER VI

THE EFFECT OF TWO HOLES ON THE LOAD CARRYING CAPACITY OF NOTCHED BARS

Two appropriately drilled holes have been shown to markedly reduce the Charpy impact transition temperature. This improvement results from the redistribution of plastic strain around the notch which was defined in the previous chapter. Associated with the modified plastic zones are corresponding changes in the local stress distribution which in turn determines the load carrying capacity of a notched bar. To determine the specific improvements in notch strength possible with two holes ($R = 0.0448"$, $\theta = 75^{o}$) Charpy bars were tested at temperatures across the transition region in slow-bend and instrumented impact-bending. From a knowledge of the material's properties, the fracture results can be used to indirectly determine the state of stress and strain in the standard notched and drilled bars. The effect of holes on the notch strength of sheet tension samples was also obtained to establish the generality of the effect.

6.1 Slow Bend Tests

Steel 0.025 was selected for these tests because the impact results had previously been obtained (Chapter III). Standard Charpy and drilled samples of optimum geometry ($R = 0.0448"$, $\theta = 75^{o}$) were tested to failure in three-point bending at various temperatures between $-196^{o}C$ and $-80^{o}C$. The results are summarized in Figure 6.1. The behavior of standard samples is similar to that observed by Knott and Cottrell[41] in low carbon, nitrogen steel. The absence of a large rise in fracture

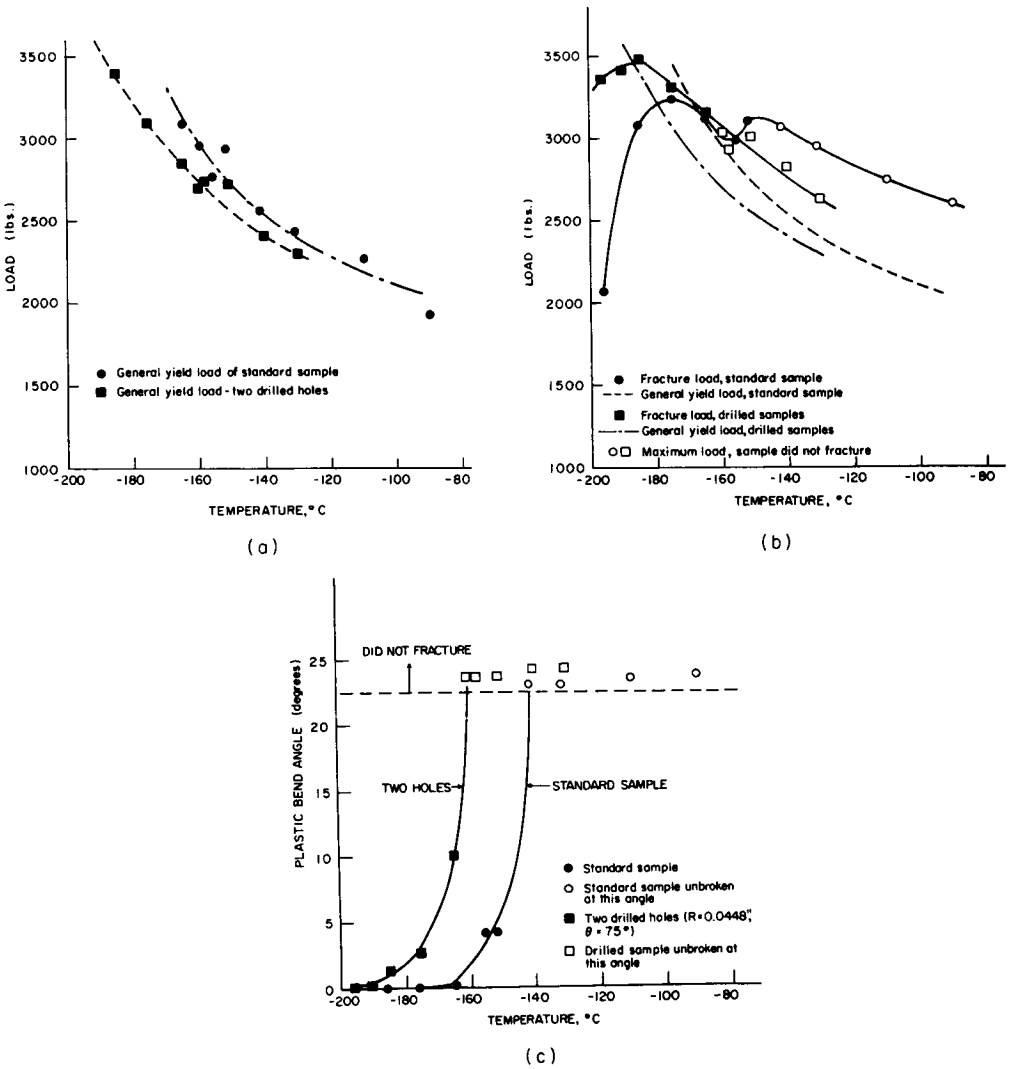

Figure 6.1 The effect of two drilled holes (H_D = 0.0292", R = 0.0448", $\theta = 75^{\circ}$) on the fracture properties of steel 0.025 tested in slow-bending;

(a) General yield load
(b) Fracture load
(c) Plastic bend angle at fracture.

load, which is usually observed in pearlitic steels when failure occurs well after general yielding, is believed to result from this alloy's low strain hardening rate.

There are four effects of the holes which should be noted.

(1) Drilled samples have considerably greater (up to 70% in these tests) load carrying capacity than standard samples at low test temperatures where both samples fracture by cleavage prior to general yielding [Figure 6.1(b)].

(2) There is a temperature range of approximately $20^{o}C$ during which standard samples fracture by cleavage at bend angles below 5^{o}, but drilled samples do not fracture at the maximum bend angle of 24^{o} imposed by the jig. Figure 6.1(c) shows quite clearly the shifting of the transition curve of drilled specimens to a lower temperature.

(3) The general yield load of drilled samples is 5 - 10% lower than standard samples throughout the entire transition temperature range [Figure 6.1(a)]. This is consistent with the 8% reduction which was observed in the Fe-3% Si samples in Chapter V.

(4) At high temperatures where neither sample failed, the ultimate (maximum) load of drilled samples was somewhat lower (10%) than that of the Charpy specimen.

6.2 Instrumented Charpy Impact Tests

In Chapter I, it was pointed out that increased strain rate modifies the transition behavior of notched bars. First, the transition curve is raised to higher absolute temperatures ($\sigma_y^* \uparrow$), and secondly, the transition region between first slip and general yielding is extended

over a wider temperature range ($d\sigma_Y^*/dT\downarrow$). Since both of these characteristics facilitate a more detailed study of the transition region, the instrumented impact test was used extensively to evaluate the effect of two holes on fracture strength.

6.2-1 Materials

Mild steel 0.24 was used to study the effect of holes on the fracture strength of impacted samples. The microstructure (Figure 2.2) and composition (Table 2.1) of this commercial mild steel were described in Chapter II. Some of the uniaxial stress strain curves which were obtained under static conditions ($\dot{\epsilon} = 0.4\ min^{-1}$) and at selected temperatures are shown in Figure 6.2, and the variation of lower yield stress with temperature is summarized in Figure 6.3.

Because the dynamic yield stress will be required in future calculations, it was estimated from the general yield load of impacted samples. Rewriting the theoretical relationship derived by Green and Hundy[39] that was given by equation (1.26)

$$\sigma_Y^* \text{ (psi)} = 33.3\ P_{GY}\text{(lb.)} \ . \qquad (6.1)$$

The dynamic yield stress (σ_Y^*), calculated by means of equation (6.1), at temperatures between -50 and +100°C is shown in Figure 6.3. There is, however, considerable uncertainty about the exact meaning of σ_Y^* calculated in this way. First, equation (6.1) is strictly valid only for an ideally plastic material, where the yield stress is equal to the flow stress at all values of strain. Since there is a strain gradient from the notch tip along the plastic hinges, σ_Y^* is actually an average flow stress over the varying strains along the plastic hinges. Equation

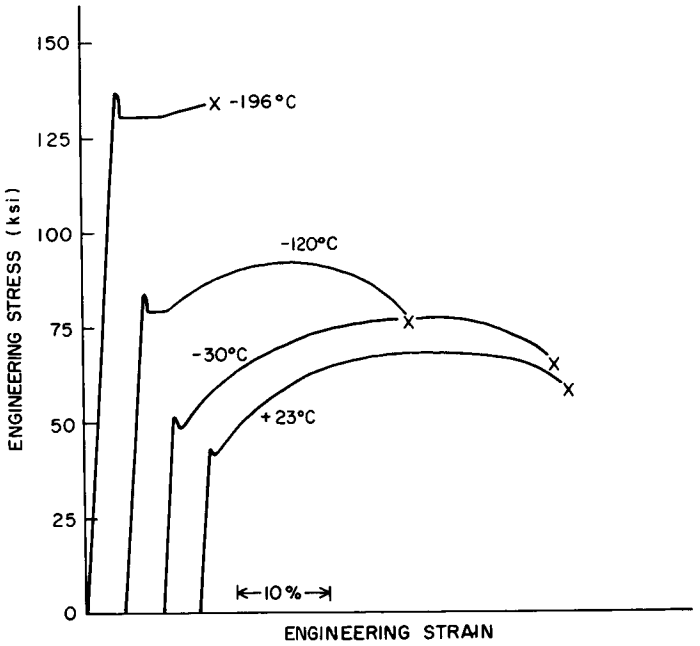

Figure 6.2 Uniaxial stress-strain curves for steel 0.24 tested at various temperatures ($\dot{\epsilon}$ = 0.4 min^{-1}).

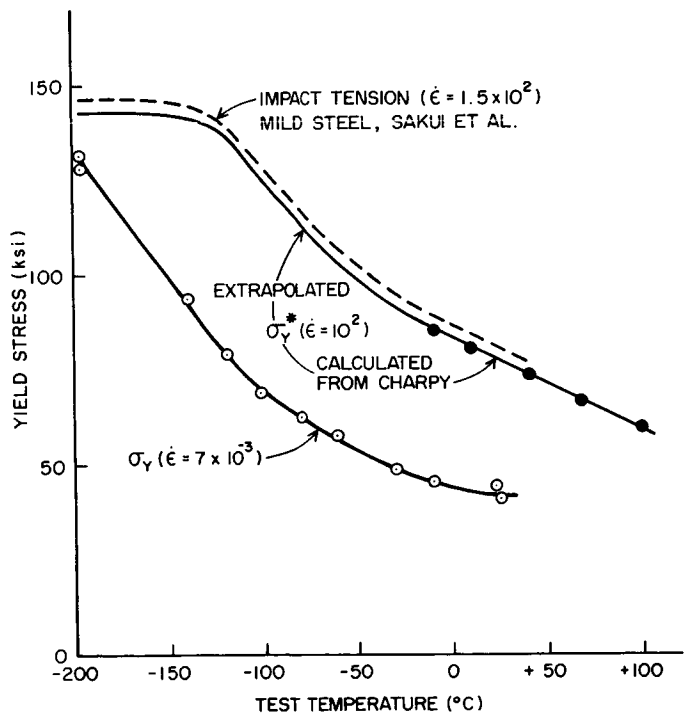

Figure 6.3 The variation of the uniaxial yield stress of steel 0.24 with test temperature under static ($\dot{\epsilon}$ = 0.4 min^{-1}) and dynamic ($\dot{\epsilon}$ = 10^2 sec^{-1}) conditions.

(6.1) therefore overestimates σ_Y^* by increasing amounts as the initial work hardening rate increases. Secondly, for a constant applied deflection rate, there is a gradient of strain rate below the notch and a corresponding variation in the local yield stress. Consequently, the controlling or average strain rate is uncertain. Experimental observations of Sakui et al[37] and Wilshaw[54] indicate that σ_Y^*, calculated from the Charpy impact P_{GY} (17 ft./sec.) by equation (6.1), corresponds to σ_Y^* measured uniaxially at a strain rate of $\dot{\epsilon} \cong 10^2$ sec^{-1}.

At temperatures below -50°C, Charpy samples failed prior to general yielding so that σ_Y^* had to be obtained in some other way. Using the impact tensile results ($\dot{\epsilon} = 1.5 \times 10^2$) of Sakui et al[37] for a similar mild steel, σ_Y^* was extrapolated as shown in Figure (6.3). The sharp decrease in the temperature dependence at -120°C results from a change in yielding mode from slip to twinning. In general, the temperature range at which twinning becomes the dominant deformation mode varies strongly with grain size; but since steel 0.24 had the same grain size as Sakui's, σ_Y^* was extrapolated in the same manner. Krafft[35] and Krafft et al[103] have also reported similar strain rate-temperature sensitivity for the dynamic yield stress of mild steels.

6.2-2 Fracture Results for Steel 0.24

Standard and drilled (R = 0.0448", $\theta = 75^\circ$) Charpy samples of steel 0.24 were impacted at temperatures ranging from -196 to +100°C. During each test, the load-time trace was recorded (as described in Chapter II), and some typical load-time traces are shown in Figure 6.4. Figure 6.5 summarizes, as a function of test temperature, the measured impact energy and the corresponding general yield, ultimate, and fracture

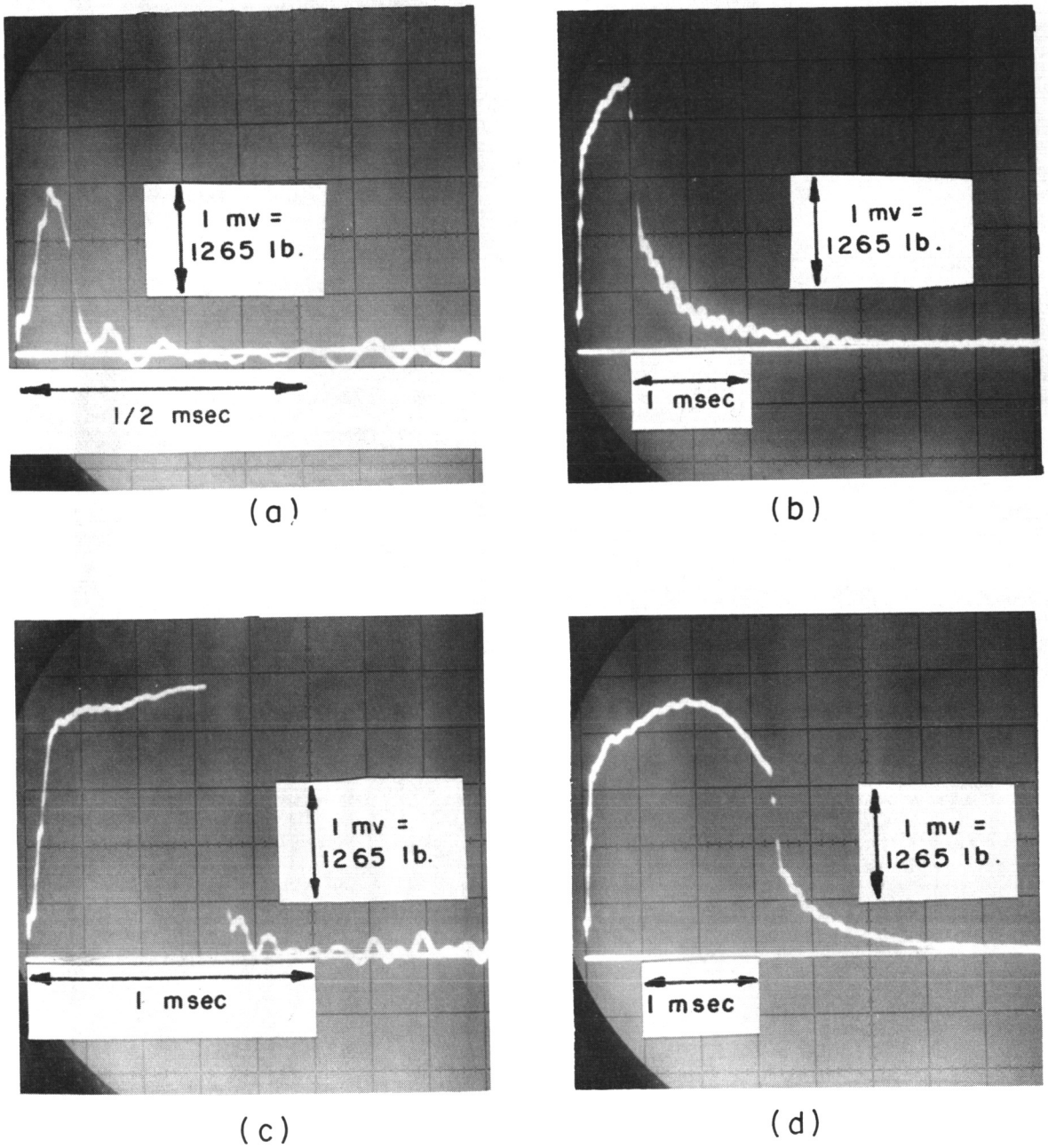

Figure 6.4 Some typical instrumented Charpy, load-time recordings for standard and drilled samples of steel 0.24;

(a) Standard Charpy, T = -37°C
(b) Standard Charpy, T = +27°C
(c) Drilled Charpy, T = -37°C
(d) Drilled Charpy, T = +27°C

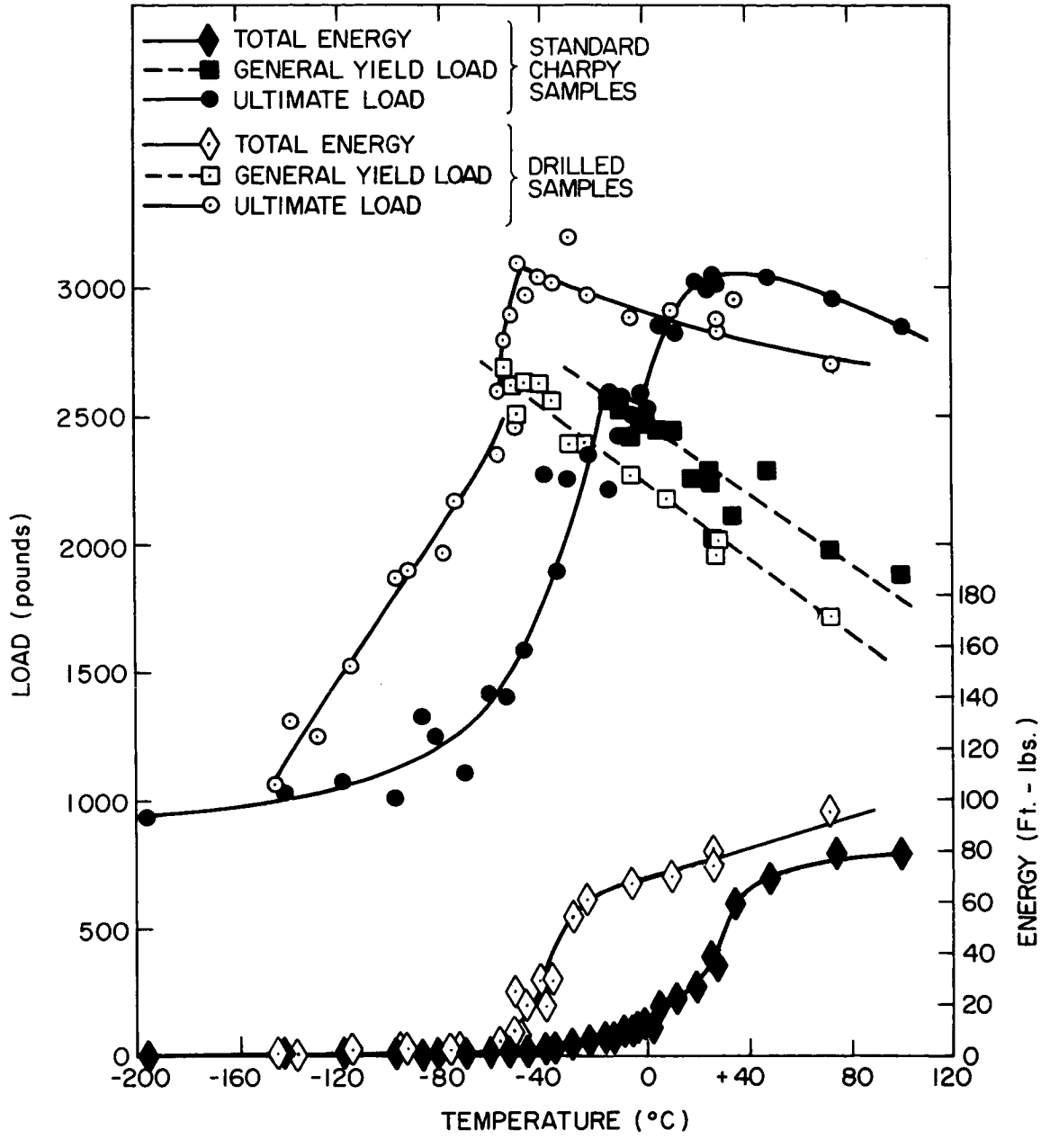

Figure 6.5 Instrumented Charpy fracture results for standard and drilled (H_D = 0.0292", R = 0.0448", $\theta = 75^{\circ}$) samples of steel 0.24 as a function of test temperature.

load obtained from the load-time curves.

Standard Charpy Samples

At temperatures below $T_D = -15^oC$, cleavage occurs prior to general yielding (Figure 6.4a), but it requires increasingly higher loads (P_F) as the nil-ductility temperature is approached. The impact energy recorded on the machine is approximately proportional to P_F in this range, but energy alone cannot be used to define P_F due to the experimental error in its measurement.

Above the nil-ductility temperature $T_D = -15^oC$, cleavage occurs only after the "plastic hinges" have traversed the entire sample ($P_F > P_{GY}$). Since plastic constraint does not increase after general yield and σ_Y^* decreases with increasing temperature, increasing amounts of work hardening are required to locally produce the cleavage stress σ_f. Since strain is still concentrated at the notch tip, the critical notch displacement [V*(c)] and measured total energy increase quite slowly with temperature above T_D. At the ductility transition temperature of $T_N = +10^oC$, there is a sharp increase in the notch displacement (time) which is required to produce σ_f locally. In fact, at temperatures above T_N, the required displacement to produce σ_f is so high that fibrous tearing occurs at the notch root before it is obtained. In steel 0.24 then, the initiation mode transition temperature T_S is approximately equal to T_N and is marked by a sharp rise in both the fracture load and impact energy.

At temperatures just above $T_N = T_S = 10^oC$, the fibrous tear acts as a sharpened notch, and the increased strain rate and triaxiality causes nucleation of a fast-running, cleavage crack. At still higher

temperatures ($T > 30^{o}C$), the fibrous tear extends through the entire thickness (at ultimate load) and causes plastic instability before cleavage initiates. The energy continues to increase with temperature above this point although the ultimate load decreases as σ_Y^* does. At still higher temperatures ($T > 65^{o}C$), σ_Y^* is so low that cleavage cannot be initiated even in front of the sharpened tear. Failure then occurs completely by fibrous tearing, and the energy (shelf energy) remains approximately constant with increasing temperature.

Drilled Charpy Samples

The effect of two drilled holes on the load carrying capacity of Charpy samples varies markedly with temperature.

(1) At very low temperatures ($T < 140^{o}C$), drilled samples are less than 10% stronger than standard Charpys. Fracture occurs by 100% cleavage at less than 30% of the extrapolated P_{GY}. The photoelastic results of Chapter IV show that holes do not reduce the elastic stress concentration factor markedly. In addition, dislocation etch-pit results (Chapter V) show that two holes produce only small changes in the size and location of the plastic zone for loads less than 35% of P_{GY} (see Figure 5.1). Therefore, when fracture occurs on or soon after initial yielding at the notch tip, very little improvement results from hole drilling.

(2) At temperatures above $-140^{o}C$, the fracture strength of drilled samples increases much more rapidly with temperature than does the strength of standard samples. At temperatures up to $-60^{o}C$, both standard and drilled samples fail prior to general yielding, but the load carrying of drilled samples is up to 70% higher than standard

Charpys. In this temperature range, the fracture path in drilled samples may include one hole or neither hole with similar improvements observed in either case. Fracture initiation occurs directly by cleavage except in some drilled samples which fail just prior to general yield. In these cases, a fibrous tear may form between the notch and one hole, but cleavage is initiated directly on the opposite side of the hole.

(3) Fulfillment of the fracture criteria locally requires general yielding of drilled samples at all temperatures above $T_{DH} = -55^{o}C$. Therefore, the nil-ductility temperature of drilled samples T_{DH} is $40^{o}C$ below T_{D}. In addition, at temperatures above T_{DH}, fibrous tearing occurs between the notch sides and each hole. Fracture initiation from the resulting "hammer head" notch is much more difficult, resulting in a sharp rise in both the fracture load and impact energy. As a result, the nil-ductility (T_{DH}), ductility (T_{NH}), and initiation mode (T_{SH}) transition temperatures of drilled samples are approximately coincident and $40^{o}C$ below T_{D} of the standard Charpy. Furthermore, since T_{N} is $25^{o}C$ above T_{D}, two holes reduce the ductility transition temperature ($\Delta T_{N} = T_{NH} - T_{N}$) by $65^{o}C$.

The 50% maximum energy transition T_{50} has no general, physical significance; but, in steel 0.24, it corresponds to the temperature at which brittle fracture first initiates from a full width fibrous crack (i.e., at maximum load). The effect of two holes on T_{50} and the other transition temperatures is summarized in Table 6.1.

Table 6.1

The effect of two holes (H_D = 0.0292", R = 0.0448", $\theta = 75^o$) on the impact transition temperatures (^oC) of steel 0.24.

Transition Temperature	Symbol	Standard Charpy	Two Drilled Holes	Difference Due to Two Holes
	T_D	-15		
Nil-ductility	T_{DH}		-55	
	ΔT_D			-40
Ductility	T_N, T_S	+10		
Initiation	T_{NH}, T_{SH}		-55	
	ΔT_N, ΔT_S			-65
50% of the	T_{50}	+27		
maximum energy	T_{50H}		-37	
	ΔT_{50}			-64

(4) The general yield load of drilled specimens is approximately 10% lower than P_{GY} of the standard Charpy specimens at all temperatures. This is consistent with the slow-bend results in steel 0.025 (section 6.1) and in Fe-Si 2 (Chapter V) where holes lowered P_{GY} by about 8 percent. Similar reductions are observed in other alloys to be discussed later, but the exact magnitude varies with the material and loading rate.

(5) At high temperatures (above T_{50}), both standard and drilled samples reach their ultimate load P_{ULT} prior to failure. Although the ultimate load of drilled samples is 10 percent lower than that of the standard Charpy, the notch displacement [V*(c)] at which it is achieved is larger. As a result, the pre-maximum load energy is increased by two

holes. Holes did not measurably change the amount of post-brittle (shear-lip) energy so that the observed increase in the total Charpy energy results from the increased V*(c) which is required for cleavage initiation.

6.3 Discussion of the Effect of Holes Prior to General Yield

6.3-1 Initial Yielding

Local yielding begins when the applied nominal stress multiplied by the elastic stress concentration factor exceeds the uniaxial yield stress at the notch root. It was shown in Chapter V (equation 5.2) that in the Charpy sample yielding begins at the notch tip at an applied load

$$P_{LY}(\text{lb.}) = 3.9 \times 10^{-3}\ \sigma_Y^* \ (\text{psi}) \qquad \begin{matrix}(5.2)\\(6.2)\end{matrix}$$

where σ_Y^* is the yield stress at the actual strain rate which exists at the notch tip.

The actual strain rate at the notch root may be estimated in the following manner. The elastic deflection δ of the loading point of an unnotched beam is given by elasticity[99]

$$\delta = \frac{P\,L^3}{6EI} \qquad (6.3)$$

where L = support length

E = elastic modulus

I = moment of inertia of beam section.

The nominal tensile stress opposite the loading point is

$$\sigma_N = \frac{PLa}{4I} \qquad (6.4)$$

where a is the beam height. The maximum stress in a notched bar is $\sigma_N K_\sigma$ and the associated elastic strain is

$$\varepsilon = \frac{\sigma_N K_\sigma}{E} . \qquad (6.5)$$

Combining equations (6.3), (6.4), and (6.5) to eliminate P and differentiating with respect to time yields

$$\dot{\varepsilon} = \frac{3 K_\sigma a}{2L^2} \dot{\delta} . \qquad (6.11)$$

In the present Charpy tests, $\dot{\delta}$ = 17 ft./sec. so that $\dot{\varepsilon} = 6.5 \times 10^2$ sec^{-1}, which is slightly higher than the average $\dot{\varepsilon} = 10^2$ sec^{-1} at general yield (section 6.2-1). However, indentation of the beam by the striker reduces $\dot{\delta}$ and $\dot{\varepsilon}$. Hendrickson et al[104] measured the indentations in Izod samples to be of the order of the elastic deflection when local yielding begins, and this reduces the local strain rate by a factor of two. In any case, the strain rate at first slip is not significantly greater than the average value at general yielding. Consequently, the effective local σ_Y^* is given by Figure 6.3 at all temperatures.

6.3-2 The Elastic-Plastic Stress Distribution

The initial plastic zones in a standard sample have been shown (Chapter V) to take the form of the logarithmic spirals predicted by plane strain slip line field analysis. The longitudinal stresses (σ_{yy}) within the plastic zone are raised above σ_Y^* by plastic constraint and are given by the equation derived by Hill[38]

$$\sigma_{yy}(x) = \sigma_Y^* \left[1 + \ell n \left(1 + \frac{x}{\rho}\right)\right] \qquad x \leq R_\beta \qquad (6.7)$$

where x is the distance below the notch tip within the plastic zone and

ρ is the radius of curvature (0.010") of the notch tip.

Figure 6.6 shows schematically the elastic stress distribution along the minimum section which exists just prior to local yielding (at load P_{LY}) and that which results after local yielding at two higher loads (P_1 and P_2). The maximum tensile stress occurs at the elastic-plastic interface x = R and is given by

$$\sigma_{yy}^{max} = \sigma_Y^* K_{\sigma(p)}$$

$$K_{\sigma(p)} \equiv 1 + \ell n \left(1 + \frac{R}{\rho}\right) \qquad R \leq R_\beta \qquad (1.23) \quad (6.8)$$

where $K_{\sigma(p)}$ is the plastic stress concentration factor.

Hill[38] has shown that there is a plastic zone size R_β beyond which the maximum stress due to constraint alone no longer increases. Green and Hundy[39] have theoretically calculated the value of $K_{\sigma(p)}$ at this point to be

$$K_{\sigma(p)} = K_{\sigma(p)}^{max} \equiv 1 + \frac{\pi}{2} - \frac{\omega}{2} \qquad R \geq R_\beta \qquad (1.24) \quad (6.9)$$

where ω is the notch flank angle. Theoretically at least, $K_{\sigma(p)}^{max}$ depends only on ω and is 2.18 for the Charpy notch. Higher applied loads can cause the plastic zone to extend beyond R_β but no further increase in $K_{\sigma(p)}$ occurs. For these cases, the stress distribution assumes the form produced by P_2 in Figure 6.6.

In order to quantitatively relate the maximum stresses to the applied load, the size of the plastic zone R must be known as a function of applied load, P. Wilshaw and Pratt[60] have experimentally measured R as a function of applied load P by etching the plastic zones in a high nitrogen mild steel. Using these measurements and equations (6.8) and

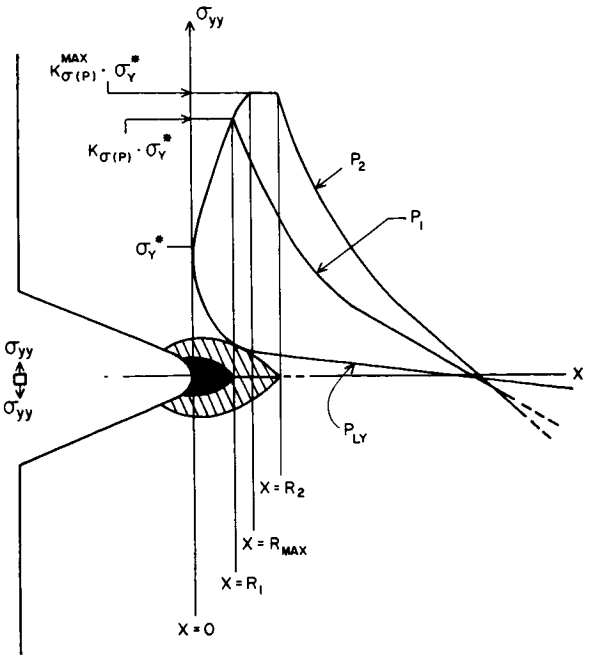

Figure 6.6 Schematic sketch of the predicted elastic and elastic-plastic stress distributions in a Charpy sample of an ideal plastic material at various applied loads ($P_{LY} < P_1 < P_2$) in three-point bending.

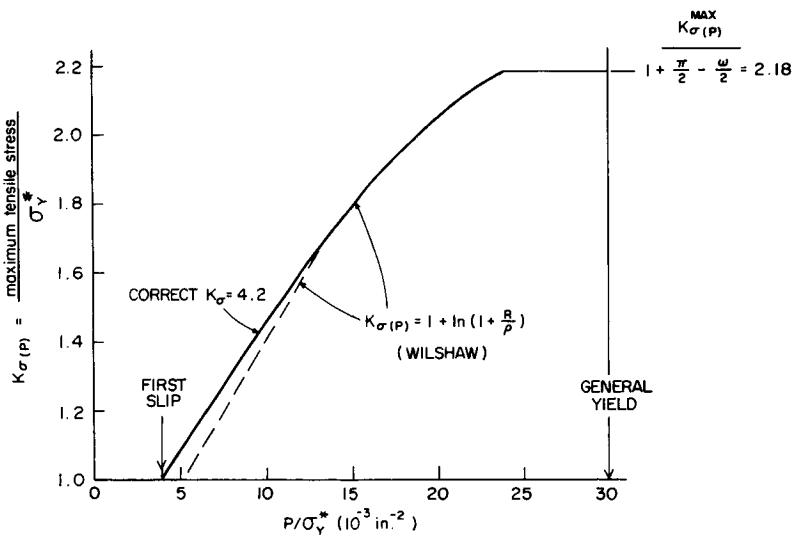

Figure 6.7 The predicted increase of plastic stress concentration factor [$K_{\sigma(p)}$] with applied load in a Charpy sample loaded in three-point bending [after Wilshaw and Pratt[60], and Wilshaw, Rau and Tetelman[59]].

(6.9), the increase of $K_{\sigma(p)}$ with applied load (P/σ_Y^*) is defined as shown in Figure 6.7. The portion of this curve between first slip at $P/\sigma_Y^* = 3.9$ and $P/\sigma_Y^* = 13.5$ has been corrected from that plotted by Wilshaw and Pratt. They used $K_\sigma = 3.2$ for a hyperbolic notch from Neuber's early work[105] rather than the actual $K_\sigma = 4.2$ and consequently overestimated P_{LY}. Figure 6.7 is also in agreement with the predictions of a recent theoretical model[59].

6.3-3 Prediction of Fracture Load

Various investigators[40, 54, 74] have shown that cleavage fracture of mild steel occurs when the maximum tensile stress exceeds a critical value (σ_f), which is approximately independent of both temperature and strain rate. In a notched sample, a fast running cleavage crack can start to grow when the maximum tensile stress below the root exceeds σ_f. As the crack grows in length and accelerates, the nominal stress required to keep it in motion [equation (1.2)] decreases, so that complete failure of the section results.

The fracture criteria for a notched bar is therefore given by

$$\sigma_{yy}^{max} = \sigma_Y^* K_{\sigma(p)}^F = \sigma_f \qquad P_F < P_{GY}$$

or

$$K_{\sigma(p)} = K_{\sigma(p)}^F = \frac{\sigma_f}{\sigma_Y^*} , \tag{6.10}$$

and the applied load required to cause fracture is related to $K_{\sigma(p)}^F$ through Figure 6.7. Since σ_Y^* decreases with increasing temperature as shown in Figure 6.3, the critical $K_{\sigma(p)}^F$ and corresponding applied load P_F must increase with increasing temperature to satisfy equation (6.10).

6.3-4 Fracture Strength of Standard Samples

In order to check the predictions of the previous section, specifically Figure 6.7, σ_Y^* and P_F were obtained from Figures 6.3 and 6.5 respectively. The ratio P_F/σ_Y^* was calculated, and the corresponding $K^F_{\sigma(p)}$ was read from Figure 6.7. According to equation (6.10), the product $K^F_{\sigma(p)} \cdot \sigma_Y^*$ should yield a constant equal to σ_f at all temperatures. The actual calculated product, shown in Figure 6.8, is nearly constant for temperatures between -196 and -50°C but somewhat higher between -50 and -15°C, where fracture is coincident with general yielding.

There are several assumptions implicit in the preceding calculation of Figure 6.7 which might cause the observed deviation when fracture occurs close to general yielding. First, the actual yield stress at the point of maximum constraint could be less than σ_Y^* ($\dot{\epsilon} = 10^2$) since the actual strain rate decreases as the elastic stresses [K_σ, (equation (6.6)] decrease with distance from the notch. This change causes, at most, a reduction in $\dot{\epsilon}$ of less than a factor of two between 0.5 P_{GY} and general yield, and thus it does not reduce σ_Y^* significantly.

Secondly, a more realistic fracture criteria might require that σ_f be achieved over some minimum area (A). In this case, the plastic stress concentration factor, given by equation (6.8), should be modified to

$$K_{\sigma(p)} = 1 + \ell n \left(1 + \frac{R - \sqrt{A}}{\rho}\right) \qquad (6.11)$$

However, for $\sqrt{A}$ of the order of the grain size, this correction is quite small and would be most significant at small R. As a result, it is not responsible for the observed deviation noted near general yield.

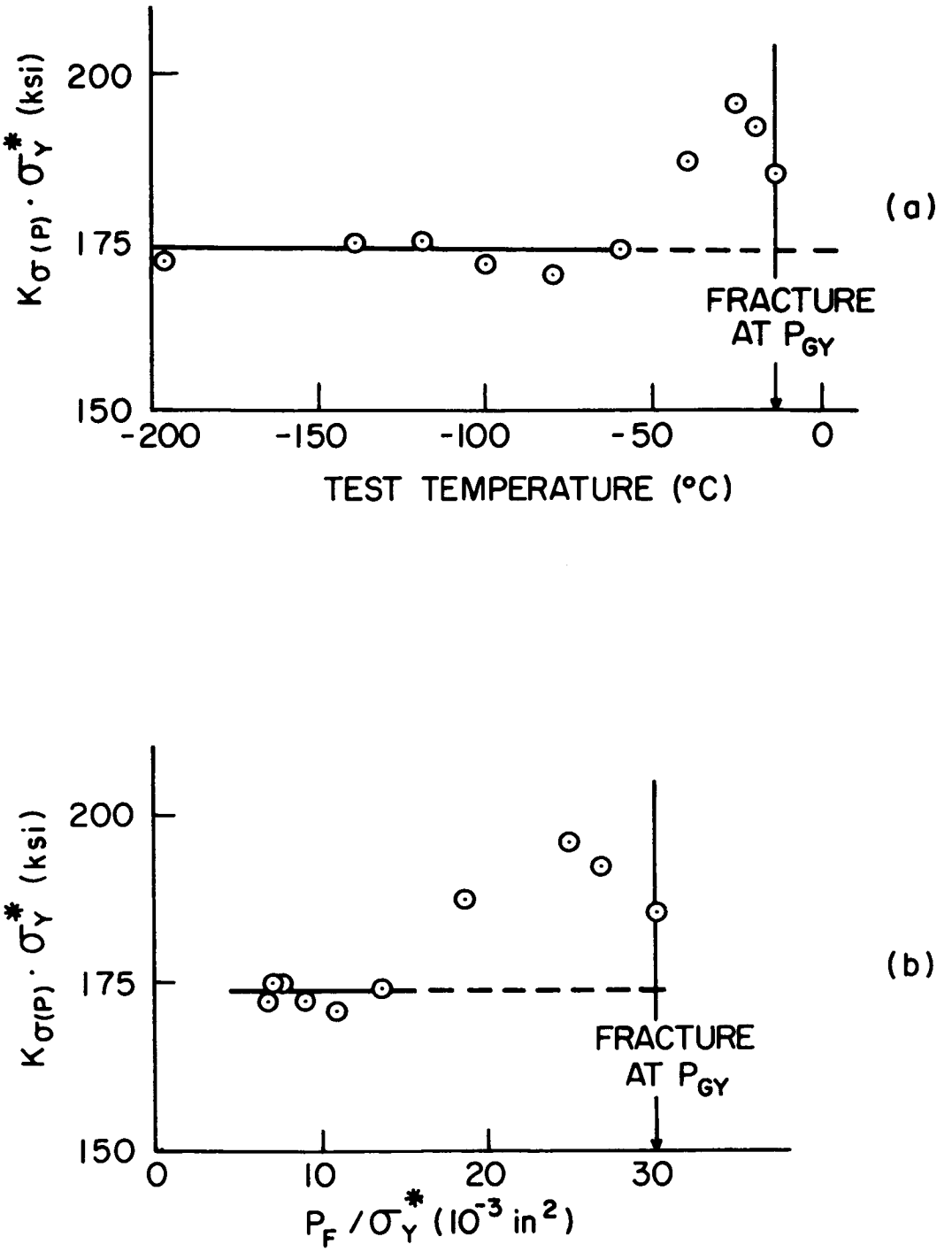

Figure 6.8 The microscopic fracture stress of steel 0.24 calculated from the measured fracture loads (Figure 6.5) and the predicted $K_{\sigma(p)}$ (Figure 6.7), i.e., $\sigma_f = K^F_{\sigma(p)}(P_F/\sigma_Y^*) \cdot \sigma_Y^*$;

(a) As a function of test temperature

(b) As a function of applied load (P/σ_Y^*).

Thirdly, there may be a straightforward deviation from the form of $K_{\sigma(p)}$ predicted by equations (6.8) and (6.9) from slip-line field analysis. That is because these equations were derived for an ideal plastic material, it is likely that work hardening causes modifications of the shape of the plastic zone and the stress distribution within the zone. This was, in fact, observed in the FeSi-2 samples of Chapter V, where plastic hinges started to form at loads between 0.55 and 0.70 P_{GY} (see Figure 5.4). In mild steel 0.24 at low temperatures, the Luders extension may cause the steel to behave very much like an ideal plastic material. On the other hand, with increasing temperature, the amount of Luders strain decreases, and the work hardening rate increases (Figure 6.2) so that $K_{\sigma(p)}$ might deviate significantly from that shown in Figure 6.7.

The actual increase of $K_{\sigma(p)}$ with applied load (P/σ_Y^*) can be calculated directly from the fracture results with the assumption that σ_f = 174 ksi from Figure 6.8. At each test temperature, P_F/σ_Y^* is obtained from the fracture results (Figures 6.5 and 6.3) and $K_{\sigma(p)}$ from

$$K_{\sigma(p)}\ (P/\sigma_Y^*) = K^F_{\sigma(p)}(T) = \frac{174{,}000}{\sigma_Y^*\ (T)}\ . \qquad (6.12)$$

By considering a range of test temperatures, the build-up of $K_{\sigma(p)}$ with P/σ_Y^* is defined as shown in Figure 6.9. This experimentally determined curve is similar to that predicted by Figure 6.7 at low P/σ_Y^*, but the deviation increases at loads approaching general yield (P/σ_Y^* = 30(in^2 x 10^{-3})). The fracture results of Wilshaw[54] in nitrogen steel, when analyzed as in Figure 6.8, also indicate that $K_{\sigma(p)}$ is overestimated by Figure 6.7 at loads near general yield.

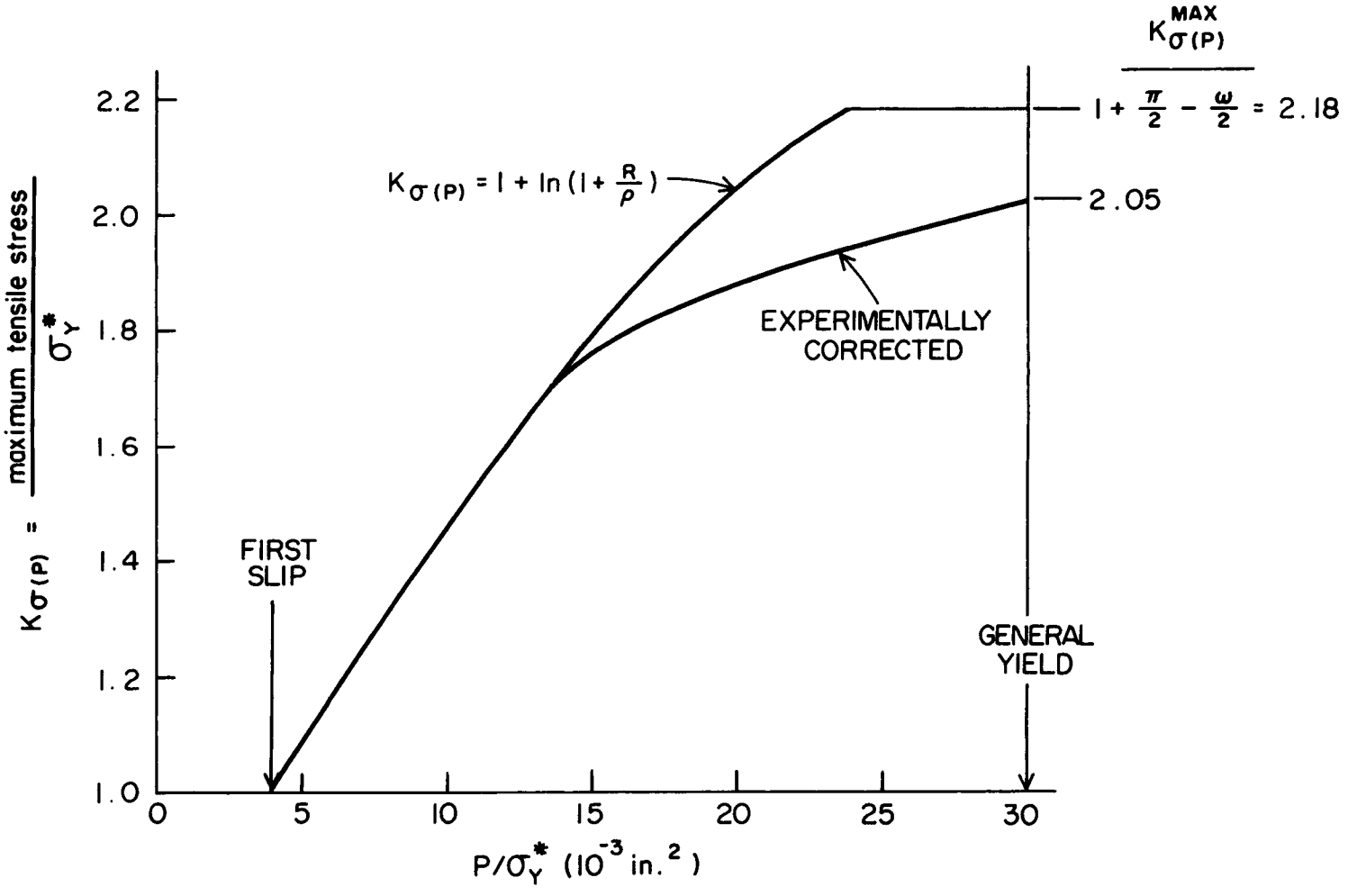

Figure 6.9 The experimentally determined increase of plastic stress concentration factor $[K_{\sigma(p)}]$ with applied load for steel 0.24, assuming that σ_f = 174 ksi.

6.3-5 The Effect of Two Holes on Fracture Strength

In drilled samples, the fracture criteria is also given by equation (6.12). Since σ_f and σ_Y^* are defined by the material and test conditions, the same stress intensification $K^F_{\sigma(p)}$ is required for fracture of both standard and drilled samples at each temperature. However, as a result of the modification of the yield zones by the holes, a higher applied load (P^H_F/σ_Y^*) is necessary to produce a given $K^F_{\sigma(p)}$ in drilled samples. By considering the fracture loads at various temperatures, the increase of $K^H_{\sigma(p)}$ with P/σ_Y^* in drilled samples was defined as it was for the Charpy sample. Figure 6.10 summarizes the plastic stress concentration factor as a function of applied load in both standard Charpy and drilled specimens.

At very low temperatures where σ_f is of the order of σ_Y^* ($K^F_{\sigma(p)} \approx 1$), cleavage requires only a small plastic constraint. Since the necessary plastic zone is quite small, two holes have very little effect on them or the corresponding $K_{\sigma(p)}$; and the fracture load is increased only slightly. However, as the critical $K^F_{\sigma(p)} = \sigma_f/\sigma_Y^*$ increases with increasing temperature and larger plastic zones are required, holes raise markedly the applied load to produce $K^F_{\sigma(p)}$. This results because holes modify the development of the plastic zones in such a way that the maximum local stress $(K_{\sigma(p)} \cdot \sigma_Y^*)$ increases much less rapidly with applied load.

Because the redistribution of plastic strain increases with the applied load, the resulting improvement in nominal fracture strength through hole drilling increases with the critical $K^F_{\sigma(p)}$ and may be obtained from Figure 6.10. For example, at -80°C, $\sigma_Y^* = 113$ ksi, $\sigma_f =$

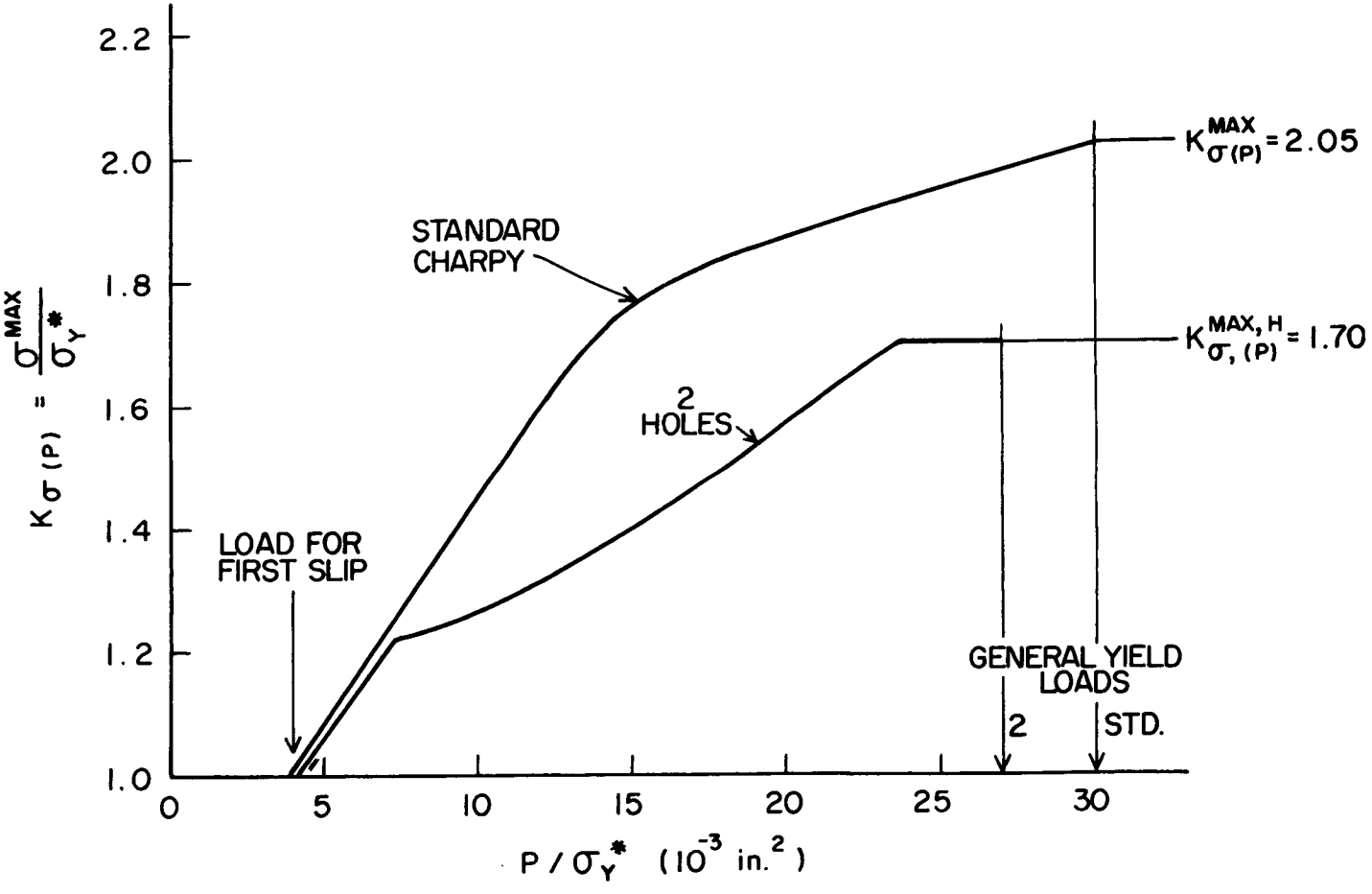

Figure 6.10 The effect of two holes (H_D = 0.0292", R = 0.0448", $\theta = 75^o$) on the increase of the plastic stress concentration factor [$K_{\sigma(p)}$] with applied load in Charpy samples of steel 0.24.

174 ksi; so that $K^{F}_{\sigma(p)} = \frac{174}{113} = 1.54$. From Figure 6.10, the fracture load of the Charpy sample is P_F = 11.2 x 113 = 1250 lb. while that of the drilled sample is P^{H}_{F} = 19.3 x 113 = 2180 lb., an increase of 75%.

6.4 Discussion of Fracture Behavior Above General Yield

6.4-1 Reduction of the Nil-Ductility Temperature

In the previous section, it was shown that the critical $K^{F}_{\sigma(p)} = \sigma_f/\sigma^*_Y$ for fracture is defined by the material and test conditions, but the fracture load to obtain it is increased by two holes. In fact, whenever the necessary $K^{F}_{\sigma(p)} > 1.70$, Figure 6.10 indicates that it cannot be reached in drilled samples prior to general yielding. Thus the nil-ductility temperature of drilled specimens (T_{DH}) is defined by

$$K^{max,H}_{\sigma(p)} = \frac{\sigma_f}{\sigma^*_Y\ (T_{DH})} = 1.7 \qquad T = T_{DH} \qquad (6.13)$$

Similarly, the nil-ductility temperature of the standard Charpy (T_D) is defined by

$$K^{max}_{\sigma(p)} = \frac{\sigma_f}{\sigma^*_Y(T_D)} = 2.05 \qquad T = T_D \qquad (6.14)$$

Because holes redistribute the local strain, $K^{max,H}_{\sigma(p)} < K^{max}_{\sigma(p)}$, and a lower temperature ($T_{DH} < T_D$) is required before σ^*_Y is high enough to satisfy equation (6.13). Using the schematic diagram shown in Figure 6.11, the reduction in nil-ductility temperature due to holes may be estimated. In this calculation, it is assumed that (1) σ_f is a constant independent of temperature and (2) the temperature dependence of the yield stress $d\sigma^*_Y/dT$ is approximately constant over the transition region. Under these conditions

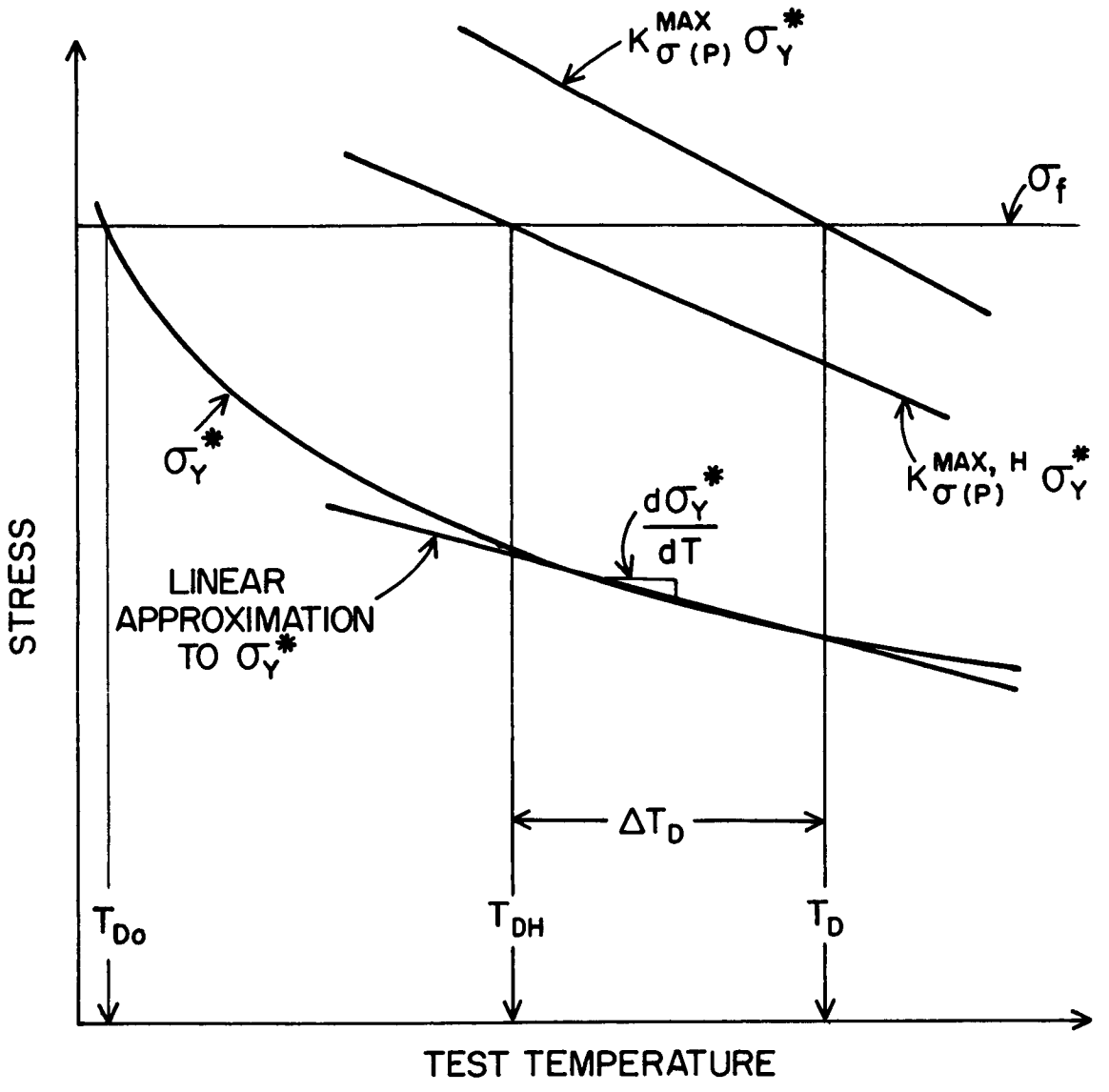

Figure 6.11 Schematic representation of the effect of holes on the nil-ductility transition temperature.

$$K^{max}_{\sigma(p)}\ \sigma^*_Y(T_D) - K^{max,H}_{\sigma(p)}\ \sigma^*_Y(T_D) = \frac{d\left[K^{max,H}_{\sigma(p)}\ \sigma^*_Y\right]}{dT} \cdot (T_{DH} - T_D)$$

$$= K^{max,H}_{\sigma(p)} \frac{d\sigma^*_Y}{dT} (T_{DH} - T_D) \cdot$$

Rearranging,

$$\Delta T_D = T_{DH} - T_D = \frac{\left[K^{max}_{\sigma(p)} - K^{max,H}_{\sigma(p)}\right]\sigma^*_Y(T_D)}{K^{max,H}_{\sigma(p)}\ d\sigma^*_Y/dT}$$

$$\Delta T_D = \frac{\left[K^{max}_{\sigma(p)} - K^{max,H}_{\sigma(p)}\right]\sigma_f}{K^{max,H}_{\sigma(p)}\ K^{max}_{\sigma(p)}\ d\sigma^*_Y/dT} \cdot \qquad (6.15)$$

Estimating $d\sigma^*_Y/dT$ from Figure 6.3 and substituting into equation (6.15) yields for steel 0.24

$$\Delta T_D = \frac{2.05 - 1.70}{(1.70)\ (2.05)} \cdot \frac{174}{(0.385)} = -45^oC\ ,$$

which is in good agreement with the experimentally observed reduction of -40^oC.

In steel 0.025, two holes were observed to reduce the impact transition temperature by 33^oC (Chapter III) but the slow-bend transition temperature by only 20^oC (section 6.1). Moreover, the slow-bend results indicate that holes reduce the initiation and nil-ductility transition temperatures by about the same amount ($\Delta T_S \cong \Delta T_D$) in alloy 0.025.

Equation (6.15) shows that the reduction in nil-ductility temperature ΔT_D which results from a particular reduction in constraint (hole geometry) is inversely proportional to $\left|\frac{d\sigma^*_Y}{dT}\right|$. Since the absolute magnitude of $\frac{d\sigma^*_Y}{dT}$ increases with decreasing temperature and the transition temperature region decreases with decreasing loading rate, $\left|\frac{d\sigma^*_Y}{dT}\right|$ over the transition region is higher under slow-bend conditions. Specific-

ally, an increase in $|d\sigma_Y^*/dT|$ of 65% in going from impact to slow-bend conditions ($T_D = -58^oC$ to $T_D = -165^oC$) is quite reasonable (note Figure 6.1(a)); and this could cause the observed difference between $\Delta T_N(\Delta T_D)$ in impact and slow-bending.

It should be noted that equation (6.15) can be used to predict ΔT_D for any geometric change (not only holes) that changes the maximum constraint, provided that the approximations of constant σ_f and $d\sigma_Y^*/dT$ are justified.

6.4-2 Reduction of the Ductility Transition Temperature

In Chapter I, it was shown that σ_f is obtained after general yielding at a critical root displacement

$$V^*(c) = \rho\ \beta\ \varepsilon_F = \rho\ \beta \left[\frac{\sigma_f - K^{max}_{\sigma(p)}\ \sigma_Y^*}{K^{max}_{\sigma(p)}\ \frac{d\sigma}{d\varepsilon}} \right] \qquad \begin{matrix}(1.16)\\(6.16)\end{matrix}$$

Because σ_Y^* decreases with increasing temperature, the cleavage fracture strain ε_F and displacement $V^*(c)$ increase with temperature. At the ductility transition temperature (T_N), the critical notch displacement $[V^*(c)]$ increases sharply due to a relaxation of constraint $[K^{max}_{\sigma(p)}\downarrow]$, which results from plastic deformation through the thickness and/or the formation of plastic "wings"[100]. In steel 0.24, the required $V^*(c)$ becomes so large that high root strains initiate ductile fracture at a smaller displacement

$$V^*(c) > V_s^*(c) = \rho\ \varepsilon_s \,. \qquad T > T_N = T_S \qquad \begin{matrix}(1.27)\\(6.17)\end{matrix}$$

In a drilled sample, the critical displacement for cleavage fracture is given

$$V^{**}(c) = \alpha\ \rho\ \beta\ \varepsilon_F^H = \alpha\ \rho\ \beta \left[\frac{\sigma_f - K_{\sigma(p)}^{max,H}\ \sigma_Y^*}{K_{\sigma(p)}^{max,H}\ \frac{d\sigma}{d\varepsilon}} \right] \tag{6.18}$$

where the factor $\alpha > 1$ is a measure of the redistribution of strain away from the notch tip. Comparing equations (6.16) and (6.18), it is apparent that under the same test conditions $V^{**}(c) \gg V^*(c)$ because (1) holes increase the critical cleavage strain $\varepsilon_F^H > \varepsilon_F$ by reducing the maximum constraint $K_{\sigma(p)}^{max,H} < K_{\sigma(p)}^{max}$ and (2) holes reduce the strain concentration ahead of the notch ($\alpha > 1$). Therefore, holes make cleavage initiation below the notch tip more difficult. While holes reduce the strain concentration at the notch root, they increase it between the notch side and each hole. Consequently, there is a critical displacement

$$V_H^*(c) = \frac{\text{const.}}{\alpha}\ \varepsilon_s \tag{6.19}$$

at which ductile tearing occurs between the notch side and a hole.

As tearing occurs to one hole there is a reduction in the net section area and thus an increase in the nominal bending stress. The depth of the "effective notch" is increased from c to c + H where H = R cos θ + H_D - ρ, but the tip radius (of the blunted hole, $\rho_H > \rho$) is also increased. Reinitiation of fracture from the one hole may occur by either cleavage or fibrous tearing, and the critical displacement [$V^*(c + H)$] is given by equations of the form of either (6.16) or (6.17). That is

$$V^*(c + H) = \begin{cases} \rho_H\ \beta_H\ \varepsilon_F' & \text{(cleavage)} \\ \rho_H\ \varepsilon_s & \text{(fibrous)} \end{cases} \tag{6.20}$$

where $\beta_H \equiv$ a constant relating the strain at the hole edge to that at

the point of maximum constraint below the hole, ϵ_F' ≡ the critical strain required for cleavage at the point of maximum triaxiality below the hole, and $\beta_H \epsilon_F' > \beta \epsilon_F$ because the magnitude and location of maximum constraint are different below the hole than below the notch.

The marked increase in fracture load and toughness of drilled samples at temperatures just above T_{DH} is achieved by altering fracture mechanism to that represented in Figure 6.12. This mechanism operates when ductile tearing occurs to <u>both</u> holes. Once this occurs, there is extensive relaxation of constraint, and the effective notch has two blunt tips, in the form of elongated holes. The critical displacement required to reinitiate failure from this notch-hole combination is so much larger that a ductility transition temperature (T_{DH}) results. Two criteria must be fulfilled for operation of this mechanism. They are

(1) fibrous tearing must occur to one hole before cleavage can be nucleated below the root,

$$V_H^*(c) < V^{**}(c) \quad \text{(criterion 1)} \tag{6.21}$$

$$\frac{\text{const.}}{\alpha} \epsilon_s < \alpha \beta \rho \epsilon_F^H$$

$$\frac{\text{const.}}{\alpha} \epsilon_s < \alpha\beta\rho \left[\frac{\sigma_f - K_{\sigma(p)}^{\max,H} \sigma_Y^*}{K_{\sigma(p)}^{\max,H} \, d\sigma/d\epsilon} \right]$$

(2) brittle fracture must not initiate on the opposite side of the hole (i.e., at point A, Figure 6.12) before tearing reaches the second hole. Therefore, $V^*(c + H)$ must be sufficiently greater than $V_H^*(c)$, i.e.

$$V^*(c + H) \gg V_H^*(c) \quad \text{(criterion 2)} \tag{6.22}$$

to assure that tearing will reach both holes when statistical variations

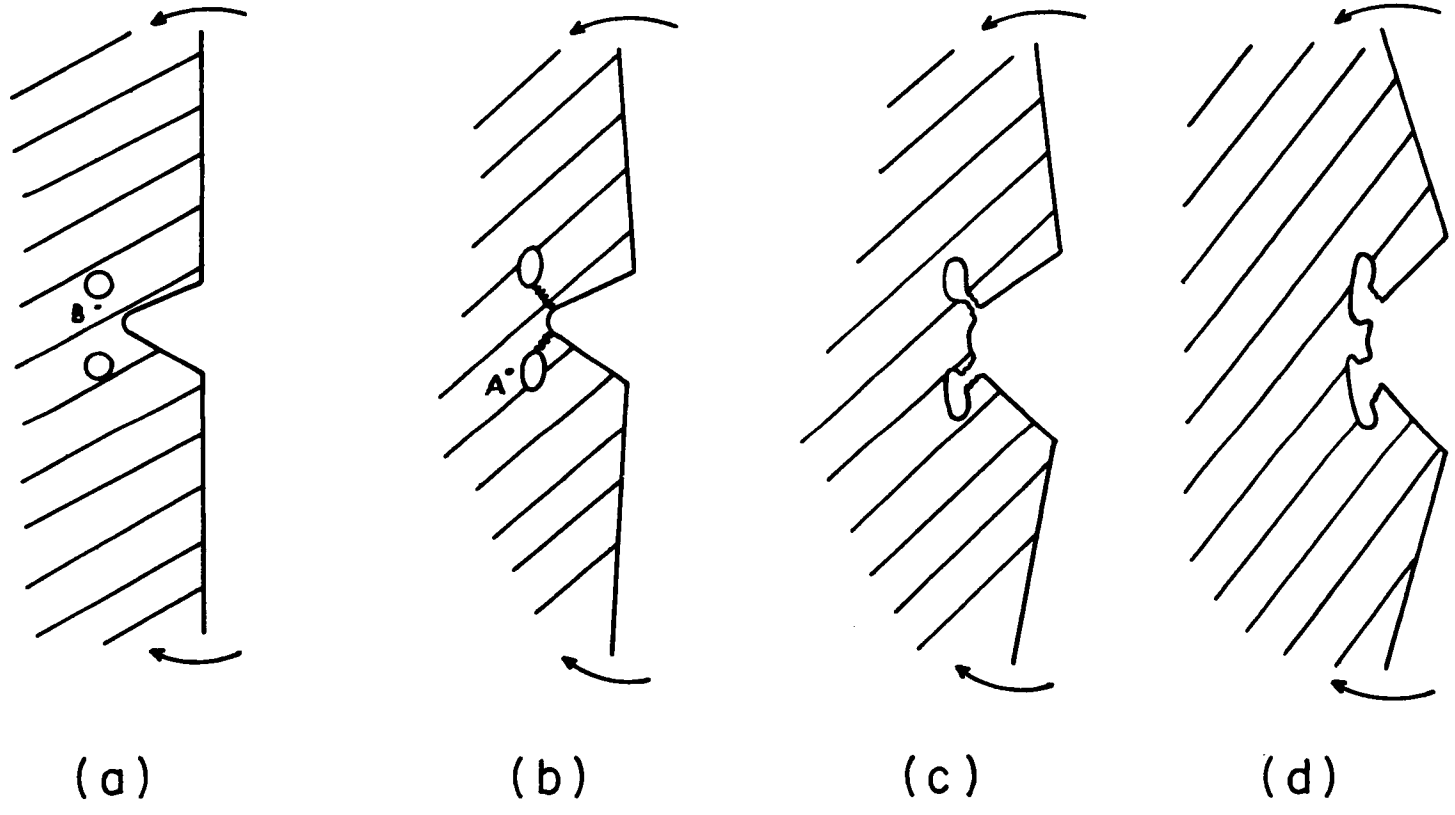

Figure 6.12 Schematic representation of the fracture mechanism in drilled samples tested at temperatures above the ductility transition temperature of drilled samples.

or slight loading asymmetry prevents simultaneous tearing to both holes.

The magnitude of the reduction in ductility transition temperature with hole drilling depends on how easily (at what temperature) these two criteria are satisfied. This, in turn, depends on the specific geometrical (α, $K^{max}_{\sigma(p)}$, $K^{max,H}_{\sigma(p)}$, β, ρ, β_H, ρ_H, etc.) and materials (σ_f, σ^*_Y, $d\sigma/d\epsilon$, ϵ_s) parameters. For a particular material and the Charpy notch, criterion (1) is more easily satisfied when strains are highly concentrated toward the holes because high α and high ϵ^H_F favor equation (6.21). Criterion (2) is more easily satisfied when the net section area which remains after tearing reaches a hole is large. In addition, criterion (2) is more easily satisfied if the holes have been blunted [ρ_H = large, equation (6.20)] by plastic deformation before the first tear forms. A low α increases $V^*_H(c)$ somewhat, but it also enables more blunting and thus favors equation (6.22).

The coordinants R and θ, which locate the holes relative to the notch, are important because they determine the nature of the redistribution of strain (α) as well as the net area which remains after tearing to one hole. The optimum hole position of R = 0.0448", $\theta = 75^o$, which was determined in Chapter III (Figure 3.6), is a compromise which best fulfills both criteria. At larger R > 0.0448" or $\theta > 75^o$, the holes interact less strongly with the plastic zone so that $\alpha \rightarrow 1$ and $K^{max,H}_{\sigma(p)} \rightarrow K^{max}_{\sigma(p)}$; therefore, criterion 1 [equation (6.21)] is not satisfied until a higher temperature ($T_{NH} \rightarrow T_N$). On the other hand, at R = 0.0448" and smaller $\theta < 75^o$, criterion 1 is satisfied quite easily. However, the net area which remains when failure reaches one hole is smaller [larger (c+H)], and criterion 2 is not satisfied until a higher tempera-

ture ($T_{NH} \rightarrow T_N$). Similarly, one 0.0292" hole ($\theta = 0^o$) does not redistribute the local strain away from the notch tip nor cause large scale blunting when failure reaches it; consequently, no improvement results.

In drilled samples ($R = 0.0448"$, $\theta = 75^o$) of steel 0.24, both criteria are satisfied at temperatures above $T_{DH} \cong T_{NH} \cong T_{SH}$. This sharp transition behavior results because the critical displacement required for cleavage [V**(c), equation (6.18)] increases very rapidly with temperature above T_{DH} [$\alpha\uparrow$, $K_{\sigma(p)}^{max,H}\downarrow$]. In standard Charpy samples, however, the high strain concentration and larger constraint [$K_{\sigma(p)}^{max}$] cause the critical displacement for cleavage [V*(c), equation (6.16)] to increase quite slowly with temperature above T_D. As a result, the ductility transition temperature (T_N) of Charpy samples of steel 0.24 occurs well above the nil-ductility temperature (i.e., $T_N - T_D = 25^oC$). Consequently, holes reduce the ductility transition temperature [$\Delta T_N = T_{NH} - T_N = -65^oC$] even more than they reduced the nil-ductility temperature [$\Delta T_D = T_{DH} - T_D = -40^oC$] in steel 0.24.

6.4-3 Reduction of the General Yield Load

The general yield load (P_{GY}) is defined as that applied load which is necessary to extend plastic hinges across the entire bar. P_{GY} is related to the distribution of longitudinal stress $\sigma_{yy}(x)$ across the minimum section, through the moment equilibrium requirement

$$\frac{P_{GY}\, L}{2} = \int_{x=0}^{x=a} x\, \sigma_{yy}(x)\, t\, dx \qquad (6.23)$$

where $2L$ = distance between anvil supports

t = bar thickness

a = bar depth.

$\sigma_{yy}(x)$ = longitudinal stress at x below the notch.

Two holes have been observed to reduce P_{GY} by approximately 10 percent in steel 0.24 and 8 percent in alloys 0.025 and FeSi 2. This lower P_{GY} implies that, at general yield, the longitudinal stress $\sigma_{yy}(x)$ is on the <u>average</u> lower than at corresponding x in the standard Charpy sample. This is consistent with the fracture results which have shown that holes reduce the <u>maximum</u> local tensile stress $[K^{max,H}_{\sigma(p)} \cdot \sigma_Y]$ which is present at general yield. Because two holes do not change the net sectional area (a · t), the lower P_{GY} is truly a reduction in the average plastic constraint which is normally developed in the Charpy sample.

6.4-4 <u>The Effect in Fully Ductile Samples</u>

At higher temperatures, both standard and drilled samples reach their ultimate load prior to failure. At these temperatures, holes reduce the load carrying capacity of the Charpy bar because (1) the cross-sectional area is reduced when tearing reaches the holes, (2) plastic constraint (triaxiality) is lower due to the blunting ($\rho_H \gg \rho$), and (3) plastic strain is spread over a large volume producing a lower average $\bar{\epsilon}$ and corresponding flow stress. Although the maximum load is reduced, it is significant that the notch displacement and total energy absorbed prior to instability are larger in drilled samples. This again results because the blunted notch-hole combination is a much less severe strain concentrator than the Charpy notch.

6.5 Notch Tension Tests

The effect of two holes on deformation and fracture has been defined in detail for Charpy bars loaded in three-point bending. This sample deforms under conditions approximating plane strain until well above general yielding. On the other hand, tensile loading even of the same notch geometry would result in significant differences in the mechanics of deformation and thus the improvement possible with hole drilling. In addition, in thin, notched, sheet-tension samples, deformation occurs under conditions approaching plane stress (no triaxiality). The embrittlement produced by the notch in sheet samples therefore results primarily from strain concentration at the notch tip which raises the flow stress by both work hardening and increased strain rate.

In order to determine whether similar improvements from two holes could be obtained under these conditions, symmetrically and singly notched tension samples shown in Figure 2.12c and d were examined. Fracture experiments were performed on steel 0.40 (50% pearlite) because its nil-ductility temperature of -100°C enabled study of fracture loads prior to general yield at convenient temperatures. All samples were surface ground to 0.035" thick from warm rolled 0.050" sheet, and cycled five times through the $\gamma \rightleftarrows \alpha$ transition to obtain the equiaxed structure shown in Figure 2.6.

Fracture tests on standard V-notch and drilled samples were performed at 0.1"/min. and temperatures between -196°C and +23°C. The results are summarized in Figure 6.13. The stress-strain properties of the unnotched material (specimen configuration Figure 2.12b) were obtained over the same range as the notched samples. At the nil-

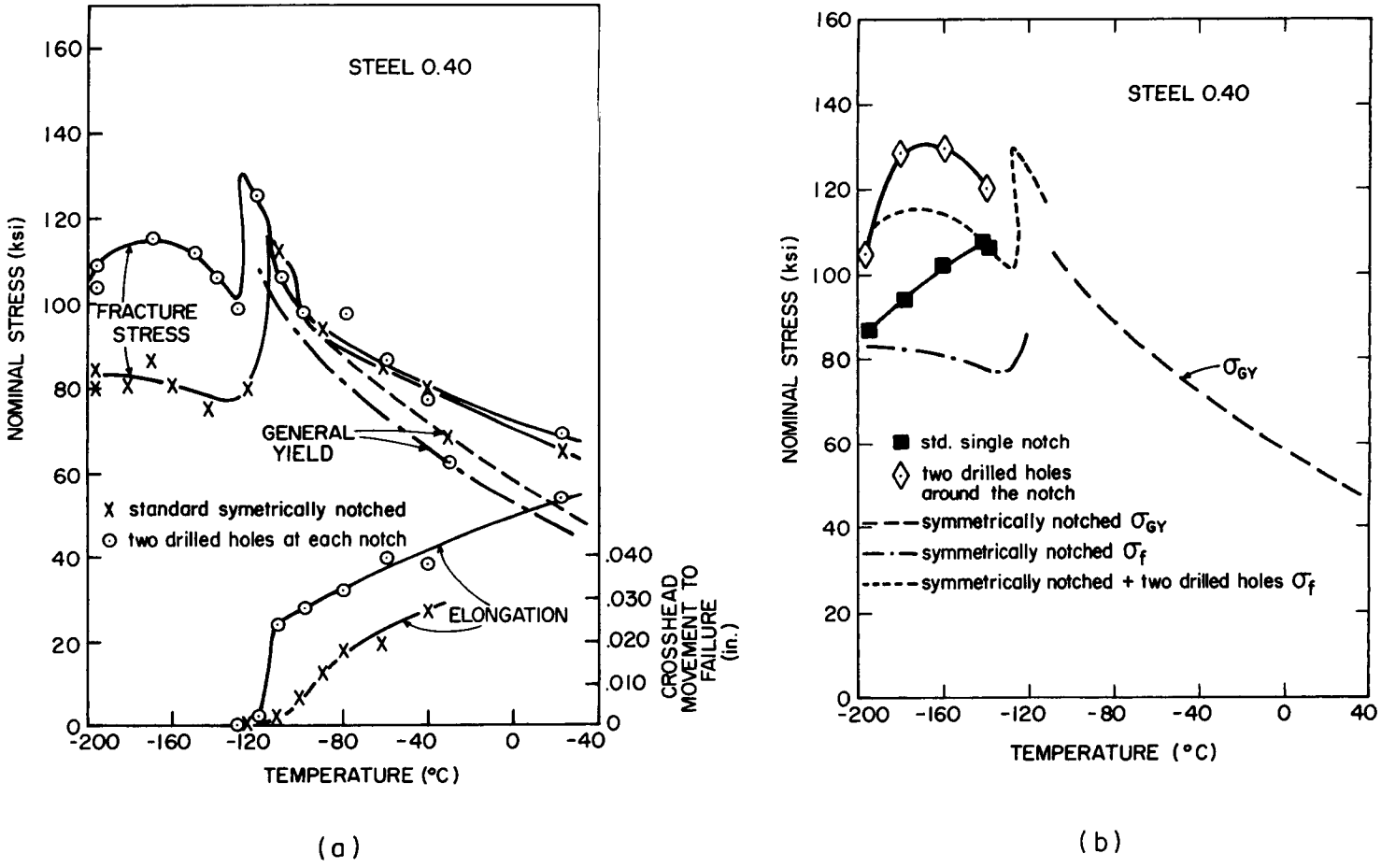

Figure 6.13 The effect of two holes (H_D = 0.0292", R = 0.0448", $\theta = 75^o$) on the fracture properties of notched sheet tension samples of steel 0.40;

(a) symmetrical Charpy notches
(b) single Charpy notch.

ductility temperature -100°C, the unnotched material has a pronounced yield drop followed by 4% Luders strain. It work hardens mildly and starts to neck after about 15% strain, finally cleaving after 30% nominal strain. The yield stress decreases with increasing temperature and is consistently 10 ksi lower than the nominal general yield stress σ_{GY} of symmetrically notched samples (Figure 6.13a). Over the same temperature range, the work hardening rate $d\sigma/d\varepsilon$ increases slightly with temperature but is still quite low at -60°C.

Standard notched samples fail by 100% cleavage prior to general yielding at all temperatures below -100°C. Above this temperature, general yielding, marked by a large drop in load, occurs; and fracture is nucleated by fibrous tearing at the notch root. Complete separation results by cleavage nucleated from the fibrous tear. The elongation prior to fracture increases slowly with temperature because more local strain is necessary for nucleation and sharpening of a fibrous tear to critical size.

Two drilled holes modify the notch tension properties of sheet samples in qualitatively the same ways that they did Charpy bend samples. That is

(1) holes increase the load carrying capacity of notched samples by 20 to 30 percent at low temperatures where fracture occurs prior to general yielding. This is true both in symmetrically and singly notched samples.

(2) Holes reduce the nil-ductility temperature (where fracture first occurs after the lower yield point) by about 20°C. Figure 6.14 compares the extent of deformation in standard and drilled samples

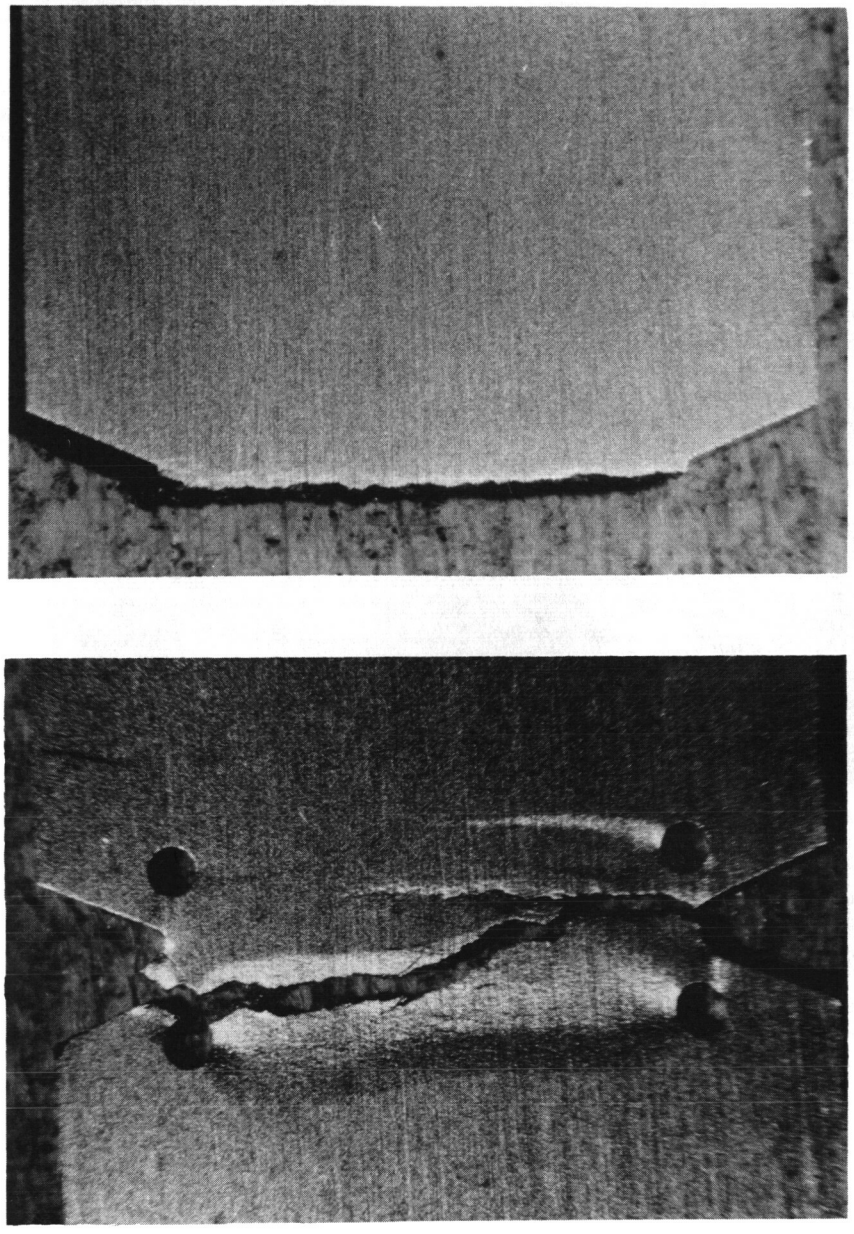

Figure 6.14 Comparison of the plastic deformation and fracture path of standard notched and drilled sheet samples of steel 0.40; Magnification = 8X,

(a) Test temperature = -125°C
(b) Test temperature = -120°C .

tested at -120°C. In the standard sample, cleavage was nucleated from a small plastic zone confined to the notch tip while in the drilled sample, fracture occurred after considerable deformation just before general yield.

(3) After general yielding, tearing occurs between the notch sides and both holes resulting in a sharp increase in the elongation necessary to cause cleavage. Figure 6.15 shows the fracture path and the deformation which was required to cause failure of both standard and drilled samples after general yielding.

(4) The general yield load (or nominal σ_{GY}) of drilled samples is approximately 8% below that of standard symmetrically notched samples. This is approximately the same reduction that was observed in bending of Charpy bars, but in this case, there are two notches contributing to the total stress on the net area so that the constraint reduction at each one is somewhat smaller.

(5) At high temperatures where failure is completely fibrous, the elongation prior to instability is consistently higher in drilled samples while the ultimate load is about the same.

These results indicate that two holes can improve the notch toughness and load carrying capacity of sheet tension samples as well as thick notched bars in bending. The modifications due to holes show the same general characteristics in both cases although the specific magnitudes appear to be less in sheet tension samples. Because the degree triaxiality is low even in standard tension samples, the primary effect of the holes is to reduce the strain concentration at the notch, and the total improvement is correspondingly less.

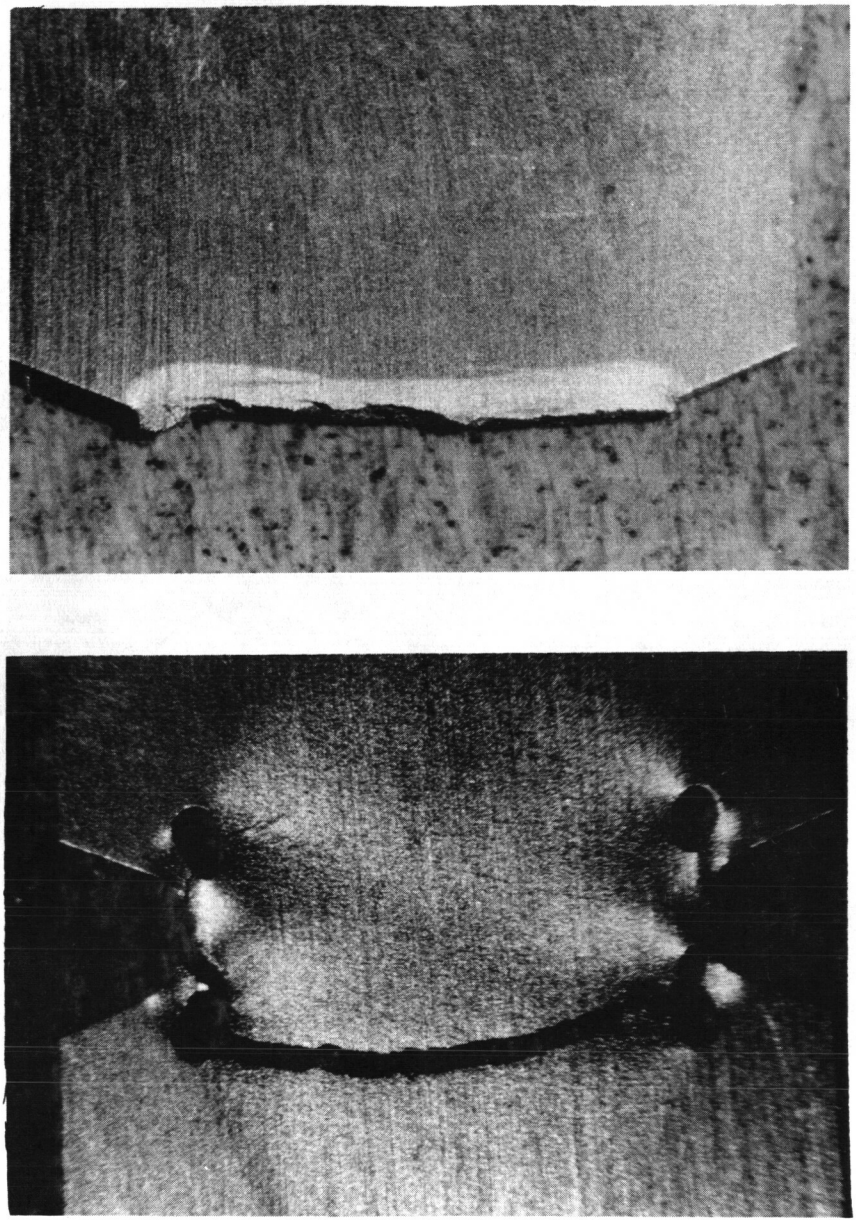

Figure 6.15 Comparison of the plastic deformation and fracture path of standard notched and drilled sheet samples of steel 0.40 tested at -99°C; magnification = 8X.

Figures 6.16 and 6.17 compare the surface yield zones revealed by dislocation etch-pitting of symmetrically notched Fe-Si 1 samples. The plastic zone of standard sample is confined very close to the net section with maximum strain occurring at the notch tip. Two holes relocate the maximum strain away from the front of the notch (Figure 6.16) and reduce its magnitude (note that the dark region, Figure 6.17a, indicates that strains exeeed 4.5%, but no such high strain region exists in Figure 6.17b).

Although the uncertainty regarding the amount of constraint (plane stress - plane strain) prevents a quantitative analysis of the problem, it is significant that improvements are obtained under conditions approaching plane stress.

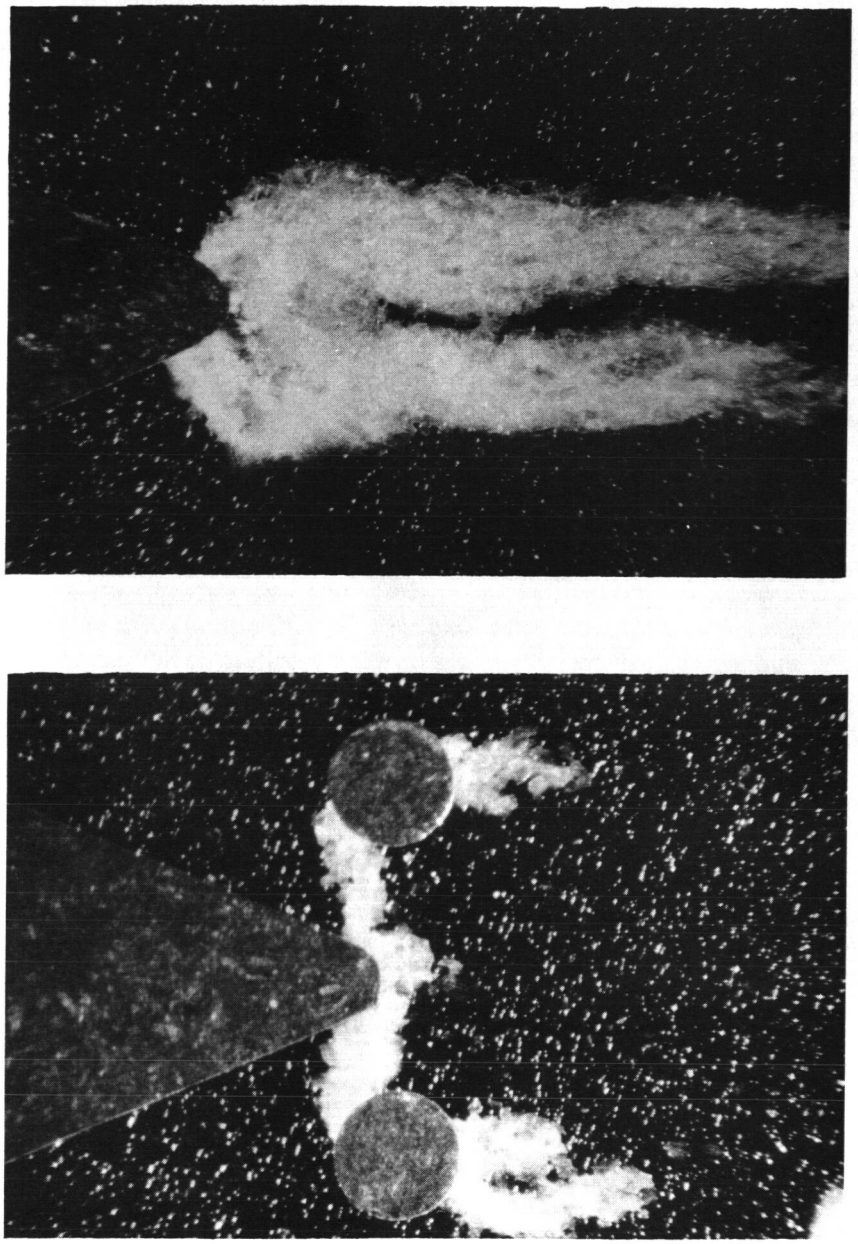

Figure 6.16 The effect of two drilled holes on the plastic zones revealed by dislocation etch pitting just below the surface of symmetrically notched (and drilled) sheet tension samples of FeSi 1; magnification = 22.9X, test temperature = $25^{o}C$,

(a) $P/P_{GY} = 0.83$ (b) $P/P^{H}_{GY} = 0.815$.

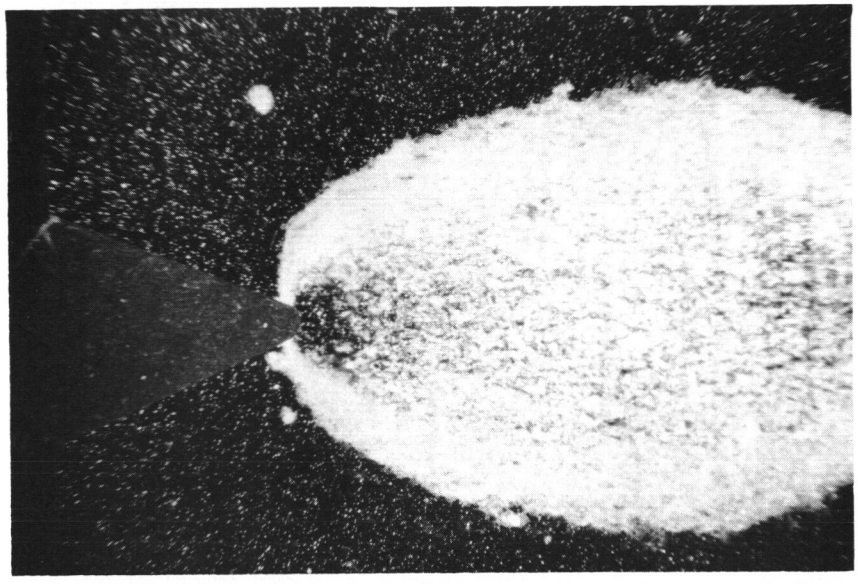

(a)

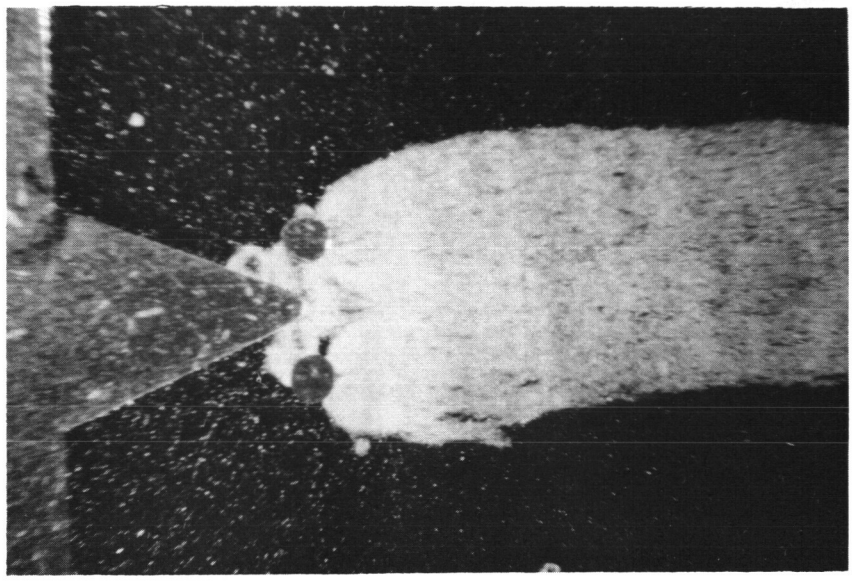

(b)

Figure 6.17 The effect of two drilled holes on the plastic zones revealed by dislocation etch pitting just below the surface of symmetrically notched (and drilled) sheet tension samples of FeSi 1; magnification = 8X, test temperature = $25^{o}C$,

(a) $P/P_{GY} = 1.07$ (b) $P/P^{H}_{GY} = 1.02$.

CHAPTER VII

THE EFFECT OF MORE COMPLEX GEOMETRIES ON NOTCH TOUGHNESS

Having now defined the improvement produced by two 0.0292" diameter holes, certain geometrical modifications were examined which were believed to have additional advantages. At the same time, these modifications served to further define important geometric variables and the generality of some of the earlier conclusions. Each geometry, with the exception of the first discussed here, was studied in steel 0.24 by means of the instrumented Charpy bend test. Each geometry is discussed separately, but comparison with the previous results is made whenever possible.

7.1 Two Holes - Drilled Part-way Through the Charpy Thickness

In all previous experiments, holes have been drilled entirely through the thickness of the Charpy bar. To investigate whether beneficial effects could be obtained if holes were drilled only part-way through the thickness, three series of Charpy samples were prepared with two 0.0292" holes located at R = 0.0448", $\theta = 75^{o}$ but drilled only 1/3, 2/3, and 5/6 of the total thickness. Holes were drilled symmetrically about the mid-thickness (i.e., the 2/3 thickness hole was drilled 1/3 of the thickness from each surface so that two holes appeared at optimum geometry on each face). For comparison, a fourth series was drilled 2/3 of the total thickness entirely from one face.

The alloy used for these tests was steel 0.025 in which the geometrical studies of Chapter III and the slow-bend tests of Chapter VI

were performed. For each series of specimens, the impact energy increased sharply from less than 20 to 240 ft. lbs. at a well defined ductility transition temperature, which varied with the drilling depth as shown in Figure 7.1. When holes are drilled completely through the thickness, the transition temperature is reduced by $\Delta T_N = -33^oC$. This optimum improvement is also obtained when holes are drilled 5/12 of the thickness from each face (5/6 total thickness) or 2/3 of the total thickness from one face. Drilling 1/3 of the thickness from each side (2/3 total depth) produces only a 10^oC lowering of T_N, and drilling 1/6 of the thickness from each side (1/3 total depth) produces no improvement at all.

For optimum improvement in partially drilled specimens, the degree of constraint and strain concentration ahead of the notch must be maintained low in whatever thickness is left undrilled. More specifically, criterion 1 [equation (6.21)] must be satisfied across the entire bar at all temperatures where it would be satisfied within the totally drilled sample. In these cases, fibrous tears spread between the notch and the holes over that portion of the thickness where holes exist, and the undrilled portion then acts very much like a shear lip. Because the notch displacement required to shear off the undrilled portion is higher than that required to reach one hole (less strain concentration), the undrilled region actually continues to support some load as the first tear forms. This, in turn, makes reinitiation from one hole more difficult [$V^*(c+H)\uparrow$] and insures that tearing will reach the second hole (criterion 2, equation (6.22) is satisfied).

At lower temperatures or when the holes are shallower, sufficient constraint exists in the undrilled portion to nucleate a cleavage crack

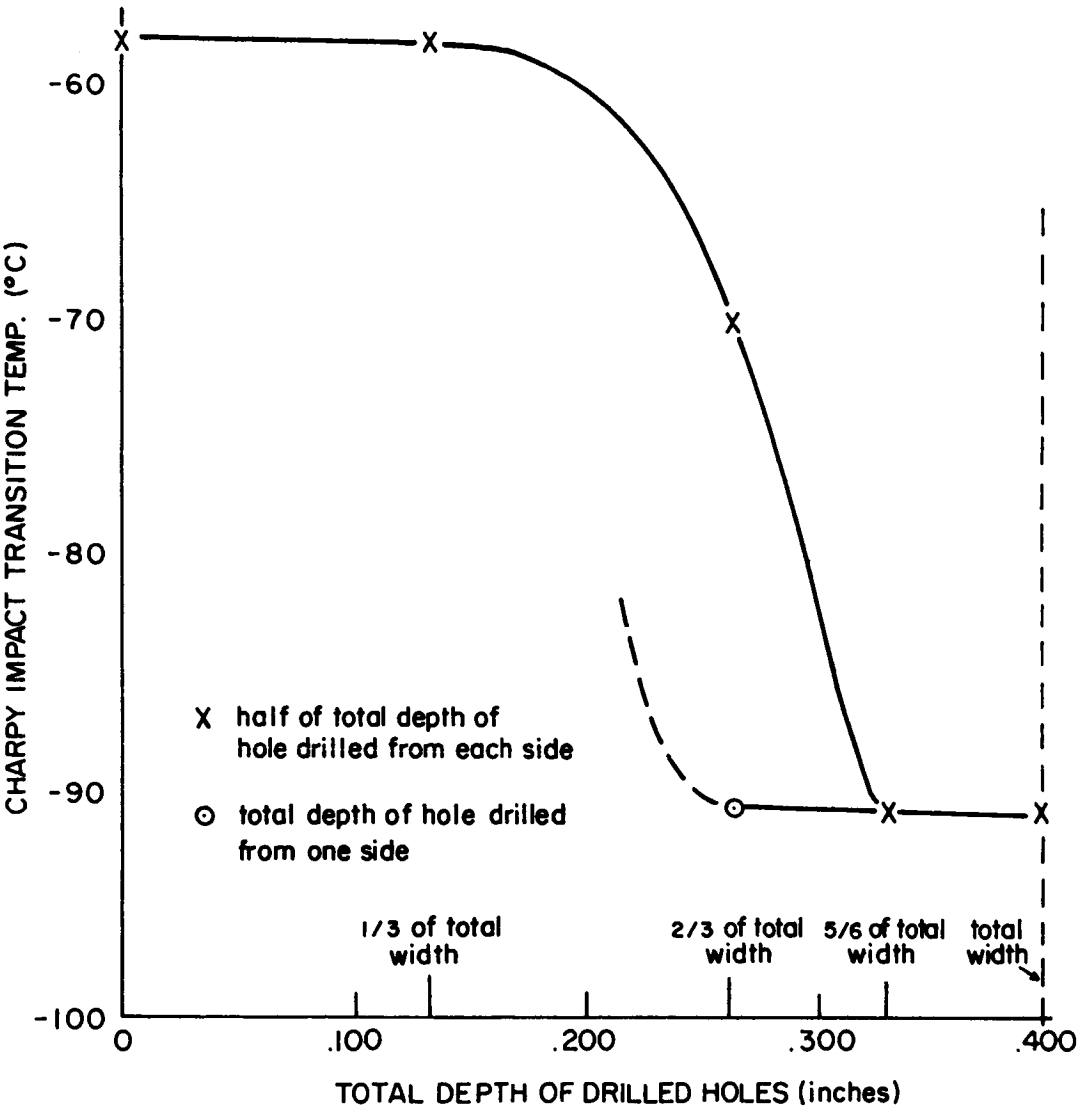

Figure 7.1 The effect of two holes (H_D = 0.0292", R = 0.0448", $\theta = 75^{\circ}$), drilled to various fractions of the total thickness, on the ductility transition temperature ($T_N = T_S$) of Charpy impact samples of steel 0.025.

ahead of the notch. This crack propagates forward in the direction of the notch and outward between the holes in the drilled portion, producing complete cleavage fracture that does not contact the drilled holes.

Conceptually, the undrilled thickness may be considered as an undrilled Charpy sample having a reduced thickness. As the sample thickness (t) decreases, the maximum obtainable value of constraint $\left[K_{\sigma(p)}^{max,t}\right]$ which is developed prior to general yield decreases[66], and it is also more easily relaxed by plastic deformation above general yield. (This will be discussed in detail in Chapter VIII.) Thus if the undrilled portion is thin enough, the amount of triaxiality is less than that present in the drilled portions $\left[\text{i.e., } K_{\sigma(p)}^{max,t} \leq K_{\sigma(p)}^{max,H}\right]$, and optimum improvement is obtained. In a partially drilled sample, the drilled portions of the thickness still contribute somewhat to the plastic constraint in the undrilled portion so that $K_{\sigma(p)}^{max,t}$ depends on whether that portion falls in the specimen center or at the surface. Consequently, a given total drilling depth is more effective (Figure 7.1) when drilled completely from one side so that the undrilled portion extends to the side surface.

7.2 Two holes connected with the notch by saw-cuts

Two holes have been shown to markedly improve the notch toughness of Charpy samples especially when test conditions are such (two criteria) that fibrous tearing occurs to both holes. A similar geometry may be formed prior to impact by physically connecting each hole (H_D = 0.0292", R = 0.0448", $\theta = 75^o$) with the side of the notch by means of a jeweler's saw cut as shown in Figure 7.2. A series of instrumented Charpy tests were performed on this geometry in steel 0.24, and the fracture results

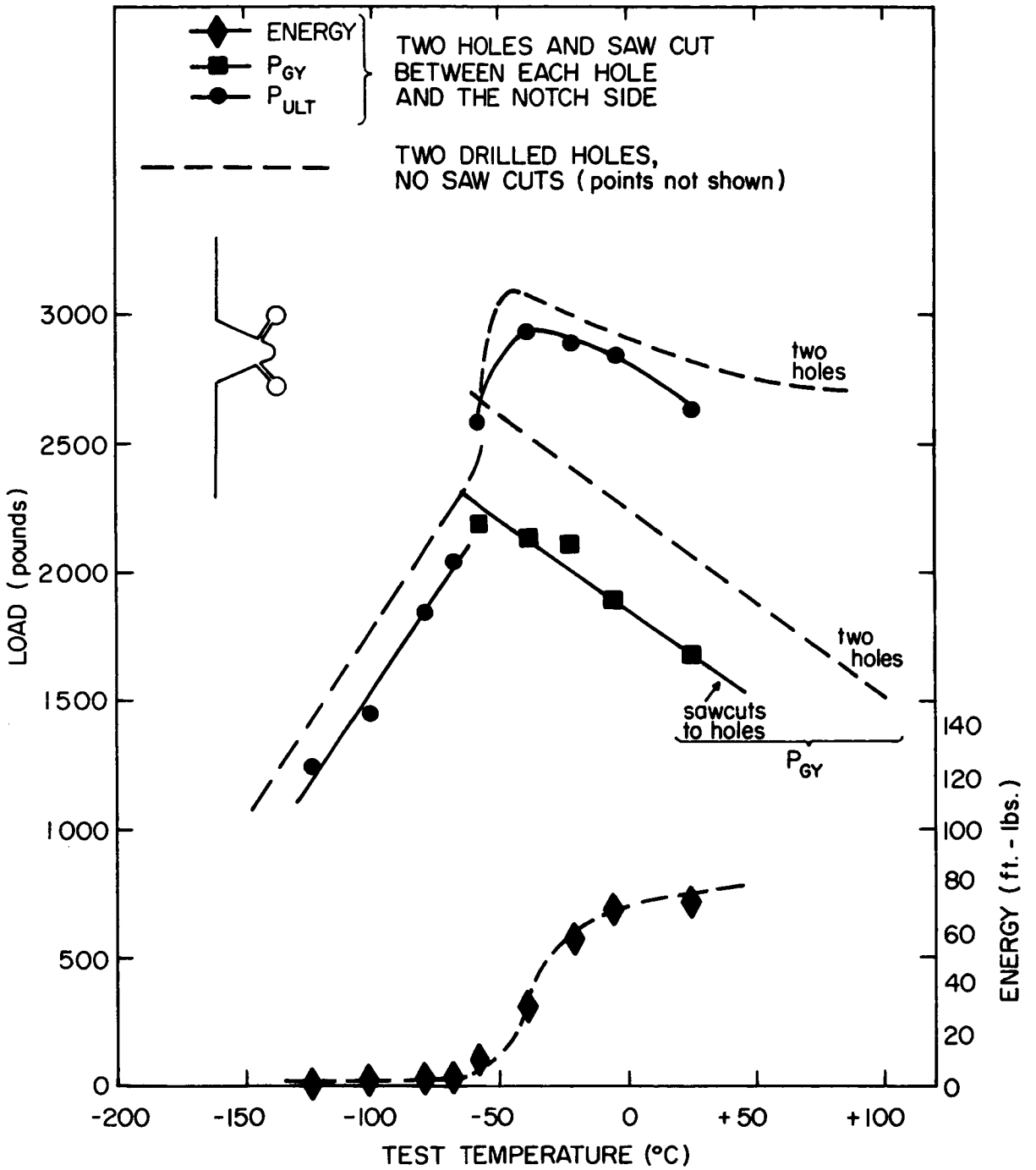

Figure 7.2 Instrumented Charpy fracture results at various test temperatures for steel 0.24 samples containing two drilled holes (H_D = 0.0292", R = 0.0448", $\theta = 75^{\circ}$) which are connected with the notch sides by saw-cuts.

are summarized in Figure 7.2.

Compared with the plain drilled sample, saw cuts produced the following changes, which reduce the beneficial effects of hole drilling.

(1) The load-carrying capacity is less at low temperatures where cleavage occurs prior to general yielding. Cleavage is initiated ahead of one of the holes and propagates to complete failure.

(2) The various transition temperatures are approximately unchanged as is the total impact energy curve.

(3) The general yield load is 15 to 20 percent lower, and the ultimate load is only slightly lower.

Proceeding as in Chapter VI, section 6.3, the critical plastic stress concentration factor for cleavage at each temperature is given by

$$K^{F}_{\sigma(p)} = \frac{174{,}000}{\sigma^{*}_{Y}\,(T)} \quad . \qquad (6.12)\ (7.1)$$

The applied load to produce $K^{F}_{\sigma(p)}$ is simply the measured fracture load at the corresponding temperature (Figure 7.2). Therefore, by considering the fracture loads at various temperatures, the build-up of $K_{\sigma(p)}$ with P/σ^{*}_{Y} for the saw-cut geometry is defined as shown in Figure 7.3. Also shown are the analogous curves for the standard Charpy and plain drilled samples from Figure 6.10.

The critical region for cleavage initiation in saw-cut specimens is ahead of the holes because the saw cuts have greatly reduced the stresses at the notch tip. Plastic zones develop from each hole producing constraint and an increase in the maximum local stresses $\left[K_{\sigma(p)} \cdot \sigma^{*}_{Y}\right]$ with applied load. Roughly speaking, the zones develop as they might in a simple notched sample with a slightly deeper but less

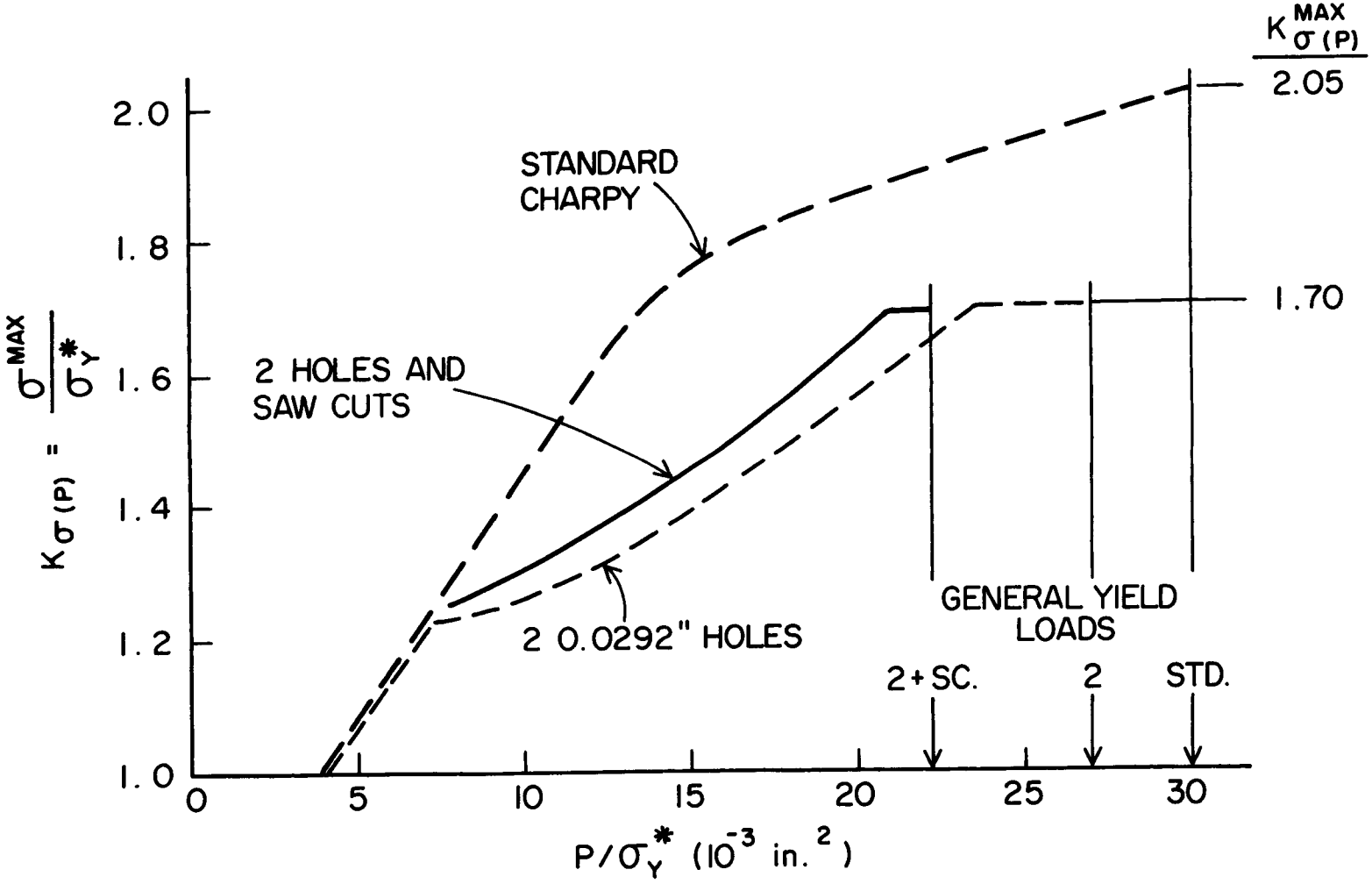

Figure 7.3 The effect of saw-cuts between the notch sides and each hole on the increase of the plastic stress concentration factor [$K_{\sigma(p)}$] with applied load in Charpy samples of steel 0.24.

sharp notch. Because there are two effective notches with larger $\rho = H_D$, neither of which is oriented normal to the minimum cross section, it requires a larger displacement and applied load to produce a given $K_{\sigma(p)}$ than it does in the standard Charpy. As a result, the saw-cut samples have higher toughness than the standard Charpy sample. However, the improvements are not as great as in drilled samples without the saw cuts because there is no mechanism whereby strain is concentrated away from the relocated critical region. $K_{\sigma(p)}$ thus builds up more rapidly with applied load ahead of the saw-cut holes than it does ahead of the notch in plain drilled samples.

In Chapter VI equation (6.23), the general yield load was shown to be related to the distribution of longitudinal stress $\sigma_{yy}(x)$ by

$$\frac{P_{GY}L}{2} = \int_{x=0}^{x=a} x\,\sigma_{yy}(x)\,t\,dx \quad . \qquad \begin{matrix}(6.23)\\(7.2)\end{matrix}$$

Because the saw-cuts isolate the notch tip, the stresses (σ_{yy}) are very small ahead of the notch; therefore, the general yield load (P_{GY}) is correspondingly smaller. In contrast to the plain drilled sample, this reduction in average constraint does not reflect a similar reduction in $K^{max}_{\sigma(p)}$ since the maximum stress no longer occurs in the notch cross section but ahead of the holes.

Although $K_{\sigma(p)}$ builds up more rapidly with applied load in saw-cut samples than in plain drilled samples, the much lower P_{GY} causes the maximum constraint at P_{GY} ($K^{max,H}_{\sigma(p)} = 1.70$) to be the same in both samples. The reduction in the Charpy nil-ductility temperature

$$\Delta T_D = \frac{\left[K^{max}_{\sigma(p)} - K^{max,H}_{\sigma(p)}\right]}{K^{max,H}_{\sigma(p)} \quad K^{max}_{\sigma(p)}} \cdot \frac{\sigma_f}{d\sigma^*_Y/dT} \qquad \begin{matrix}(6.15)\\(7.3)\end{matrix}$$

is consequently the same for both samples. The ductility transition temperature is also about the same because deformation during and after general yielding effectively blunts the holes in both cases making cleavage initiation (saw-cut) or reinitiation (plain drilled) from the holes equally difficult. Once tears reach both holes in the plain drilled sample, the resulting geometry is very similar to a saw-cut specimen deformed a similar amount. It is therefore not surprising that both samples obtain the same ultimate load (P_{ULT}) and generally behave alike at high temperatures.

7.3 Four 0.0292" holes

This geometry consisted of the standard two 0.0292" diameter holes located at R = 0.0448", $\theta = 75^o$ and two additional holes of the same size positioned at R = 0.0584", $\theta = 60^o$ from the center of the other holes. It was hoped that this modification could (1) encourage shear failure to the close holes by better concentrating strain away from the notch tip, but (2) make reinitiation of cleavage from these holes more difficult, thereby reducing the ductility transition temperature. The transition behavior of four-hole Charpy samples of steel 0.24 is summarized in Figure 7.4.

The changes induced by four drilled holes are considerably different from those produced by two holes alone.

(1) At low temperatures, the load carrying capacity (fracture strength) of 4-hole samples is as much as 150% greater than the standard

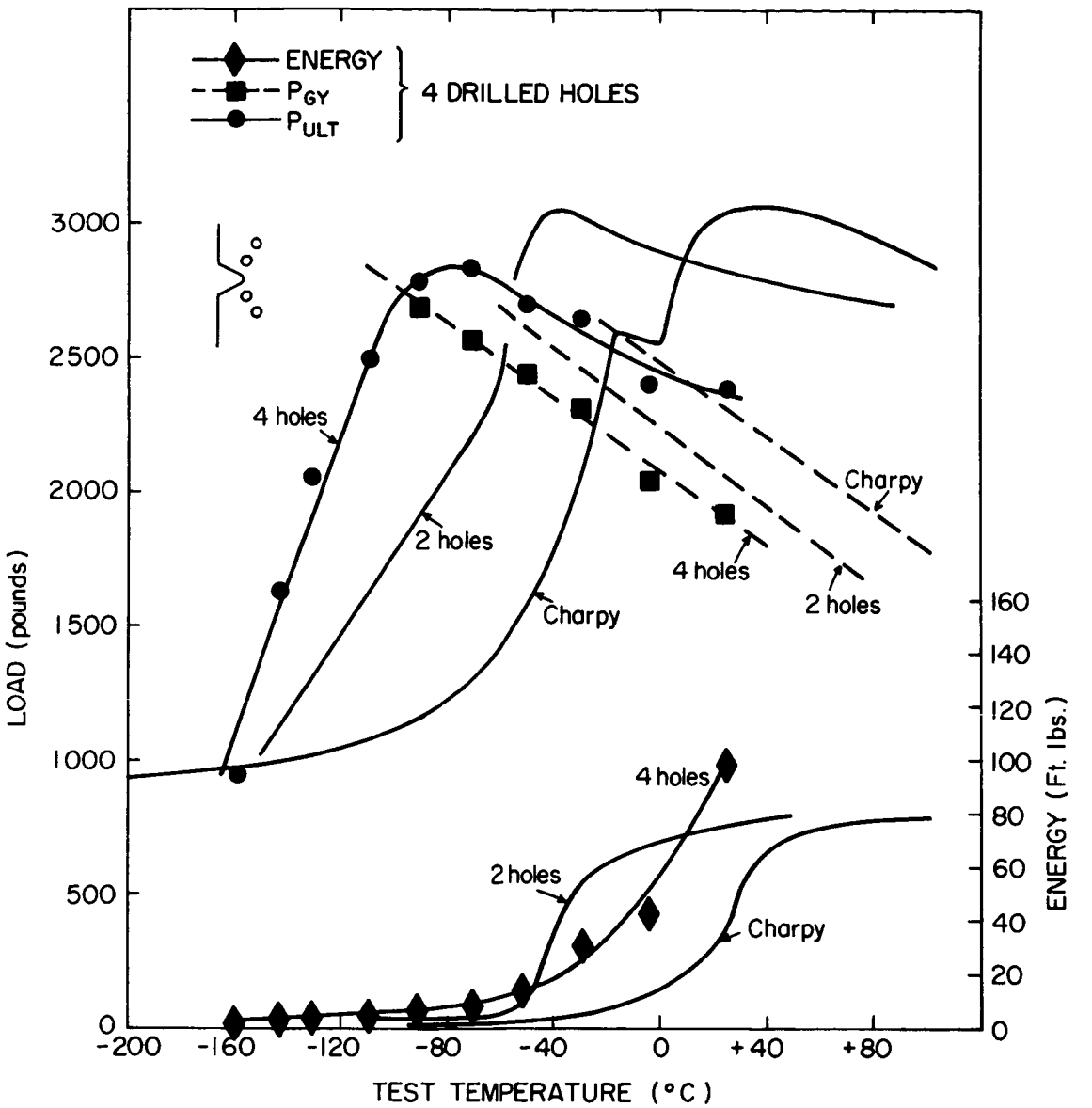

Figure 7.4 Instrumented Charpy fracture results at various test temperatures for steel 0.24 samples containing four 0.0292" diameter holes.

Charpy, which is almost twice the improvement produced by two holes. This improvement is obtained when cleavage is nucleated below the notch root and propagates across the bar without encountering any of the holes.

(2) Four drilled holes reduce the nil-ductility temperature of the Charpy sample by $\Delta T_D = -85^oC$ compared to -40^oC with two holes.

(3) At temperatures between -90^o and -40^oC, fracture occurs after general yielding (at a lower P_{GY}) by fibrous tearing to one hole, propagation of this tear to the second hole on the same side of the notch, and initiation of cleavage from the second hole. Because tearing has not occurred to both sides of the notch, the total displacement and impact energy are below 20 ft. lbs. This behavior differs markedly from the two-hole samples in which the ductility transition temperature is almost coincident with the nil-ductility temperature.

(4) At temperatures above -40^oC but less than $+10^oC$, tearing reaches both holes on one side of the notch and the closest hole on the other side; but cleavage still initiates directly below the outermost hole. There is a marked increase in the notch displacement and thus the total energy prior to fracture so that $T = -40^oC$ represents the ductility transition temperature. However, Figure 7.5a shows that there is no sharp increase in the applied load accompanying the increased deflection like that which is observed at T_{NH} with only two holes. Instead the mechanical instability and area reduction associated with the tearing causes a drop in load which then increases only slightly with further displacement. As a result, the fracture or ultimate load remains quite low regardless of the ductility.

(5) At temperatures above $+10^oC$, tearing reaches all four holes,

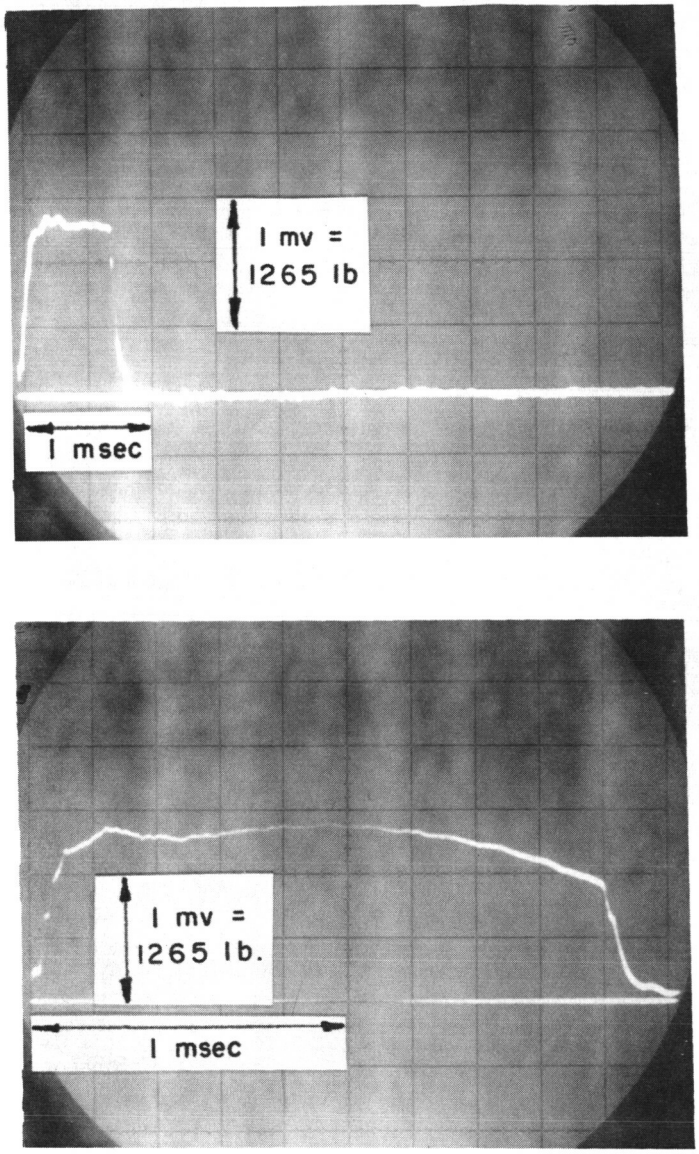

Figure 7.5 Load-time traces for steel 0.24 samples containing:
(a) Four 0.0292" holes, test temperature = -29°C,
(b) Two 0.0595" holes, test temperature = -29°C.

and the total energy shows another sharp rise. Final fracture now occurs by fibrous initiation from one of the outer holes. Because of the drop in load when tearing occurs to the holes, the ultimate load is actually lower than the load at which tears first form. Compared with either two drilled holes or the standard Charpy, the load carrying capacity of four-hole samples is much lower at high temperatures even though the toughness is increased.

Since four holes produced such dramatic improvements at low temperature, their effect on the shape of the local plastic zones was observed directly. Proceeding as in Chapter V, Fe-Si 2 samples were machined and recrystallized to obtain a strain-free homogeneous grain size. Samples were then loaded to various P/σ_Y^*, and the yielded regions revealed by dislocation etch-pitting. Figures 7.6 - 7.9 show the observed zones along with those previously obtained for standard Charpy and two-hole samples. Although two holes alone reduce the size of the plastic zone at the notch tip, four holes are even more effective in minimizing deformation at and below the notch root as the load increases. The strain concentration between the notch sides and the holes nearest the notch is similar to that when only two holes are present. At higher loads, the additional holes cause extension of high strain regions further away from the minimum section and thereby reduce the strain concentration in the secondary hinges ahead of the two closest holes.

Again proceeding as in Chapter VI, section 6.3, the rate of increase in $K_{\sigma(p)}$ with applied load in the four-hole samples was determined from the fracture loads (P_F/σ_Y^*) at various temperatures ($K^F_{\sigma(p)}$). The results, summarized in Figure 7.10, indicate that constraint builds up

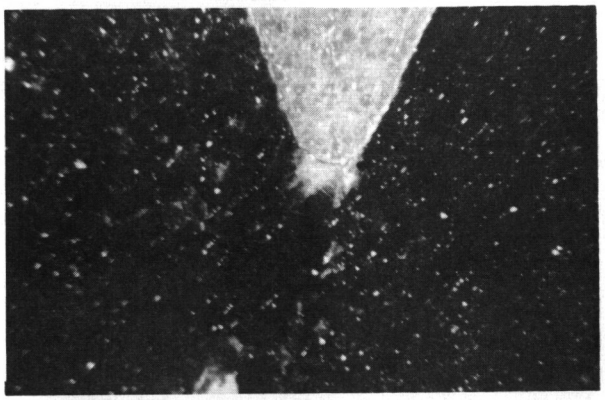

(a)

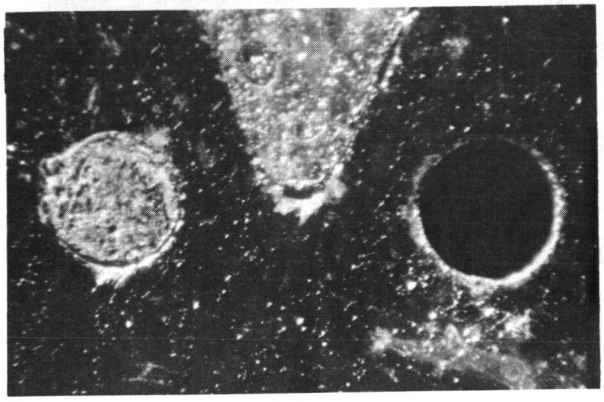

(b)

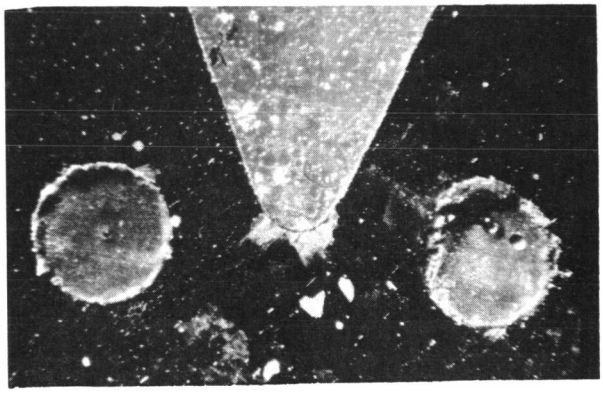

(c)

Figure 7.6 Comparison of the yield zones which result in Charpy, two-hole, and four-hole samples after loading to P = 750 lb.; $P/\sigma_Y = 9.7\ (10^{-3}\ in^2)$, magnification = 24X; (a) $P/P_{GY} = .33$, (b) $P/P_{GY} = .36$, (c) $P/P_{GY} = .39$.

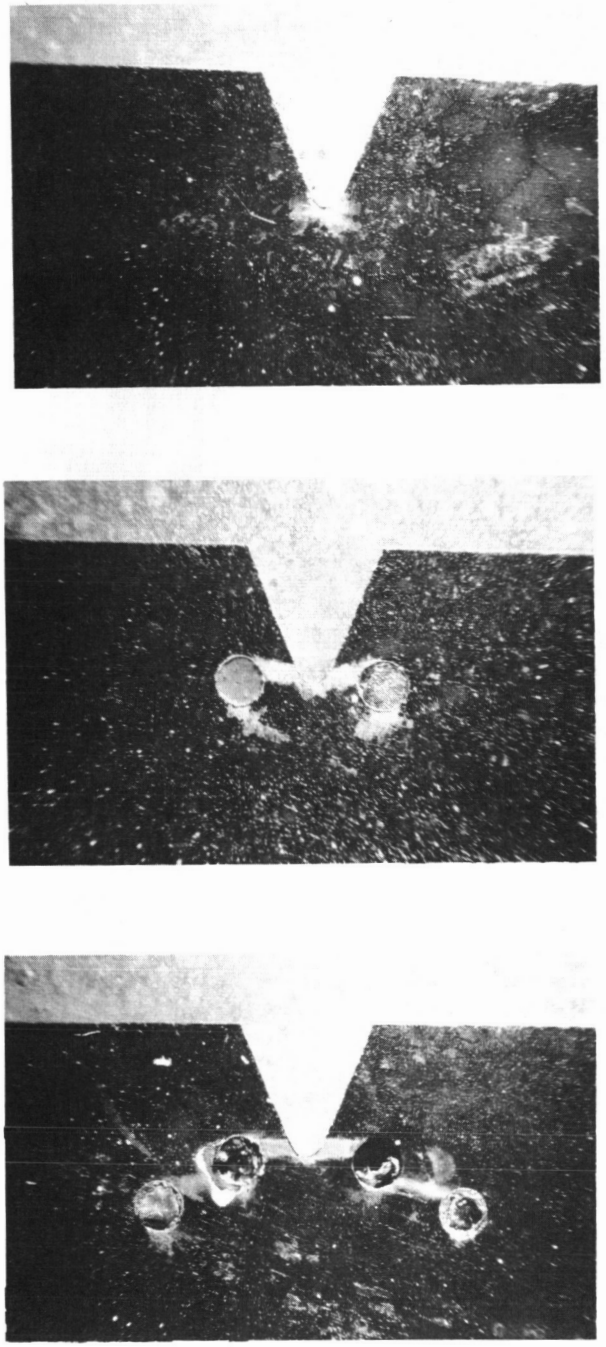

Figure 7.7 Comparison of the yield zones which result in Charpy, two-hole, and four-hole samples after loading to P = 1250 lb.; P/σ_Y = 16.0 (10^{-3} in^2), magnification = 8.9X;

(a) P/P_{GY} = .53, (b) P/P_{GY} = .60, (c) P/P_{GY} = .63.

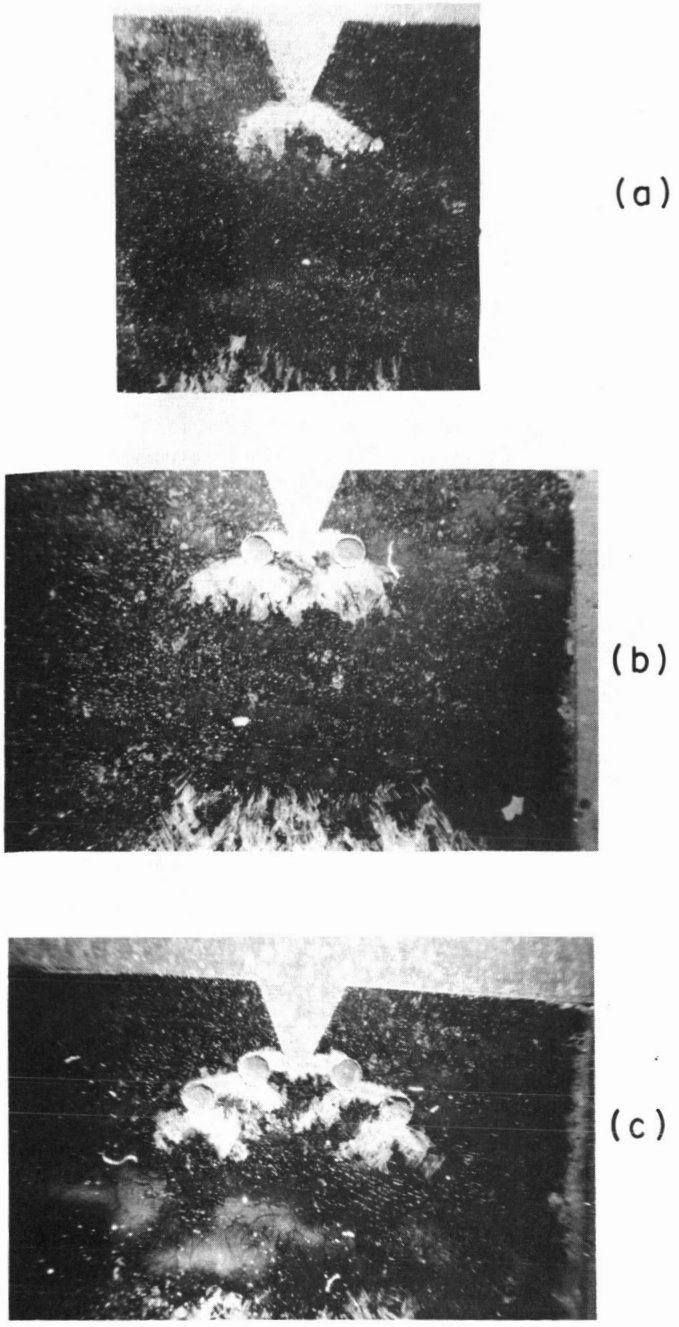

Figure 7.8 Comparison of the yield zones which result in Charpy, two-hole, and four-hole samples after loading to P = 1750 lb.; P/σ_Y = 22.4 (10^{-3} in^2), magnification = 5.6X;

(a) P/P_{GY} = .75, (b) P/P_{GY} = .82, (c) P/P_{GY} = .91.

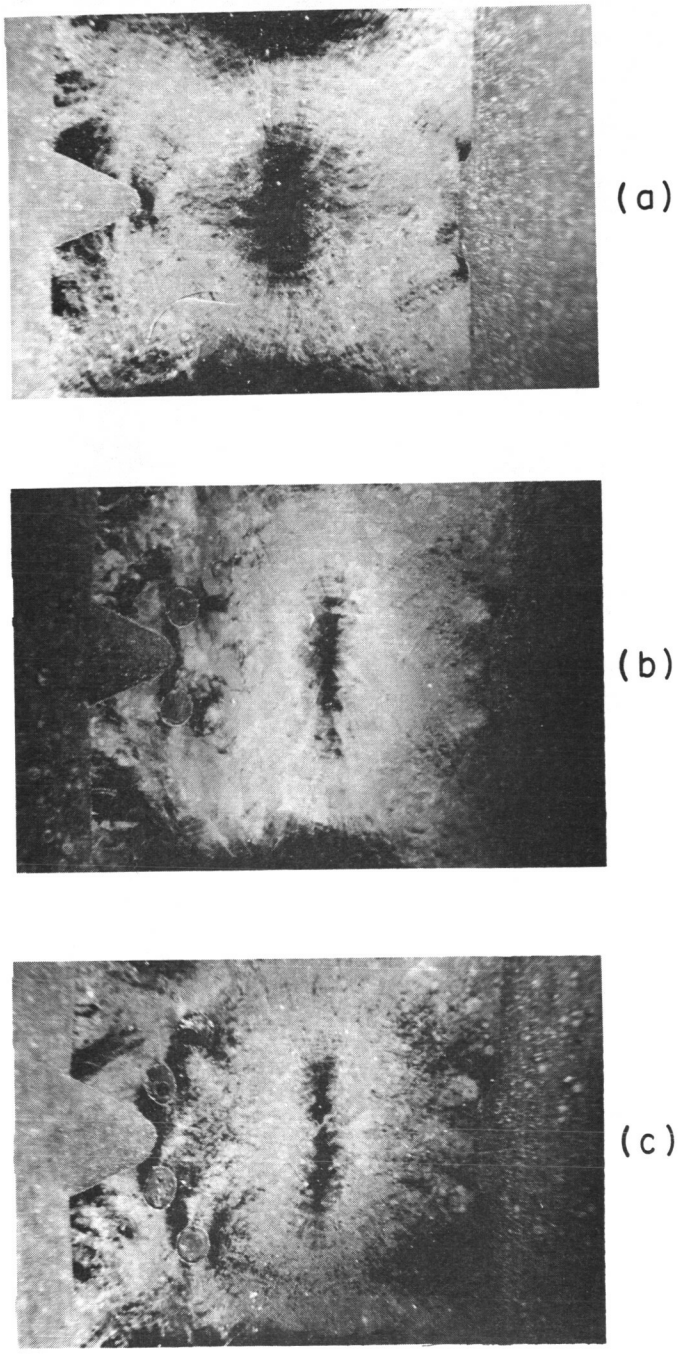

Figure 7.9 Comparison of the yield zones in Charpy, two-hole, and four-hole samples after loading to P = 2550 lb.; P/σ_Y = 32.7 (10^{-3} in^2), magnification = 5.6X; (a) P/P_{GY} = 1.09, (b) P/P_{GY} = 1.20, (c) P/P_{GY} = 1.33.

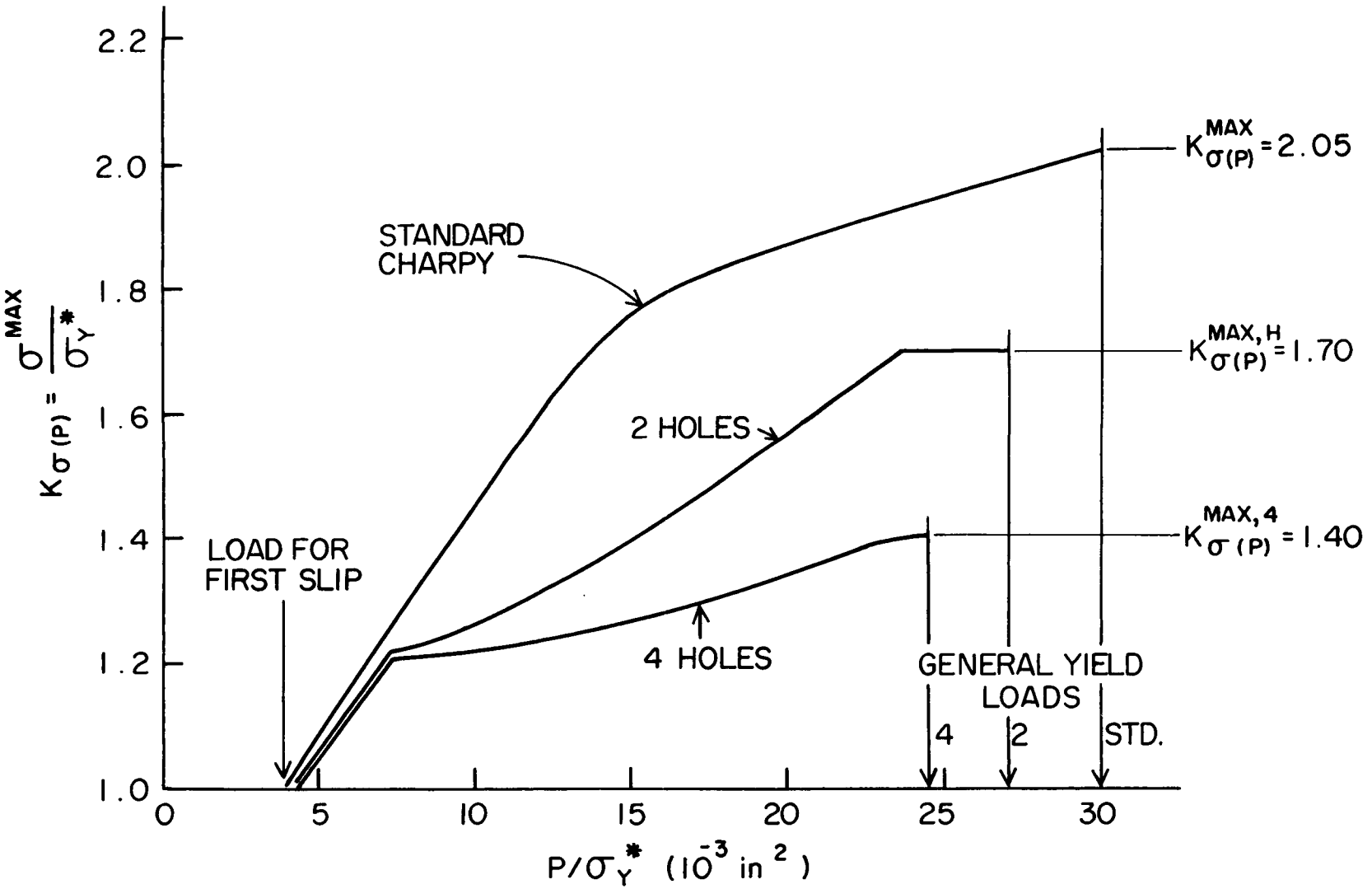

Figure 7.10 Comparison of the increase in plastic stress concentration factor $[K_{\sigma(p)}]$ with applied load in Charpy, two-hole, and four-hole samples of steel 0.24.

much less rapidly with applied load and reaches a lower maximum $\left[K_{\sigma(p)}^{max,4}\right] = 1.40$ when four holes are present. This large improvement over two holes is a little surprising in view of the similarity between the shape of the plastic zones. However, it is the amount of triaxiality at the elastic-plastic boundary rather than the size of the zone that determines the maximum tensile stress $\sigma^{max} = K_{\sigma(p)}\sigma_Y^*$. For the Charpy notch, $K_{\sigma(p)}$ is directly related to R by equation (6.8), but in general no simple relationship exists. Consequently, quite different $K_{\sigma(p)}$ may result from the same zone size depending on the notch geometry.

Although four holes greatly improve the fracture strength at low temperatures, their effect at intermediate and high temperatures is much less desirable than two holes alone (Figure 7.4). Low energy fractures can still occur through the holes on one side of the notch at temperatures up to 50°C above the nil-ductility temperature while the ductility transition is approximately coincident with T_{DH} in the two-hole samples. Even when tearing reaches both sets of holes ($T > T_{NH} = -40$), cleavage reinitiation occurs at temperatures up to +10°C (T_N of standard Charpy), and the total energy in this range is less than that absorbed by the standard two-hole geometry.

Four holes reduce the general yield load of Charpy samples even more than two holes do. By reference to equation (7.2), this results from the lower average tensile stress ahead of the notch when four holes are present. In addition, the fracture or ultimate load remains low at higher deflections because tearing to the holes reduces the effective load bearing area significantly. In other words, because the applied load depends on the stresses in the net section

$$P = \frac{2}{L}\, t \int_{x=0}^{x=a} x\, \sigma_{yy}(x)\, dx \qquad (7.4)$$

[the symbols have the same meaning as in equations (6.23) and (7.2)], unobtainable amounts of strain hardening are necessary to compensate for the large region of low σ_{yy} that is isolated below the notch by tearing.

7.4 Two holes - larger diameter

To investigate whether further improvements could be obtained by increasing the hole diameter, instrumented Charpy transition curves were obtained in steel 0.24 for two larger hole sizes (H_D = 0.0465", 0.0595"). In both cases, the angular coordinant ($\theta = 75^o$) was maintained constant and the radial positions (R = 0.0624", 0.0690") were chosen to maintain the spacing between the notch side and the hole edge at constant 0.0292". The fracture results for both hole sizes are summarized in Figure 7.11.

Qualitatively, the larger holes produce effects similar to two 0.0292" diameter holes, but the magnitudes of the changes are significantly different. Specifically, increased hole diameter:

(1) improves the fracture strength at low temperatures (for H_D = 0.0465", the improvement is almost the same as for H_D = 0.0292"; but for H_D = 0.0595", the fracture load is 15 to 20% higher);

(2) lowers the nil-ductility temperature by 10 to 15°C more than 0.0292" holes (reduction is largest for H_D = 0.0465");

(3) lowers the ductility transition temperature by about the same amount as 0.0292" holes, but as in the four-hole samples, the sharp increase in impact energy and critical displacement at the ductility transition T_{NH} is not accompanied by a rise in applied fracture

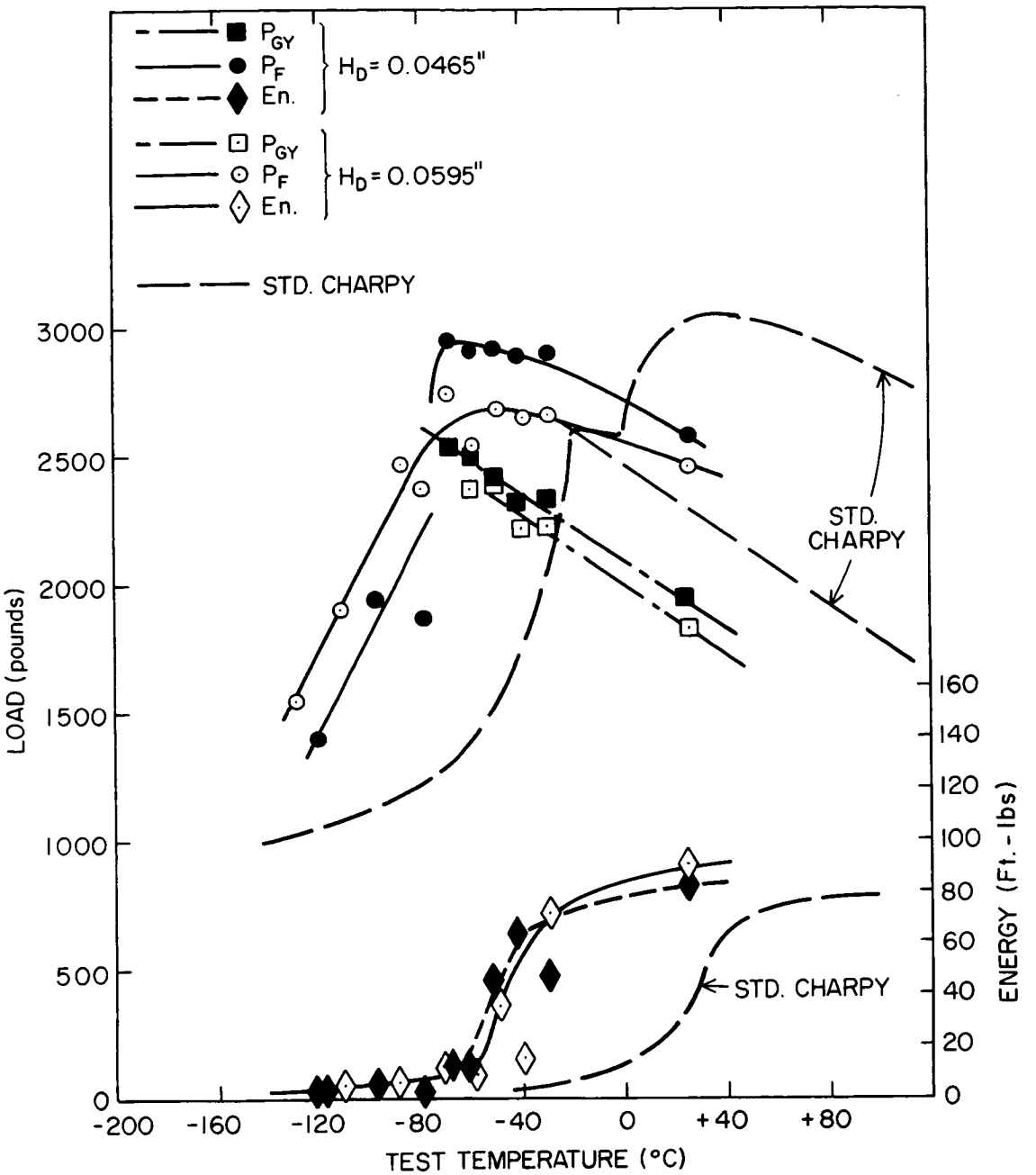

Figure 7.11 Instrumented Charpy fracture results at various test temperatures for steel 0.24 samples containing two holes of larger diameter (H_D = 0.0465", 0.0595"), $\theta = 75^o$ for both, and R = 0.0624" and 0.0690" respectively.

load; Figure 7.5(b) shows a load-time trace at a temperature just above T_{NH}, indicating that the bar deforms at nearly constant load after tearing reaches both holes;

(4) reduces the general yield load (P_{GY} (0.0292") > P_{GY} (0.0465") > P_{GY} (0.0595");

(5) reduces the ultimate load substantially below that of H_D = 0.0292" and much more than the corresponding P_{GY} is reduced.

The rate of increase $K_{\sigma(p)}$ with applied load was obtained from the fracture results as described in the previous sections and originally in Chapter VI, section 6.3. The results are summarized in Figure 7.12 for the standard Charpy and the various hole sizes. The low temperature fracture strength increases somewhat with hole diameter because the local redistribution of plastic strain produced by larger holes is able to more efficiently prevent the increase of constraint [$K_{\sigma(p)}$] with applied load. Furthermore, since the reduction in nil-ductility temperature [equation (7.3)] is controlled by $K^{max}_{\sigma(p)}$, ΔT_D is greater for the larger hole sizes.

For 0.0292" holes, the nil-ductility and ductility transitions were approximately coincident (i.e., $T_{DH} = T_{NH}$). However, for the larger hole diameters there is a temperature range of about 15°C above T_{DH} where fracture occurs by shearing to one hole and cleavage reinitiation. As a result, the reduction in the ductility transition temperature with larger hole sizes is about the same as that for 0.0292" holes. Apparently, the larger increase in the effective notch depth, when tearing occurs to one hole, is just compensated by the larger hole radius ($\rho_H = H_D$); the critical displacement required for cleavage re-

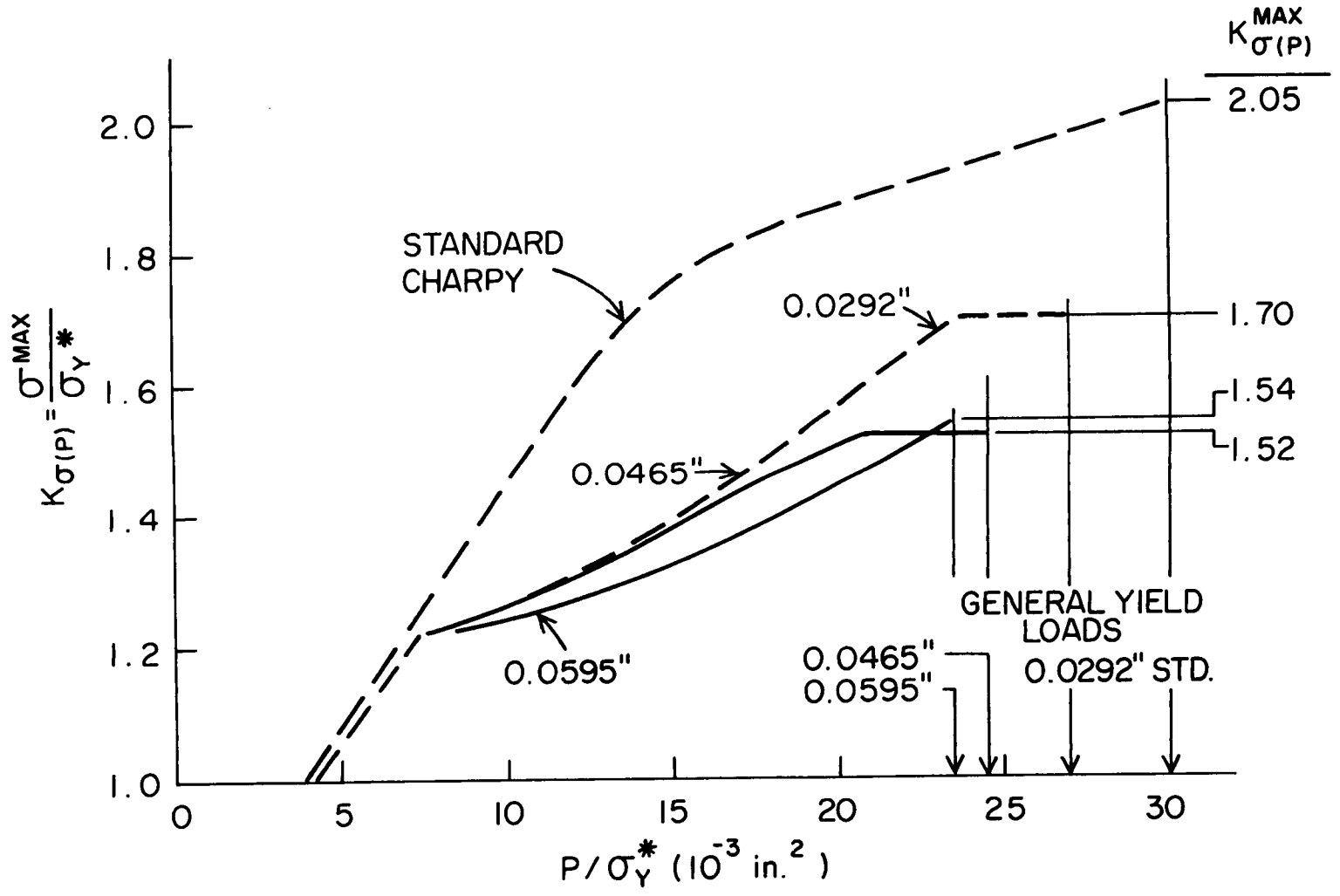

Figure 7.12 The effect of hole size on the increase of the plastic stress concentration factor $[K_{\sigma(p)}]$ with applied load in Charpy samples of steel 0.24.

initiation [$V^*(c+H)$], and thus the temperature (T_{NH}) where tears reach both holes, are about the same for all hole sizes.

As in four-hole samples, the general yield load [equation (7.2)] decreases with increasing hole size because the average tensile stresses [like $K^{max}_{\sigma(p)}$] are lower ahead of the notch. When tearing reaches both holes, the tensile stresses near the "isolated" notch tip are suddenly reduced. The applied load given by equation (7.4) must then decrease momentarily, as shown in Figure 7.5(b). However, the applied load increases gradually with additional notch displacement as the material in the net section strain hardens. Nevertheless, the "isolated" region is larger for larger hole sizes, and consequently the ultimate load, that can be reached by work hardening prior to failure, decreases with hole size.

7.5 Stress relieving notches

Under some circumstances the embrittling effects of a notch can be reduced by locating an additional notch on each side of the original. This well known design technique, called stress relieving notches, is based on reduction of the elastic stress concentration factor, K_σ. The technique has been successfully applied to completely brittle materials[106] and low stress fatigue failure of normally ductile metals[107]. In both cases, K_σ is the controlling factor. Little is known about the improvements possible when considerable amounts of local or general yielding occur. For comparison with the various hole geometries, a series of 0.24 steel Charpy samples was prepared with two additional Charpy notches located with their tips 0.090" from that of the central notch. The instrumented Charpy fracture results at various temperatures

are summarized in Figure 7.13.

In all cases, regardless of test temperature or fracture initiation mode, fracture initiates ahead of one of the outer notches and propagates to failure. At temperatures between -130 and -90°C, "stress relieving notches" increase the fracture strength of the Charpy sample but to a lesser extent than two 0.0292" holes. At still lower temperatures, where fracture occurs on first slip and two holes have little effect, three notch samples would be somewhat stronger[106]. Between -70 and -40°C, the three-notch specimens failed at or just before general yielding and absorbed less than 7 ft. lbs. energy. Although these fracture loads are a significant improvement over the standard Charpy, drilled samples (H_D = 0.0292") are both tougher and stronger over the same temperature range. There is a sharp increase in the total deflection, applied load, and total energy at the ductility transition temperature of about -30°C, but fracture still initiates by cleavage. Above -5°C, the displacement for cleavage is so large that initiation and 70% of the total fracture is fibrous. The ultimate load and total energy of three-notch samples at high temperatures are somewhat better than in two-hole samples.

As in previous cases, the increase of $K_{\sigma(p)}$ with applied load prior to general yield (P_{GY}) was calculated from the fracture results and is given by Figure 7.14. The maximum tensile stress $\sigma^{max} = K_{\sigma(p)}\sigma_Y^*$ ahead of the outside notches is comparable to that ahead of the Charpy notch when two 0.0292" holes are present. Improvements are observed in the three-notch sample because the total strain is distributed around three notches rather than one, thereby producing a lower effective

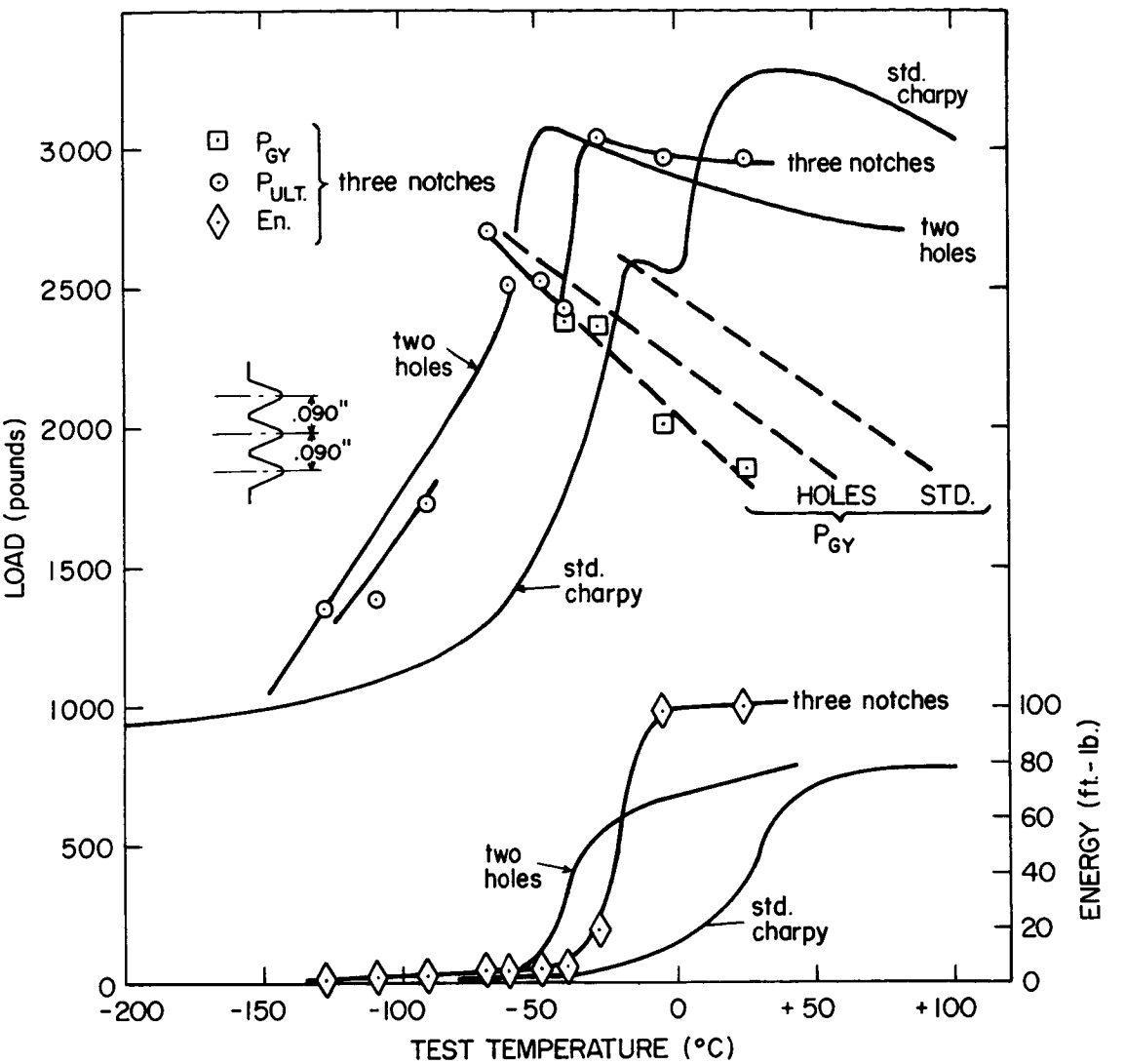

Figure 7.13 Instrumented Charpy fracture results at various test temperatures for steel 0.24 samples containing three Charpy notches (two "stress relieving notches" around the standard notch).

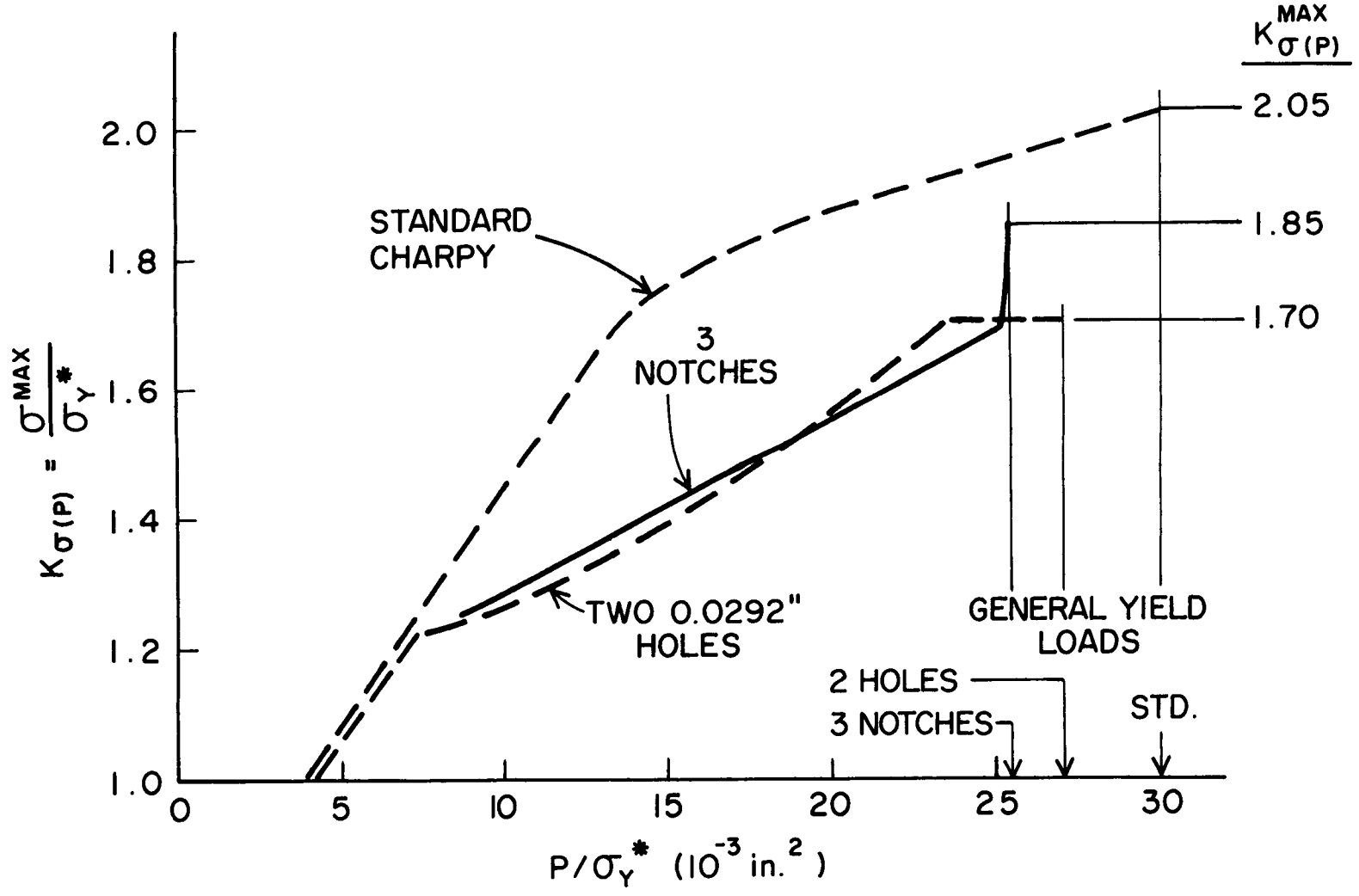

Figure 7.14 The effect of two additional Charpy notches on the increase of the plastic stress concentration factor [$K_{\sigma(p)}$] with applied load in Charpy specimens of steel 0.24.

strain rate (σ_Y^*) and a lower strain concentration (zone size) at any one notch. However, the instability associated with general yielding of the three-notch geometry produces a sudden increase in both strain rate and strain hardening, and the effective $K_{\sigma(p)}$ increases from 1.70 to 1.85 at P_{GY}. Therefore, fracture occurs at P_{GY} over the range of temperatures where $\sigma_f/\sigma_Y^* \equiv K^F_{\sigma(p)}$ is between 1.7 and 1.85, and the ductility transition is moved to a temperature considerably above the nil-ductility temperature.

The general yield load of three-notch samples is much less than that of standard Charpys and even less than that of the two-hole samples. However, as in the case of the saw-cut samples, this reduction in <u>average</u> constraint is not necessarily indicative of lower <u>maximum</u> constraint since the critical region no longer occurs in the section of symmetry. Finally at high temperatures, the shelf energy for the three-notch samples is higher than either the standard Charpy or the drilled sample. This simply reflects (1) the larger volume of plastically deformed material which is present when a full thickness fibrous crack develops (P_{ULT}) and (2) the larger area over which the fibrous crack must propagate for complete separation.

7.6 <u>The effect of smaller notch tip radius (ρ = 0.002") on the improvement from hole drilling</u>

In order to determine whether similar improvements from hole drilling could be obtained when the initial stress concentration is more severe, the root radius of the Charpy notch was reduced. Instrumented impact bend tests were performed on two series of 0.24 steel samples: (1) a standard 45° V-notch with root radius ρ = 0.002" and

(2) the same sharp notch with two 0.0292" diameter holes located as shown in Figure 7.15. The fracture results for both are summarized in Figure 7.15.

The fracture load of standard samples prior to general yielding increases with temperature much like the standard Charpy sample except that the entire transition curve is shifted to temperatures about 40°C higher. The total energy absorbed by sharp-notch samples reaches 20 ft. lbs. at temperatures below the nil-ductility temperature (T_D = +30) even though fracture initiates directly by cleavage at low displacements. This higher energy in brittle samples results from the much larger shear lip (post-brittle) energy present at the higher temperatures just prior to T_D. In contrast to Charpy samples, cleavage is not observed after P_{GY} ($T > 30^{\circ}C$), and T_S is coincident with T_D. The smaller notch radius has little effect on P_{GY}, but does reduce P_{ULT} by about 300 lbs. below that of standard Charpys at corresponding temperatures. This implies that the increased strain concentration at the sharper notch reduces the notch displacement and corresponding load which is required to produce a full width fibrous tear.

Two drilled holes produce significant improvements in the notch toughness of the sharply notched samples. Specifically, two holes reduce the nil-ductility temperature by 60°C down to $T_{DH} = -30^{\circ}C$. Between $T_{DH} = -30^{\circ}C$ and $+10^{\circ}C$, drilled samples show a bimodal behavior failing either by (1) cleavage initiation at the notch tip and propagation between the holes or (2) fibrous tearing to both holes and fibrous reinitiation after very large displacements. In either case, the load carrying capacity of drilled samples is very much greater than the

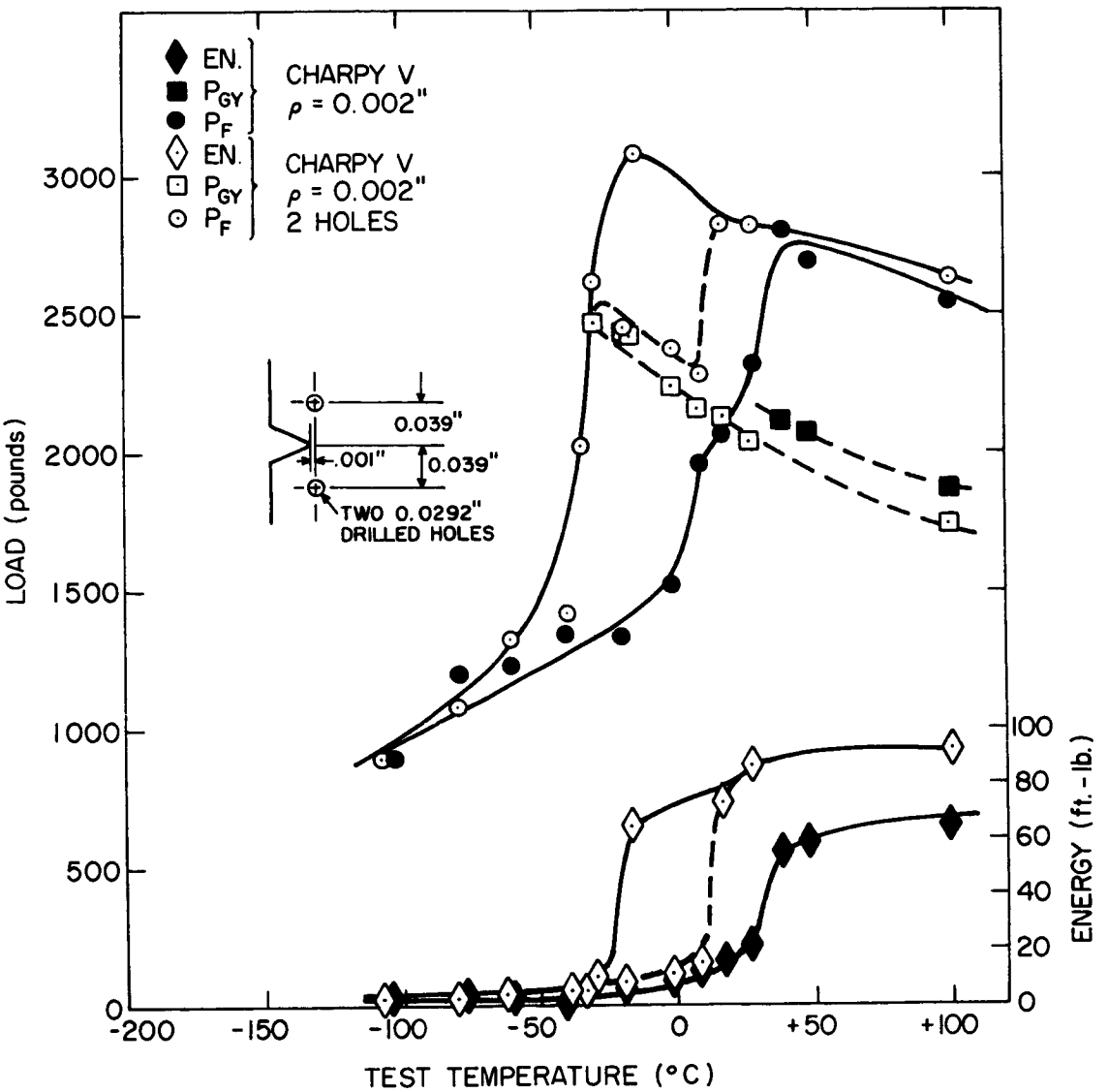

Figure 7.15 The effect of two 0.0292" holes on the instrumented "Charpy" transition behavior of steel 0.24 samples containing a sharper (ρ = 0.002") notch.

standard samples which fail by cleavage at loads well below P_{GY}. Above $T = +10^{o}C$, fracture always reaches both holes so that drilled samples behave like drilled Charpy samples, independent of notch radius.

Due to the reduced root radius, the effective strain rate at the notch tip will be larger than in the standard Charpy samples, especially during the early stages of deformation. Consequently, when fracture occurs prior to general yield, the effective local yield stress will be somewhat greater than that obtained from P_{GY} by equation (6.1) (Figure 6.3). However, at each temperature, we may calculate an effective plastic stress concentration factor for fracture

$$K^{EFF}_{\sigma(p)} = \frac{\sigma^{max}}{\sigma^{*}_{Y}} = \frac{\sigma_{f}}{\sigma^{*}_{Y}} = \frac{174{,}000}{\sigma^{*}_{Y}(T)} \qquad \sigma^{*}_{Y}\ (\dot{\varepsilon} = 10^{2}\ sec^{-1}) \tag{7.5}$$

which is related to actual constraint factor

$$K^{F}_{\sigma(p)} = K^{EFF}_{\sigma(p)} \frac{\sigma^{*}_{Y}\ (\dot{\varepsilon} = 10^{2}\ sec^{-1})}{\sigma^{*}_{Y}\ (actual\ \dot{\varepsilon})} \ . \tag{7.6}$$

That is, the local stresses are raised above $\sigma^{*}_{Y}\ (\dot{\varepsilon} = 10^{2}\ sec^{-1})$ by both constraint and increased strain rate. Without attempting to separate the two effects, the rate of increase of $K^{EFF}_{\sigma(p)}$ (given by equation (7.5)) with applied load P/σ^{*}_{Y} is defined by the fracture load (P_{F}/σ^{*}_{Y}) at various temperatures. The curve for drilled samples is developed in the same way, and the two are compared in Figure 7.16.

In general, two holes cause the maximum local stress to increase less rapidly with applied load, and thereby increase the load carrying capacity at any given temperature $(\sigma_{f}/\sigma^{*}_{Y})$. However, because higher strains are concentrated around the sharp notch, two holes do not exert a strong influence until higher fractions of P_{GY} where the larger zones

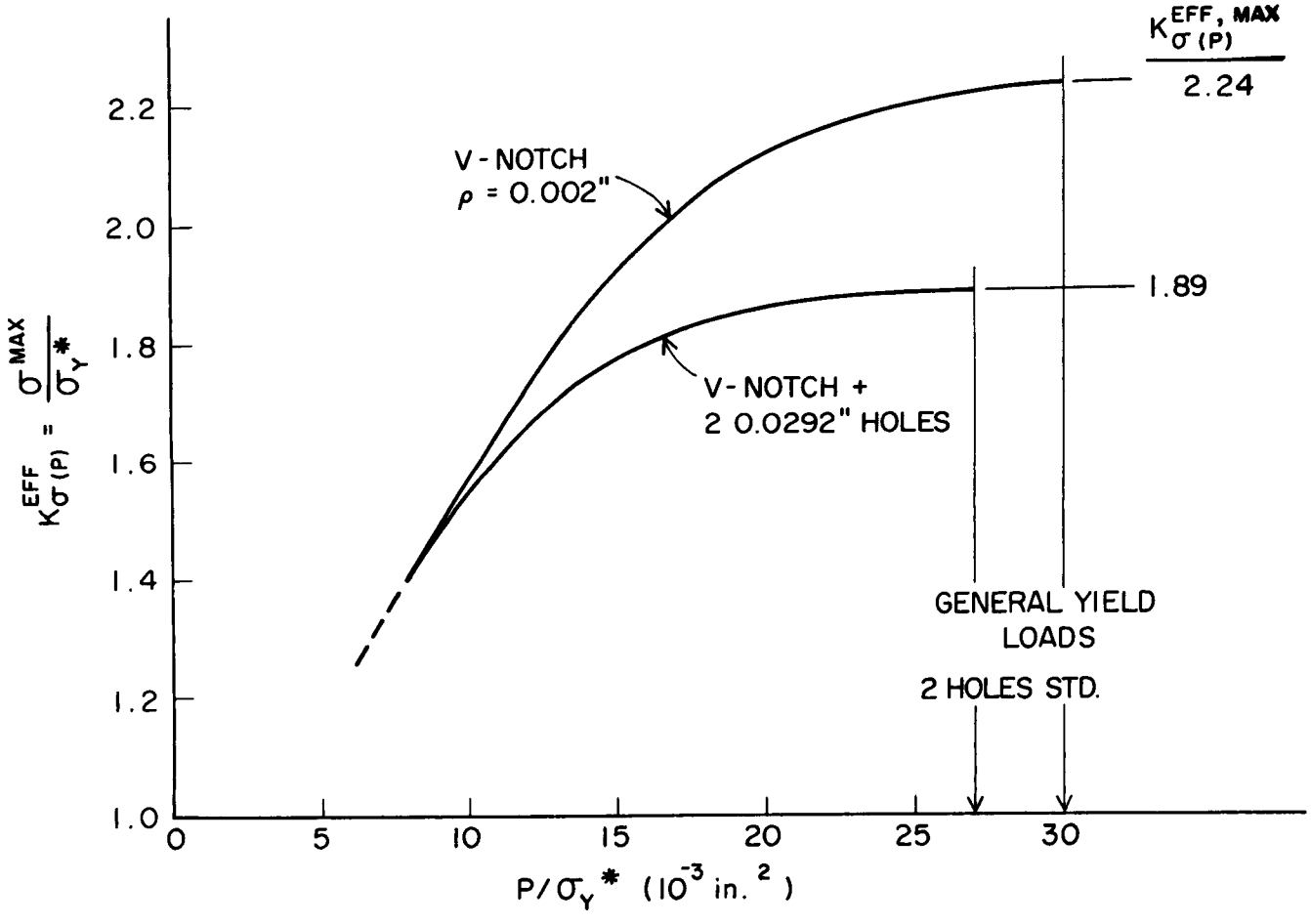

Figure 7.16 The effect of two holes on the increase in the effective plastic stress concentration factor [$K^{EFF}_{\sigma(p)}$] with applied load in steel 0.24 samples containing a sharper (ρ = 0.002") notch.

can interact with the holes. Consequently, the load to produce any $K^{EFF}_{\sigma(p)} < 1.7$ is relatively unaffected by two holes since R is small compared to the spacing between the notch and the holes; but drilled holes cause large increases in the applied load required to obtain higher $K^{EFF}_{\sigma(p)}$. In fact, in the temperature range where $1.89 < \sigma_f/\sigma^*_Y < 2.24$ general yielding and subsequent strain hardening occur prior to failure in drilled samples while standard samples fail prior to general yield. It is interesting to note that the ratio of $K^{EFF,max}_{\sigma(p)}$ in sharply notched standard and drilled samples $\left(\frac{2.24}{1.89}\right)$ is approximately equal to the analogous ratio in samples of Charpy ($\rho = 0.010"$) tip radius $\left(\text{i.e., } \frac{2.05}{1.70} \cong \frac{2.24}{1.89}\right)$. This implies that the additional effects of increased strain rate and local strain hardening at the sharper notch have similar effects in both standard and drilled samples.

The bimodal behavior of drilled samples just above the nil-ductility temperature results because the severe strain concentration at the sharp notch tip can produce enough work hardening to initiate cleavage at temperatures considerably above T_{DH}. That is, the critical displacement required for cleavage in drilled samples

$$V^{**}(c) = \alpha\,\beta\,\rho\,\varepsilon_F = \alpha\,\beta\,\rho\left[\frac{\sigma_f - K^{EFF,max}_{\sigma(p)}\,\sigma^*_Y}{K^{EFF,max}_{\sigma(p)}\,d\sigma/d\varepsilon}\right] \qquad (7.7)$$

increases less rapidly with temperature due to smaller α, ρ, and β and larger $K^{EFF,max}_{\sigma(p)} = 1.89$. The smaller ρ reduces the gauge length of the "miniature tensile specimen" and thus reduces the tip displacement required to produce a given strain at the notch root. β is reduced because the point of maximum triaxiality is closer to the notch root and experiences a strain closer to that at the root. α is also lower because

the effective redistribution of strain away from the point of maximum constraint is less as that point approaches the notch root.

Criterion (1) for reduction in the ductility transition temperature

$$V_H^*(c) < V^{**}(c) \qquad \begin{matrix}(6.21)\\(7.8)\end{matrix}$$

is not surely satisfied until temperatures well above T_{DH}. However, if (7.8) is satisfied prematurely due to unfavorable grain orientation for cleavage, tearing reaches one hole; then the second criterion, that cleavage must not reinitiate from the hole, is easily satisfied at this higher temperature. In other words, for $-30^{\circ} < T < +10^{\circ}C$, tearing reaches both holes if statistical variations allow equation (7.8) to be satisfied prematurely.

At high temperatures ($T > +10^{\circ}C$), tearing always occurs to both holes, and the notch tip is isolated. It is therefore not surprising that drilled samples are relatively independent of the root radius. However, the standard sharp-notch sample can fail fibrously at a lower displacement and ultimate load than the Charpy sample because of the higher strain concentration at the notch tip. At high temperatures drilled holes are thus more effective in the sharply notched samples and are able to increase both the total energy and ultimate load.

7.7 General Discussion of More Complex Geometries

The previous examples have demonstrated that the fracture properties of notched bars can be changed greatly by modifications to the $H_D = 0.0292"$, $R = 0.0448"$, $\theta = 75^{\circ}$ hole geometry. However, no one geometry shows a complete superiority across the entire temperature range

since those which increase notch strength at low temperatures also reduce the general yield and ultimate strength at high temperatures. Each test temperature represents a material with a particular intrinsic toughness $\left[K^{F}_{\sigma(p)} \equiv \sigma_f/\sigma^*_Y\right]$, and the improvement from each geometry varies with this ratio. Consequently, the optimum hole geometry depends on the material's intrinsic toughness under test conditions as well as the severity of the notch.

Figure 7.17 summarizes the percentage improvement in notch strength that can be produced by the various modifications (hole geometries) to the standard Charpy notch as a function of the intrinsic toughness (σ_f/σ^*_Y). In each case, the curve has been calculated from the respective $K_{\sigma(p)}$ vs P/σ^*_Y, and the vertical arrow indicates the intrinsic toughness above which general yielding precedes fracture for the particular hole geometry, i.e., $\sigma_f/\sigma^*_Y > K^{max,H}_{\sigma(p)}$. The maximum improvement in fracture strength prior to P_{GY} (160% increase) is produced by the four 0.0292" diameter holes when $\sigma_f/\sigma^*_Y = 1.4$. With the other geometries, the maximum possible improvement is less and is obtained at higher σ_f/σ^*_Y.

The effect of the various hole geometries on the transition temperatures of steel 0.24 are summarized in Table 7.1. Since the reduction in the nil-ductility temperature

$$\Delta T_D = \frac{\left[K^{max}_{\sigma(p)} - K^{max,H}_{\sigma(p)}\right]}{K^{max,H}_{\sigma(p)}\ K^{max}_{\sigma(p)}} \cdot \frac{\sigma_f}{d\sigma^*_Y/dT} \qquad \begin{matrix}(6.15)\\(7.3)\end{matrix}$$

depends on the maximum plastic stress concentration factor $\left[K^{max,H}_{\sigma(p)}\right]$, the four-hole geometry also produces the largest ΔT_D.

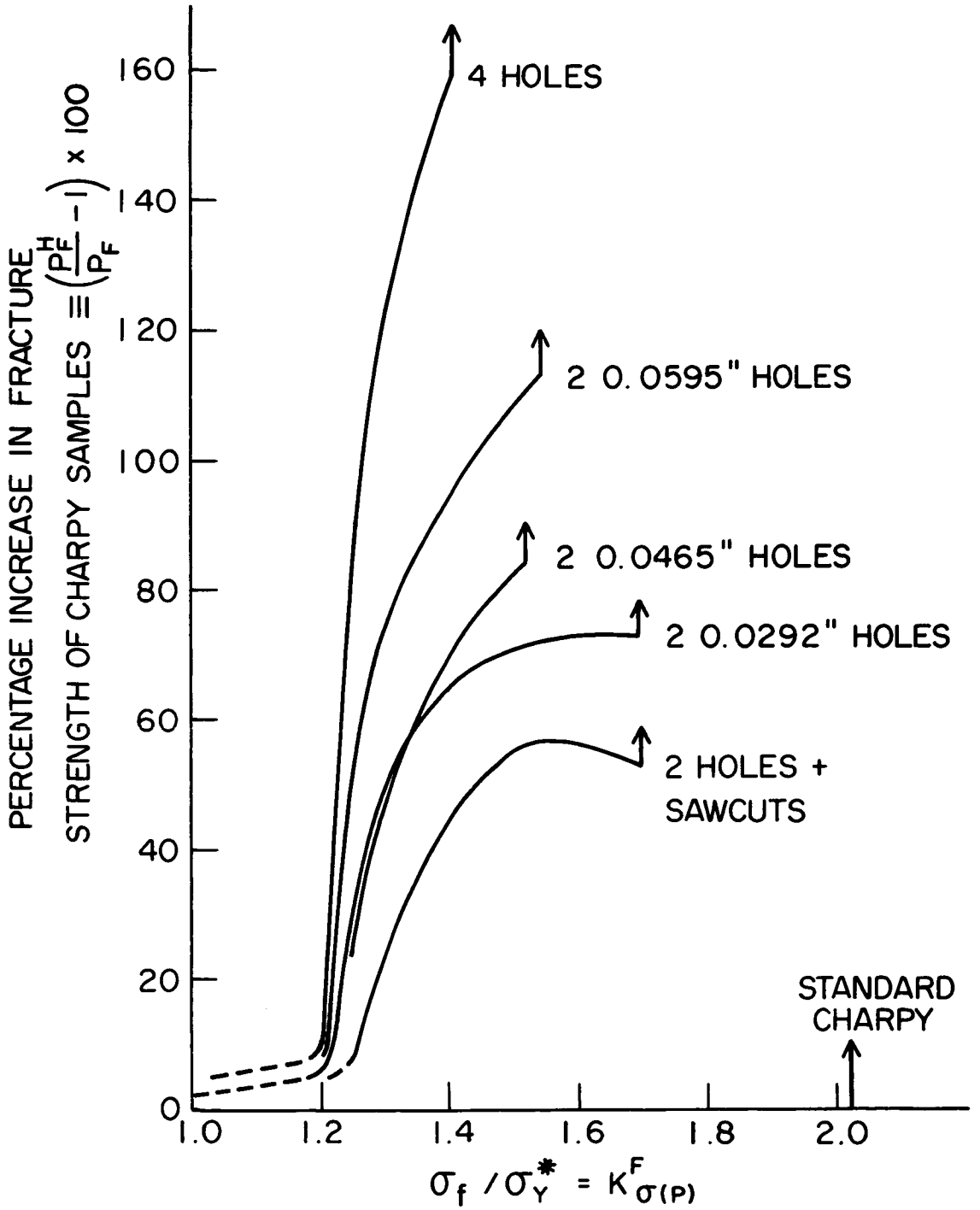

Figure 7.17 The effect of intrinsic toughness (σ_f/σ_Y^*) on the percentage improvement in the nominal fracture strength of Charpy bars which results from various hole geometries; the vertical arrows indicate the intrinsic toughness above which general yielding is required to cause failure of the particular geometry.

Table 7.1

The effect of various hole geometries on the measured Charpy impact transition temperatures and room temperature general yield and ultimate loads of steel 0.24

	T_D	ΔT_D	T_N	ΔT_N	T_{50}	ΔT_{50}	P_{GY}	ΔP_{GY}	P_{ULT}	ΔP_{ULT}
	(← ^oC →)						(lb.)	(%)	(lb.)	(%)
Standard Charpy	-15	-	+10	-	+27	-	2310	-	3100	-
2 0.0292" Holes	-55	-40	-55	-65	-37	-64	2060	-10.8	2820	-9.0
2 0.0292" Holes and Saw Cuts	-58	-43	-55	-65	-37	-64	1680	-27.3	2650	-14.5
4 0.0292" Holes	-100	-85	-40	-50	-10	-37	1910	-17.3	2380	-23.2
2 0.0465" Holes	-70	-55	-55	-65	-50	-77	1940	-16.0	2580	-16.8
2 0.0595" Holes	-65	-50	-50	-60	-45	-72	1830	-20.8	2450	-21.0
3 Notches	-40	-25	-25	-35	-20	-47	1860	-19.5	2970	-4.2

On the other hand, the reduction in ductility transition temperature ΔT_N by these same geometries is never greater than, and in some cases substantially less than, by two 0.0292" diameter holes. In addition, those geometries which are most effective when the intrinsic toughness (σ_f/σ_Y^*) is low (i.e., for ΔT_D and prior to general yielding) have inferior properties (smaller P_{GY}, P_{ULT}, and ΔT_N) at high σ_f/σ_Y where fibrous failure or plastic instability controls behavior. Table 7.1 also summarizes the effect of each of these geometries on the room temperature P_{GY} and P_{ULT}. For example, four holes reduce the Charpy P_{GY}

by 17.3% and P_{ULT} by 23.2% compared to 10.8% and 9.0% for the two 0.0292" holes. Furthermore, four holes reduce the ductility transition temperature by only 50°C compared to 65°C for two 0.0292" holes. This means that for $\sigma_f/\sigma_Y^* > 1.7$, two 0.0292" holes would be substantially better than the four holes or larger diameter holes.

The optimum hole geometry can only be chosen if the material and service conditions (σ_f/σ_Y^*) are specified. If, in fact, a large range of temperatures or strain rates were to be encountered, a compromise geometry with less improvement at low temperatures but more toughness and strength at higher temperatures might be best.

The severity of the initial stress raiser will also affect the magnitude of the improvement from each hole geometry, especially at low σ_f/σ_Y^* where the critical $K_{\sigma(p)}^{EFF}$ can be developed at the notch before holes start to affect the yield zone. The geometries which (1) reduce the elastic stress concentration factor or (2) interact with the plastic zones soon after local yielding will be most effective for more severe notches or cracks at low σ_f/σ_Y^*. However, for intermediate σ_f/σ_Y^* where failure requires fairly large plastic zones, the values of $K_{\sigma(p)}^{max,H}$ developed at P_{GY} and thus the nil-ductility temperatures (T_D) can be reduced by hole drilling much as they were in the Charpy samples (i.e., four holes largest ΔT_D, etc.). Finally at very large σ_f/σ_Y^*, when shear failure reaches the holes, the ultimate load of drilled samples is independent of ρ (i.e., same trends as in Charpy, four holes have the lowest P_{ULT}, etc.). These results indicate that for materials with sufficient intrinsic toughness (σ_f/σ_Y^*), improvements could be obtained with the same geometries in sharply cracked (i.e., fatigue) samples.

CHAPTER VIII

THE EFFECT OF SPECIMEN THICKNESS ON THE IMPROVEMENT POSSIBLE WITH HOLE DRILLING

Hole drilling reduces the nil-ductility temperature and increases notch strength at low temperatures by reducing the maximum local stress developed in the Charpy bar. The magnitude of the improvement depends on (1) the constraint in the standard sample and (2) how efficiently the holes can retard the build-up of this constraint. The standard Charpy specimen deforms under approximately plane strain conditions until well above general yield and in steel 0.24 develops a maximum stress of

$$\sigma^{max} = K^{max}_{\sigma(p)} \; \sigma^{*}_{Y} = \sigma_{f} \qquad (8.1)$$

$$K^{max}_{\sigma(p)} = 2.05$$

at T_D.

Various authors[66, 67, 73] have shown in both impact and slow bend tests that for the same notch, T_D decreases with decreasing specimen thickness (t). That is, as the deformation conditions approach plane stress, the maximum constraint at general yield $\left[K^{max,t}_{\sigma(p)}\right]$ is lower, thus requiring a higher σ^{*}_{Y} (lower T^{t}_{D}) for stress controlled cleavage fracture,

$$\sigma^{max} = K^{max}_{\sigma(p)} \; \sigma^{*}_{Y}(T_D) = \sigma_{f} \qquad (8.2)$$

where the superscript, t, means associated with a specimen of reduced thickness, t.

For thicknesses less than 0.2 - 0.3", a sharp decrease in the

initiation transition temperature (T_S^t) has been reported[66, 73] which does not correspond to the more gradual changes in $K_{\sigma(p)}^{max,t}$ and T_D^t. There is, however, some question about the reason for this transition since it has been observed in mild steel where stable microcracks complicate the ductility and initiation transitions. In any case, the relaxation of constraint after general yielding occurs more easily in thin samples; but it does not depend on thickness in the same way as the build-up of constraint does.

In order to study the effect of specimen thickness on the improvements from hole drilling, instrumented impact-bend tests were performed on three thicknesses (0.100", 0.200", standard 0.394") of Fe-Si 2 samples. This single-phase material was chosen because it obeys a critical cleavage stress criterion, and the ductility transition is not complicated by fibrous initiation or by slow growth of cleavage cracks prior to failure. All specimen dimensions were those of the standard Charpy except the thickness (t) as specified. Standard notch and drilled (H_D = 0.0292", R = 0.0448", $\theta = 75^o$) samples were prepared by surface grinding from top and bottom of a 1/2" plate so that all specimen centers coincided with the plate center regardless of their thickness. Machining and hole drilling were completed prior to vacuum annealing for one hour at 875°C to produce an equiaxed grain size (d = 0.021").

Instrumented impact-bend tests were performed at various temperatures between -80° and +100°C, and the results are summarized in Figures 8.1 - 8.9 and Table 8.1. To facilitate comparison between thicknesses, all loads and energies have been normalized to the standard Charpy area

by the ratio of the initial areas. For example,

$$E'^{.2}(\text{Plotted}) = E'^{.2}(\text{Measured}) \times \frac{.394}{.200}$$
$$P'^{.1}(\text{Plotted}) = P'^{.1}(\text{Measured}) \times \frac{.394}{.100} \qquad (8.3)$$

8.1 The Effect of Two Holes in Standard Thickness Samples

As shown in Figure 8.1, standard Charpy samples fracture by 100 percent cleavage prior to general yielding at all temperatures below 90°C. At temperatures above 90°C, samples undergo general yielding and large deflections before ductile tearing occurs. The transition is so sharp that cleavage initiation is not observed between general yield and ultimate load and $T_D = T_N = 90°C$. At 94°C, cleavage does initiate from the ductile tear after very large deflection; but at 100°C, the 240 ft.lb. hammer is stopped without failure of the sample.

Two 0.0292" holes reduce the nil-ductility temperature (ΔT_D = -50°C) down to $T_{DH} = 40°C$. However, between 40 and 60°C, failure occurs by ductile tearing to one hole and cleavage reinitiation from that hole. In this range, the notch displacement is quite small, and the total energy less than 20 ft. lbs. This behavior differs slightly from that of mild steel where T_{DH} and T_{NH} are approximately coincident for the same hole geometry. The temperature range where cleavage initiates after general yield, but before tearing reaches both holes, is extended because (1) the higher $d\sigma/d\varepsilon$ raises the local stresses at one hole when sufficient constraint is not present [lower $V^*(c+H)$] and (2) the lower $\left|\frac{d\sigma_Y^*}{dT}\right|$ extends the temperature range associated with any change in critical displacement. At temperatures above $T_{NH} = 60°C$, tearing reaches both

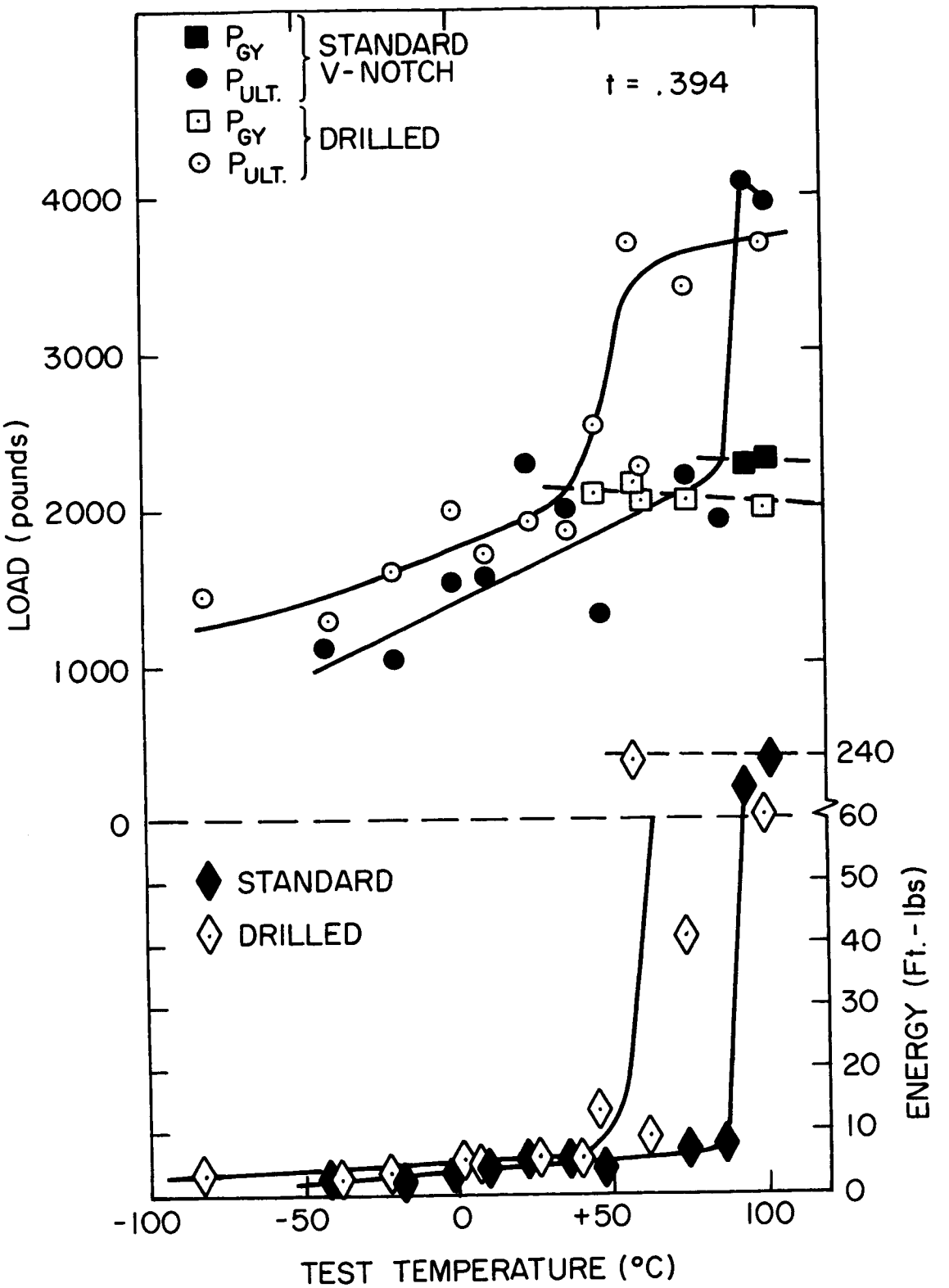

Figure 8.1 The effect of two holes (H_D = 0.0292", R = 0.0448", $\theta = 75^{o}$) on the instrumented Charpy fracture behavior of Fe-Si 2.

holes, and large notch displacements (high energy) precede cleavage nucleation from one of the holes. As in the previous results with other materials, holes reduce both the general yield (P_{GY}) and ultimate (P_{ULT}) loads by about 10 percent at high temperatures.

The fracture strength is considerably improved by holes at low temperatures where both samples fail completely by cleavage. From the extrapolated general yield load [a linear extrapolation is justified by the linear temperature dependence of P_{GY} in thinner samples between $+100^{o}$ and $-20^{o}C$ (Figure 8.4)], the local yield stress is obtained from equation (6.1)

$$\sigma_Y^* \text{ (psi)} = 33.3\ P_{GY} \text{ (lb.)} \ .$$

Knowing σ_Y^*, the ratio P_F/σ_Y^* (or P_F^H/σ_Y^*) was calculated from the fracture results at various temperatures. If FeSi 2 and steel 0.24 had identical stress-strain curves, then $K_{\sigma(p)}$ would increase with applied load P/σ_Y^* as shown in Figure 6.10 for standard and drilled samples. In addition, if Figure 6.10 described the behavior of Fe-Si samples, the critical fracture stress

$$\sigma_f(T) = K^F_{\sigma(p)}(T) \cdot \sigma_Y^*(T) \qquad (8.4)$$

would have the same value at each temperature whether $K^F_{\sigma(p)}$ is calculated from the measured fracture loads of standard (P_F/σ_Y^*) or drilled (P_F^H/σ_Y^*) samples. Figure 8.2(a) shows that $\sigma_f(T)$ calculated from standard samples is about 10% higher than that calculated from drilled samples. Because Fe-Si 2 work hardens more rapidly than steel 0.24 and thus deviates from ideal plastic behavior sooner, Figure 6.10 does not describe the exact $K_{\sigma(p)}$ for either standard or drilled Fe-Si 2 samples. This points out

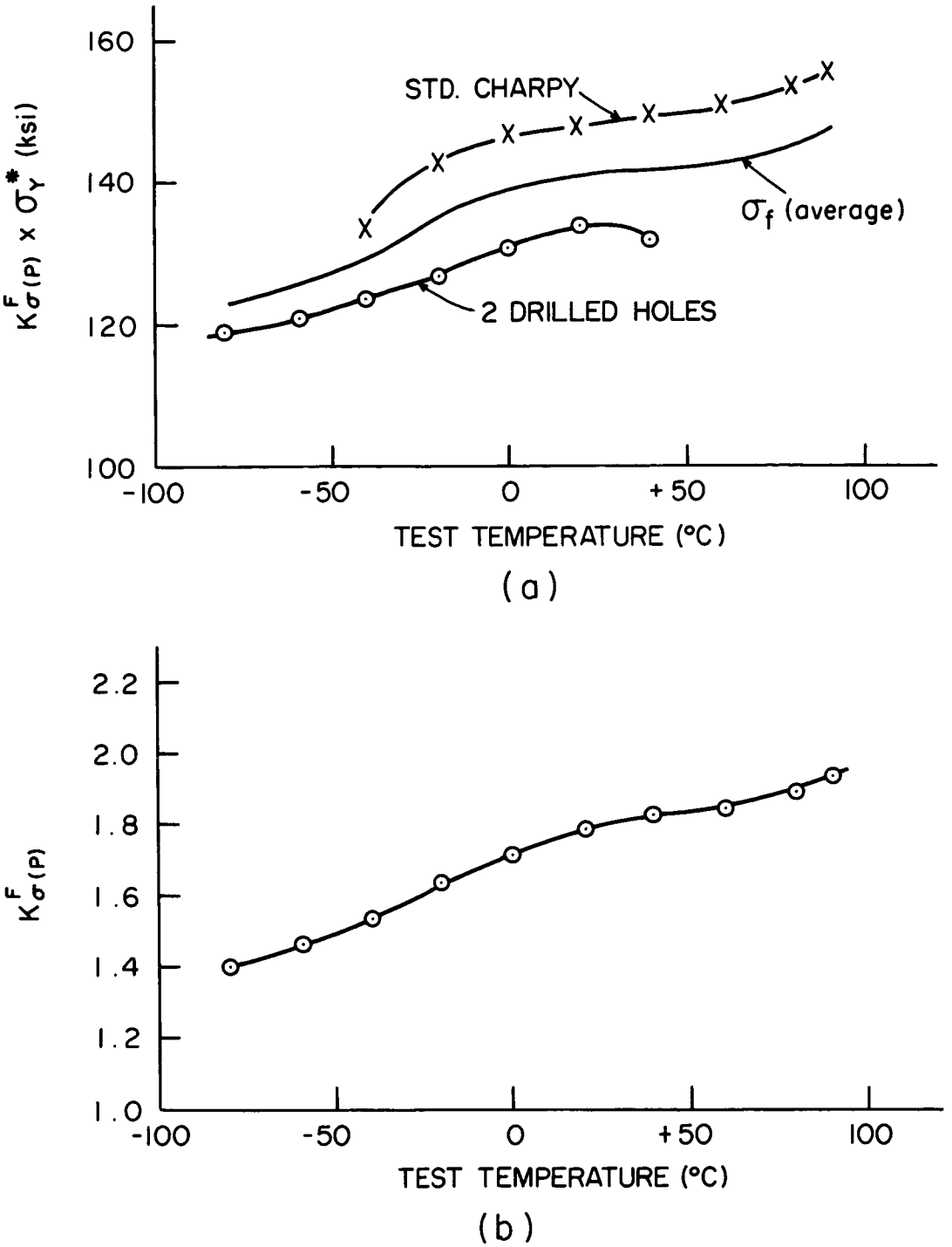

Figure 8.2 The critical fracture stress (σ_f) and critical plastic stress concentration factor [$K^F_{\sigma(p)}$] at various test temperatures, calculated from the impact-bend results of Fe-Si 2 samples at various test temperatures.

that the increase of triaxiality with applied load, which is usually considered a function only of geometry, actually depends on the material's deformation characteristics.

In order to determine the actual increase of $K_{\sigma(p)}$ with applied load in Fe-Si 2, the fracture stress $\sigma_f(T)$ must be estimated. Because neither the calculations based on the standard or drilled curves of Figure 6.10 is exact, the mean value of $\sigma_f(T)$ [Figure 8.2(a)] was used to compute the critical $K^F_{\sigma(p)} \equiv \sigma_f/\sigma^*_Y$ at each temperature [Figure 8.2(b)]. The fracture loads (P_F/σ^*_Y and P^H_F/σ^*_Y) at corresponding temperatures, then redefine the increase of $K_{\sigma(p)}$ with applied load in both standard and drilled FeSi 2 samples as shown in Figure 8.3. Although the assumed $\sigma_f(T)$ leaves some uncertainty about the specific $K^F_{\sigma(p)}$, the effects of holes (or thickness) on the load to produce it is exact. That is, an error in the assumed $\sigma_f(T)$ would shift the curves of Figure 8.3 up or down slightly but would maintain the same horizontal spacing.

Based on this assumption, the build-up of triaxiality in the standard Charpy sample is lower in Fe-Si 2 than in steel 0.24. Two holes still reduce the rate of increase of $K_{\sigma(p)}$ with applied load, but holes are not quite as effective as in mild steel. In Chapter V, it was observed that in Fe-Si 2, the plastic zone shape deviates from the logarithmic spiral yield zone when $P/P_{GY} \geq .6$. This could cause the less rapid increase of $K_{\sigma(p)}$ with applied load and the reduced $K^{max}_{\sigma(p)}$ at P_{GY}. In drilled samples, however, where constraint is lower, the higher strain hardening rate actually increases the maximum local stress between the notch side and hole and thus the effective $K^H_{\sigma(p)}$ above that produced below the notch in mild steel. The importance of strain hardening is

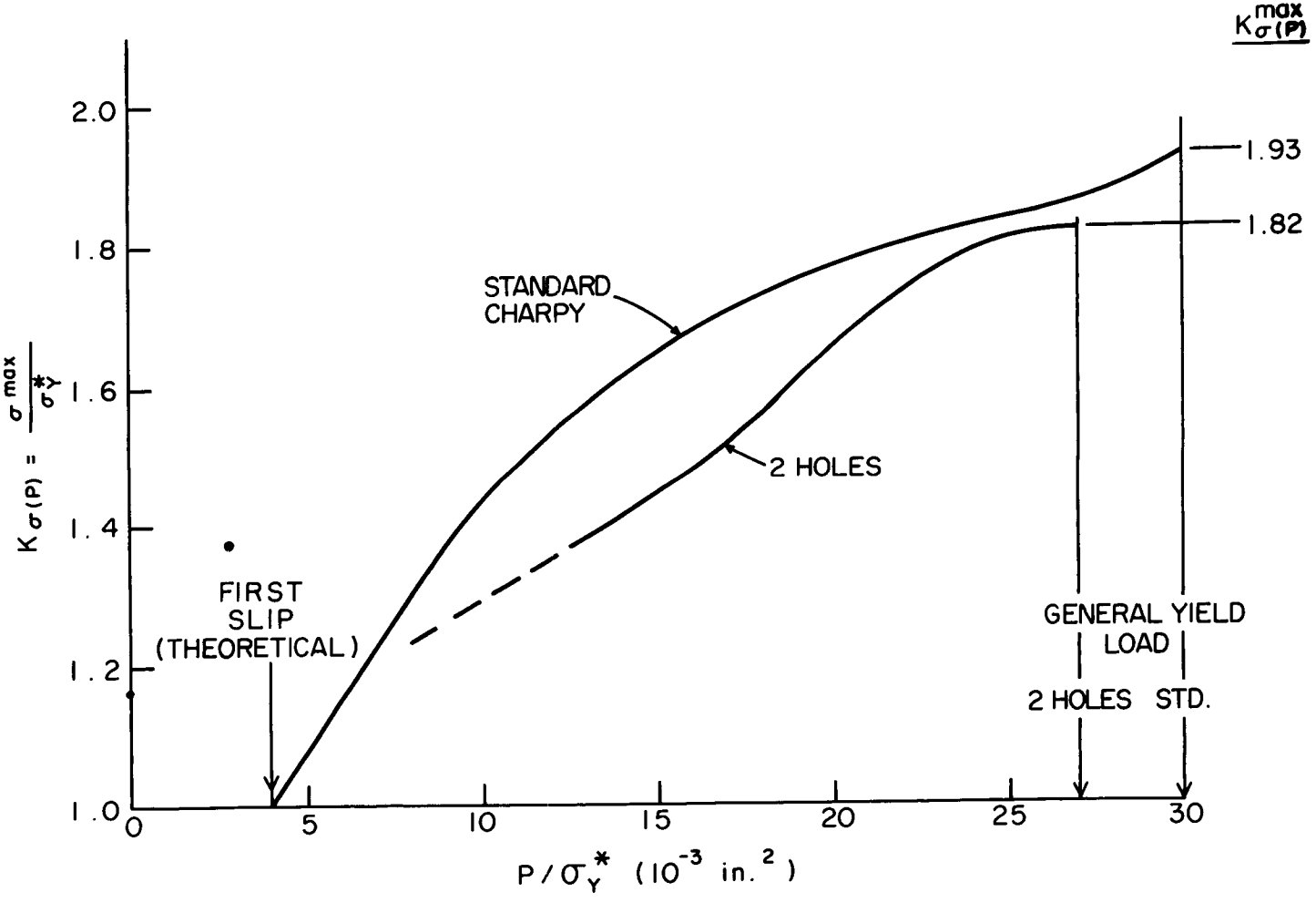

Figure 8.3 The increase of the plastic stress concentration factor with applied load in standard Charpy and drilled (H_D = 0.0292", R = 0.0448", θ = 75°) samples of Fe-Si 2.

evidenced by the fact that at temperatures above -30°C, cleavage initiates between the notch side and hole where strains are higher rather than at the notch tip as in steel 0.24.

It seems surprising at first that such a large ΔT_D = -50°C is produced by a small reduction in $K^{max}_{\sigma(p)}$. However, allowing σ_f to be linearly temperature dependent in schematic Figure 6.11 and proceeding as in section 6.4-1, a general equation for ΔT_D [analogous to equation (6.15)] is derived

$$\Delta T_D = \frac{\left[K^{max}_{\sigma(p)} - K^{max,H}_{\sigma(p)}\right] \cdot \sigma^*_Y (T_D)}{K^{max,H}_{\sigma(p)} \frac{d\sigma^*_Y}{dT} - \frac{d\sigma_f}{dT}} \quad . \tag{8.5}$$

Equation (8.5) indicates that ΔT_D can be quite large even for a small change $K^{max}_{\sigma(p)}$ if $\left|\frac{d\sigma^*_Y}{dT}\right|$ and $\frac{d\sigma_f}{dT}$ are small. In Fe-Si 2, $\left|\frac{d\sigma^*_Y}{dT}\right|$ is very small, thereby resulting in a large ΔT_D from small changes in constraint. Substitution of appropriate values in equation (8.5) yields ΔT_D = -40°C, which is fair agreement with the observed value (-50°C) considering the variation of $\frac{d\sigma_f}{dT}$, shown in Figure 8.2a.

8.2 Standard Samples of Reduced Thickness

8.2-1 Fracture Results

Figure 8.4 summarizes the impact properties of standard notched samples which are 0.100", 0.200", and standard 0.394" thick. In each case, the measured loads and impact energy of the thinner samples have been normalized to standard Charpy area as illustrated by equations (8.3). Compared on this basis, reduced thickness produces the following changes:

(1) The notch strength of thinner samples is up to 50% greater

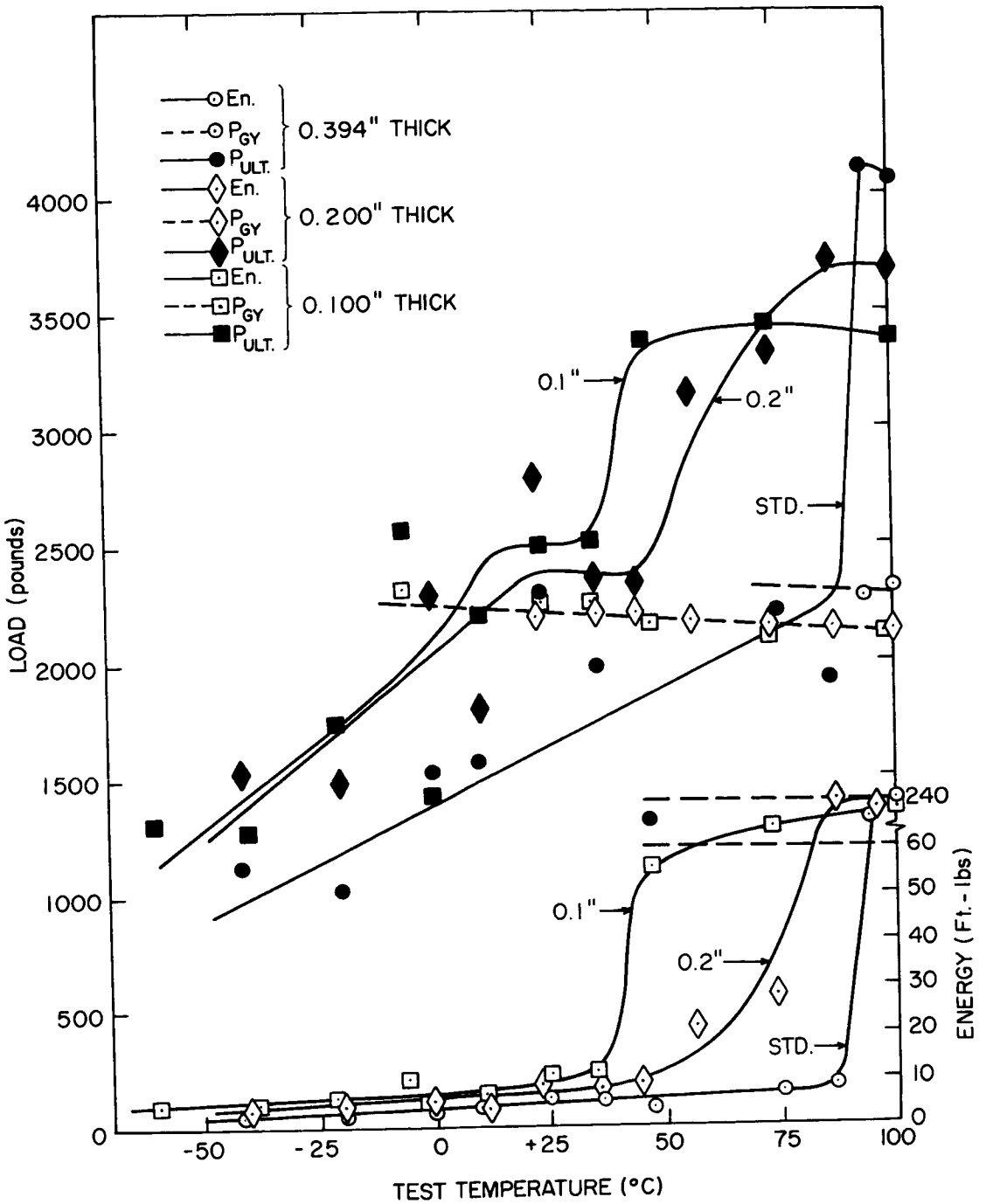

Figure 8.4 The instrumented "Charpy" faacture results at various test temperatures for Fe-Si 2 samples of various thicknesses (t = 0.100", 0.200", 0.394"); all measured loads and energies have been normalized to account for the net area differences.

than standard Charpys at low temperatures, where all samples cleave prior to P_{GY}. The results of Sakui, et al[67] indicated similar increases just below T_D in instrumented impact tests with mild steel. However, these are the first conclusive results verifying the effect of thickness prior to general yield. The improvement is quite small at very low temperatures (small zone sizes) and increases with increasing temperature. Although there is some experimental scatter, the 0.200" thick samples always require a considerably higher P_F than standard Charpys, and the 0.100" thick samples show on the average a still larger improvement.

(2) The nil-ductility temperatures of 0.200" samples ($T_D^{\cdot 2} = 15^oC$) and 0.100" samples ($T_D^{\cdot 1} = 10^oC$) are 75^o and 80^oC respectively below that of the standard Charpy sample. The magnitude of the reduction is related to the maximum constraint at P_{GY} through equation (8.5) and will be discussed later.

(3) Above the nil-ductility temperature, there are temperature ranges of 45^oC and 30^oC for .200" and 0.100" samples respectively where cleavage initiates after small displacements beyond general yield. That is, local work hardening is able to produce

$$\sigma_f = K_{\sigma(p)}^{max,t} \ (\sigma_Y^* + \Delta\sigma) \tag{8.6}$$

at a small displacement

$$V^*(c) = \beta \rho \epsilon_F^t = \beta \rho \left[\frac{\sigma_f - K_{\sigma(p)}^{max,t} \sigma_Y^*}{K_{\sigma(p)}^{max,t} \, d\sigma/d\epsilon} \right] \tag{8.7}$$

(4) At the ductility transition temperatures of $T_N^{\cdot 2} = 60^oC$ and $T_N^{\cdot 1} = 40^oC$, there is a sharp rise in the impact energy and fracture load. In 0.2" thick samples, this increase in fracture strength occurs although

fracture still occurs by 100% cleavage at temperatures up to 80°C; but in 0.1" samples failure initiates by ductile tearing at temperatures above $T_N^{.1} = 40^oC$. Although the nil-ductility temperature (T_D^t) is similar for both thinner samples, the ductility transition temperature (T_N^t) is considerably lower in 0.100" samples ($T_N^{.1} < T_N^{.2} < T_N$). The effect of thickness on the various transition temperatures is summarized in Table 8.1.

(5) The normalized general yield loads of 0.200" and 0.100" samples are identical and about 6% below those of the standard thickness (0.394") samples. This is consistent with the observations of Knott[66] where the differences were small, but P_{GY} for thinner samples (0.1", 0.2") were consistently on the low side of the scatter band.

(6) At high temperatures where specimens of all thicknesses are ductile, the ultimate load is lower in thinner samples implying lower average constraint in the fully plastic section.

8.2-2 Discussion of the Effect of Thickness Prior to General Yield

Since the critical $K^F_{\sigma(p)} \equiv \sigma_f/\sigma_Y^*$ has been defined at each temperature [Figure 8.2(b)], the corresponding fracture loads P_F^t/σ_Y^* (Figure 8.4) define the increase of $K_{\sigma(p)}$ with applied load in each thickness as shown in Figure 8.5. Thinner samples are stronger at low temperatures because a higher load is required to produce the critical triaxiality. Physically, this results because the stress in the thickness direction, which controls the triaxiality, is less in the 0.200" and 0.100" thicknesses even though the plastic zone size (R) is small compared to t. The extent of this deviation from plane strain condi-

TABLE 8.1

The effect of two 0.0292" holes on the impact transition temperatures, general yield load, and ultimate load of various thickness samples of Fe-Si

		t = 0.394"		t = 0.200"		t = 0.100"	
		Standard	Drilled	Standard	Drilled	Standard	Drilled
Nil-ductility Temperature	T_D(°C)	90		15		10	
	T_{DH}		40		-20		-15
	ΔT_D	-50		-35		-25	
Ductility Temperature	T_N	90		60		40	
	T_{NH}		60		45		0
	ΔT_N	-30		-15		-40	
Fracture to Both Holes	T'_{NH}		60		60		60
General Yield Load at 100°C	P_{GY}(lb.)	2260		2120		2120	
	P^H_{GY}(lb.)		2000		1930*		1930*
	ΔP_{GY}(%)	-11.5		-9		-9	
Ultimate Load at 100°C	P_{ULT}(lb.)	4060		3700		3400	
	P^H_{ULT}(lb.)		3700		3400*		3150*
	ΔP_{ULT}(%)	-9		-8		-7.5	

* Extrapolated to 100°C for comparison.

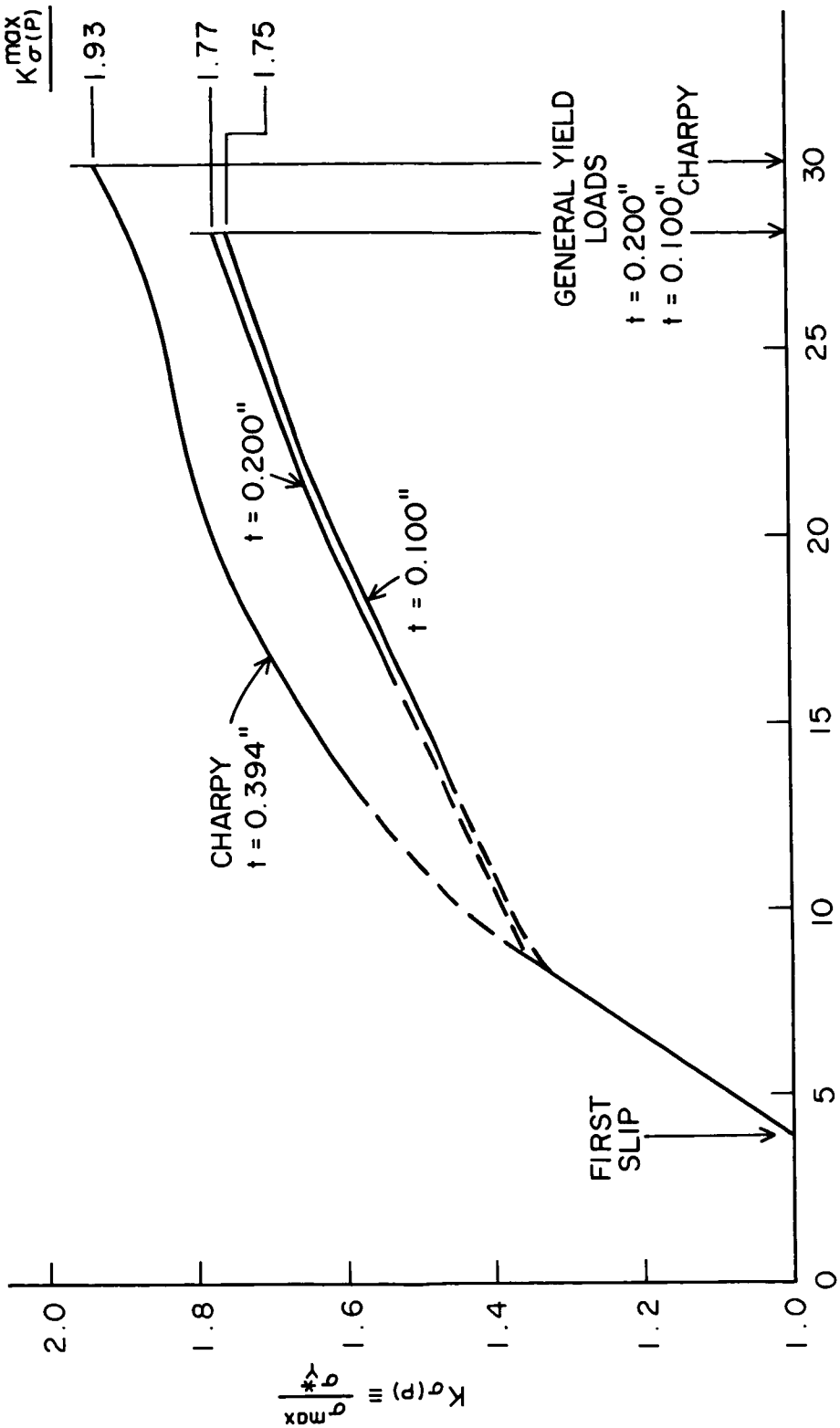

Figure 8.5 The effect of specimen thickness on the increase of the plastic stress concentration factor with applied load in Charpy-type samples of Fe-Si 2.

tions decreases with decreasing zone size, and all thicknesses behave alike at low P/σ_Y^*.

The observed reductions in the nil-ductility temperature ($T_D^{.394} - T_D^t$) with decreasing thickness results from the reduced $K_{\sigma(p)}^{max,t}$ at P_{GY} and is predicted by equation (8.5). Knott[66] has attempted to correlate his own observed T_D^t in various thickness slow bend samples with that obtained in thick samples of variable notch flank angle (T_D^ω). He assumed that the maximum constraint in the latter samples was given by equation (1.24)

$$K_{\sigma(p)}^{max} = 1 + \pi/2 - \omega/2 \qquad \begin{matrix}(1.24)\\(8.8)\end{matrix}$$

and that this $K_{\sigma(p)}^{max}$ is just sufficient to produce fracture at T_D^ω. For a thinner sample of the same material [same $\sigma_f/\sigma_Y^* = K_{\sigma(p)}^F(T)$], the same $K_{\sigma(p)}^{max}$ given by equation (8.8) must exist when $T_D^t = T_D^\omega$. By matching T_D^t and T_D^ω, Knott calculated the value of $K_{\sigma(p)}^{max,t}$ in reduced thicknesses.

Although qualitatively this calculation predicts the effect of reduced thickness, there is much uncertainty about the specific values. The dislocation etch-pitting results of Chapter V, as well as the mild steel fracture results in Chapter VI, indicate a marked deviation from ideal plastic behavior at loads approaching P_{GY}. Specifically, the results indicate that $K_{\sigma(p)}^{max}$ is actually lower than given by equation (8.8) in Charpy samples of mild steel and even lower in Charpy samples of FeSi. Similar deviations from equation (8.8) would be expected for other flank angles (ω), and the magnitude of the deviation may itself vary with ω. Consequently, the specific values of $K_{\sigma(p)}^{max,t}$ calculated by Knott for thinner samples are uncertain even in mild steel and definitely not applicable in materials with a high initial strain hardening rate.

8.2-3 Discussion of the Effect of Thickness after General Yield

Above P_{GY}, cleavage is initiated at a critical displacement $V^*(c) = f(T)$ [equation (8.7)] which produces σ_f locally by strain hardening at the point of maximum constraint. The ductility transition results when $V^*(c)$ shows a sharp increase, and the temperature T_N^t at which this occurs depends on the specimen thickness (Table 8.1). In mild steel, Knott[66] has proposed that this sudden increase in $V^*(c)$ might be associated with plastic strain acting as a barrier to growth of crack nuclei and raising σ_f [by blunting or increasing γ_m, equation (1.6)]. This, in turn, increases the necessary strain hardening to reach σ_f, and the additional strain raises σ_f still more. In this explanation, thickness should affect T_N^t in the same way as T_D^t because $K_\sigma^{max,t}$ defines ϵ_F^t at any temperature.

In Fe-Si, stable microcracks are not formed, and the first cleavage crack nucleated leads to failure. It is unlikely that the small plastic strains involved ($\epsilon_F < 10\%$) could increase σ_f so markedly. A more likely explanation is that there is a displacement $[V^{RLX,t}(c)]$ at which deformation occurs in the thickness direction causing a reduction in triaxiality $[K_{\sigma(p)}^{max,t}]$. This relaxation of plane strain conditions causes $V^*(c)$ [equation (8.7)] to increase sharply at that temperature (T_N^t) where $V^{RLX,t}(c) \leq V^*(c)$, and this depends strongly on the thickness. It is important to note that in this model, T_N^t depends both on the magnitude of $K_{\sigma(p)}^{max,t}$ which determines $V^*(c)$ and on the displacement $[V^{RLX,t}(c)]$ at which it can be relaxed. Thus, T_N^t need not vary with thickness in the same way as T_D^t, and in fact, should be independent of t for sample thickness where $K_{\sigma(p)}^{max}$ is relaxed by plane strain deforma-

tion such as wing formation. Knott[66], in fact, observed a constant T_N^t for $t \geq 0.3$" although T_D^t continued to increase with thickness up to $t = 0.5$". In the present results (Figure 8.4), $T_N^{.1}$ is well below $T_N^{.2}$ even though $K_{\sigma(p)}^{max,t}$ and T_D^t are similar for both; this is consistent with the mechanism of relaxation by deformation through the thickness.

The general yield load decreases only slightly with decreasing thickness indicating that the average constraint across the net section like $K_{\sigma(p)}^{max,t}$ is slightly lower at P_{GY}. However, the ultimate load, which depends on the degree of relaxation after P_{GY}, decreases considerably with decreasing thickness. Apparently there is more complete relaxation of constraint at and above $V^{RLX,t}(c)$ in the thinner samples so that a lower applied load can produce the displacement where ductile tearing begins.

8.3 The Effect of Two Holes in Thinner Samples

8.3-1 Fracture Results - t = 0.200"

Figure 8.6 summarizes the effect of two holes on the impact properties of 0.200" thick samples. The nil-ductility temperature ($T_{DH}^{.2} = -20^oC$) of drilled samples is 35^oC below the standard 0.200" sample ($\Delta T_D^{.2} = -35^oC$). Below -20^oC, both standard and drilled samples fail by 100% cleavage through one hole, but holes increase the nominal notch strength. Between -20^o and $+40^oC$, drilled samples fail after P_{GY} but still by 100% cleavage either between the holes or through one hole. Ductile tearing occurs to one hole at temperatures above $T_{NH}^{.2} = 45^oC$, and there is a marked increase in both applied load and impact energy before cleavage reinitiates from the one hole. At 60^oC (T_{NH}'), tearing reaches

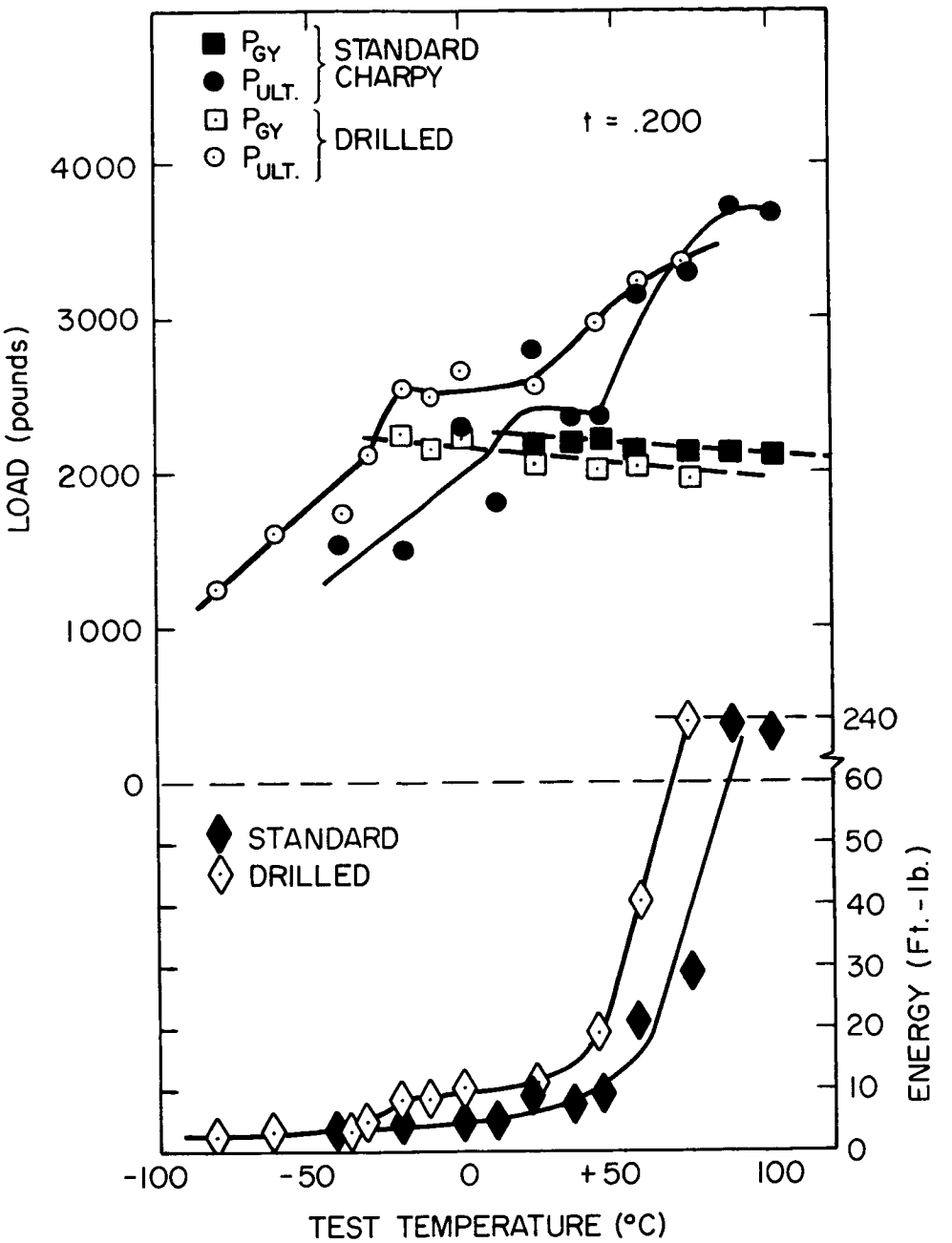

Figure 8.6 The effect of two holes (H_D = 0.0292", R = 0.0448", $\theta = 75^{\circ}$) on the instrumented "Charpy" transition behavior of 0.200" thick samples; all measured loads and energies have been normalized to the net area of the standard thickness.

both holes prior to cleavage, and the impact energy again increases sharply. At higher temperatures, tearing reaches both holes, and failure occurs completely by ductile tearing. Both the general yield and ultimate load of drilled samples are about 10 percent below the corresponding values in standard 0.200" thick samples.

8.3-2 Fracture Results - t = 0.100"

Figure 8.7 summarizes the fracture results for standard and drilled 0.100" thick specimens. At low temperatures ($T < -10^{o}C$), two holes strengthen the samples by as much as 60%. Failure occurs by 100% cleavage, sometimes through one hole but usually without encountering either hole. The nil-ductility temperature of drilled samples ($T'^{.1}_{DH} = -15^{o}C$) is $\Delta T^{.1}_{D} = -25^{o}C$ below that of standard samples, but this reduction is less than that produced in the thicker samples. At temperatures above $T^{.1}_{NH} = 0^{o}C$, drilled samples require a large increase in applied load and notch displacement before failing by ductile tearing to one hole and cleavage reinitiation. At temperatures above $T'_{NH} = 60^{o}C$, tearing occurs to both holes, and there is another sharp increase in absorbed energy. It should be noted that the temperature ($T'_{NH} = 60^{o}C$) at which tearing first reaches both holes is the same in 0.394", 0.200", and 0.100" thick samples. As in the thicker samples, holes reduce the general yield and ultimate loads by about 10%.

8.3-3 Discussion of the Effect of Thickness on the Improvement from Hole Drilling Prior to General Yield

Having defined $K^{F}_{\sigma(p)} \equiv \sigma_f/\sigma^{*}_{Y}$ as a function of temperature by means of the standard thickness samples [Figure 8.2(b)], the fracture loads at corresponding temperatures (Figures 8.6, 8.7) serve to define

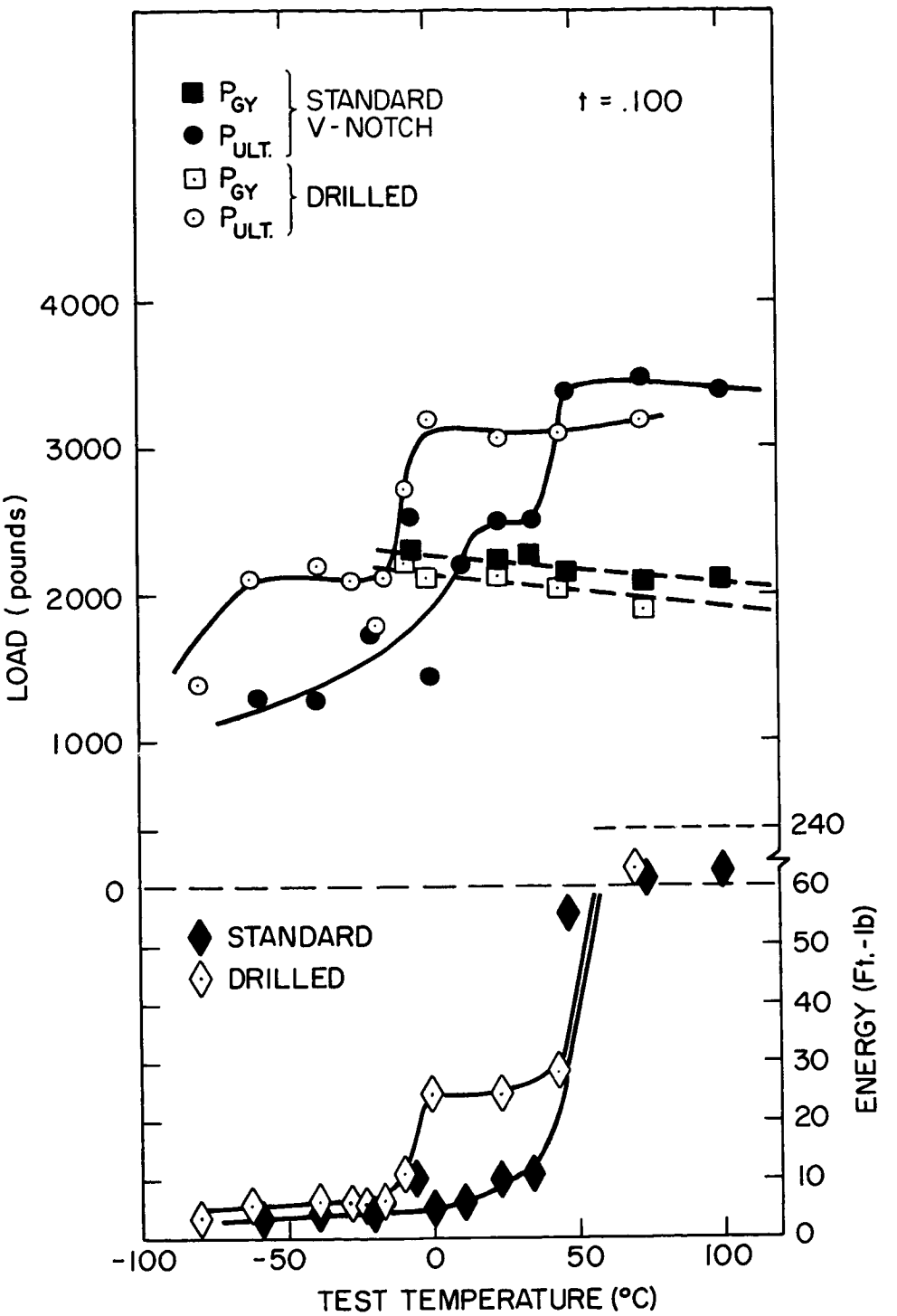

Figure 8.7 The effect of two holes (H_D = 0.0292", R = 0.0448", $\theta = 75^{\circ}$) on the instrumented "Charpy" transition behavior of 0.100" thick samples; all measured loads and energies have been normalized to the net area of the standard thickness.

the increase of $K_{\sigma(p)}$ with P/σ_Y^* for the thinner specimens. The curves for standard and drilled specimens, developed in this way, are compared in Figures 8.8a and 8.8b for 0.200" and 0.100" thick samples respectively. In reduced thicknesses, holes still reduce the build-up of triaxiality with applied load despite the lower triaxiality in the undrilled samples. In general, the plastic stress concentration factor can be written

$$K^t_{\sigma(p)} = K^\infty_{\sigma(p)} \cdot X\ (t, R) = \frac{\sigma^{max}}{\sigma_Y^*} \qquad (8.9)$$

where $K^\infty_{\sigma(p)}$ is the plane strain value and $X < 1$ is a factor (depending on thickness and plastic zone size) which represents the degree relaxation of stress in the thickness direction.

Holes have been shown to reduce $K^\infty_{\sigma(p)}$ by preventing plastic deformation ahead of the notch. Specifically, holes prevent the increase of longitudinal strain ahead of the notch which is necessary to produce high transverse stresses when plastic flow in those directions cannot occur. The reduction in $K^\infty_{\sigma(p)}$ has some physical meaning even in thinner samples because holes still reduce the longitudinal strain by about the same amount. Although $K^t_{\sigma(p)}$ is lower than $K^\infty_{\sigma(p)}$ by X (t, R), the relative reduction in $K^t_{\sigma(p)}$ which is produced by holes is directly proportional to their effect on $K^\infty_{\sigma(p)}$ because X(t, R) has about the same value in standard and drilled samples.

In reality, the amount of relaxation [X (t, R)] depends on the size of the plastic zone as well as the bar thickness. Moreover, the whole meaning of zone size (R) in a drilled sample differs from that in a standard one. As a result, there are slight differences in the relative reduction of $K^t_{\sigma(p)}$ from hole drilling in thinner samples. For

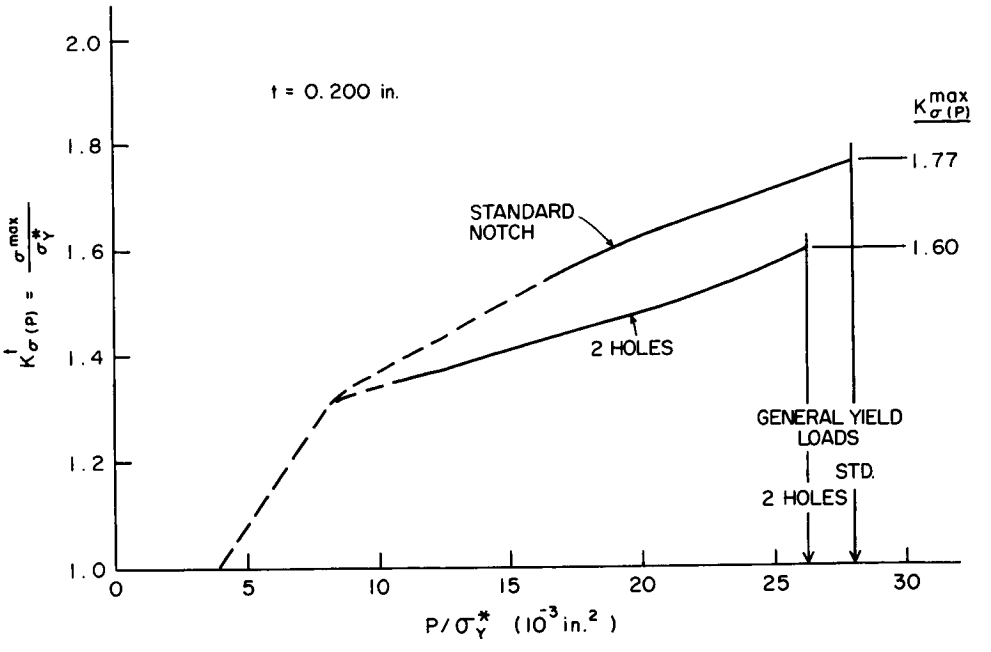

(a)

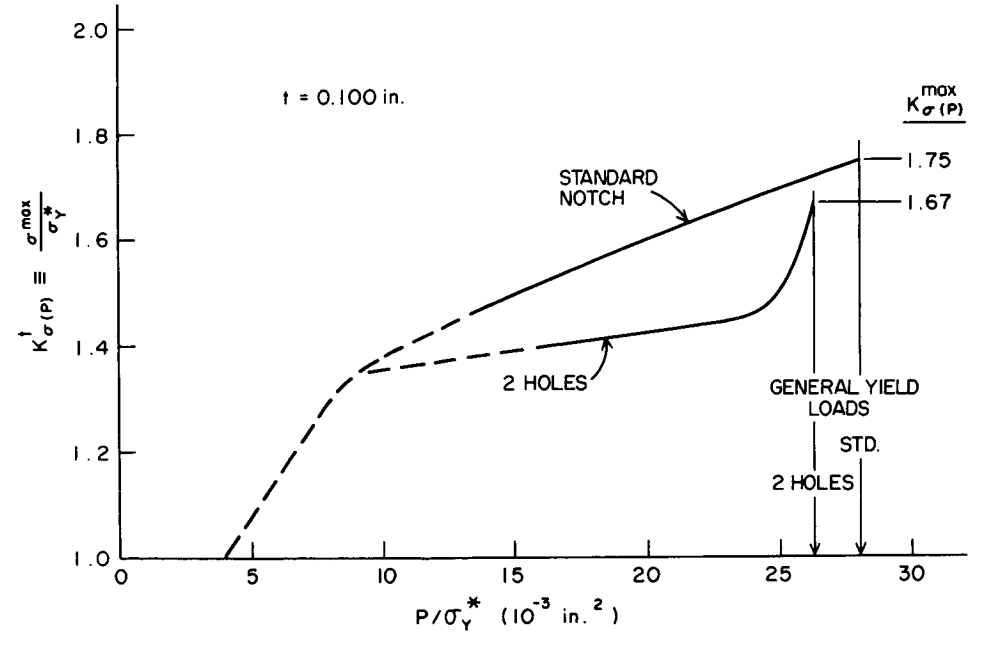

(b)

Figure 8.8 The effect of two holes (H_D = 0.0292", R = 0.0448", $\theta = 75^{o}$) on the increase of the plastic stress concentration factor $[K^{t}_{\sigma(p)}]$ with applied load in Charpy-type samples of thickness: (a) t = 0.200", (b) t = 0.100".

instance, the drilled 0.100" samples show a sharp increase in the plastic stress concentration factor [$K^{H,.1}_{\sigma(p)}$] just prior to P_{GY} (Figure 8.8b). This is responsible for the fractures observed just below general yield at temperatures between -60 and -20°C (Figure 8.7). The exact cause of this rise in X and thus $K^{H,.1}_{\sigma(p)}$ is not known, but it is likely that as the plastic zones extend rapidly at P_{GY}, local work hardening between the notch and hole causes a rapid increase in the maximum local stress.

The measured reduction in nil-ductility temperature caused by holes (ΔT^t_D) were -50, -35, and -20°C in 0.394", 0.200", and 0.100" thick samples respectively (Table 8.1). Because ΔT^t_D is related to the reduction in maximum plastic stress concentration factor through equation (8.5), this trend indicates that holes are less effective in reducing triaxiality in thinner samples. It should be noted that these observed ΔT^t_D are not directly proportional to the change in $K^{max,t}_{\sigma(p)}$ because $\frac{d\sigma_f}{dT}$ is not constant. The actual $K^{max,t}_{\sigma(p)}$ are noted in Figures 8.3 and 8.8 and are consistent with the observed ΔT^t_D with the exception of the standard thickness, where the difference in $K^{max}_{\sigma(p)}$ is smaller than expected. In this instance, $K^{max}_{\sigma(p)}$ = 1.93 for standard Charpy may have been underestimated. Since $d\sigma_f/dT$ is increasing very rapidly at high temperatures, the extrapolated σ_f and $K^{F}_{\sigma(p)}$ in Figure 8.2 may be low at temperatures above 60°C. Any error in this temperature range affects only the standard Charpy specimen and a 5% error in σ_f would account for the discrepancy.

8.3-4 Discussion of the Effect of Thickness on the Improvement from Hole Drilling Above General Yield

After general yielding, the effect of holes varies markedly

with thickness. In standard thickness drilled specimens, the ductility transition is well defined at that temperature ($T'_{NH} = 60^{o}C$) where ductile tearing reaches both holes. When this occurs, there is large scale blunting and a sharp rise in the fracture load and total impact energy (Figure 6.12). However, in the drilled 0.100" samples, there is a sharp rise in energy and fracture strength at $T'^{.1}_{NH} = 0^{o}C$ (see Figure 8.7) when tearing reaches only one hole. In 0.200" drilled samples, there is also an increase in toughness when tearing reaches one hole, but this does not occur until $T'^{.2}_{NH} = 40^{o}C$ (Figure 8.6). This is a form of ductility transition resulting from relaxation of stresses in the thickness direction as tearing occurs to one hole. In all thicknesses, ductile tearing reaches both holes at $T'_{NH} = 60^{o}C$, and there is extensive blunting and another sharp increase in energy.

It thus appears that there are two possible ductility transitions in drilled samples. In terms of equation (8.9), one (1) results from relaxation of stress in the plane of the sample when tearing reaches both holes $[K^{\infty}_{\sigma(p)}{}^{\downarrow}]$, and it is independent of thickness; the other (2) results from relaxation of stress by plastic deformation in the thickness direction $[X(t, R)\downarrow]$, and therefore it depends on thickness.

The first (1) transition depends on satisfying two criteria which were discussed in detail for the standard thickness samples in Chapter VI, section 6.4-2. In the thinner samples, criterion 1 is satisfied more easily, due to the lower $K^{H,t}_{\sigma(p)}$, and tearing reaches one hole at a lower temperature. However, criterion 2 [equation (6.22)] is not satisfied any more easily in thinner samples so that tearing reaches both holes at the same $T'_{NH} = 60^{o}C$. Apparently, the critical displace-

ment for cleavage reinitiation from one hole [V*(c+H)] is influenced more by strain hardening ahead of the hole, which is independent of thickness, than by plastic constraint.

The second (2) transition results when the stresses in the thickness direction are relaxed by plastic deformation. The longitudinal stresses which had been stable in the triaxial stress state now exceed the yield criteria and are relaxed by plastic deformation. This ductility transition temperature is thus defined by the condition

$$V_H^{RLX}(c) < V^{**}(c) \tag{8.10a}$$

or

$$V_H^{RLX}(c) < V^{*}(c+H) \tag{8.10b}$$

where $V_H^{RLX}(c)$ is the displacement at which extensive plastic relaxation occurs through the thickness and either equation (8.10a) or (8.10b) is controlling depending on whether tearing has reached neither (a) or one (b) hole.

Because larger transverse stresses can be supported at and above P_{GY} in thicker samples,

$$K_{\sigma(p)}^{H,.394} > K_{\sigma(p)}^{H,.2} > K_{\sigma(p)}^{H,.1} \tag{8.11}$$

Consequently, the critical displacement required for cleavage below the notch [analogous to equation (6.18)]

$$V^{**}(c) = \alpha\ \beta\ \rho \left[\frac{\sigma_f - K_{\sigma(p)}^{H,t}\ \sigma_Y^*}{K_{\sigma(p)}^{H,t}\ d\sigma/d\varepsilon} \right] \tag{8.12}$$

is smaller in thicker drilled samples at corresponding temperatures. Specifically, in 0.200" thick samples tested at temperatures up to $T_{NH}^{.2} = 45^oC$, which is 65^oC above $T_{DH}^{.2}$,

$$V^{**}(c) < V_H^*(c) < V_H^{RLX}(c) \quad . \tag{8.13}$$

Therefore, equation (8.10a) is not fulfilled, and cleavage occurs before relaxation.

In 0.100" samples, $V^{**}(c)$ increases more rapidly with temperature, and $V_H^{RLX}(c)$ is smaller. Thus, tearing reaches one hole

$$V_H^*(c) < V^{**}(c) \tag{8.14}$$

and relaxation occurs prior to failure

$$V_H^{RLX}(c) < V^*(c+H) \tag{8.10b}$$

at all temperatures above $T_{NH}^{0.1} = 0^oC$, which is only 15^oC above $T_{DH}^{.1}$. Theoretically, relaxation through the thickness is also possible in drilled samples of standard (0.394") thickness. In this case, $V_H^{RLX}(c)$ is so large that relaxation occurs within the thickness (by tearing to both holes) at a smaller displacement (i.e., $T_{NH} > T'_{NH} = 60^oC$).

The same two modes of stress relaxation also control behavior of undrilled samples. In the standard Charpy, relaxation of stress by plane strain deformation results by formation of plastic wings between the plastic hinges and the top surface[100]. However, there is also relaxation of the stress in the thickness direction (notch contraction) occurring coincident with and after wing formation. In both 0.200" and 0.100" thickness samples, relaxation by deformation through the thickness can occur at a $V^{RLX,t}(c)$ which is less than that required for wing formation so that the ductility transition occurs at a lower temperature. Plastic wings still form in 0.200" thick samples and contribute to the complete stress relaxation, but their role is secondary. More-

over, in the 0.100" thick samples, wings are not observed even in completely ductile samples because almost all deformation beyond $V^{RLX,.1}(c)$ occurs at 45° to the specimen surface along the net section (plane stress type deformation[84]).

Table 8.1 summarizes the effect of thickness on the reduction in the ductility transition temperature produced by hole drilling. Holes reduce the ductility transition temperature (ΔT_N^t) considerably in both thick (t = 0.394") and thin (t = 0.100") samples, but they are less effective in intermediate thickness (t = 0.200") samples. This results because T_N^t of the standard samples decreases with decreasing thickness ($K_{\sigma(p)}^{max,t}\downarrow$) while tearing does not reach both holes any more easily ($T'_{NH} = 60°C$). If tearing to both holes were the only possible relaxation mechanism, ΔT_N^t would decrease continuously with decreasing thickness. However, in thin samples, tearing to one hole allows sufficient deformation to cause stress relaxation in the thickness direction. Therefore, ΔT_N^t initially decreases but then increases with decreasing thickness when tearing to one hole is sufficient to cause relaxation.

Also summarized in Table 8.1 are the effects of two holes on the general yield and ultimate loads in the various thickness samples. The general yield loads of both standard and drilled samples decrease by about 5 percent in going from t = 0.394" to 0.200" but are approximately unchanged in going from t = 0.200" to 0.100". The ultimate load of standard and drilled samples decreases by 8 percent between t = 0.394" and 0.200" and another 8 percent between t = 0.200" and 0.100". Despite these reductions due to thickness alone, two holes reduce P_{GY} and P_{ULT} by the same amount (10%) within each of the three thicknesses. This is

a further indication that holes act directly to reduce the longitudinal stress and strain in the notch section, and therefore can produce improvements in both thin and thick samples.

CHAPTER IX

THE EFFECT OF MICROSTRUCTURE ON THE IMPROVEMENT FROM HOLE DRILLING

In defining the relevant geometric parameters which determine the effectiveness of drilled holes, three alloys (steels 0.025, 0.24, and FeSi 2) have been employed. Although holes produced generally similar improvements in all three, the specific magnitude of the changes varied from one alloy to another. In order to determine in more detail the effect of microstructure on the toughness improvements from hole drilling, impact transition curves were obtained for Charpy and two hole (H_D = 0.0292", R = 0.0448", $\theta = 75^o$) specimens for a series of hypoeutectoid steels (0.02, 0.10, 0.20, 0.40, 0.41, 0.57, 0.72). The number designation of each steel represents the approximate weight percent carbon while a more specific composition analysis was given in Table 2.1 and the respective microstructures in Figures 2.1 - 2.9 (Chapter II). In addition, an 18 Ni - 8 Co maraging steel (18-8, σ_Y = 250 ksi) was also examined.

In each alloy, the impact energy was obtained over a temperature range where failure went from 100% cleavage to 100% fibrous failure (except steel 18-8 which fails by low energy tearing over the entire range studied). In alloys 0.1, 0.2, 0.44, and 0.57 as well as the previous series of FeSi 2 and 0.24, the Charpy tests were instrumented to record the corresponding load-time traces. In addition, a limited number of specimens containing four 0.0292" holes (see section 7.3) were tested in alloys 0.1, 0.2, and 18-8.

9.1 Experimental Results

The impact results for standard and drilled samples of the various steels are shown in Figures 9.1 - 9.6. Table 9.1 summarizes, for all the alloys investigated, the effect of holes on the (1) various transition temperatures, (2) maximum or shelf energy (E_{max}) at high temperatures, (3) general yield load (P_{GY}), and (4) ultimate load (P_{ULT}). For those alloys where the tests were instrumented, the nil-ductility (T_D, T_{DH}), ductility (T_N, T_{NH}), and initiation (T_S, T_{SH}) transition temperatures were obvious from the load time traces and fractured surfaces. In the others, T_D (or T_{DH}) was determined by observation of the plastic bend angle ($\theta_p > 1^o$) and surface deformation of fractured samples. T_{NH} was taken as the lowest temperature at which tearing reached both holes (reinitiation from the holes was always fibrous so that $T_{SH} = T_{NH}$). In standard samples, the initiation transition temperature [$T_S = T_N$, except for high carbon alloys where $T_S < T_N$, and a fibrous crack initiates prior to $V^{RLX}(c)$] was obtained by observations of the fracture surface ahead of the notch root.

9.2 Discussion

9.2-1 The Effect of Increased Carbide Content on the Standard Charpy Transition

All the present steels with the exception of 18-8 and FeSi were tested in the hot rolled condition. Their microstructures (Figures 2.1 - 2.9) consist of continuous ferrite and various fractions of lamellar pearlite. For carbon contents greater than 0.4, the continuous ferrite is located primarily at the prior austenite grain boundaries, pearlite occupying what was the inside of austenite grains. The 18-8

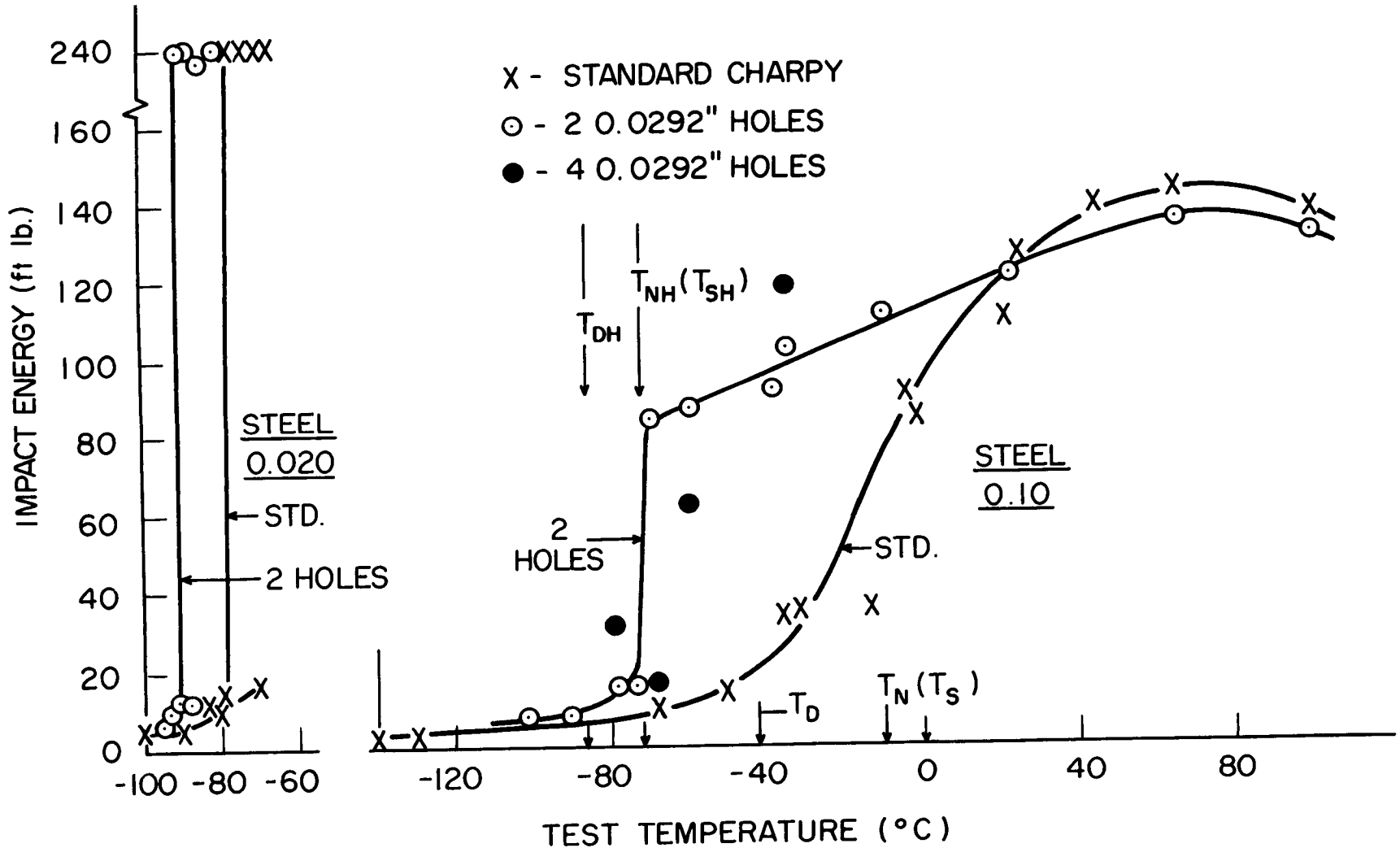

Figure 9.1 The effect of two holes (H_D = 0.0292", R = 0.0448", θ = 75°) on the Charpy impact transition curves of steels 0.020 and 0.10.

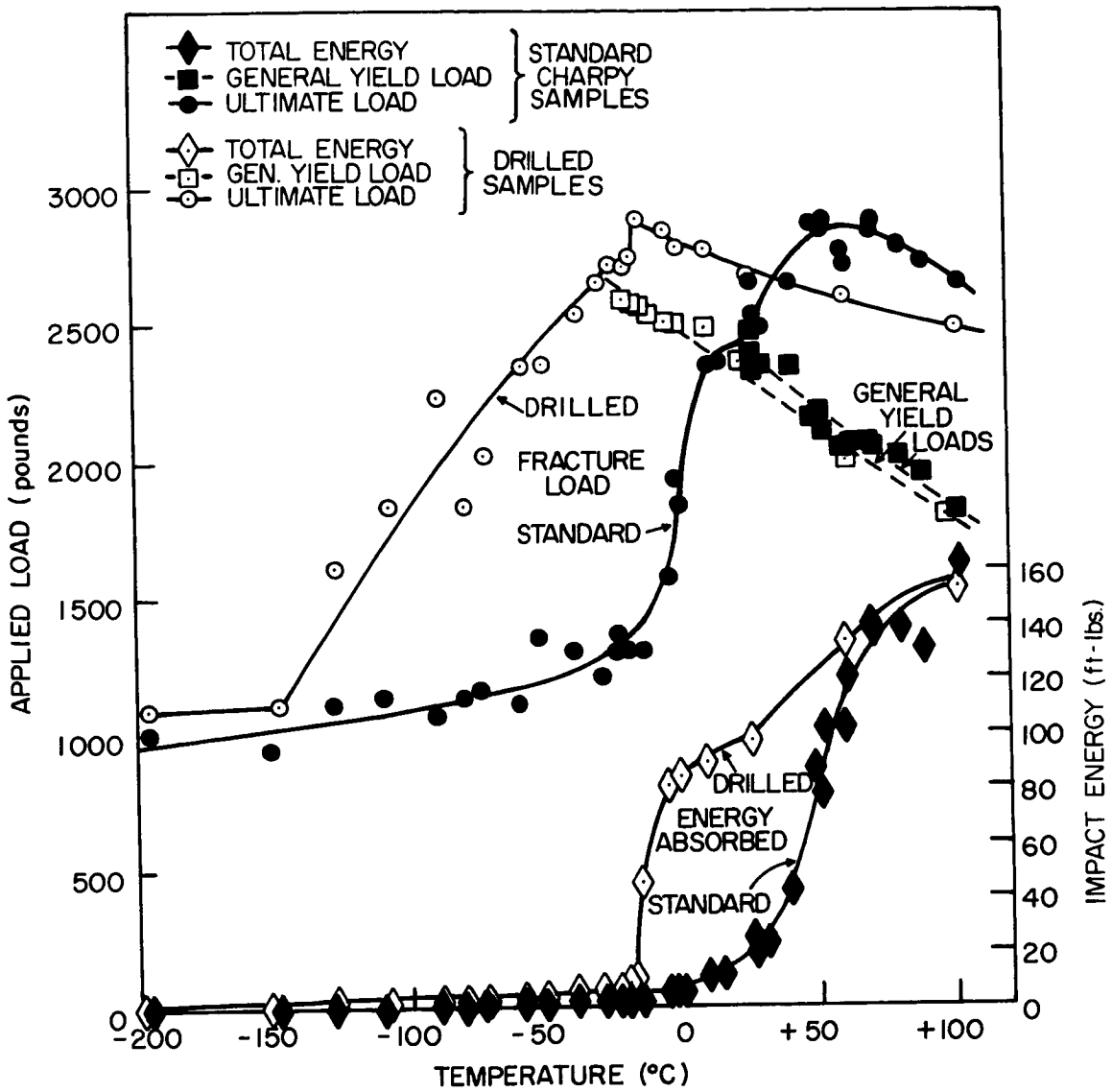

The effect of two drilled holes on the Charpy impact properties of 0.24% carbon steel.

Figure 9.2 The effect of two holes (H_D = 0.0292", R = 0.0448", $\theta = 75^{\circ}$) on the instrumented Charpy transition behavior of steel 0.20.

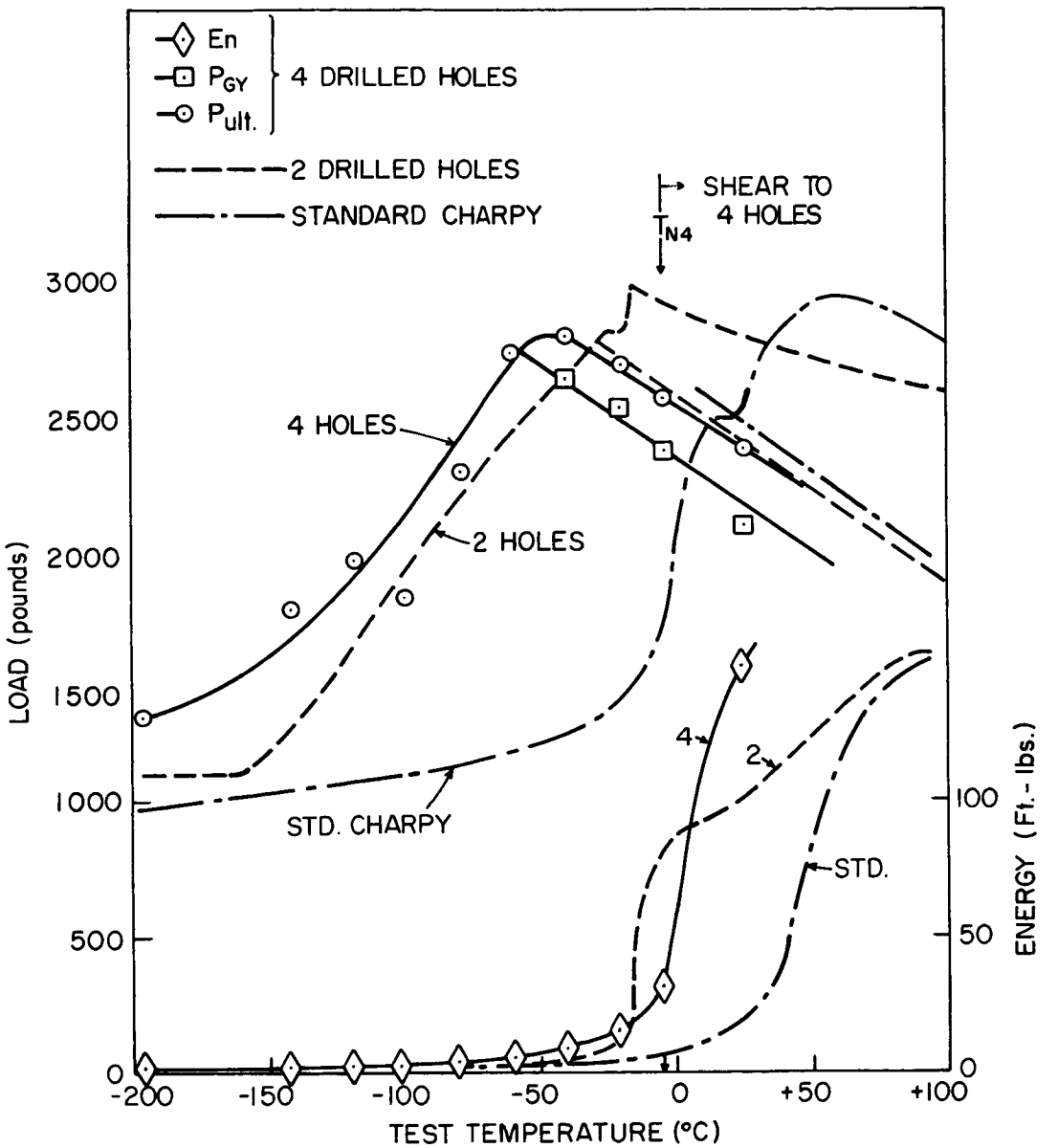

Figure 9.3 The effect of four holes on the instrumented Charpy transition behavior of steel 0.20.

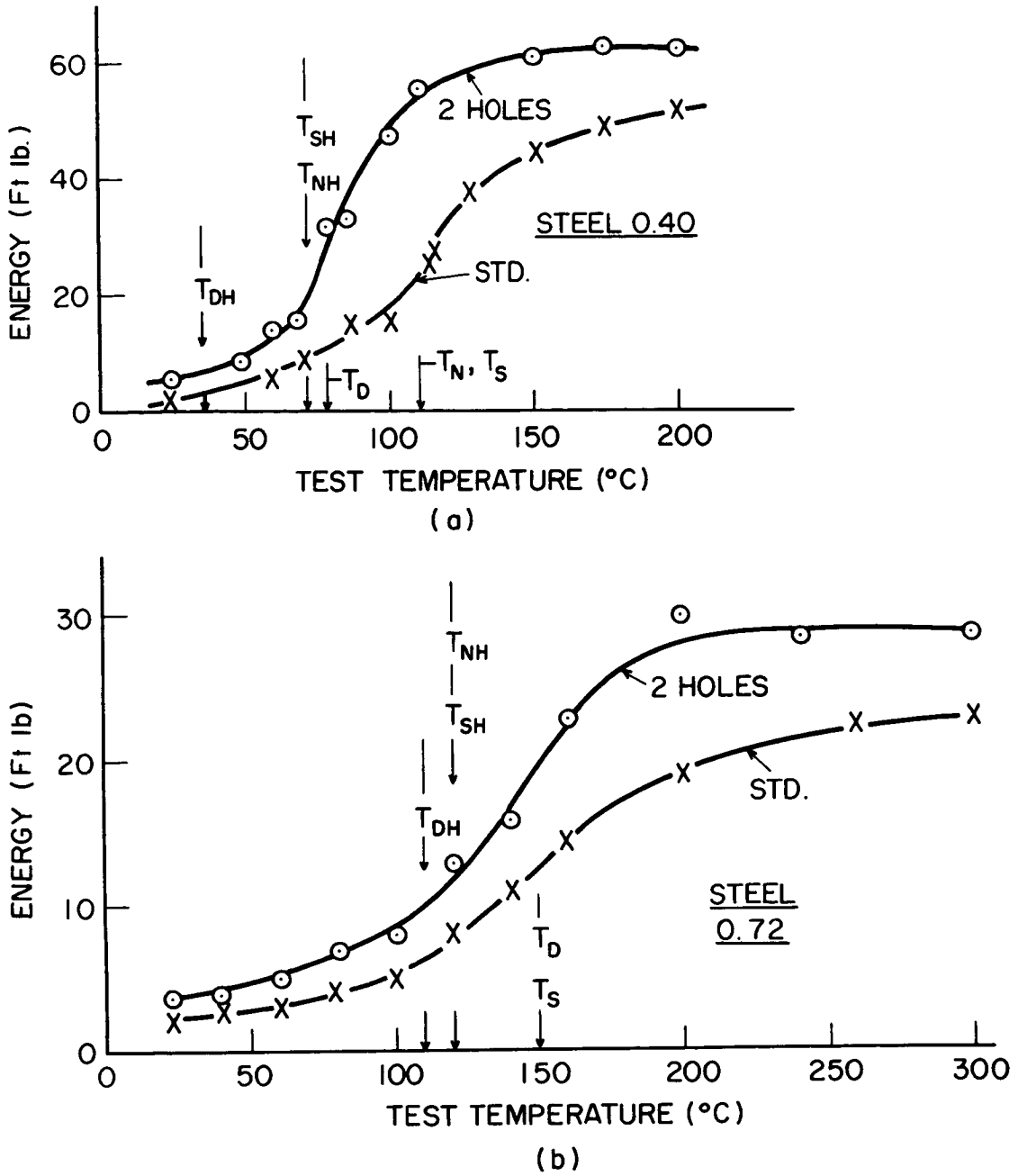

Figure 9.4 The effect of two holes (H_D = 0.0292", R = 0.0448", $\theta = 75^{\circ}$) on the Charpy impact transition curves of steels 0.40 and 0.72.

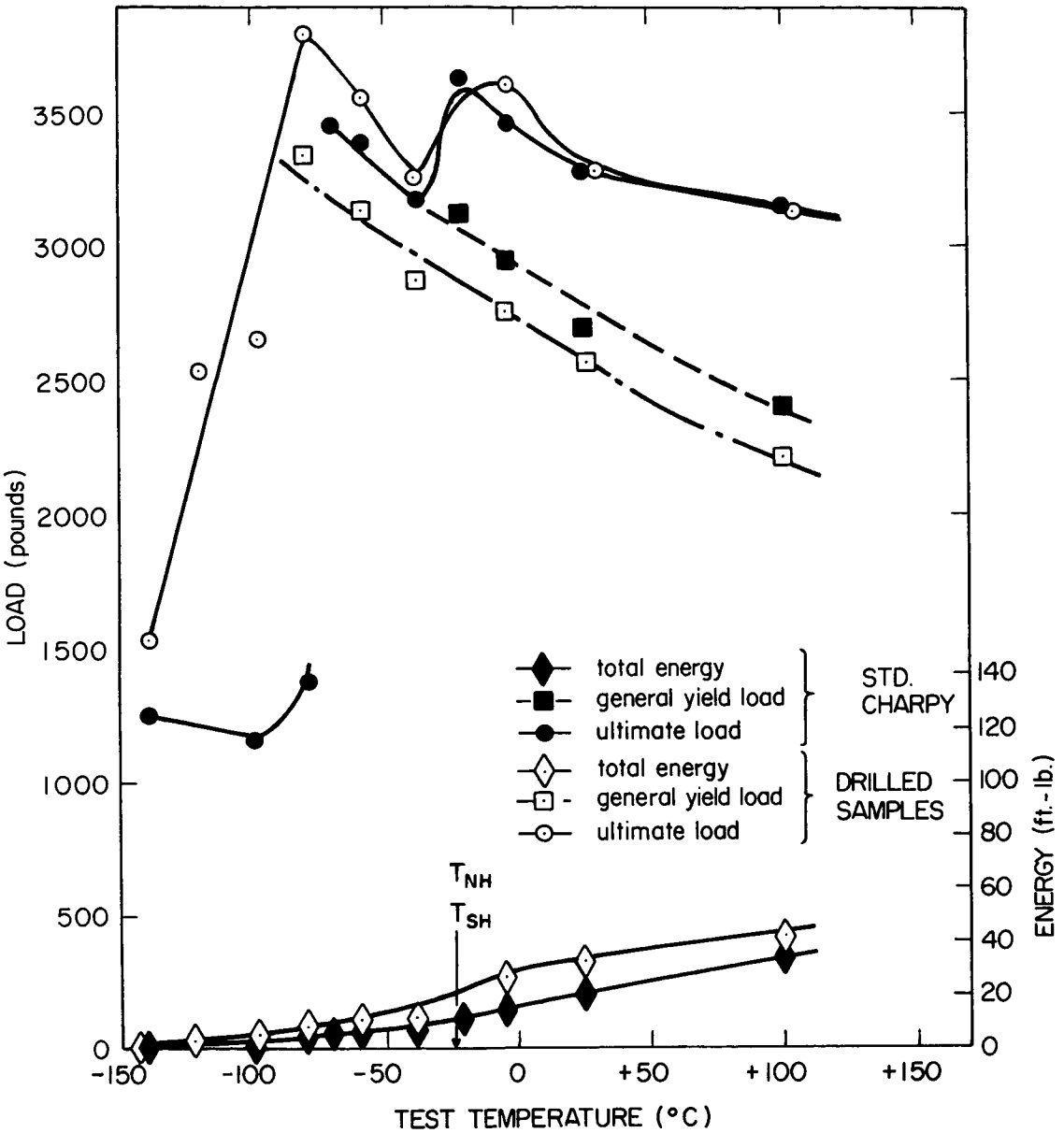

Figure 9.5 The effect of two holes (H_D = 0.0292", R = 0.0448", $\theta = 75^{\circ}$) on the instrumented Charpy transition behavior of steel 0.41.

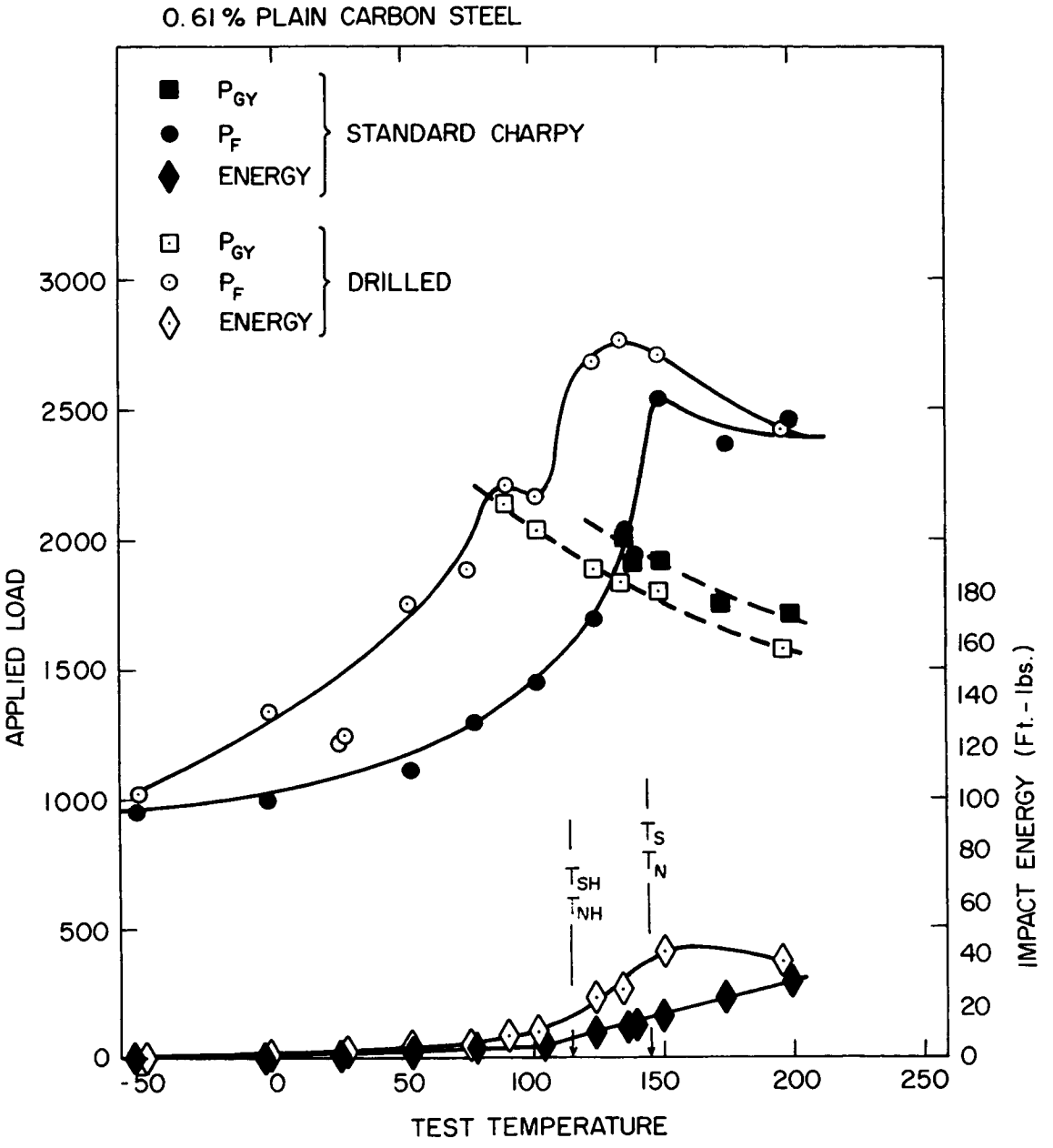

Figure 9.6 The effect of two holes (H_D = 0.0292", R = 0.0448", $\theta = 75^{\circ}$) on the instrumented Charpy transition behavior of steel 0.57.

Table 9.1

The Effect of Drilled Holes on the Charpy Impact Properties of Various Iron - Base Alloys

Material	$\frac{d\sigma_Y^*}{dT}$ (T_D)	ΔT_D T_D	T_{DH}	ΔT_N ΔT_S T_N, T_S	T_{NH}, T_{SH}	ΔT_{50} T_{50}	T_{50H}	ΔE_{max} (%) E_{max}	E^H_{max}	ΔP_{GY}	ΔP_{ULT}
	(psi/°C)	(°C)		(°C)		(°C)		(ft.lb.)	(ft.lb.)	(%)	(%)
Fe-Si 2 (d=0.021")	-110	90	40	90	60	90	60	240	240	-10	-10
		-50		-30		-30		-			
0.02 (d=0.0024")	-	-	-	-78	-91	-78	-91	240	240	-	-
		-		-13		-13		-			
0.025 (d=0.0011")	-	-	-	-58	-91	-58	-91	240	240	-9*	-9*
		-		-33		-33		-			
0.10 (d=0.00067")	-300	-42	-86	-10	-72	-10	-70	143	135	-9	-10
		-44		-62		-60		-5.5			
0.20 (d=0.0012")	-240	20	-20	40	-15	49	-11	160	154	-4	-10
		-40		-65		-60		-4.0			
0.24 (d=0.0008")	-260	-15	-55	10	-55	27	-37	80	95	-10.8	- 9
		-40		-65		-64		+18.0			
0.40 (d=0.0011")	-	78	35	110	70	118	80	51	62	-	-
		-43		-40		-38		+21.5			
0.41	-240	-30	-80	T_S=-5	-25	10	-25	34	44	-8	0
		-50		-20		-35		29			
0.57	-230	135	90	T_S=145	115	170	140	30	40	-9	0
		-45		-30		-30		33			
0.72	-	150	110	T_S=150	120	157	130	23	29	-	-
		-40		-30		-27		26			
18-8	-	-	-	-	-	-	-	17.7	36.9	-15*	-5*
		-		-		-		109			
0.10 (4 holes)	-300	-42	<-80	-10	-60	-10	-60	143	>118	-14	-24
		-		-50		-50		+			
0.20 (4 holes)	-240	20	-55	35	-5	49	+5	160	>150	-13	-20
		-75		-40		-44		+			
0.24 (4 holes)	-260	-15	-100	10	-40	27	-10	80	>98.5	-17.3	-23.2
		-85		-50		-37		+			
18-8 (4 holes)	-	-	-	-	-	-	-	17.7	39.4	-	-
								122			

* Determined from slow bend tests.

maraging steel was solution treated for one hour at 815°C, air cooled, and aged at 480°C after machining and hole drilling. The microstructure consists of precipitation hardened (fine alloy carbides) low carbon martensite[108, 109].

There are three major effects of increased carbon content on the Charpy transition behavior[64, 65]. First, the yield strength $\sigma_Y^*(T)$ is increased ($\sigma_i\uparrow$, $d\downarrow$), and the cleavage strength is decreased (more and larger carbides). Both changes shift the nil-ductility transition where

$$K_{\sigma(p)}^{max} \cdot \sigma_Y^* = \sigma_f \qquad T = T_D \qquad (9.1)$$

to a higher temperature. Secondly, the maximum or shelf energy of fully ductile samples decreases with increasing carbide content because the energy to nucleate and propagate a fibrous crack is lower. That is, the formation of voids at cracked carbides and the necking between these voids which is necessary to cause failure both require less plastic strain and less energy when there is more carbide. Thirdly, the transition region from fully brittle (cleavage) to fully ductile (fibrous) failure is extended over a larger temperature range.

This broader transition region results for primarily two reasons. (1) Increased carbide content causes the cleavage fracture strain

$$\epsilon_F = \frac{\sigma_f - K_{\sigma(p)}^{max}\ \sigma_Y^*}{K_{\sigma(p)}^{max}\ d\sigma/d\epsilon}$$

to increase less rapidly with temperature above T_D (due to higher $d\sigma/d\epsilon$[110], lower $|d\sigma_Y^*/dT|$, and higher $K_{\sigma(p)}^{max}$ around stable microcracks[100]). The ductility transition, defined by

$$V^*(c) = \beta \rho \varepsilon_F \geq V^{RLX}(c) \qquad T = T_N , \qquad (9.2)$$

therefore doesn't occur until a higher temperature above T_D. (2) When the amount of carbide is low, relaxation of constraint (at $V^{RLX}(c)$, T_N) requires a sharp increase in the displacement required to initiate a fibrous tear and to sharpen it to the point where cleavage can initiate. However, with higher carbide contents, the critical strain to initiate fibrous tearing ε_S is reduced, and no large increase in energy results at T_N. In fact, for very high carbide contents, fibrous tearing initiates at the notch root prior to relaxation of constraint

$$\rho \varepsilon_S = V_S^*(c) < V^{RLX}(c) \qquad T_S < T_N . \qquad (9.3)$$

In either case, the effective sharpness of the fibrous crack also decreases with increasing carbide content[111], and therefore, cleavage occurs at temperatures well above T_S and further broadens the transition region.

Maraging steel behaves differently because its microstructure consists of very fine tempered martensite plates and no large carbides to initiate cleavage cracks. In addition, the yield stress (σ_Y^*) increases very slowly with decreasing temperature[112] so that failure involves void formation and coalescence at all temperatures between -196° and 450°C where the microstructure becomes unstable[113].

The Charpy transition curves shown in Figures 9.1 - 9.6 definitely demonstrate the broader transition and lower E_{max} with increasing carbide content. There is some variation in the absolute temperature of the transition region, but this is probably associated with differences in

Mn and Ni (which tend to lower T_D), Si (which tends to raise T_D), or simply processing variables which control the resulting ferrite grain size. The reasons for the effects of the alloying additions as well as carbon have been discussed by various authors[64, 65, 114] and will not be repeated here. For the present study, the important variables are (1) the relative ease of fibrous tearing (ε_S) compared with cleavage initiation (ε_F) since this determines the initiation mode

$$V_S^*(c) \begin{matrix} > \\ < \end{matrix} V^*(c) \quad \begin{matrix} \text{cleavage (a)} \\ \text{fibrous (b)} \end{matrix} \tag{9.4}$$

where

$$V_S(c) = \rho\, \varepsilon_S \tag{1.27) (9.5}$$

and

$$V^*(c) = \beta\, \rho\, \varepsilon_F = \beta\, \rho \left[\frac{\sigma_f - K^{max}_{\sigma(p)}\, \sigma_Y^*}{K^{max}_{\sigma(p)}\, d\sigma/d\varepsilon} \right] \tag{1.16) (9.6}$$

and (2) the effective sharpness (ρ_{eff}) of the propagating fibrous tear since this determines V*(c) ahead of the tear and thus the highest temperature where cleavage is produced.

9.2-2 The Effect of Microstructure on the Improvements from Hole Drilling Prior to General Yielding

The instrumented Charpy results shown in Figures 9.2, 9.5 and 9.6 confirm that two holes increase the load-carrying capacity of Charpy samples at low temperatures in each of the steels. Prior to general yielding, cleavage initiation requires that σ_f be produced locally; the fracture criterion is

$$K_{\sigma(p)} \left(\frac{P}{\sigma_Y^*} \right) \cdot \sigma_Y^* = \sigma_f \,, \qquad P_F < P_{GY} \tag{6.10) (9.7}$$

The effect of holes on the increase of $K_{\sigma(p)}$ with P/σ_Y^* is approximately a geometric property, except for small changes resulting from different initial strain hardening rates. Consequently, similar improvements in the nominal fracture strength (P_F) are expected and observed at corresponding σ_f/σ_Y^* in all of the steels.

Although the exact general yield loads are not known below T_{DH}, σ_Y^* may be estimated from a linear extrapolation of P_{GY} using equation (6.1). With this assumption, the ratios P_F/σ_Y^* and P_F^H/σ_Y^* at each temperature were calculated from the fracture results of steel 0.20 (Figure 9.2) and steel 0.57 (Figure 9.6). Using the $K_{\sigma(p)}$ vs P/σ_Y^* curves derived for steel 0.24 (Figure 6.10), the corresponding $K_{\sigma(p)}$ and $K_{\sigma(p)}^H$ were obtained. Substituting these values into equation (9.7) for steel 0.20 yields the same constant fracture stress (σ_f = 160 ksi) in both standard and drilled samples. This implies that Figure 6.10 also represents very closely the effect of two holes on $K_{\sigma(p)}$ in steel 0.20.

In steel 0.57, substitution in equation (9.7) yields nearly constant σ_f for both standard (140 ksi) and drilled (132 ksi) samples, but the value is 5% lower for the drilled samples. This implies that holes do not reduce constraint ($K_{\sigma(p)} - K_{\sigma(p)}^H$) by quite as much in steel 0.57 as in mild steels. As was the case of Fe-Si, an increased initial strain hardening rate ($d\sigma/d\varepsilon$) may be responsible for this small difference. Because of the uncertainty in σ_Y^* below T_{DH}, no attempt is made to adjust Figure 6.10 to describe the specific $K_{\sigma(p)}$ vs P/σ_Y of steel 0.57, which would be very similar to Figure 6.10.

In Chapter VI, it was shown that the reduction in nil-ductility temperature (when σ_f = const)

$$\Delta T_D = T_{DH} - T_D = \frac{(K^{max}_{\sigma(p)} - K^{max,H}_{\sigma(p)})}{K^{max,H}_{\sigma(p)} \quad K^{max}_{\sigma(p)}} \cdot \frac{\sigma_f}{d\sigma^*_Y/dT} \qquad \begin{matrix}(6.15)\\(9.8)\end{matrix}$$

depends only on the reduction in maximum stress intensification at P_{GY} and the temperature dependence of σ^*_Y. Since the various steels have similar $d\sigma^*_Y/dT$ (noted in Table 9.1), ΔT_D represents a good measure of the reduction in $K^{max}_{\sigma(p)}$ produced by holes. Table 9.1 shows that in all of the steels investigated, ΔT_D was between -40 and -50°C. This is further evidence that the relative effect of holes at a given σ_f/σ^*_Y prior to P_{GY} is nearly independent of microstructure as long as failure depends on achieving a critical fracture stress. That is, holes produce a local redistribution of plastic strain and resulting stress which is, at most, only slightly affected by the increased work hardening rates (deviation from ideal plastic behavior) of the high carbon steels.

9.2-3 The Effect of Microstructure on the Improvement with Holes in the Transition Region

Although microstructure has little effect prior to P_{GY}, it causes quite different improvements after P_{GY}, where the work hardening rate and relative ease of fibrous (ϵ_S) to cleavage (ϵ_f) failure control behavior. Figure 9.7 shows the reduction in ductility (initiation) ΔT_N (ΔT_S) and 50% maximum energy ΔT_{50} transition temperatures as a function of the steel's carbon content. ΔT_N is quite small in the very clean alloys, but the improvement increases with carbon content up to the mild steels 0.1 - 0.25%C. With further increases in carbon toward eutectoid composition, ΔT_N decreases so holes produce a maximum reduction in the ductility transition temperature in the mild steels.

The reduction in ductility transition temperature due to holes

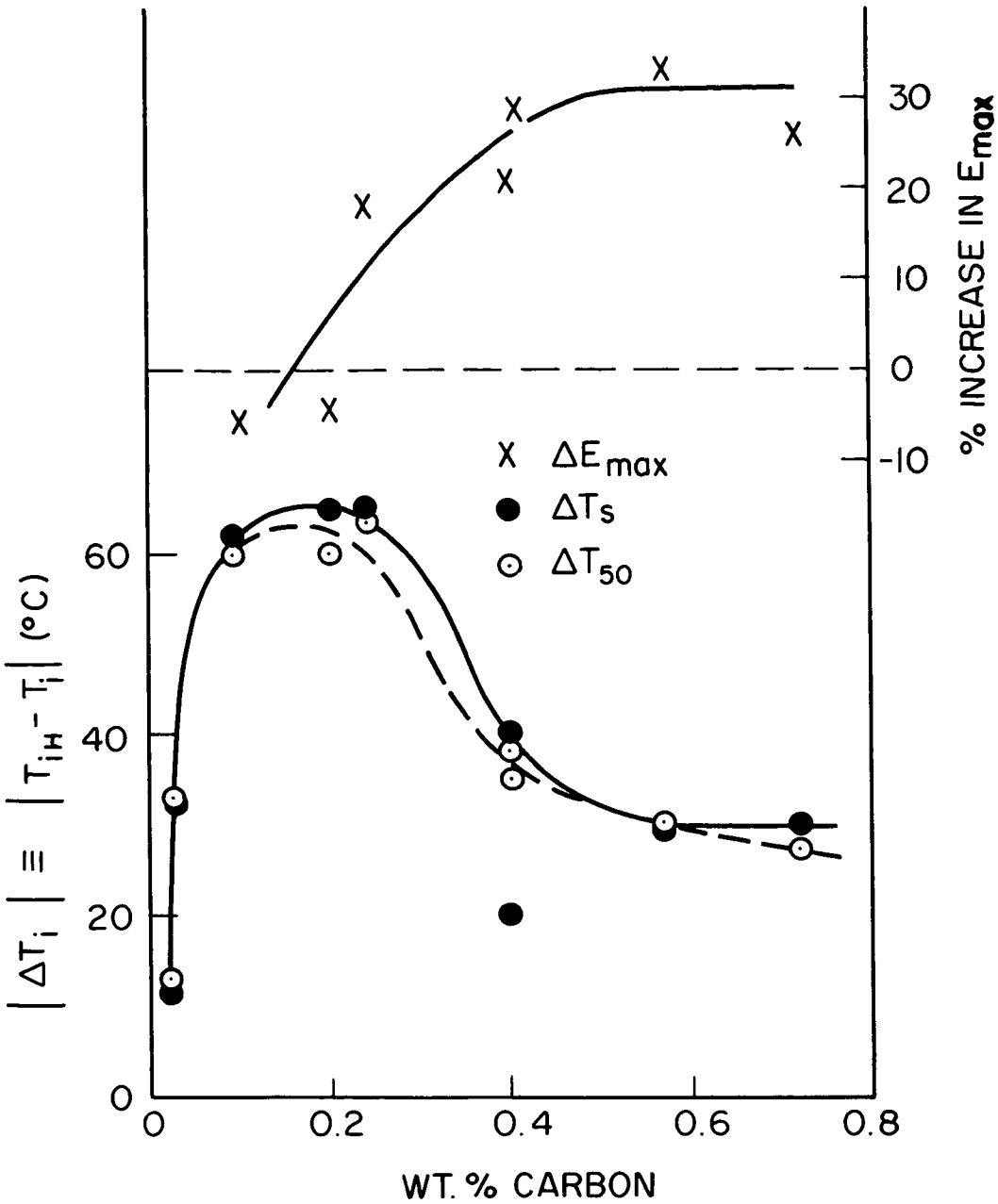

Figure 9.7 The effect of the steel's carbon content on the reduction in the Charpy transition temperatures (ΔT_L) and the percentage increase in the shelf energy which result from hole drilling (H_D = 0.0292", R = 0.0448", θ = 75°).

may be written as

$$\Delta T_N = T_{NH} - T_N$$

$$= T_{DH} - T_D + (T_{NH} - T_{DH}) - (T_N - T_D)$$

$$\Delta T_N = \Delta T_D + (T_{NH} - T_{DH}) - (T_N - T_D) \qquad (9.9)$$

In the previous section, it was shown that microstructure has very little effect on ΔT_D so that the effect of microstructure on ΔT_N results from the different amounts by which the ductility transition is raised above the nil-ductility temperature in the standard $(T_N - T_D)$ and drilled $(T_{NH} - T_{DH})$ specimens. That is, $|\Delta T_N|$ will be quite large if the microstructure encourages cleavage initiation after P_{GY} in standard samples ($T_N - T_D$ large) but allows tearing to reach both holes very soon after P^H_{GY} ($T_{NH} - T_{DH}$ small). Table 9.2 shows the transition temperatures compared in this way.

Table 9.2

The difference between the nil-ductility and ductility transition temperatures of standard and drilled samples of the various steels

Alloy	$\frac{T_D - T_N}{(^oC)}$	$\frac{T_{DH} - T_{NH}}{(^oC)}$	$\Delta T_D \equiv \frac{T_{DH} - T_D}{(^oC)}$	$\Delta T_N \equiv \frac{T_{NH} - T_N}{(^oC)}$
Fe-Si	0	20	-50	-30
0.02	-	-	-	-13
0.025	-	-	-	-33
0.10	32	14	-44	-62
0.20	20	5	-40	-65
0.24	25	0	-40	-65
0.40	32	35	-43	-40
0.41	25	55	-50	-20
0.57	10	25	-45	-30
0.72	0	10	-40	-30

To understand the total effect of microstructure on ΔT_N, consider its effect on the Charpy ($T_N - T_D$) and drilled samples ($T_{NH} - T_{DH}$) individually. In the standard sample, T_N is defined as the lowest temperature where

$$V^{RLX}(c) < V^*(c) \tag{9.10a}$$

or where

$$V_S^*(c) < V^*(c) \tag{9.10b}$$

($V_S^*(c)$ and $V^*(c)$ are given by equations (9.5) and (9.6) respectively) depending on whether fibrous tearing occurs after (9.10a) or before (9.10b) relaxation of constraint. The first case, equation (9.10a), determines T_N in all steels except 0.57 and 0.72. Since $V^{RLX}(c)$ depends only on the geometry, $T_N - T_D$ depends on how the microstructure affects the increase of $V^*(c)$ with temperature above T_D.

Table 9.2 shows that $T_N - T_D$ is approximately constant in steels 0.1 through 0.41 implying that $V^*(c)$ increases with temperature at the same rate in each steel. Apparently, the increase of $d\sigma/d\varepsilon$ with carbon content is quite small up to 0.41% C. In steels 0.57 and 0.72, fibrous tearing occurs very soon after general yield at $V_S^*(c)$. Consequently, equation (9.10b) is satisfied at temperatures near T_D, and ($T_S - T_D$) decreases as eutectoid composition is approached.

The ductility transition of drilled samples occurs at that temperature (T_{NH}) where tearing reaches both holes. The two criteria necessary for this to occur were discussed in detail in section 6.4-2, Chapter VI. The first requires that fibrous tearing occur to one hole before cleavage initiates ahead of the notch. That is

$$V_H^*(c) < V^{**}(c)$$

$$\frac{\text{const.}}{\alpha}\,\varepsilon_s < \alpha\,\beta\,\rho\,\varepsilon_F^H \qquad \text{[criterion 1]}$$

$$\frac{\text{const.}}{\alpha}\,\varepsilon_s < \alpha\,\beta\,\rho\left[\frac{\sigma_f - K_{\sigma(p)}^{\max,H}\,\sigma_Y^*}{K_{\sigma(p)}^{\max,H}\,d\sigma/d\varepsilon}\right] \qquad \begin{matrix}(6.21)\\(9.11)\end{matrix}$$

The second requires that fracture must not reinitiate on the opposite side of the hole [at $V^*(c+H)$] before tearing reaches the second hole. This is assured if

$$V^*(c+H) \gg V_H^*(c) \qquad \text{[criterion 2]} \qquad \begin{matrix}(6.22)\\(9.12)\end{matrix}$$

where

$$V^*(c+H) = \begin{cases} \rho_H\,\beta_H\,\varepsilon_F' & \text{(cleavage)} \qquad (9.12a) \\ \rho_H\,\varepsilon_S & \text{(fibrous)} \qquad (9.12b) \end{cases}$$

and $\beta_H\,\varepsilon_F' > \beta\,\varepsilon_F$ because the magnitude and location of maximum constraint below the hole differ from that ahead of the Charpy notch.

Criterion 1 [equation (9.11)] is satisfied at a critical ratio of $\varepsilon_F^H/\varepsilon_S$. How soon above T_{DH} this ratio is reached depends on how rapidly $\varepsilon_F^H/\varepsilon_S$ increases with temperature. The cleavage strain

$$\varepsilon_F^H = \frac{\sigma_f - K_{\sigma(p)}^{\max,H}\,\sigma_Y^*}{K_{\sigma(p)}^{\max,H}\,d\sigma/d\varepsilon}$$

is temperature dependent, and $d\varepsilon_F^H/dT$ increases with $|d\sigma_Y^*/dT|\uparrow$, $d\sigma_f/dT\uparrow$, $d\sigma/d\varepsilon\downarrow$, and $d\sigma_f/d\varepsilon\uparrow$. Increased carbide content increases $d\sigma/d\varepsilon$ and reduces $d\sigma_f/d\varepsilon$ slightly, so that $d\varepsilon_F^H/dT$ decreases slightly. The fibrous fracture strain (ε_S) is approximately temperature dependent, but its mag-

nitude decreases markedly with increasing carbide content. As a result, $d[\epsilon_F^H/\epsilon_S]/dT$ increases with carbon content, and criterion 1 is satisfied at temperatures closer to T_{DH}.

Criterion 2 [equation (9.12)] is most easily satisfied when (1) holes are blunted ($\rho_H\uparrow$) by plastic deformation prior to $V_H^*(c)$ and (2) ϵ_S and $\beta_H\epsilon_F'$ are large. Both these changes make reinitiation from one hole more difficult [$V^*(c+H)\uparrow$] and allow tearing to reach both holes. Large ϵ_S is especially important because it allows more blunting of the holes ($\rho_H\uparrow$) before tearing and thus raises $V^*(c+H)$ whether reinitiation occurs by cleavage or by tearing. Except in steel 0.72, reinitiation from one hole, when it occurred, was by cleavage, and criterion 2 is given by equation (9.12a). Since

$$\epsilon_F' = \frac{\sigma_f - K'_{\sigma(p)}\,\sigma_Y^*}{K'_{\sigma(p)}\,d\sigma/d\epsilon}$$

(where $K'_{\sigma(p)} \equiv \sigma^{max}/\sigma_Y^*$ ahead of one hole) depends on the same parameters as ϵ_F^H, $d\epsilon_F'/dT$ decreases slightly with increasing carbon content. Due to the lower ϵ_S and lower $d\epsilon_F'/dT$, criterion 2 becomes more difficult to satisfy with increasing carbon content [$(T_{NH} - T_{DH})\uparrow$].

Table 9.2 summarizes the observed variation of $(T_{NH} - T_{DH})$ with carbon content. In single phase ferrite 0.020, ϵ_S is so large that tearing can't reach one hole until temperatures well above T_{DH} where ϵ_H^H/ϵ_S reaches the required value. Consequently, $(T_{NH} - T_{DH})$ is large, and the observed ΔT_N is quite small. Increases in the carbide content up through the mild steels reduce ϵ_S markedly. Furthermore, the initial work hardening rate remains very low (Lüders strain) so that $d(\epsilon_F^H/\epsilon_S)/dT$ increases with carbon content. Equations (9.11) and (9.12a) are there-

fore satisfied at temperatures nearer T_{DH}, and $(T_{NH} - T_{DH})$ decreases $(\Delta T_N \uparrow)$ with increasing carbon content, approaching zero in steel 0.24. For still higher carbon contents, tearing reaches one hole at an even lower $V_H^*(c)$; but because the holes are less blunt $(\varepsilon_S \downarrow, \rho_H \downarrow)$ and $d\varepsilon_F'/dT$ is smaller, cleavage reinitiates from one hole at temperatures well above T_{DH}. Consequently, $(T_{NH} - T_{DH})$ increases with carbon content above 0.24, resulting in a maximum improvement (ΔT_N) in mild steels.

Holes are most effective in mild steels because (1) $d(\varepsilon_F^H/\varepsilon_S)/dT$ is large and the critical $\varepsilon_F^H/\varepsilon_S$ is reached at temperatures just above T_{DH}, but (2) ε_S and ε_F' are large enough to assure that criterion 2 is also satisfied. It should be noted that in standard Charpy samples of high carbon steels (0.57, 0.72), fracture initiates fibrously just after P_{GY}. In these cases $V_S^*(c) < V^{RLX}(c)$ and $T_S < T_N$. The smaller $(T_S - T_D)$ in standard samples, as well as larger $(T_{NH} - T_{DH})$ in drilled samples, contribute to the smaller total ΔT_S, given by equation (9.9).

Whether final failure initiates by shear or cleavage, the single most important material's variable is the fibrous fracture strain (ε_S), since it determines the effective hole geometry (ρ_H) at failure. On the other hand, σ_Y^*, σ_f, $d\sigma_Y/dT$, $d\sigma/d\varepsilon$, $d\sigma_f/dT$, $d\sigma_f/d\varepsilon$ and other materials variables affect both standard and drilled samples in nearly the same way.

9.2-4 The Effect of Microstructure on the Changes from Two Holes in Fully Ductile (Fibrous) Samples

Table 9.1 summarizes the effect of holes on the maximum energy, general yield, and ultimate loads of Charpy samples of the various steels. The general yield load of drilled samples is about 9% less

than the standard Charpy in most of the alloys tested. As described previously in Chapter VI, Section 6.4-3, P_{GY} depends only on the average longitudinal stresses (average constraint) in the net section, and they are nearly a geometric property. Differences in the initial strain hardening rate may modify these stresses slightly, but at the low strains present (on the average) at P_{GY}, the effect of holes is nearly independent of the microstructure.

Two holes also reduce the ultimate load by about 10% in all of the steels except 0.57 and 0.7 where $P_{ULT} \approx P^{H}_{ULT}$. Observation of the fracture surfaces of samples which broke around P_{ULT} indicated that in all alloys (as in mild steel[55]), a fibrous tear initiates at the specimen center prior to P_{ULT}. This tear grows outward extending across the entire thickness at P_{ULT} and then advances under decreasing applied load. In drilled samples full width tears have reached both holes, but P^{H}_{ULT} represents that load at which a full width fibrous tear develops ahead of one or both holes. Holes reduce P_{ULT} for the reasons discussed in Chapter VI, section 6.4-4, which are approximately independent of microstructure. The strains are, of course, quite large at P_{ULT}, and strain hardening is a strong contribution to the local stresses and the corresponding applied load; but the contribution is similar in both standard and drilled samples. The smaller reduction of P_{ULT} by holes in the high carbon steels is not believed to be significant since probably the standard samples had not reached their maximum energy.

Although holes reduce P_{ULT}, they have previously been shown (Chapter VI) to increase the total displacement at which it is reached and thus the pre-maximum load energy. On the other hand, the fracture

area (between the hole and loading striker) is reduced slightly by the holes, and this may reduce the amount of post-maximum load energy. Figure 9.7 shows the percentage change in E_{max} that is produced by two holes as a function of the steel's carbon content. In the low carbon irons, two holes reduce E_{max} slightly (5%), but for all steels where %C > 0.2, holes increase E_{max}. The percentage improvement in E_{max} from hole drilling increases with the carbon content because the increased energy associated with plastic deformation prior to P_{ULT} becomes a larger fraction of the total energy as the fibrous tear energy decreases. For the same reason, holes have a very large effect in maraging steel 18-8 (ΔE_{max} = 109%) where the tear energy is very low; but a smaller and even negative effect when the post maximum energy is large (low carbon alloys).

9.2-5 The Effect of Microstructure on the Improvement with Four Holes

A limited number of four-hole samples (Chapter VII, section 7.3) were also tested in steels 0.10, 0.20, and 18-8 for comparison with the previous results in steel 0.24. Table 9.1 and Figures 9.1b and 9.3 summarize the results of these tests.

Two holes produced similar changes in each of the three mild steels 0.10, 0.20, and 0.24. This was also the case with four holes. At low temperatures, four holes increase the load carrying capacity of Charpy bars considerably more (Figure 9.3) than do two holes. The improvement results from a much less rapid increase of $K_{\sigma(p)}$ with applied load when four holes are present. The maximum plastic stress concentration factor when four holes are present [$K^{max,4}_{\sigma(p)}$] is also lower than in

Charpy or two-hole samples so that the resulting ΔT_D given by equation (9.8) is greater. The magnitude of the improvements prior to P_{GY} are relatively independent of microstructure at corresponding σ_f/σ_Y^* because the local strains are too small for different $d\sigma/d\varepsilon$ to cause any marked changes in the local stress state or geometry.

Above general yielding, four holes also had similar effects in each of the mild steels tested. The reduction in ductility transition temperature (ΔT_N^4) is approximately 50°C, and no sharp increase in load accompanies the transition. The general yield load (P_{GY}^4) is about 15% below P_{GY} of the Charpy specimen, and the ultimate load (P_{ULT}^4) is between 20 and 24% lower in all of the steels tested. In Chapter VII, section 7.3, it was shown that four holes allow tearing to occur on one side of the notch (criterion 1) more easily than do two holes. However, because of the larger reduction in net area, fracture is initiated directly from the outer hole (criterion 2 not satisfied) at temperatures well above the nil-ductility temperature (T_{D4}). As a result, ΔT_N^4 is less than produced by two holes in steel 0.24. Because criterion 2 is controlling behavior, ΔT_N^4 would certainly decrease with increasing carbon contents above 0.24. In addition, the largest ΔT_N from four-hole samples may not be obtained in mild steels, but in some cleaner alloy where ε_S is higher (favors criterion 2). For example, a plot of ΔT_N^4 such as Figure 9.7) for four-hole samples would be lower on the average and might show its maximum reduction at a lower carbon content.

Four holes have been observed to increase the deflection at which P_{ULT} is reached and thereby the pre-maximum load energy. As in the two-hole samples, the percentage increase in the shelf energy E_{max} with four

holes should increase as the tear energy decreases, and plastic deformation prior to P_{ULT} becomes a larger fraction of the total energy. Although pearlitic steel samples were not tested at high temperatures to directly compare with ductile standard samples, four-hole samples were tougher than ductile two-hole samples at the same temperature. In maraging steel 18-8, both standard and four-hole samples fail completely by low energy tear fracture, and the shelf energy (E^4_{max}) is 122% larger than that of the standard sample (Table 9.1).

Four holes increase the Charpy shelf energy because they increase (1) the volume of plastic deformation prior to instability and (2) the total area over which fibrous tearing must occur. As for two-hole samples, the percentage improvement in E_{max} increases as the tear energy decreases because (1) becomes more dominant. However, E_{max} may also be increased by four holes in low carbon alloys as a result of (2) although two holes reduce E_{max} slightly in the same alloy.

CHAPTER X

SUMMARY AND GENERAL DISCUSSION

10.1 The Improvement of Notch Toughness at Various Temperatures

Two or more appropriately drilled holes have been shown to increase the notch toughness under a variety of test conditions. The exact nature of the improvement with holes, like the notch toughness of the standard sample, depends on (1) the intrinsic toughness (σ_f/σ_Y^*, ϵ_f, ϵ_s) of the material and (2) the mechanics of deformation (plastic constraint, local $\dot{\epsilon}$, and strain concentration) in each of the geometries. Varying the test temperature of mild steel is a convenient way of changing σ_f/σ_Y^* and thus providing materials of different intrinsic toughness. Figure 10.1 summarizes the effect of two holes on the notch strength and impact energy of mild steel 0.24 and illustrates the characteristic changes resulting from two holes (H_D = 0.0292", R = 0.0448", $\theta = 75^o$) in each of the ranges of intrinsic toughness.

At very low temperatures ($T < -200^oC$) where $\sigma_f/\sigma_Y^* < 1$, unstable cleavage can propagate as soon as local yielding reaches the first grain boundary. The applied load to cause fracture depends only on the elastic stress concentration factor K_σ of the notch (at the first grain boundary) and the yield stress at the notch tip σ_Y^*,

$$P_F = \frac{4}{L}\frac{I}{a}\frac{\sigma_Y^*}{K_\sigma} = (0.0163\ in^2) \cdot \frac{\sigma_Y^*}{K_\sigma} \qquad (10.1)$$

where I is the moment of inertia of the net section. The photoelastic results of Chapter V indicate that two 0.0292" holes do not significantly reduce the elastic stress concentration factor (K_σ) of the Charpy notch.

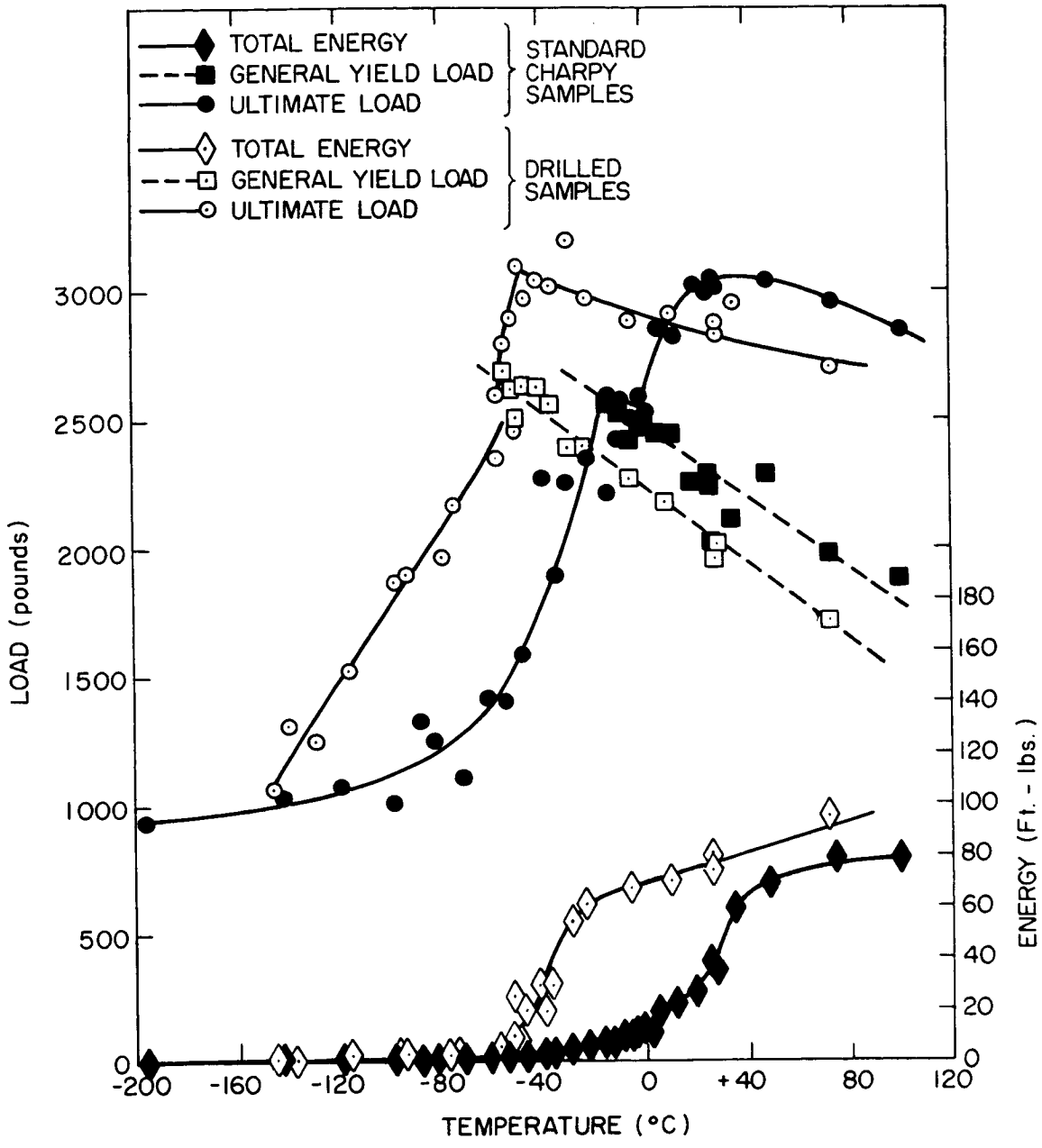

Figure 10.1 Instrumented Charpy fracture results for standard and drilled (H_D = 0.0292", R = 0.0448", θ = 75°) samples of steel 0.24 as a function of test temperature.

Consequently, no significant change in P_F is expected when failure occurs on local yielding. Other geometries such as one larger hole at the notch tip and "stress relieving notches" which do reduce K_σ will increase P_F. The choice of an optimum geometry in this region is governed by the well established techniques to reduce K_σ (increased ρ, increased ω, stress relieving notches).

For $\sigma_f/\sigma_Y^* > 1$, unstable cleavage cannot propagate on initial yielding, and additional plastic deformation is necessary to produce stress intensification by plastic constraint. The fracture criterion becomes

$$K_{\sigma(p)}(P/\sigma_Y^*) = \sigma_f/\sigma_Y^* \equiv K^F_{\sigma(p)}(T) \quad . \tag{10.2}$$

The nominal fracture strength depends on how rapidly $K_{\sigma(p)}$ builds up with applied load (P/σ_Y^*) for the particular notch and specimen geometry. For temperatures up to -140°C $(\sigma_f/\sigma_Y^* < 1.2)$, drilled samples fail at about the same load as the standard Charpy. This implies that in both Charpy and drilled samples, $K_{\sigma(p)}$ increases with applied load at the same rate during the early stages of plastic deformation. Dislocation etch-pit results (Chapter V) also showed that two holes have little effect on the size or shape of the initial plastic zone. With further increases in the applied load, plastic zones extend between the notch side and each hole but not very far below the notch tip. Therefore, $K_{\sigma(p)}$ builds up much less rapidly with applied load when holes are present. As a result, the nominal fracture strength of drilled bars (Figure 10.1) becomes increasingly larger than that of the standard Charpy as the critical $K^F_{\sigma(p)}$ (intrinsic toughness) increases with temperature. Figure 10.2 summarizes the rate of increase of $K_{\sigma(p)}$ and $K^H_{\sigma(p)}$ with applied

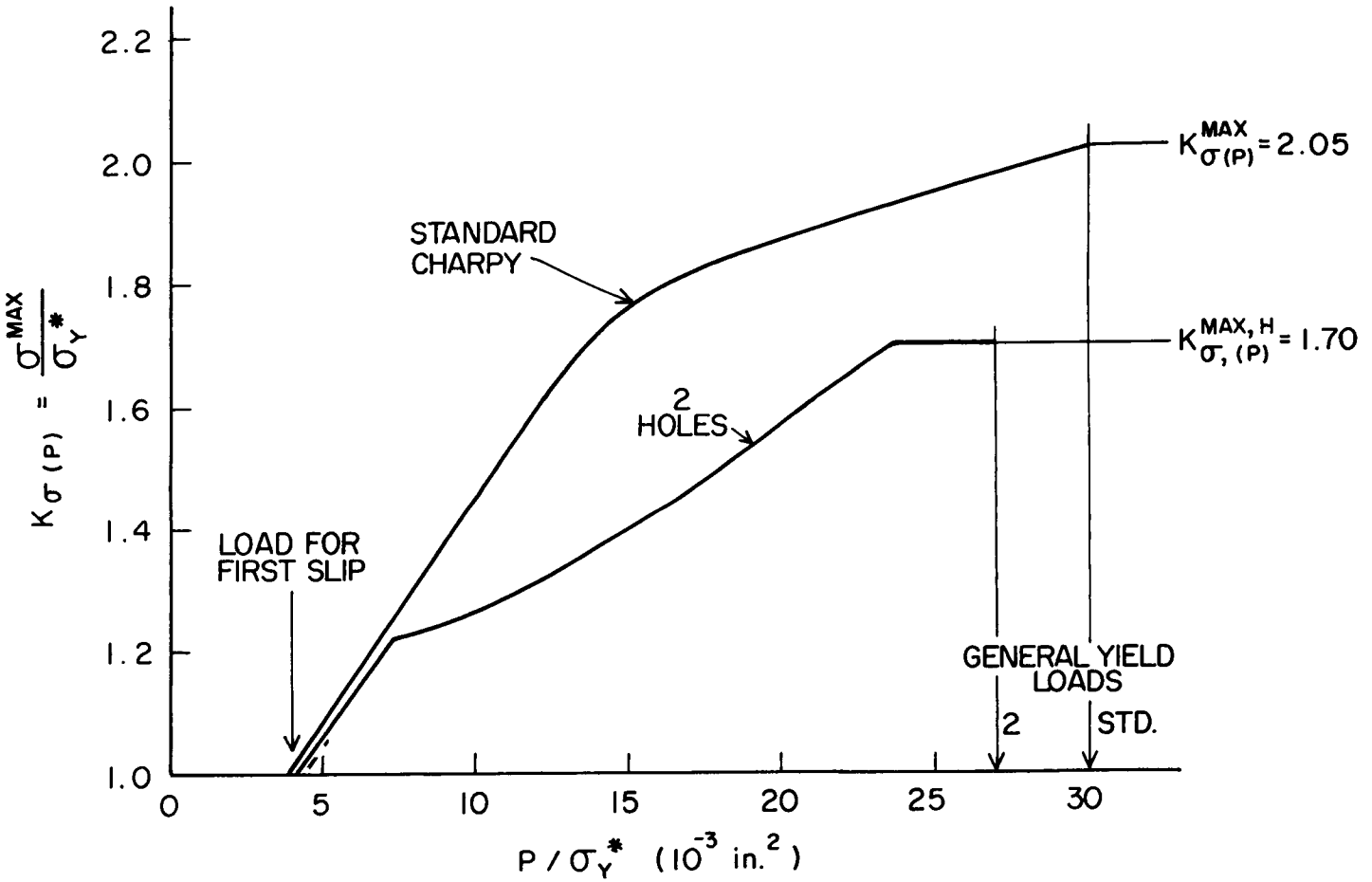

Figure 10.2 The effect of two holes (H_D = 0.0292", R = 0.0448", θ = 75°) on the increase of the plastic stress concentration factor with applied load in Charpy samples of steel 0.24.

load and indicates why for a specific $K^{F}_{\sigma(p)}$, the fracture strength of drilled samples is larger. For instance, if $\sigma_f/\sigma^*_Y = 1.6$, the applied loads to produce $K_{\sigma(p)} = 1.6$ are $P/\sigma^*_Y = 12$ and $P^H/\sigma^*_Y = 20.7$ (10^{-3} in^2) in standard and drilled samples respectively.

Figure 10.2 also shows that whenever $\sigma_f/\sigma^*_Y > 1.7$, the critical stress intensification cannot be produced in drilled samples by constraint alone; general yielding and local work hardening are necessary to cause failure. In fact, within the temperature range where $1.7 < \sigma_f/\sigma^*_Y < 2.05$, Charpy samples reach $K^{F}_{\sigma(p)}$ at low loads prior to general yield, but drilled samples undergo large scale deformation before failure. Since the nil-ductility temperature (T_D) is determined by the $K^{max}_{\sigma(p)}$ produced at general yield, two holes reduce T_D by

$$\Delta T_D = T_{DH} - T_D = \frac{K^{max}_{\sigma(p)} - K^{max,H}_{\sigma(p)}}{K^{max,H}_{\sigma(p)} \; K^{max}_{\sigma(p)}} \cdot \frac{\sigma_f}{d\sigma^*_Y/dT} \qquad (6.15)\ (10.3)$$

It should be noted that ΔT_D corresponds to a $\Delta(\sigma_f/\sigma^*_Y) = 2.05 - 1.70 = 0.35$ over which the constraint developed in the Charpy sample is sufficient to cause cleavage while that in a drilled sample is not. The magnitude of ΔT_D also is inversely proportional to the temperature dependence of the yield stress. Therefore, ΔT_D may be considerably larger at higher loading rates where $d\sigma^*_Y/dT$ is lower.

At temperatures just above T_{DH}, drilled samples fail by fibrous tearing to both holes and fibrous reinitiation after much larger displacements. Two criteria must be satisfied to cause this type of tough failure. The first requires that tearing reach one hole before cleavage occurs ahead of the notch. That is

$$V_H^*(c) < V^{**}(c)$$

Criterion 1

$$\frac{\text{const}}{\alpha}\,\varepsilon_s < \alpha\,\rho\,\beta\,\varepsilon_F^H$$

$$\frac{\text{const}}{\alpha}\,\varepsilon_s < \alpha\,\rho\,\beta\left[\frac{\sigma_f - K_{\sigma(p)}^{\max,H}\,\sigma_Y^*}{K_{\sigma(p)}^{\max,H}\,d\sigma/d\varepsilon}\right] \qquad (6.21)\ (10.4)$$

Equation (10.4) is satisfied at temperatures just above T_{DH} in steel 0.24 because (1) the large relocation of strain ($\alpha\uparrow$, $K_{\sigma(p)}^{\max}\downarrow$) away from the notch tip increases $\frac{d\,V^{**}(c)}{dT}$ while (2) the concentration of strain between the notch side and each hole ($\alpha\uparrow$) reduces $V_H^*(c)$. The second criterion requires that fracture must not reinitiate ahead of one hole before tearing reaches the second hole. This is assured if

$$V_H^*(c) \ll V^*(c+H)$$

Criterion 2

$$\frac{\text{const}}{\alpha}\,\varepsilon_s \ll \rho_H\,\beta_H\,\varepsilon_F'$$

$$\frac{\text{const}}{\alpha}\,\varepsilon_s \ll \rho_H\,\beta_H\,\frac{\sigma_f - K'_{\sigma(p)}\,\sigma_Y^*}{K'_{\sigma(p)}\,d\sigma/d\varepsilon} \qquad (10.5)$$

Equation (10.5) is also satisfied at temperatures just above T_{DH} in steel 0.24 because (1) the holes are blunted by plastic deformation ($\rho_H\uparrow$) prior to tearing, (2) β_H increases with ρ_H since the point of maximum constraint (R_β) occurs further away from the hole, and (3) the maximum constraint $K'_{\sigma(p)}$ ahead of one hole is much less than that below the notch tip.

When $\sigma_f/\sigma_Y^* > 2.05$ ($T > T_D = -10^oC$), even standard Charpy samples cannot obtain the necessary stress intensification by constraint alone. However, Charpy samples still fail by 100% cleavage at small notch dis-

placements [V*(c)] after general yielding until T_N, some 25°C above T_D (Figure 10.1). At this temperature (where $\sigma_f/\sigma_Y^* = 2.2$), relaxation of constraint occurs before cleavage can be initiated, i.e.

$$V^{RLX}(c) < V^*(c)$$

$$V^{RLX}(c) < \beta \rho \varepsilon_F$$

$$V^{RLX}(c) < \beta \rho \frac{\sigma_f - K^{max}_{\sigma(p)} \sigma_Y^*}{K^{max}_{\sigma(p)} d\sigma/d\varepsilon} \qquad (10.6)$$

Equation (10.6) is more difficult to satisfy than equation (10.4) because $dV^*(c)/dT$ is much smaller than $\frac{dV^{**}(c)}{dT}$ due to the higher $K^{max}_{\sigma(p)}$ and lower $\alpha = 1$ (no redistribution coefficient). Consequently, $T_N - T_D = 25^oC$ while $T_{NH} - T_{DH} = 0$, and holes are even more effective in reducing the ductility transition temperature ($\Delta T_N \equiv T_{NH} - T_N$) than they are in reducing the nil-ductility transition temperature (ΔT_D). In mild steel, there is a range of intrinsic material's toughness $1.7 < \sigma_f/\sigma_Y^* < 2.2$ where drilled samples absorb large energies in fibrous failure but Charpy samples fail by 100% cleavage.

At high temperatures ($\sigma_f/\sigma_Y^* > 2.3$), both Charpy and drilled samples fail fibrously. The general yield load of drilled samples is about 10 percent below that of standard Charpys at a given temperature. Since two holes reduce the tensile stresses ahead of the notch, they also reduce the total bending moment produced by these stresses and consequently the general yield load to produce them. Similarly, holes reduce the ultimate load by about 10 percent because (1) the net load bearing area is reduced slightly by tearing to both holes and (2) the longitudinal stresses are on the average lower due to more complete relaxation

of triaxiality and slightly lower local strain rate ($\rho\uparrow$).

10.2 Geometric Parameters which Influence the Improvement of Notch Toughness in Charpy Samples

Hole location (R, θ) is important because it determines the nature and extent of the redistribution of local strain around the notch. In Chapter III, it was shown that two 0.0292" holes at $\theta = 30^{o}$ and 90^{o} produced significantly smaller reductions of the ductility transition temperature (ΔT_N) than did holes at $\theta = 45$, 60, and 75^{o}, for R = 0.0448". The most effective hole positions are those which most easily (at the lowest temperature) satisfy the two criteria given by equations (10.4) and (10.5). The first is favored by a high concentration of strain between the notch sides and holes ($\alpha\uparrow$) but away from the notch tip ($\alpha\uparrow$, $K^{max,H}_{\sigma(p)}\downarrow$). Since at $\theta = 90^{o}$ holes are further removed from high shear stress regions of the Charpy notch (plastic hinges), there is less concentration of strain toward the hole and away from the notch. Equation (10.4) is not satisfied until a higher temperature, and a smaller ΔT_N results. The second criterion, equation (10.5), is favored if (1) the holes are blunted ($\rho_H\uparrow$) prior to failure and (2) the remaining area after failure reaches one hole is large [$K'_{\sigma(p)}\downarrow$]. The $\theta = 30^{o}$ holes, like one hole ahead of the notch, are not blunted as much by plastic deformation and leave a smaller net area when failure reaches one hole. Therefore, cleavage reinitiation occurs from one hole until a higher temperature, and ΔT_N is smaller. Larger radial spacings R > 0.0448" at any θ also reduce the improvements because there is less strain concentration to cause initial tearing ($\alpha\downarrow$) and hole blunting ($\rho_H\downarrow$) as well as a smaller net area ($K'_{\sigma(p)}\uparrow$) when tearing does reach one hole.

Certain geometric modifications to the two 0.0292" holes, such as increased hole size and four drilled holes, produce even larger increases in the notch strength of Charpy samples when $1.2 < \sigma_f/\sigma_Y^* < 1.7$. For instance, four holes increase the fracture strength of Charpy samples by 160% when $\sigma_f/\sigma_Y^* = 1.4$, and reduce the nil-ductility temperature by $\Delta T_D = -85^oC$. These further improvements result because four holes reduce the rate of increase of $K_{\sigma(p)}$ with applied load by redistributing plastic strain away from the notch tip even more efficiently than two holes do. $K^{max}_{\sigma(p)}$, which is reached at general yield, is correspondingly lower, causing the larger ΔT_D which is predicted by equation (10.3).

In contrast to samples containing two 0.0292" holes where $T_{DH} = T_{NH}$, samples containing four holes (or two larger holes) fail by tearing from one side of the notch and cleavage reinitiation from the outermost hole at temperatures well above their nil-ductility temperature (T_{D4}). This results because equation (10.5) (criterion 2) is not satisfied as easily as equation (10.4). In four-hole samples, the temperature (σ_f/σ_Y^*) range between T_{D4} and T_{N4} is quite large since the outermost holes are blunted much less ($\rho_H\downarrow$) by plastic deformation, and the effective load bearing area is reduced markedly [$K'_{\sigma(p)}\uparrow$] when tearing occurs to both holes on one side of the notch. Specifically, tearing does not occur on both sides of the notch until T_{N4}, 60^oC above T_{D4}, and the reduction in the ductility transition temperature by four holes is much less than the reduction of the nil-ductility temperature. Furthermore, four holes are actually less effective than two holes in reducing T_N. In larger hole size samples, the effective load bearing area is also reduced somewhat by tearing to one hole ($K'_{\sigma(p)}\uparrow$). However, the larger ρ_H allows equation

(10.5) to be satisfied at temperatures only 15°C above its T_{DH} so that the ΔT_N produced by two larger holes is about equal to that produced by two 0.0292" holes.

Compared with the two 0.0292" holes, both these geometries reduce the general yield load (due to lower tensile stresses below the notch) and the ultimate load (due to both smaller load bearing area and lower constraint after tearing) considerably.

There is no specific hole geometry which produces the maximum improvement over the entire range of intrinsic toughness (σ_f/σ_Y^*). Four holes are superior when $\sigma_f/\sigma_Y^* < 1.5$, and two 0.0465" holes produce the largest nominal strength and toughness when $1.5 < \sigma_f/\sigma_Y^* < 1.7$. Nevertheless, when $\sigma_f/\sigma_Y^* > 1.7$, two 0.0292" holes at R = 0.0448" and $\theta = 75^o$ increase the toughness with a minimum reduction in both the general yield and ultimate loads. In general, the optimum hole geometry can only be specified if the material and service conditions which determine σ_f/σ_Y^* and ϵ_s are specified. If, for instance, a range of service temperatures or strain rates were to be encountered, a compromise geometry with less improvement at low temperatures (σ_f/σ_Y^*) but more strength at higher temperatures might be best.

10.3 Toughness Improvements in Other Than Charpy Samples

A smaller notch root radius in the Charpy type sample reduces the notch toughness and strength at each temperature (σ_f/σ_Y^*) and shifts the transition region to higher temperatures. Because higher stresses can be produced locally by smaller yield zones at a sharp notch, holes are not effective until larger σ_f/σ_Y^* and P/P_{GY}. However, at loads near or above general yield, holes redistribute the local plastic strain and

produce marked improvements in notch toughness ($T_D\downarrow$, $T_N\downarrow$, $P_F\uparrow$, $E_{max}\uparrow$).

Various authors have suggested[41, 43, 69] that there is a notch tip radius ρ_{min}, determined by some microstructural feature, below which reducing ρ causes no further reduction in toughness. Most estimates predict that $\rho_{min} \geq 0.002"$. Consequently, sharply cracked samples might behave much like the $\rho = 0.002"$ samples examined in this study. However, a crack ($\omega = 0^o$) would still be somewhat more severe than the sharp ($\omega = 45^o$) notch due to the higher $K^{max}_{\sigma(p)}$ [equation 1.24]. Nevertheless, improvements are surely possible even in cracked samples when the intrinsic toughness (σ_f/σ^*_Y) is large enough to require considerable local plasticity prior to failure.

Conditions of plane strain and high constraint are not necessary prerequisites for holes to produce improvements. In Charpy samples of reduced thickness, the tensile stress which can be supported in the thickness direction is lowered, and the degree of triaxiality is reduced. Consequently, the plastic stress concentration factor, $K^t_{\sigma(p)} = \frac{\sigma^{max}}{\sigma^*_Y}$, is less than the plane strain value at a given zone size (R) or applied load, i.e.

$$K^t_{\sigma(p)} = K^{\infty}_{\sigma(p)} \cdot X\ (t, R) \qquad (10.7)$$

where $X\ (t, R) < 1$ represents the degree of relaxation of stress in thickness direction. Similarly, the maximum triaxiality $[K^{max,t}_{\sigma(p)}]$ is lower, and the associated nil-ductility temperature (T^t_D) is below that of the standard Charpy sample. In 0.394", 0.200", and 0.100" thick samples, two holes have been shown to increase the nominal fracture strength by similar amounts at corresponding P/σ^*_Y. This implies that holes are able to retard the increase of $K^t_{\sigma(p)}$ with applied load in a

way which is nearly independent of the amount of relaxation which occurs through the thickness. Specifically, this results because holes reduce directly the longitudinal strains ahead of the notch, and thus, the hypothetical plane strain constraint factor is reduced from $K^{\infty}_{\sigma(p)}$ to $K^{\infty,H}_{\sigma(p)}$. Since the difference $[K^{\infty,H}_{\sigma(p)} - K^{\infty}_{\sigma(p)}]$ is independent of X (t, R), the total reduction $[K^{t,H}_{\sigma(p)} - K^{t}_{\sigma(p)}]$ will vary with thickness only as X (t, R) varies with R. Consequently, holes produce similar improvements prior to general yield in each thickness with certain peculiarities caused by the difference between X (t, R) in the standard and drilled samples.

In samples of reduced thickness, drilled holes produce similar changes in (1) notch strength prior to general yielding, (2) the nil-ductility temperature (T_D, T_{DH}, ΔT_D), and (3) fully ductile samples (P_{GY}, P_{ULT}). However, in the transition region, the effect of holes depends strongly on thickness. There are two forms of stress relaxation and two possible ductility transitions in both standard and drilled samples. The first (1) results from stress relaxation within the plane of the bar by "wing formation" in standard samples and by ductile tearing to both holes (effective blunting) in drilled samples. The second (2) results from extensive plastic deformation through the thickness and a complete breakdown of the triaxial stress state. The required notch tip displacement $V^{RLX,t}(c)$ [equation (10.6)] to produce the second depends strongly on thickness, while $V^{RLX}(c)$ for the first is independent of thickness but varies with other geometric parameters such as notch depth (in standard samples) and hole position (in drilled samples).

In standard Charpy thickness, plane strain relaxation (1) requires the smaller $V^{RLX}(c)$ and thus determines the ductility transition

temperatures of standard and drilled samples (T_N, T_{NH}, ΔT_N) as described by equations (10.4), (10.5) and (10.6). In 0.200" and 0.100" thick samples, both types of relaxation occur; but "through the thickness" (1) relaxation requires the smaller $V^{RLX}(c)$ and thus controls T_N^t, T_{NH}^t, and ΔT_N^t. In thin drilled samples, tearing need not reach both holes for relaxation of constraint to occur; tearing to one hole allows sufficient deformation to produce the ductility transition (T_{NH}^t). Thus ΔT_N^t is considerable for thick (plane strain) samples as previously discussed and also for very thin samples where $K_{\sigma(p)}^{max,t}$ is low enough that tearing reaches one hole easily (near T_{DH}^t). For intermediate thicknesses ($t \approx .2"$), $T_N^{.2}$ (of the standard sample) is below that of the standard Charpy, but sufficient constraint is maintained in the drilled sample to cause cleavage below the notch at temperatures well above $T_{DH}^{.2}$. Consequently, tearing does not reach one hole, to encourage through-the-thickness deformation, until a much higher temperature; and $\Delta T_N^{.2}$ is quite small.

10.4 The Improvement of Notch Toughness in Various Microstructures

It has been noted that each test temperature corresponds to a particular σ_f/σ_Y^* and thus to a different intrinsic toughness. Moreover, the notch toughness of the structure, as well as the improvement from holes, depends strongly on the particular σ_f/σ_Y^*. First, the microstructure determines σ_f/σ_Y^* at a particular temperature and thus the possible improvement from holes. Secondly, the microstructure determines the temperature dependence of σ_Y^* and/or σ_f. In Chapter VIII, it was shown that

$$\Delta T_D = \frac{\left[K^{max}_{\sigma(p)} - K^{max,H}_{\sigma(p)}\right] \sigma^*_Y(T_D)}{K^{max,H}_{\sigma(p)} \cdot \frac{d\sigma^*_Y}{dT} - \frac{d\sigma_f}{dT}} \qquad (10.8)$$

where $d\sigma^*_Y/dT$ and $d\sigma_f/dT$ are approximated as constants. This expression indicates that for a given geometric change ($K^{max}_{\sigma(p)} \rightarrow K^{max,H}_{\sigma(p)}$), the resulting change in nil-ductility temperature depends on the intrinsic material's properties.

Both of the previous effects are only apparent effects of microstructure in that holes produce the same effect at equivalent intrinsic toughness (σ_f/σ^*_Y) values. Viewed in this way, the effect of holes is independent of microstructure when failure occurs prior to general yield and is controlled by a critical fracture stress criterion. Microstructure does, however, have a direct effect on the improvements within the transition region and in fully ductile samples.

The ductility transition temperature of drilled samples T_{NH} depends on the ease with which fibrous tearing reaches one [equation (10.4)] and both [equation (10.5)] holes. This, in turn, depends strongly on the strain required for fibrous tearing (ε_s) as well as those required for cleavage (ε^H_F and ε'_F). Because equation (10.4) is satisfied at a critical ratio of $\varepsilon^H_F/\varepsilon_s$, it is fulfilled more easily when ε_s is low. On the other hand, reinitiation of failure from one hole is most difficult, and equation (10.5) is thus most easily satisfied when holes are blunted ($\rho_H\uparrow$, $\beta_H\uparrow$) by plastic deformation prior to tearing; this is favored by a high ε_s. In a particular material, ε_s is approximately temperature independent, but its magnitude decreases markedly with increasing volume fractions of second phases (carbide content in steels).

Since both equations (10.4) and (10.5) must be satisfied at the ductility transition temperature (T_{NH}), the magnitude of ΔT_N is quite low for both single phase ferrite where ϵ_s is very high and high carbon steels where ϵ_s is quite low. The maximum reduction is obtained in mild steels where ϵ_s is just low enough to cause tearing to one hole prior to cleavage, but high enough that holes are blunted significantly before the tearing occurs. In this respect, microstructure determines the geometry from which failure occurs, and thus it has a direct effect on the possible improvement from holes.

In fully ductile samples, the toughness depends on (1) the plastic deformation required to initiate an unstable fibrous tear, and (2) the deformation required to propagate this tear and cause complete separation. With increasing amounts of second phases, the tear energy decreases, and the energy associated with initial deformation becomes a larger fraction of the total energy. Since holes increase the deformation to initiate a fibrous tear but reduce the area over which it must propagate, they produce a larger percentage increase in the shelf energy in microstructures which have a lower tear energy.

10.5 Practical Implications and Future Work

This study indicates that drilled holes can be used to reduce the embrittling effects of design notches or incipient cracks in semi-brittle materials. The location of holes should be chosen for maximum redistribution of plastic strain away from the notch tip rather than solely for reduction of the elastic stress concentration factor whenever loading might extend beyond initial yielding either by design or by overload. Etch-pittable model materials such as Fe-Si or high nitrogen steel can be

used to experimentally evaluate those hole locations which produce a favorable redistribution of plastic strain around any complex keyway.

Although all the present work was done in simple static or dynamic tests, improvements should also be possible under conditions of fatigue loading. Certainly for hole locations which do not affect the elastic stress concentration factor (K_σ) markedly, little improvement can be expected in high cycle - low stress fatigue where K_σ controls the behavior. On the other hand, in low cycle-high stress fatigue, there is considerable local plastic deformation, and improvements from hole drilling might be quite pronounced. That is, because the regions of maximum strain are relocated at the notch side away from the maximum tensile stresses, initiation and initial growth of fatigue cracks might be more difficult than in a standard notched structure. In addition, if unstable failure initiates from a fatigue crack at the notch side, it may be stopped by one of the holes, preventing catastrophic failure of the part. In any case, this is an area which deserves future consideration.

There are still many unknowns regarding the details of the elastic-plastic stress and strain distributions in simply loaded bars. Specifically, the variation of the plastic zones from the sample surface to center and the effect of holes on this variation could be determined in more detail by dislocation etch pitting studies on various sections (like Figure 5.8). Microhardness measurements within the plastic zones could also be performed to estimate the magnitude of plastic strains when they exceed the etch-pit resolution. These measurements themselves would

relate the notch tip displacement to the various local strains and thereby define some of the parameters in equations (10.4) to (10.6).

Although knowledge of the path of local yielding provides insight into the maximum local stresses, the exact stress distribution must for the foreseeable future be determined by experimental methods. The measurement of the nominal fracture strength at known σ_f/σ_Y^* provides one way to determine the relationship between the maximum local stress $[K_{\sigma(p)} \equiv \sigma^{max}/\sigma_Y^*]$ and the applied load (P/σ_Y^*). A recently developed technique of thermally cycling some photoelastic materials[115], may be capable of simulating elastic-plastic behavior; although tedious, it might also be used to determine in detail the distribution of stress around partially plastic notch-hole combinations.

REFERENCES

1. A. A. Griffith, Phil. Trans. Roy. Soc., A221 (1920), 163.
2. A. A. Griffith, Proc. Int. Congr. Appl. Mech., 55 (1924).
3. E. Orowan, Repts. Prog. Phys., XII (1948), 185.
4. E. Orowan, Trans. Inst. Eng. Shipbuild. Scotland, 89 (1945), 165.
5. D. K. Felbeck and E. Orowan, Welding J. Res. Suppl. (1955), 570s.
6. J. R. Low, Jr., Relation of Properties to Microstructure, A.S.M., Cleveland (1953), 163.
7. A. Gilbert, et.al., Acta Met., 12 (1964), 754.
8. C. J. McMahon, Jr. and M. Cohen, Acta Met., 13 (1965), 591.
9. G. T. Hahn, et.al., Fracture, B. L. Averbach, et.al., eds. M.I.T., Wiley, New York (1959), 91.
10. C. Zener, Fracturing of Metals, A.S.M. (1948), 3.
11. A. N. Stroh, Advanc. In Phys., 6 (1957), 418.
12. D. Hull, Acta Met., 8 (1960), 11.
13. D. Hull, A.I.M.E. Int. Conf. on Fract., Seattle (1962).
14. R. Honda, J. Phys. Soc. Japan, 16 (1961), 1309.
15. R. Ku and T. L. Johnston, Phil. Mag., 9 (1964), 231.
16. A. J. McEvily, Jr. and T. L. Johnston, Int. Conf. on Fracture, Sendai, Japan, B-I (1965), 23.
17. W. G. Johnston and J. J. Gilman, J. Appl. Phys., 30 (1962), 129.
18. J. J. Gilman, Cranfield Symposium on Crack Prop., Cranfield (1961), 95.
19. A. S. Tetelman, Fracture of Solids, Wiley, New York (1963), 461.
20. A. S. Tetelman and A. J. McEvily, Jr., Fracture of Structural Materials, Wiley, New York (1967), 258.
21. A. H. Cottrell, Trans. A.I.M.E., 212 (1958), 192.
22. D. J. Petch, Fracture, B. L. Averbach, et.al., eds., M.I.T., Wiley, New York (1959), 54.

REFERENCES

23. N. J. Petch, J. Iron Steel Inst., 173 (1953), 25.

24. W. G. Johnston and J. J. Gilman, J. Appl. Phys., 30 (1959), 129.

25. W. G. Johnston, J. Appl. Phys., 33 (1962), 2050.

26. D. F. Stein and J. R. Low, Jr., J. Appl. Phys., 31 (1960), 362.

27. H. W. Schadler, Acta Met., 12 (1964), 861.

28. D. Hull, Acta Met., 9 (1960), 191.

29. T. L. Johnston, R. G. Davies, and N. S. Staloff, Phil. Mag., 12 (1965), 305.

30. E. E. Smith and P. J. Worthington, Int. Conf. on Fract., Sendai, Japan, B-III (1965), 3.

31. A. S. Tetelman and A. J. McEvily, Jr., op.cit., 266.

32. A. S. Tetelman, Acta Met., 12 (1964), 993.

33. A. H. Cottrell, The Mechanical Prop. of Matter, Wiley, New York (1964), 365.

34. J. M. Krafft and A. M. Sullivan, Trans. A.S.M., 56 (1963), 160.

35. J. M. Krafft, J. Appl. Mat'ls. Res., 3 (1964), 88.

36. A. R. Rosenfield and G. T. Hahn, "Numerical Description of the Ambient, Low-Temperature, and High Strain Rate Flow and Fracture Behavior of Plain Carbon Steel", Battelle Memorial Institute, Columbus Lab.Rept.(1967).

37. S. Sakui, et.al., J. Iron Steel Inst., Japan, 49 (1963), 996.

38. R. Hill, Mathematical Theory of Plasticity, Oxford, London (1950).

39. A. P. Green and B. B. Hundy, J. Mech. Phys. Solids, 4 (1956), 128.

40. J. R. Hendrickson, D. S. Wood, and D. S. Clark, Trans. A.S.M., 50 (1958), 656.

41. J. F. Knott and A. H. Cottrell, J. Iron Steel Inst., 201 (1963), 249.

42. F. A. McClintock and G. R. Irwin, Fracture Toughness Testing, A.S.T.M., Philadelphia, S.T.P. No. 381 (1965), 84.

43. A. H. Cottrell, Proc. Roy. Soc., A285 (1965), 10.

REFERENCES

44. A. A. Wells, Proc. Roy. Soc., A285 (1965), 34.

45. B. A. Bilby, A. H. Cottrell, and K. H. Swinden, Proc. Roy. Soc., A272 (1963), 304.

46. G. R. Irwin, Encyclopedia of Physics, VI, Springer, Heidelburg (1958).

47. M. Tanaka and S. Umekawa, Proc. First Japan Cong. Test. Mat'ls. (1958), 95.

48. B. Cotterell, Brit. Welding J., 9, 83.

49. B. Augland, Brit. Welding J., 9, 434.

50. D. E. W. Stone, Ph.D. Thesis, London (1963).

51. H. P. Tardiff and H. Marquis, Canadian Met. Quart., 2, 373.

52. G. D. Fearnehough and C. J. Hoy, J. Iron and Steel Inst., 202 (1964), 912.

53. W. D. Biggs, The Brittle Fracture of Steel, MacDonald and Evans, Ltd., London (1960).

54. T. R. Wilshaw, Ph.D. Thesis, London (1965).

55. J. D. Lubahn, Welding J., 34 (1955), 518.

56. C. Crussard, et.al., J. Iron Steel Inst., 183, 146.

57. J. F. Knott, Ph.D. Thesis, Cambridge (1962).

58. A. S. Tetelman and A. J. McEvily, Jr., op. cit., 311.

59. T. R. Wilshaw, C. A. Rau, Jr., and A. S. Tetelman, "A General Model to Predict the Elastic - Plastic Stress Distribution and Fracture Strength of Notched Bars in Plane Strain Bending", to be presented at the National Fracture Mechanics Conf., Lehigh U. (1967).

60. T. R. Wilshaw and P. L. Pratt, J. Mech. Phys. Solids, 14 (1966), 7.

61. A. P. Green, Quart. J. Mech. Appl. Math., 6 (1953), 223.

62. G. Lianis and H. Ford, J. Mech. Phys. Solids, 7 (1958), 1.

63. J. M. Alexander and T. J. Komoly, J. Mech. Phys. Solids, 10 (1962), 265.

REFERENCES

64. J. A. Rineholt and W. J. Harris, Jr., Trans. A.S.M., 43 (1951), 1175.

65. K. W. Burns and F. B. Pickering, J. Iron Steel Inst., 202 (1964), 899.

66. J. F. Knott, Proc. Roy. Soc., A285 (April, 1965), 150.

67. S. Sakui, et.al., Iron Steel, 4 (1963), 672.

68. A. S. Tetelman and A. J. McEvily, Jr., op. cit., 319.

69. T. R. Wilshaw and P. L. Pratt, Int. Conf. on Fract., Sendai, Japan, B-III (1965), 3.

70. H. Neuber, Kerbspannungs Lehre, Springer-Verlag, AEC TR 45-47 (1958).

71. G. Oates, Proc. Roy. Soc., A285 (1965), 166.

72. A. S. Tetelman and A. J. McEvily, Jr., op. cit., 326.

73. R. Castro and A. Gueussier, Rev. Metal, 46 (1949), 517.

74. J. F. Knott, J. Iron Steel Inst. (Feb., 1966), 104.

75. W. S. Pellini, et.al., N.R.L. Rept. 6300 (June, 1965).

76. V. Weiss and S. Yukawa, Fracture Toughness Testing and Its Applications, Am. Soc. for Test. Mat'ls., Philadelphia, Pa. (1965).

77. W. Weibull, Proc. Roy. Swed. Inst. for Engr. Res., Stockholm, 149, 27; 151, 45; 153, 55.

78. A. H. Cottrell, Proc. Roy. Soc., A282 (1964), 2.

79. J. Cook and J. E. Gordon, Proc. Roy. Soc., A282 (1964), 508.

80. A. Kelly and W. R. Tyson, High Strength Materials, Wiley, New York (1965), 578.

81. A. J. McEvily, Jr. and R. H. Bush, Trans. A.S.M., 55 (1962), 654.

82. R. J. Stokes and C. H. Li, Trans. A.I.M.E., 230 (1964), 1104.

83. T. L. Johnston, R. J. Stokes, and C. H. Li, Trans. A.I.M.E., 221 (1961), 221.

84. G. T. Hahn and A. R. Rosenfield, Acta Met., 13 (1965), 293.

85. A. S. Tetelman and W. D. Robertson, Trans. A.I.M.E., 224 (1962), 224.

REFERENCES

86. J. R. Griffiths and A. H. Cottrell, J. Mech. Phys. Solids, 13 (1965), 306.

87. C. G. Dunn and W. R. Hibbard, Jr., Acta Met., 4 (1956), 306.

88. F. T. Wessel and R. D. Olleman, A.S.T.M. Bulletin No. 187 (1953), 56.

89. C. E. Morris, Metals Prog. (1949), 696.

90. R. S. Zeno and J. R. Low, Jr., Weld. J. Res. Suppl., 27 (1948), 1455.

91. E. P. Klier and M. Gensamer, "Final Rept. on Correlation of Lab. Tests with Full-Scale Ship Plate Fracture Tests", S.S.C. 30 (Jan., 1953).

92. G. M. Boyd, Symp. on Notch-Bar Testing and Its Relation to Welded Construction, London Inst. of Welding (1953).

93. D. Brewster, Trans. Roy. Soc., London (1816), 156.

94. F. G. Coker and L. N. G. Filon, Photoelasticity, Cambridge University Press (1931).

95. M. Hetenyi, Handbook of Experimental Stress Analysis, Wiley (1950).

96. M. M. Frocht, Photoelasticity, 2 vols. (1941 and 1948), Wiley, New York.

97. H. T. Jessop and F. C. Harris, Photoelasticity, Dover Publications (1950).

98. J. Nunes, "Slow-Bend Tension Test Correlations of Short Beams with Special Reference to the Charpy Type Specimens", AMRA TR 64-45.

99. S. Timoshenko and J. N. Goodier, Theory of Elasticity, McGraw-Hill, New York (1951), 99.

100. T. R. Wilshaw, J. Iron Steel Inst., 204 (Sept., 1966), 936.

101. J. C. Suits and J. R. Low, Jr., Acta Met., 5 (1957), 285.

102. G. T. Hahn, Trans. AIME, 224 (1962), 395.

103. J. M. Krafft, A. H. Sullivan and C. F. Tipper, Proc. Roy. Soc., 221A (Jan., 1954), 114.

104. J. A. Hendrickson, D. S. Wood, and D. S. Clark, Trans. A.S.M., 51 (1959), 629.

REFERENCES

105. H. Neuber, Theory of Notch Stresses, J. W. Edwards, ed., Ann Arbor, Michigan (1946).

106. A. Thum and S. Berg, Forschung auf dem Gebiete des Ingenieurwesens, 2 (1931), 345.

107. S. Berg, Forschung auf dem Gebiete des Ingenieurwesens, 12 (1941), 205, Translation RSIC-161 (1964).

108. A. J. Baker and P. R. Swann, Trans. A.S.M., 57 (1964), 1008.

109. S. Floreen and G. R. Speich, Trans. A.S.M., 57 (1964), 714.

110. D. J. Petch, Progr. in Metal Phys., 5 (1954), 1.

111. A. S. Tetelman and A. J. McEvily, Jr., op. cit., 501.

112. J. Nunes and F. R. Larson, Trans. A.I.M.E., 227 (1963), 1369.

113. E. B. Kula and C. F. Hickey, Jr., Watertown Arsenal Rept. ASD-TDR-63-262 (1963), 236.

114. E. C. Bain and H. W. Paxton, Alloying Elements in Steel, 2nd ed., A.S.M., Cleveland (1961).

115. A. R. Hunter and M. E. Schwartz, "Development and Application of a Photo-Plastic Method to Study Stress Distributions in the Vicinity of a Simulated Crack", Lockheed M. & S. Rept. 4-05-66-3 (31 May, 1966).